REACTIVITY AND CHARACTERIZATION OF GOLD(I) CARBENES: KEY INTERMEDIATES IN GOLD(I) CATALYSIS

Cristina García Morales

UNIVERSITAT ROVIRA i VIRGILI

Reactivity and Characterization of Gold(I) Carbenes: Key Intermediates in Gold(I) Catalysis

Cristina García Morales

DOCTORAL THESIS
2019

Cristina García Morales

Reactivity and Characterization of Gold(I) Carbenes:

Key Intermediates in Gold(I) Catalysis

DOCTORAL THESIS

Supervised by Prof. Antonio M. Echavarren

Institut Català d´Investigació Química (ICIQ)

UNIVERSITAT ROVIRA i VIRGILI

Tarragona 2019

I STATE that the present study, entitled "Reactivity and Characterization of Gold(I) Carbenes: Key Intermediates in Gold(I) Catalysis", presented by Cristina García Morales to award the degree of Doctor, has been carried out under my supervision at the Institut Català d´Investigació Química (ICIQ).

Tarragona, March 8th, 2019

Doctoral Thesis Supervisor

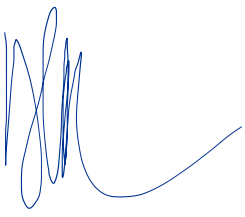

Prof. Antonio M. Echavarren Pablos

A mis padres, Lucía y mis hermanos

"Si te dan un papel pautado, escribe por detrás"

Juan Ramón Jiménez

Acknowledgments

En primer lugar, me gustaría agradecer a mi director de Tesis, Prof. Antonio M. Echavarren, por haberme aceptado en su grupo. Sus enseñanzas, consejos y críticas sobre los temas más diversos, entre ellos química, me han hecho crecer a pasos agigantados como científica y como persona. Asimismo, le agradezco su plena confianza en mí y las innumerables oportunidades que me ha brindado a lo largo de estos años. Pero, sobre todo, quiero agradecerle el apoyo y comprensión que me ha ofrecido en los no tan buenos momentos. Me depare lo que me depare el futuro, espero estar siempre a la altura de la persona en la que me he convertido bajo su supervisión.

Quisiera también agradecer toda la ayuda proporcionada por Sònia Gavaldà e Imma Escofet. Sin ellas, dedicarnos únicamente a investigar sería imposible.

I would like to thank Prof. Melanie S. Sanford for welcoming me in her group for three months at the University of Michigan, Ann Arbor, USA. Thanks for making me feel a member of the group from the very first day and also for your absolute confidence in me. I would also like to extend the warmest thank to all my lab mates, specially: Pablo Cabrera, Melissa Lee and Nomon Rezayee for making me have such a great time back there.

I would like to thank all the members (past and present) of the Echavarren group. Specially, those I had the pleasure to collaborate with: Dr. José María Muñoz Molina, Imma Escofet, Dr. Laura López-Suarez, Dr. Andrey I. Konovalov, Xiang Yi, Dr. Juan Manuel Sarria Toro and Dr. Xiao-Li Pei. Specially, I am very grateful to Dr. Juan M. Sarria Toro for being so patience with me at the beginning and to Dr. Xiao-Li Pei for putting my health first to her interests.

Quiero agradecer a todos aquellos compañeros que se convirtieron en mucho más que eso. A Oscar por sus discusiones y su horrible gusto musical. A mis compañeras de pasillo, Pilar Calleja y Ruth Dorel, gracias por tantísima ayuda y por aún más risas. A la Dr. Ana Pereira, por traer un trocito de Huelva a Tarragona. A Víctor Laserna, por su cariño incondicional. A Eloísa Serrano, por el tiempo compartido en Ann Arbor y Tarragona. Por último, quiero agradecer a la nueva generación de doctorandos, compuesta por Mauro Mato, Otilia Stoica, Joan Mayans, Inma Martín, Alba Pérez, Ana Arroyo y Bruna Sánchez. Por haber traído con ellos la alegría y la música que le faltaba al laboratorio. Por haber aparecido al final y, aún así, haberse convertido en maravillosos compañeros y amigos. Con ellos todo ha sido más fácil.

Quiero agradecer a todos mis compañeros de piso a lo largo de estos años. Especialmente a Pilar Calleja, por nuestras horas en el sofá, los bailes en la Wii, las conversaciones de hermana mayor, los viajes, los mejores consejos que me han dado nunca y por quererme tanto siempre. A Joan, por ser tan distinto a mí y abrirme los ojos a un mundo nuevo. A Ale, por todas las

visitas. A Ángel, por no haber parado ni un solo segundo de cuidar de mí y por todo el tiempo dedicado a iniciarme en el mundo de las DFTs. Además, quiero darle las gracias por haberse convertido en mi mejor compañero de viaje en esta aventura y por no haberme dejado caer jamás.

Quiero agradecer a las "Drama Queens": Mari Carmen, María Garrido, María Macías, Obdulia, Rocío, Carmen y Ana. Por haber compartido toda nuestra vida juntas, los buenos y los malos momentos durante casi 20 años ya. Vuestro apoyo y ayuda incondicional han sido un pilar fundamental para mí. Quiero agradecer especialmente a Ana, porque desde el 13/07/2008 no ha faltado ni un día en mi vida. Estoy tremendamente agradecida por tener unas amigas con las que he compartido tanto, con las que he crecido y que, incluso estando tan lejos, han estado ahí.

Quisiera extender mi más sincero agradecimiento a toda mi familia. Especialmente quiero agradecer a mis abuelos, Encarna y Pepe, por su amor, por confiar siempre en mí, por sus llamadas y todas las tardes sentados hablando de cualquier cosa. También a mis primas Teresa, Ester, Isabel y mi tía Ana, por ser simplemente especiales para mí. Por último, mi tío Fran por haber plasmado a la perfección mis deseos en la portada de esta Tesis.

I could not forget how my commercially available JosiPhos ligands caught the attention of a charming Italian PhD back in OMCOS 2015 and, specially, how years later, he shown up and turned my life upside down. Since then, he has been my strongest supporter, my best cook, my laziest friend and my permanent doses of happiness and positivism. Thanks Giacomo E. M. Crisenza for being completely opposite to me and, at the same time, my perfect half.

Quiero agradecer a mis hermanos, Antonio y Pablo. Por haberme permitido disfrutar de ellos como madre-hermana. Ver como han crecido ha sido todo un regalo. A mi pequeño Marcos, por quererme tanto aunque siempre haya sido su hermana en la distancia. A mi hermana Lucía, quiero agradecerle haber sido mi mejor amiga y haber sabido ser la hermana mayor cuando yo no podía. Quiero darle las gracias por todos los viajes que ha hecho para visitarme allá donde fuese y por todas las horas al teléfono que nos han permitido sentirnos cerca.

Por último, quisiera agradecer a mis padres, Antonio y Rosa, por la educación que nos han brindado, por enseñarnos que todo se consigue con esfuerzo y que nunca hay que rendirse. A mi padre quiero agradecerle todas las clases con naranjas para explicarnos la rotación y la traslación de la Tierra, los cálculos mentales para resolver ecuaciones cuando era niña y su afán por entenderlo todo. Gracias a esto, la pasión por investigar se despertó en mí desde pequeña. Pero, sobre todo, quiero agradecerles a los dos que hayan dedicado su vida a hacernos felices y el amor incondicional que nos han profesado siempre a mí y a mis hermanos.

This work was carried out with the support of the Agencia Estatal de Investigación (AEI)/FEDER, UE (projects CTQ2013-42106-P, CTQ2016-75960-P, FPI predoctoral fellowship to C. G.-M and Severo Ochoa Excellence Acreditation 2014-2018 (SEV-2013-0319)), the European Research Council (Advanced Grant No. 321066), the Agency of Management of University and Research Grants (AGAUR, 2014 SGR 818, 2017 SGR 1257), the Atomic Scale and Single Molecule Logic Gate Technologies (ATMOL, European Integrated Research Project, contract No. FP7-270028), and the Institute of Chemical Research of Catalonia (ICIQ).

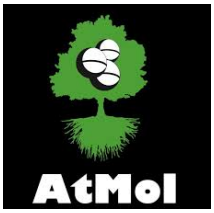

Publications arising from this work at the time of writing this manuscript:

"Direct Observation of Aryl Gold(I) Carbenes that Undergo Cyclopropanation, C–H Insertion, and Dimerization Reactions"

García-Morales, C.; Pei, X.-L.; Sarria Toro, J. M.; Echavarren, A. M. *Angew. Chem. Int. Ed.* **2019**, DOI: 10.1002/anie.201814577.

"Generation of Gold(I) Carbenes by Retro-Buchner Reaction: From Cyclopropanes to Natural Products Synthesis"

Mato, M.; García-Morales, C.; Echavarren. A. M. *ChemCatChem* **2019**, 11, 53–72.
Special Issue: 10th Anniversary Issue of ChemCatChem

"From Straightforward Gold(I)-Catalyzed Enyne Cyclizations to More Demanding Intermolecular Reactions of Alkynes with Alkenes"

García-Morales, C.; Echavarren A. M. *Synlett,* **2018***, 29*, 2225–2237.

"Enantioselective Synthesis of Cyclobutenes by Intermolecular [2+2] Cycloaddition with Non-C_2 Symmetric Digold Catalysts"

García-Morales, C.; Ranieri, B.; Escofet, I.; López-Suárez, L.; Obradors, C.; Konovalov, A.; Echavarren. A. M. *J. Am. Chem. Soc.* **2017**, *139*, 13628–13631.
Highlighted in *Synfacts*, **2018**, *14*, 66.

"Gold(I) Carbenoids: On-Demand Access to Gold(I) Carbenes in Solution"

Sarria Toro, J. M.; García-Morales, C.; Raducan, M.; Smirnova, E. S.; Echavarren. A. M. *Angew. Chem. Int. Ed*. **2017**, *56*, 1859–1863.

Table of Contents

Prologue

This thesis manuscript has been divided into four main parts, a general introduction on gold(I) catalysis and three research chapters, which are preceded by the abstract and general objectives of the Thesis, and followed by the overall conclusions. Each research chapter contains five sections including a specific introduction on the research topic, the objectives to be achieved in the chapter, the results and discussion of the investigation, the conclusions reached and the experimental section. The references and numbering are organized by chapters.

The **General Introduction** provides an overview of the basic principles of homogeneous gold(I) catalysis comprising general aspects on the catalysts, the activation of alkynes, the cycloisomerization of enynes, the intermolecular reactions of alkynes with alkenes and the enantioselective gold(I) catalysis.

Chapter I, *"Enantioselective Gold(I)-Catalyzed [2+2] Cycloaddition of Alkynes with Alkenes",* presents the development of a broad scope enantioselective synthesis of cyclobutenes by intermolecular [2+2] cycloaddition of alkynes with alkenes using Josiphos digold(I) catalysts. In-depth experimental mechanistic investigations allowed the elaboration of a full mechanistic proposal. This work was initiated by Dr. Laura López-Suárez and Imma Escofet and thus, for coherence some of their results have been discussed briefly. The reaction optimization and the scope expansion were performed in collaboration with Imma Escofet. The computed enantioinduction model was performed by Dr. Andrey I. Konovalov. This work has been published in *J. Am. Chem. Soc.* **2017**, *139*, 13628–13631. An account on this work was published in *Synlett,* **2018**, *29*, 2225–2237.

Chapter II, *"Synthesis and Reactivity of Chloromethylgold(I) Carbenoids",* discloses the development of a simple and reliable method for the preparation of chloro(methyl)gold complexes which upon activation with a chloride scavenger exhibit the reactivity expected from free gold carbenes in solution. This work was based on the research developed by Mihai Raducan and Ekaterina Smirnova and thus, for coherence, some of their results have been discussed briefly. The research presented in this chapter was done in collaboration with Dr. Juan M. Sarria Toro. This work has been published in *Angew. Chem. Int. Ed.* **2017**, *56*, 1859–1863. Part of this information has been published in a review in *ChemCatChem* **2019**, *11*, 53–72.

Chapter III, *"Characterization of Mesityl Gold(I) Carbenes: Genuine Intermediates in the Retro-Buchner Reaction"*, presents the spectroscopically characterization of monosubstituted gold(I) carbenes for the first time in solution, which undergo representative transformations of gold(I) carbene intermediates formed under catalytic conditions. At the end of the project, Dr. Xiao-Li Pei joined me to finish the experimental work. I thank Angel L. Mudarra Alonso for

fruitful discussions about Density Functional Theory. This work has been recently published in *Angew. Chem. Int. Ed.* **2019**, DOI: 10.1002/anie.201814577.

Abbreviations and Acronyms

In this manuscript, the abbreviations and acronyms most commonly used in organic and organometallic chemistry have been used following the recommendations of "Guidelines of Authors" of the Journal of Organic Chemistry.

Additional abbreviations and acronyms used in this manuscript are listed below:

APCI	atmospheric pressure chemical ionization
BAr_4^{F-}	tetrakis[3,5-bis(trifluoromethyl)phenylborate]
CHT	cycloheptatriene
DPCb	*o*-carborane diphosphine
dr	diastereomeric ratio
ee	enantiomeric excess
er	enantiomeric ratio
ESI	electrospray ionization
JohnPhos	(2-biphenyl)di-*tert*-butylphosphine
IBO	intrinsic bond orbital
Int	intermediate
IPr	1,3-bis(2,4,6-trimethylphenyl)imidazole-2-ylidene
IPr**	1,3-bis[2,6-bis[(4-*tert*-butylphenyl)methyl]-4-methylphenyl]imidazol-2-ylidene
L	ligand
MALDI	matrix assisted laser desorption ionization
MS	mass spectrometry/molecular sieves
MW	microwave irradiation
NBO	natural bond orbital
NCD	norcaradiene
NLMO	natural localized molecular orbital
NTf_2^-	bis(trifluoromethyl)imidiate
OTf^-	triflate
ORTEP	oak ridge thermal ellipsoid plot
*t*BuXPhos	2-(di-*tert*-butylphosphino)-2´,4´,6´-triisopropyl-1,1´-biphenyl
tht	tetrahydrothiophene
tmbn	trimethoxybenzonitrile
TS	transition state

Abstract

Previous endeavors of our group demonstrated that the gold(I)-catalyzed [2+2] cycloaddition of terminal alkynes with alkenes provides a straightforward route to obtain regioselectively cyclobutenes in a racemic manner. It is important to note that, despite the developments in enantioselective gold(I) catalysis, the induction of good levels of enantioselectivity in intermolecular gold(I) catalyzed reactions of alkynes with alkenes remains a challenge.

In this context, we developed the enantioselective intermolecular gold(I)-catalyzed [2+2] cycloaddition of terminal alkynes and alkenes using non C_2-chiral Josiphos digold(I) complexes as catalysts (Scheme 1). Our mechanistic studies indicate that only one of the gold(I) centers is directly involved in the activation of the alkyne, although the second one is required to induce the enantioselectivity. Our work also reveals that both ligand exchange and electrophilic addition can be turnover-limiting steps in this catalytic cycloaddition.

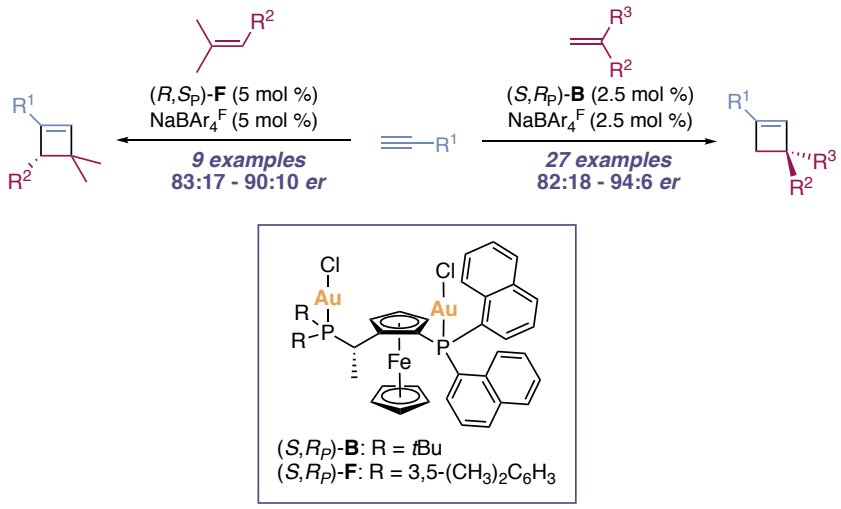

Scheme 1. Enantioselective gold(I)-catalyzed [2+2] cycloaddition of alkynes with alkenes.

As part of our efforts towards the in-depth understand mechanisms, we next focused our attention on highly electrophilic gold(I) carbenes, which have been proposed as key players in a wide variety of gold(I)-catalyzed transformations. Despite their importance in gold(I) homogeneous catalysis, a debate is underway regarding the nature and the electronic structure of these intermediates. The lack of consensus can be understood by the limited structural information obtained from reactive gold(I) carbene complexes.

To this end, we developed a convenient approach to access chloromethylgold(I) carbenoids bearing phosphines, NHC carbenes and phosphites as ligands. We demonstrated that upon chloride abstraction, these complexes display the typical reactivity of gold(I) carbenes in solution, namely: homocoupling, cyclopropanation and Buchner reaction (Scheme 2).

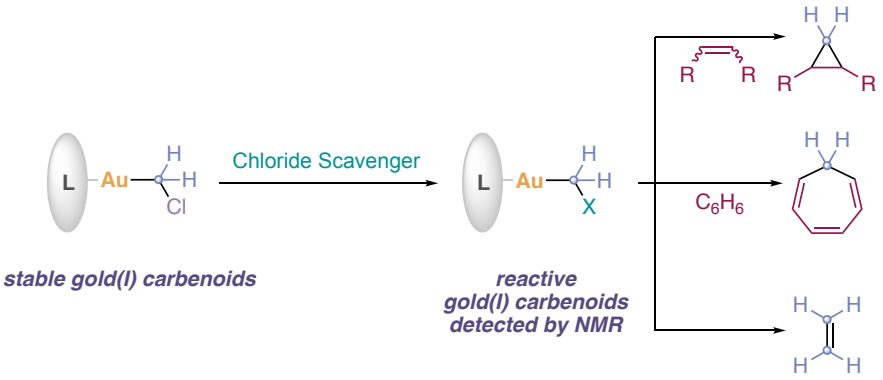

Scheme 2. Synthesis and reactivity of chloromethylgold(I) carbenoids.

As an extension of the work referred above, mesityl gold(I) carbenes lacking heteroatom stabilization or shielding ancillary ligands have been generated from chloro(mesityl)methylgold(I) carbenoids bearing JohnPhos-type ligands by chloride abstraction with $GaCl_3$ (Scheme 3). These new family of aryl gold(I) carbenes have been characterized spectroscopically at low temperatures. The latter complexes promote cyclopropanation, C–H insertion and oxidation. In the absence of nucleophiles, a bimolecular reaction, similar to that observed for other metal carbenes, leads to a symmetrical alkene. Computational studies have been carried out to gain more insights into the reactivity and the gold-carbon bond situation in these highly electrophilic complexes.

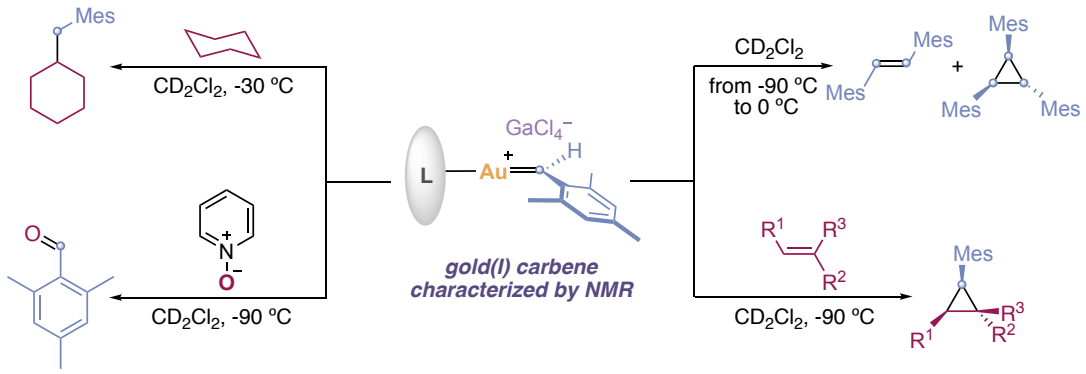

Scheme 3. Reactivity of detectable gold(I) carbenes.

General Objectives

The aims of this Doctoral Thesis were the development of new enantioselective gold(I)-catalyzed transformations and the characterization of highly electrophilic gold(I) catalytic intermediates. In particular, the objectives of this work were:

- The development of a general enantioselective gold(I)-catalyzed [2+2] cycloaddition of alkynes with alkenes and the experimental elucidation of the reaction mechanism.
- The development of a convenient approach to prepare chloro(methyl)gold(I) carbenoid complexes and the study of their reactivity.
- The spectroscopy characterization of aryl gold(I) carbenes, the demonstration of their role as catalytic intermediates and the detailed examination of the nature of the gold-carbon bond by Density Functional Theory.

Each chapter of this PhD Thesis manuscript contains a more detailed description of the objectives of the corresponding chapter.

General Introduction

Origin of Gold Chemistry

Gold, in its metallic form, occurs in a virtually pure state. It is ductile, malleable, appealing and imperishable. The earliest decorative items crafted using this precious metal, date back to 5000 BC in ancient Egypt.[1] Ever since, every human culture has associated gold to beauty, power and success.

Figure 1. Gold diadem concealed beneath the death mask of Tutankhamun´s mummy.

However, due to its assumed inertness, the potential of gold as catalyst was neglected for centuries. It was not until the very end of the 20th century when pioneering work by Teles[2] and later by Tanaka[3] on the gold(I)-catalyzed selective addition of alcohols and water to alkynes paved the way for the advent of homogeneous gold catalysis. Likewise, the development of the phenol synthesis by Hashmi using simple gold(III) salts as catalyst provided a seminal grounding to this field.[4] In the ensuing years, cationic gold(I) complexes have been extensively used to selectively activate unsaturated C–C bonds, triggering chemical transformations to furnish complex structures difficult to access by other means, in an atom-economical fashion.[5]

Gold(I) Catalysis: General Aspects

The exceptional ability of gold(I) complexes to selectively activate π-bonds has been attributed to relativistic effects.[6] The latter can be related to the acceleration of the electrons spinning around a heavy nucleus. The resulting mass increase of the electrons leads to an energetic

1 Cartwright, M. **2014**, *Ancient History Encyclopedia*, "Gold in Antiquity".

2 Teles, J. H.; Brode, S.; Chabanas, M. *Angew. Chem. Int. Ed.* **1998**, *37*, 1415–1418.

3 Mizushima, E.; Sato, K.; Hayashi, T.; Tanaka, M. *Angew. Chem. Int. Ed.* **2002**, *41*, 4563–4565.

4 Hashmi, A. S. K.; Frost, T. M.; Bats, J. W. *J. Am. Chem. Soc.* **2000**, *122*, 11553–11554.

5 (a) Hashmi, A. S. K. *Chem. Rev.* **2007**, *107*, 3180–3211. (b) Li, Z.; Brouwer, C.; He, C. *Chem. Rev.* **2008**, *108*, 3239–3265. (c) Fürstner, A. *Chem. Soc. Rev.* **2009**, *38*, 3208–3221. (d) Shapiro, N.; Toste, F. D. *Synlett* **2010**, 675–691. (e) Nolan, S. P. *Acc. Chem. Res.* **2011**, *44*, 91–100. (f) Obradors, C.; Echavarren, A. M. *Acc. Chem. Res.* **2014**, *47*, 902–912. (g) Fensterbank, L.; Malacria, M. *Acc. Chem. Res.* **2014**, *47*, 953–965. (h) Dorel, R.; Echavarren, A. M. *Chem. Rev.* **2015**, *115*, 9028–9072. (i) Pflästerer, D.; Hashmi, A. S. K. *Chem. Soc. Rev.* **2016**, *45*, 1331–1367. (j) Echavarren, A. M.; Muratore; M.; López-Carrillo, V.; Escribano-Cuesta, A.; Huguet, N.; Obradors, C. *Org. React.* **2017**, *92*, 1.

6 (a) Pyykkö, P. *Angew. Chem. Int. Ed.* **2002**, *41*, 3573–3578. (b) Schwarz, H. *Angew. Chem. Int. Ed.* **2003**, *42*, 4442–4445. (c) Pyykkö, P. *Angew. Chem. Int. Ed.* **2004**, *43*, 4412–4456.

stabilization and contraction of the *s* and *p* orbitals of the nucleus, whose electrons will exhibit a stronger nuclear attraction. As a consequence, the *d* and *f* orbitals experience destabilization and expansion, and thus, the electrons occupying those orbitals are weakly attracted by the nucleus. This phenomenon becomes significant for metals that have the *4f* and *5d* orbitals filled, reaching a maximum in the case of gold ([Xe] $6s^1 5d^{10}$) in the periodic table. Therefore, the high electrophilicity and the soft Lewis acidic character displayed by gold can be understood by this phenomenon. In the case of gold, the filled *5d* orbital, in which the electron-electron repulsion is minimized due to the expansion, can interact with the filled *p* orbitals of unsaturated bonds attracting their electrons towards gold and, thus, activating them towards nucleophilic attack.

The Lewis acidity has dominated gold(I) chemistry because gold(I) complexes prefer to adopt a linear dicoordinated geometry (Scheme 1, species **1**), which hampers typical organometallic elementary steps.[7,8] Specifically, common linear dicoordinated gold(I) complexes do not easily undergo oxidative addition or promote β-hydride elimination. However, recent new discoveries have demonstrated that by rational ligand design, and using appropriate substrates, gold(I) complexes can promote oxidative addition.[9] However, to date, β-hydride elimination has only been described from square planar gold(III) complexes.[10]

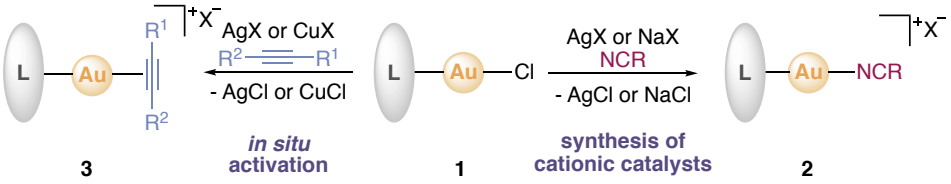

Scheme 1. Gold(I) complexes activation mode.

In order to be catalytically active, gold(I) complexes must undergo ligand substitution. Considering that cationic monocoordinated gold(I) species have never been observed, two different approaches can be used to facilitate the ligand substitution from neutral linear two-coordinate gold(I) complexes (Scheme 1). The first adopted strategy relies on the *in situ*

7 Gimeno, M. C.; Laguna, A. *Chem. Rev.* **1997**, *97*, 511–522.

8 For a review on the topic: Joost, M.; Amgoune, A.; Bourissou, D. *Angew. Chem. Int. Ed.* **2015**, *54*, 15022–15045.

9 Zeineddine, A.; Estévez, L.; Mallet-Ladeira, S.; Miqueu, K.; Amgoune, A.; Bourissou, D. *Nat. Commun.* **2017**, *8*, 565–572.

10 (a) Mankad, N. P.; Toste, F. D. *Chem. Sci.* **2012**, *3*, 72–76. (b) Kumar, R.; Krieger, J.-P.; Gómez-Bengoa, E.; Fox, T.; Linden, A.; Nevado, C. *Angew. Chem. Int. Ed.* **2017**, *56*, 12862–12865.

activation of neutral two-coordinate gold(I) species **1** *via* chloride abstraction by a copper[11] or a silver[12] salt (Scheme 1, left). However, those methods present downsides due to the formation of inactive gold(I) species or the promotion of side reactions by the chloride scavengers used.[13] A most effective procedure takes advantages of cationic complexes **2** in which gold is bounded to both an ancillary ligand and to a labile ligand. For the reaction to occur, the latter has to be replaced by the substrate through an associative ligand exchange mechanism.[14]

The ancillary ligand plays an important role to modify the steric and electronic properties of gold(I) species. To this end, in general, complexes bearing less σ-donatig phosphites ligands **6** are more electrophilic and less selective catalysts than those containing better σ-donating phosphines (**5**) or *N*-heterocyclic carbenes (**4**) (Figure 2).[15] Among the phosphine ligands, bulky Buchwald-type ligands (Figure 2, ligands in complexes **5**) have been found to be competent ligands for gold(I) complexes capable of activating alkynes in intra- and intermolecular transformations.[14,15]

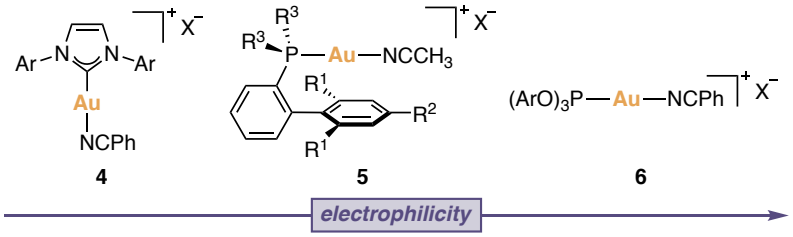

Figure 2. Electrophilicity increased by ancillary ligand modification for cationic gold(I) complexes.

11 Guérinot, A.; Fang, W.; Sircoglou, M.; Bour, C.; Bezzenine-Lafollée, S.; Gandon, V. *Angew. Chem. Int. Ed.* **2004**, *52,* 5848–5852.

12 (a) Partyka, D. V.; Robilotto, T. J.; Zeller, M.; Hunter, A. D.; Gray, T. G. *Organometallics* **2008**, *27*, 28–32. (b) Pérez-Galán, P.; Delpont, N.; Herrero-Gómez, E.; Maseras, F.; Echavarren, A. M. *Chem. –Eur. J.* **2010**, *16*, 5324–5332. (c) Hashmi, A. S. K.; Hengst, T.; Lothschütz, C.; Rominger, F. *Adv. Synth. Catal.* **2010**, *352*, 1315–1337. (d) Fortman, G. C.; Nolan, S. P. *Organometallics* **2010**, *29*, 4579–4583. (e) Fortman, G. C.; Nolan, S. P. *Chem. Soc. Rev.* **2011**, *40*, 5151–5169.

13 (a) Zhu, Y.; Day, C. S.; Zhang, L.; Hauser, K. J.; Jones, A. C. *Chem –Eur. J.* **2013**, *19*, 12264–12271. (b) Homs, A.; Escofet, I.; Echavarren, A. M. *Org. Lett.* **2013**, *15*, 5782–5785.

14 (a) Nieto-Oberhuber, C.; López, S.; Echavarren, A. M. *J. Am. Chem. Soc.* **2005**, *127*, 6178–6179. (b) Nieto-Oberhuber, C.; López, S.; Muñoz, M. P.; Cárdenas, D. J.; Buñuel, E.; Nevado, C.; Echavarren, A. M. *Angew. Chem. Int. Ed.* **2005**, *44*, 6146–6148.

15 Ranieri, B.; Escofet, I.; Echavarren, A. M. *Org. Biomol. Chem.* **2015**, *13*, 7103–7118.

Cycloisomerization of 1,*n*-Enynes

Gold(I) complexes react with alkynes generating (η^2-alkyne)gold(I) species **3**, which can be subjected to nucleophilic addition by soft nucleophiles.[5] In general, the nucleophilic attack occurs in a Markovnikov fashion to generate *trans*-alkenyl-gold complexes **7**, as a result of an *anti*-addition (Scheme 2). A rich selection of both carbon- and heteroatomic-based nucleophilic partners successfully participated in this type of gold(I)-catalyzed transformations delivering selectively *anti*-addition products.[5,16]

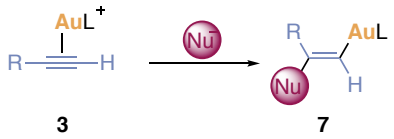

Scheme 2. *anti*-Nucleophilic attack to (η^2-alkyne)gold species.

Gold(I) triggers a series of fascinating skeletal rearrangements of 1,*n*-enynes that lead to a wide diversity of cyclic products through rather complex mechanisms (Scheme 3). In the case of 1,6-enynes, gold(I) initially coordinates to the alkyne forming (η^2-alkyne)gold(I) complexes **8** that react intramolecularly with the alkene in an electrophilic addition process to generate cyclopropyl gold(I) carbene intermediates **9** and/or **10** by *anti*-5-*exo*-dig or 6-*endo*-dig cyclization respectively (Scheme 3).[14,17] According to DFT calculations, both intermediates **9** and **10** are highly delocalized cationic structures.[14, 17]

Cyclopropyl gold(I) carbene intermediates **9** can give rise to 1,3-dienes **11** by single-cleavage skeletal rearrangement, since only the alkene moiety at the substrate (carbons in red) suffers carbon-carbon bond cleavage. Intermediates **9** can also undergo a so-called double-cleavage rearrangement by the formal insertion of the terminal alkene carbon (carbon in red bound to R^2) into the alkyne carbons (carbons in blue) of the original 1,6-enynes giving rise to new gold(I) carbenes **12** that undergo α-proton elimination to form product **13**.

16 (a) Reetz, M. T.; Sommer, K. *Eur. J. Org. Chem.* **2003**, 3485–3496. (b) Nevado, C.; Echavarren, A. M. *Synthesis* **2005**, *2*, 167–182. (c) Hashmi, A. S. K.; Haufe, P.; Schmid, C.; Rivas Nass, A.; Frey, W. *Chem. –Eur. J.* **2006**, *12*, 5376–5382. (g) Kusama, H.; Miyashita, Y.; Takay, J.; Iwasawa, N. *Org. Lett.* **2006**, *8*, 289–292. (j) Nakamura, I.; Sato, T.; Yamamoto, Y. *Angew. Chem. Int. Ed.* **2006**, *45*, 4473–4475. (e) Istrate, F. M.; Gagosz, F. *Org. Lett.* **2007**, *9*, 3181–3184. (h) Shapiro, N. D.; Toste, F. D. *J. Am. Chem. Soc.* **2007**, *129*, 4160–4161. (i) Ye, L.; Cui, L.; Zhang, L. *J. Am. Chem. Soc.* **2010**, *132*, 3258–3259. (d) Krauter, C. M.; Hashmi, A. S. K.; Pernpointner, M. *ChemCatChem* **2010**, *2*, 1226–1230. (f) Qian, J.; Liu, Y.; Cui, J.; Xu, Z. *J. Org. Chem.* **2012**, *77*, 4484–4490.

17 Escribano-Cuesta, A.; Pérez-Galán, P.; Herrero-Gómez, E.; Sekine, M.; Braga, A. A. C.; Maseras, F.; Echavarren, A. M. *Org. Biomol. Chem.* **2012**, *10*, 6105–6111.

On the other hand, intermediates **10**, resulting from an initial 6-*endo*-dig cyclization of intermediate **8**, also undergo α-proton elimination leading to the formation of bicyclo[4.1.0]hept-2-ene derivatives **14**. Alternatively,[17,18] intermediates **10** can suffer ring expansion forming (η^2-cyclobutene)gold(I) complexes **15** leading finally to product **16**. Interestingly, intermediates **15** can also open up to form (η^2-alkene)gold(I) complexes **17**, which generate 1,3-dienes **11**.

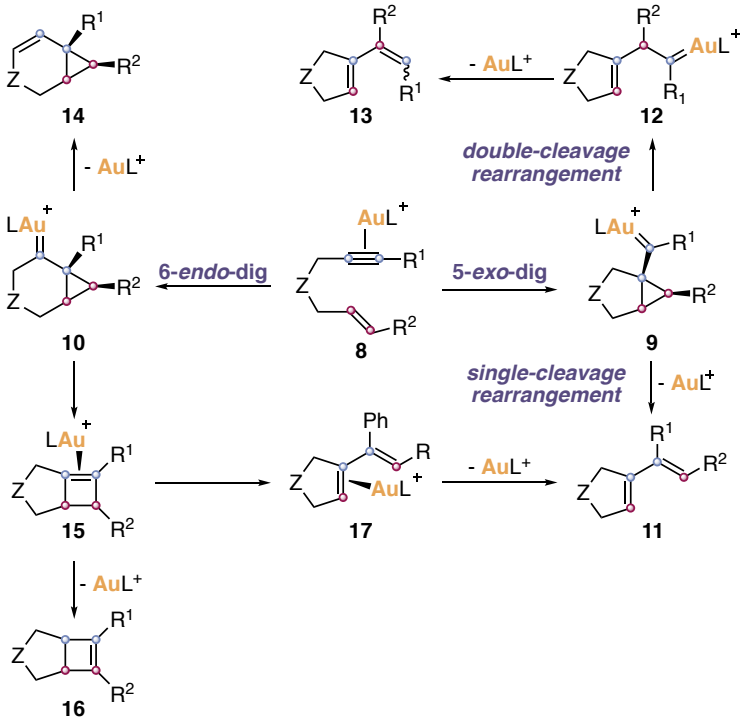

Scheme 3. Main pathways for the gold(I)-catalyzed cycloisomerization of 1,6-enynes.

The mechanism by which intermediates of type **15** evolve into products such **16** has been experimentally studied in detail by Widenhoefer and co-workers (Scheme 4).[19] Specifically, the conversion of **15a** to **16a** occurs *via* a hidden Brønsted acid catalyzed pathway in which gold(I) is not directly involved. Accordingly, complex **15a** first suffers deauration to liberate cyclobutene **18**. The latter undergoes a rapid and reversible protonation generating benzylic carbocation **19**, which is followed by the rate-limiting deprotonation step to give rise product **16a**, which is in equilibrium with complex **20**. Further studies showed that the nature of the

18 Nieto-Oberhuber, C.; Pérez-Galán, P.; Herrero-Gómez, E.; Lauterbach, T.; Rodríguez, C.; López, S.; Bour, C.; Rosellón, A.; Cárdenas, D. J.; Echavarren, A. M. *J. Am. Chem. Soc.* **2008**, *130*, 269–279.

19 (a) Brooner, R. E. M.; Brown, T. J.; Widenhoefer, R. A. *Angew. Chem. Int. Ed.* **2013**, *52*, 6259–6261. (b) Brooner, R. E. M.; Robertson, B. D.; Widenhoefer, R. A. *Organometallics* **2014**, *33*, 6466–6473.

Brønsted acid, which is generated *in situ* from the gold(I) catalyst counterion, can influence the reaction outcome.[20]

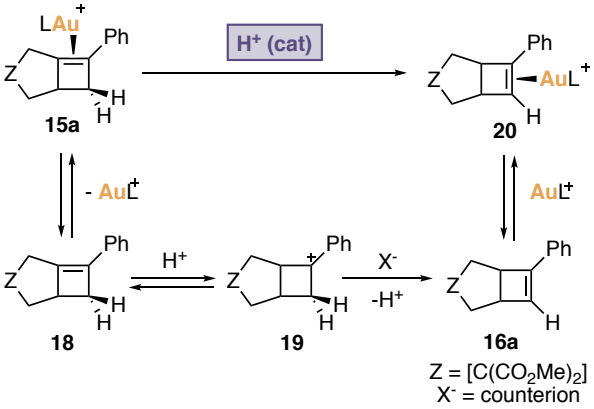

Scheme 4. Proposed mechanism for the acid-catalyzed conversion of **15a** to **20**.

Large 1,*n*-enynes (n ≥ 7) react intramolecularly by a formal [2+2] cycloaddition to afford cyclobutene-fused bicyclic compounds.[21] In particular, 1,*n*-enynes (n = 10-16) of the type of **21** react with gold catalysts by a click-type [2+2] cycloaddition of alkynes with alkenes (Scheme 5) forming cyclobutene-fused **22**.[22] Furthermore, a diastereoselective gold(I)-catalyzed [2+2] macrocyclization of 1,10-enyne **21** was used to build the tetrasubstitued cyclobutane moiety presented in both rumphellaone A and hushinone (Scheme 5).[23]

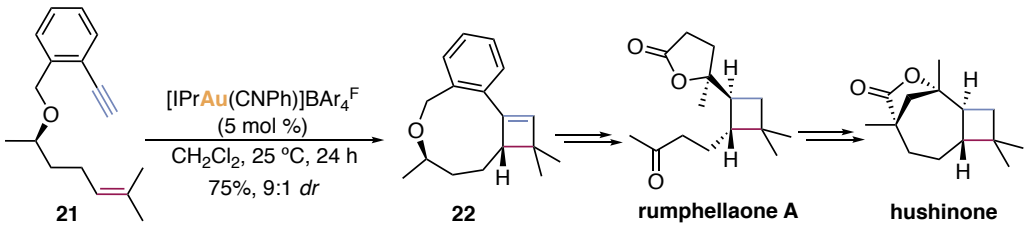

Scheme 5. Gold(I)-catalyzed [2+2] cyclization and application to the enantioselective total synthesis of rumphellaone A and hushinone.

20 Kim, N.; Brooner, R. E. M.; Widenhoefer, R. A. *Organometallics* **2017**, *36*, 673–678.

21 (a) Odabachian, Y.; Gagosz, F. *Adv. Synth. Catal.* **2009**, *351*, 379–386. (b) Inagaki, F.; Matsumoto, C.; Okada, Y.; Maruyama, N.; Mukai, C. *Angew. Chem. Int. Ed.* **2015**, *54*, 818–822. (c) Iwai, T.; Ueno, M.; Okochi, H.; Sawamura, M. *Adv. Synth. Catal.* **2018**, *360*, 670–675.

22 Obradors, C.; Leboeuf, D.; Aydin, J.; Echavarren, A. M. *Org. Lett*. **2013**, *15*, 1576–1579.

23 Ranieri, B.; Obradors, C.; Mato, M.; Echavarren, A. M. *Org. Lett*. **2016**, *18*, 1614–1617.

Intermolecular Reactions of Terminal Alkynes with Alkenes

As described in the previous section, much work has been done on the development of intramolecular reactions of alkynes with alkenes. The corresponding intermolecular transformations are much more challenging (Scheme 6).[24] In these processes, two independent unsaturated substrates are involved and can compete for the binding to the gold(I) center with similar association constants.[25] Additionally, gold catalysts are inherently acidic, and consequently can promote alkene dimerization and polymerization by cationic mechanisms.[26]

Nonetheless, in the last few years a number of intermolecular reactions with synthetic applications have been reported using gold(I) catalysts.[24] All these reactions proceed by mechanistically complex scenarios that follow the same basic principles of gold(I)-catalyzed cycloisomerization of 1,*n*-enynes. Furthermore, they all share a common key intermediate that can be seen as a distorted cyclopropyl gold(I) carbenes **23** (Scheme 6). To guarantee the success of these transformations, catalysts bearing bulky ligands and soft non-coordinating counterion must be employed.[27a,b]

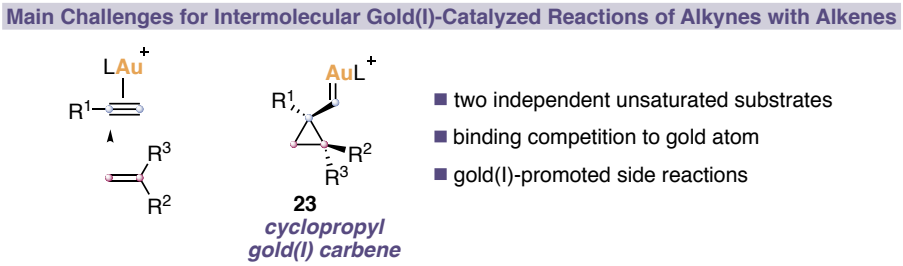

Scheme 6. Main challenges for intermolecular gold(I)-catalyzed reactions of terminal alkynes with alkenes.

Thereby, aryl alkynes, 1,3-enynes and 1,3-dienes react with non-activated alkenes *via* [2+2] gold(I)-catalyzed cycloaddition to form cyclobutenes **24** (Scheme 7, up right) (this transformation will be discussed in detail in the introduction of Chapter 1).[27] Interestingly,

24 For reviews on the topic: (a) Muratore, M. E.; Homs, A.; Obradors, C.; Echavarren, A. M. *Chem. Asian. J.* **2014**, *9*, 3066–3082. (b) García-Morales, C.; Echavarren, A. M. *Synlett* **2018**, *29*, 2225–2237.

25 (a) Brown, T. J.; Dickens, M. G.; Widenhoefer, R. A. *J. Am. Chem. Soc.* **2009**, *131*, 6350–6351. (b) Brown, T. J.; Dickens, M.G.; Widenhoefer, R. A. *Chem. Commun.* **2009**, 6451–6453. (c) Brown, T. J.; Widenhoefer, R. A. *J. Organomet. Chem.* **2011**, *696*, 1216–1220. (d) Brooner, R. E. M.; Widenhoefer, R. A. *Angew. Chem. Int. Ed.* **2013**, *52*, 11714–11724.

26 Urbano, J.; Hormigo, A. J.; de Frémont, P.; Nolan, P.S.; Díaz-Requejo, M. M.; Pérez, P. J. *Chem. Commun.* **2008**, 759–761.

27 (a) López-Carrillo, V.; Echavarren, A. M. *J. Am. Chem. Soc.* **2010**, *132*, 9292–9294. (b) Homs, A.; Obradors, C.; Leboeuf, D.; Echavarren, A. M. *Adv. Synth. Catal.* **2014**, *356*, 221–228. (c) de Orbe, M. E.;

under the same conditions, *ortho*-substituted aryl alkynes can give rise not only to cyclobutenes **24** but also to 1,3-dienes **25** in different ratios (Scheme 7, bottom right).[27c] Propiolic acid and some of its esters react in the presence of cationic gold(I) catalysts with 1,1-di- or trisubstituted alkenes by a formal [4+2] cycloaddition to afford *α,β*-unsaturated *δ*-lactones **26** (Scheme 7, up left).[28] Surprisingly, when 1,2-disubstituted alkenes were used as reaction counterpart, 1,3-dienes **25** were obtained stereoespecifically (Scheme 7, bottom left).

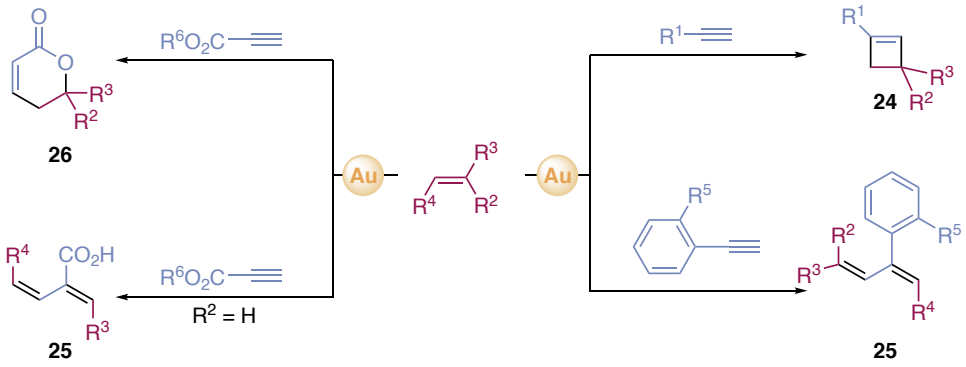

Scheme 7. Intermolecular gold(I)-catalyzed reactions of terminal alkynes with non-activated alkenes.

Furthermore, terminal alkynes can also take part of a [2+2+2] cycloaddition process with 5-oxoalkenes **27** leading to the formation of 8-oxabicyclo[3.2.1]oct-3-enes **28** (Scheme 8a),[29] or react with furans **29** giving rise to phenols **30** (Scheme 8b).[30]

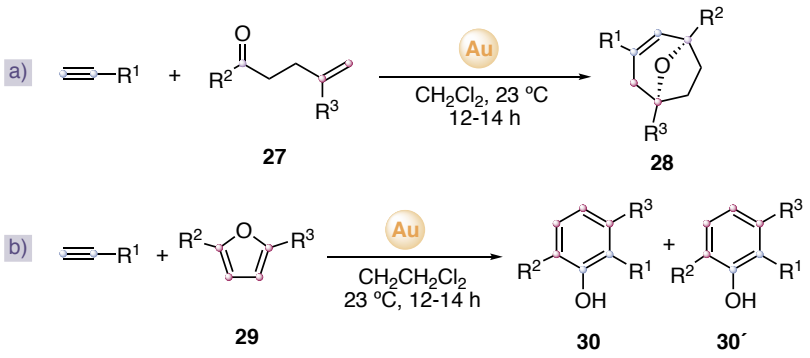

Scheme 8. Gold(I)-catalyzed reactions of alkynes with 5-oxoalkenes and furans.

Amenós, L.; Kirillova, M. S.; Wang, Y.; López-Carrillo, V.; Maseras, F.; Echavarren, A. M. *J. Am. Chem. Soc.* **2017**, *139*, 10302–10311. (d) de Orbe, M. E.; Echavarren, A. M. Eur. *J. Org. Chem.* **2018**, *22*, 2740–2752.

28 Yeom, H-S.; Koo, J.; Park, H-S.; Wang, Y.; Liang, Y.; Yu, Z-X.; Shin, S. *J. Am. Chem. Soc.* **2012**, *134*, 208–211.

29 Obradors, C.; Echavarren, A. M. *Chem. –Eur. J.* **2013**, *19*, 3547–3551.

30 Huguet, N.; Leboeuf, D.; Echavarren, A. M. *Chem. –Eur. J.* **2013**, *19*, 6581–6585.

Enantioselective Gold(I) Catalysis

The development of efficient asymmetric gold(I) catalysis has taken place at a relatively slow pace,[31] which can be ascribed to the linear geometry of gold(I) dicoordinated complexes. This geometry locates the chiral ligand far away from the reaction center, where the addition of the nucleophile to the activated π-bond takes place through an outer-sphere mechanism (Figure 5).

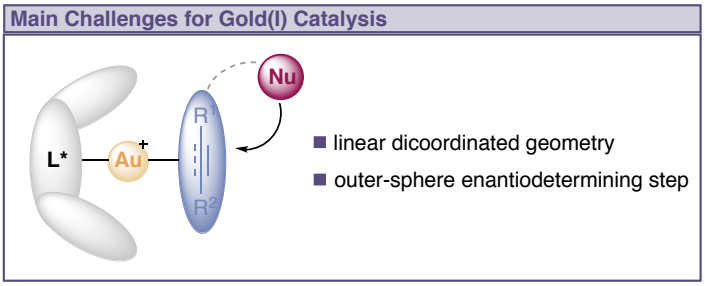

Figure 5. General coordination mode for enantioselective gold(I) catalysis.

One of the most common strategies to successfully induced chirality is based on the use of bimetallic gold(I) complexes bearing atropoisomeric bidentate phosphines (Figure 6, upper). For these catalysts, it became clear that the second gold plays a crucial role in the enantiodiscrimination. Alternatively, monogold complexes based on phosphoramidites have also demonstrated to be general enantioselective catalysts (Figure 6, bottom).[31]

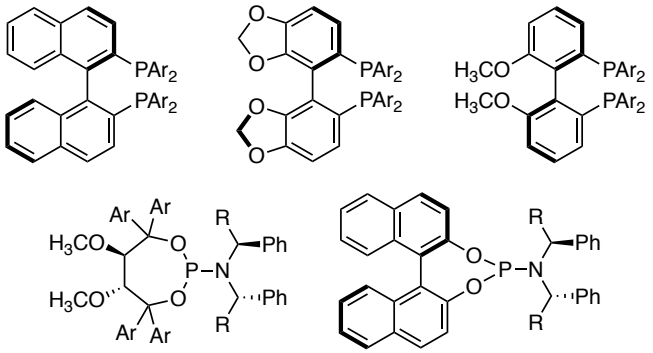

Figure 6. Commonly used ligands in asymmetric gold(I) catalysis.

In 2007, Toste demonstrated that the chiral information could be successfully transfer from

31 (a) Widenhoefer, R. A. *Chem. –Eur. J.* **2008**, *14*, 5382–5391. (b) Sengupta, S.; Shi, X. *ChemCatChem*, **2010**, *2*, 609–619. (c) Pradal, A.; Toullec, P. Y.; Michelet, V. *Synthesis*, **2011**, 1501–1514. (d) Wang, Y. M.; Lackner, A. D.; Toste, F. D. *Acc. Chem. Res.*, **2014**, *47*, 889–901. (e) Zi, W.; Toste, F. D. *Chem. Soc. Rev.* **2016**, *45*, 4567–4589. (f) Li, Y.; Li, W.; Zhang, J. *Chem. –Eur. J.* **2017**, *23*, 467–512.

chiral phosphate counterions **29** *via* tight ion pairs in allene cyclizations (Scheme 9).[32]

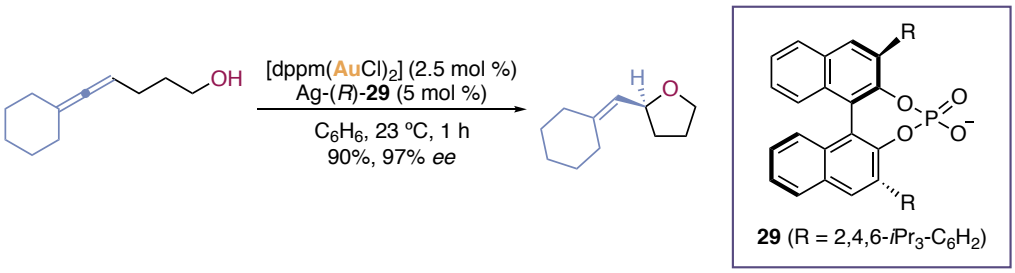

Scheme 9. Asymmetric hydroalkoxylation using chiral counterion **29**.

However, it was later demonstrated that phosphates **29** deprotonate terminal alkynes forming inactive alkynylgold(I) complexes **30**, which have hampered the implementation of the chiral counterion concept to these substrates (Scheme 10).[33]

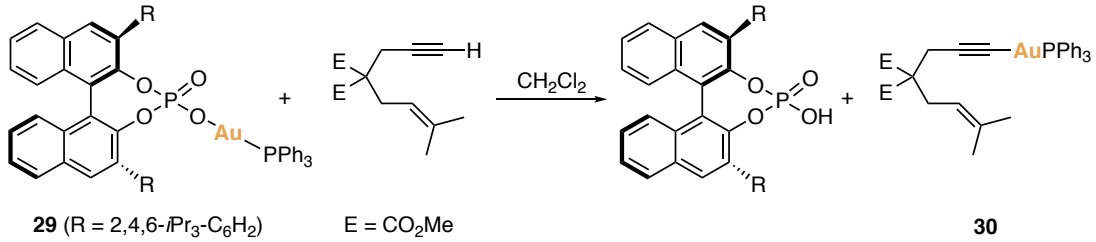

Scheme 10. Formation of alkynylgold(I) complex **30**.

32 (a) Hamilton, G. L.; Kang, E. J.; Mba, M.; Toste, F. D. *Science* **2007**, *317*, 496–499. (b) Aikawa, K.; Kojima, M.; Mikami, K. *Angew. Chem. Int. Ed.* **2009**, *48*, 6073–6077. (c) Aikawa, K.; Kojima, M.; Mikami, K. *Adv. Synth. Catal.* **2010**, *352*, 3131–3135. (d) Tu, X.; Gong, L. *Angew. Chem. Int. Ed.* **2012**, *51*, 11346–11349.

33 Raducan, M.; Moreno, M.; Bour, C.; Echavarren, A. M. *Chem. Commun.* **2012**, *48*, 52–54.

Chapter I: "Enantioselective Gold(I)-Catalyzed [2+2] Cycloaddition of Alkynes with Alkenes"

Introduction

Cyclobutenes

Cyclobutenes are strained four-membered carbocycles with a double carbon-carbon bond, which have be found in naturally occurring substances (Figure 1). They are highly reactive, and thereby very useful synthetic intermediates.[1] In particular, these carbocyclic compounds are valuable synthons for the preparation of cyclobutanes,[2] which are relative common motifs present in a variety of natural products[3] as well as in pharmaceuticals.[4]

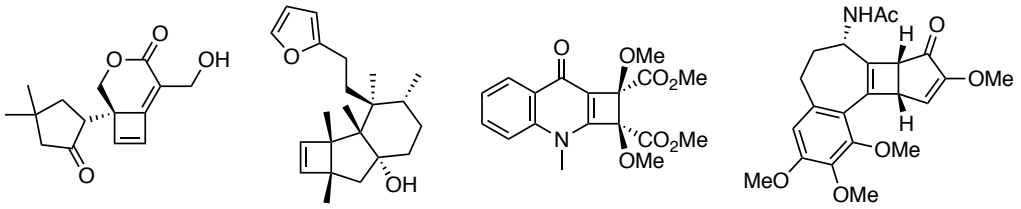

Figure 1. Natural occurring molecules containing cyclobutenes.

The photocycloaddition of maleic anhydride with acetylene or dichloroethylene is a well stablished method for the synthesis of cyclobutene-fused analogues, which can be further functionalized *via* nucleophilic ring opening (Scheme 1).[2a] However, the substitution pattern accessed by this method is always limited to the presence of two carboxylic acid groups directly attached to the four-membered ring.

1 (a) White, B. H.; Snapper, M. L. *J. Am. Chem. Soc.* **2003**, *125*, 14901–14904. (b) Xu, Y.; Conner, M. L.; Brown, M. K. *Angew. Chem. Int. Ed.* **2015**, *54*, 11918–11928. (c) Arichi, N.; Yamada, K.; Yamaoka, Y.; Takasu, K. *J. Am. Chem. Soc.* **2015**, *137*, 9579–9582. (b) Misale, A., Niyomchon, S.; Maulide, N. *Acc. Chem. Res.* **2016**, *49*, 2444–2458.

2 (a) Lee-Ruff, E.; Mladenova, G. *Chem. Rev.* **2003**, *103*, 1449–1484. (b) Namyslo, J. C.; Kaufmann, D. E. *Chem. Rev.* **2003**, *103*, 1485–1538.

3 (a) Collado, I. G.; Hanson, J. R.; Macías-Sánchez, A. J. *Nat. Prod. Rep.* **1998**, *15*, 187–204. (b) Wessjohann, L. A.; Brandt, W.; Thiemann, T. *Chem. Rev.* **2003**, *103*, 1625–1648. (c) Dembitsky, V. M. *J. Nat. Med.* **2008**, *62,* 1–33.

4 (a) Grongsaard, P.; Bulger, P. G.; Wallace, D. J.; Tan, L.; Chen, Q.; Dolman, S. J.; Nyrop, J.; Hoerrner, R. S.; Weisel, M.; Arredondo, J.; Itoh, T.; Xie, C.; Wen, X.; Zhao, D.; Muzzio, D. J.; Bassan, E. M.; Shultz, C. S. *Org. Process Res. Dev.* **2012**, *16*, 1069–1081. (b) Lukin, K.; Kishore, V.; Gordon, T. *Org. Process Res. Dev*. **2013**, *17*, 666–671. (c) Kallemeyn, J. M.; Ku, Y.-Y.; Mulhern, M. M.; Bishop, R.; Pal, A.; Jacob, L. *Org. Process Res. Dev.* **2014**, *18*, 191–197.

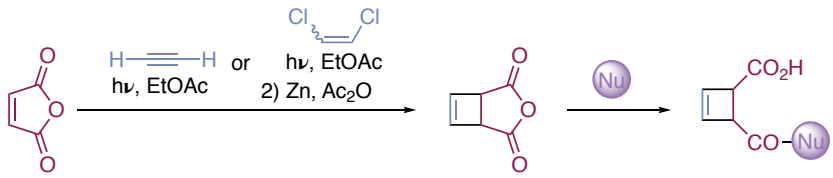

Scheme 1. Benchmark synthesis of cyclobutenes by photocycloaddition of maleic anhydride.

Enantioselective Synthesis of Cyclobutenes

The [2+2] cycloaddition of an alkyne with an alkene is a straightforward way to construct cyclobutenes in an atom-economical manner.[1c] Although the reaction is thermally forbidden, many stepwise formal [2+2] cycloadditions have been reported in the last decades using Lewis acids,[5] the Ficini reaction of ynamines or ynamides,[6] or transition metals.[7] Particularly important for the aim of this thesis is the gold(I)-catalyzed synthesis of cyclobutenes that will be further discussed in the next section (Scheme 2).[8]

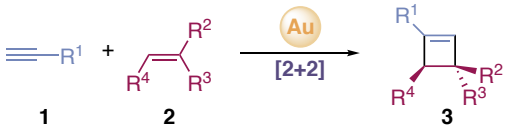

Scheme 2. Gold(I)-catalyzed synthesis of cyclobutenes.

However, regarding the asymmetric version, it was not until 2004 that the first enantioselective catalytic [2+2] cycloaddition was reported.[9] The enantioselective methodologies are based on the same chemistry principles as the synthesis of racemic compounds and can be classified as follows.

---

5 Racemic [2+2] cycloaddition catalyzed by Lewis acid: (a) Snider, B. B.; Brown, L. A.; Conn, R. S. E.; Killinger, T. A. *Tetrahedron Lett.* **1977**, *18*, 2831–2834. (b) Clark, R. D.; Untch, K. G. *J. Org. Chem.* **1979**, *44*, 248–255. (c) Clark, R. D.; Untch, K. G. *J. Org. Chem.* **1979**, *44*, 248–253. (d) Fienemann, H.; Hoffmann, H. M. R. *J. Org. Chem.* **1979**, *44*, 2802–2804. (e) Snider, B. B.; Rodini, D. J.; Conn, R. S. E.; Sealfon, S. *J. Am. Chem. Soc.* **1979**, *101*, 5283–5293. (f) Snider, B. B.; Roush, D. M.; Rodini, D. J.; Gonzalez, D.; Spindell, D. *J. Org. Chem.* **1980**, *45*, 2773–2785. (g) Rosenblum, M.; Scheck, D. *Organometallics* **1982**, *1*, 397–399. (h) Quendo, A.; Rousseau, G. *Tetrahedron Lett.* **1988**, *29*, 6443–6446. (i) Franck-Neumann, M.; Miesch, M.; Gross, L. *Tetrahedron Lett.* **1992**, *33*, 3879–3882. (j) Sweis, R. F.; Schramm, M. P.; Kozmin, S. A. *J. Am. Chem. Soc.* **2004**, *126*, 7442–7443. (k) Okamoto, K.; Shimbayashi, T.; Tamura, E.; Ohe, K. *Org. Lett.* **2015**, *17*, 5843–5845.

6 Li, H.; Hsung, P. R.; DeKorver, K. A.; Wei, Y. *Org. Lett.* **2010**, *12*, 3780–3783.

7 Sakari, K.; Kochi, T.; Kakiuchi, F. *Org. Lett.* **2013**, *15*, 1024–1027.

8 López-Carrillo, V.; Echavarren, A. M. *J. Am. Chem. Soc.* **2010**, *132*, 9292–9294.

9 Ito, H.; Hasegawa, M.; Takenaka, Y.; Kobayashi, T.; Iguchi, K. *J. Am. Chem. Soc.* **2004**, *126*, 4520–4521.

Enantioselective transition metal-catalyzed [2+2] cycloaddition

In the first enantioselective metal-catalyzed reported example, a chiral rhodium complex catalyzed the reaction between norbornene derivatives **5a** and electron deficient alkynyl esters **4** to form chiral fused cyclobutenes **6a** in moderate to excellent enantioselectivities (Scheme 3a).[10] In 2010, the asymmetric iridium [2+2] cycloaddition of non-activated terminal alkynes **1** with oxabicyclic alkenes **5b** was reported, which leads to strained cyclobutenes **6b** in excellent enantioselectivities (Scheme 3b).[11] Years later, Cramer and co-workers demonstrated that a neutral chiral ruthenium(II) (**Ru-cat**) complex was able to catalyze the formal [2+2] cycloaddition of norbornene derivatives **5c** and electron deficient non-terminal alkynes **4** (Scheme 3c).[12] The same ruthenium(II) catalyst was suitable to induce high levels of enantioselectivities in the formal [2+2] cycloaddition of 1-alkynyl triazenes **7** and bicyclic alkenes **5d** (Scheme 3d).[13] The resulting strained cyclobutenyl triazenes **6d** were further converted into a variety of structures with good to excellent enantiospecificity. Chiral palladium complexes bearing bisoxazoline **9** were also good catalysts for the synthesis of highly strained cyclobutenes **6e** *via* an asymmetric Heck reaction of propargylic acetates **8** with cycloalkenes **5e** (Scheme 3e).[14] As before, the resulting fused cyclobutenes **5e** were easily derivatized with no loss of enantiomeric excess. Recently, the asymmetric [2+2] cycloaddition of internal non-activated alkynes **1** with hetero-bicyclic alkenes **5f** has been reported using nickel catalysis (Scheme 3f).[15] All these methods require the use of cyclic alkenes **5**, which limits the scope of this method to the preparation of highly strained polycyclic cyclobutenes **6**.

10 Shibata, T.; Takami, K.; Kawachi, A. *Org. Lett.* **2006**, *8*, 1343–1345.

11 (a) Fan, B.-M.; Li, X.-J.; Peng, F.-Z.; Zhang, H.-B.; Chang, A. S. C.; Shao, Z.-H. *Org. Lett.* **2010**, *12*, 304–306. (b) Hu, J.; Yang, Q.; Yu, L.; Xu, J.; Liu, S.; Huang, C.; Wang, L.; Zhou, Y.; Fan, B. *Org. Biomol. Chem.* **2013**, *11*, 2294–2301.

12 Kossler, D.; Cramer, N. *Chem. Sci.* **2017**, *8*, 1862–1866.

13 Kossler. D.; Perrin, F. G.; Suleymanov, A. A.; Kiefer, G.; Scopelliti, R.; Severin, K.; Cramer, N. *Angew. Chem. Int. Ed.* **2017**, *56*, 11490–11493.

14 Jiao, Z.; Shi, Q.; Zhou, J. S. *Angew. Chem. Int. Ed.* **2017**, *56*, 14567–14571.

15 Qin, H.; Chen, J.; Li, K.; He, Z.; Zhou, Y.; Fan, B. *Chem. Asian J.* **2018**, *13*, 2431–2434.

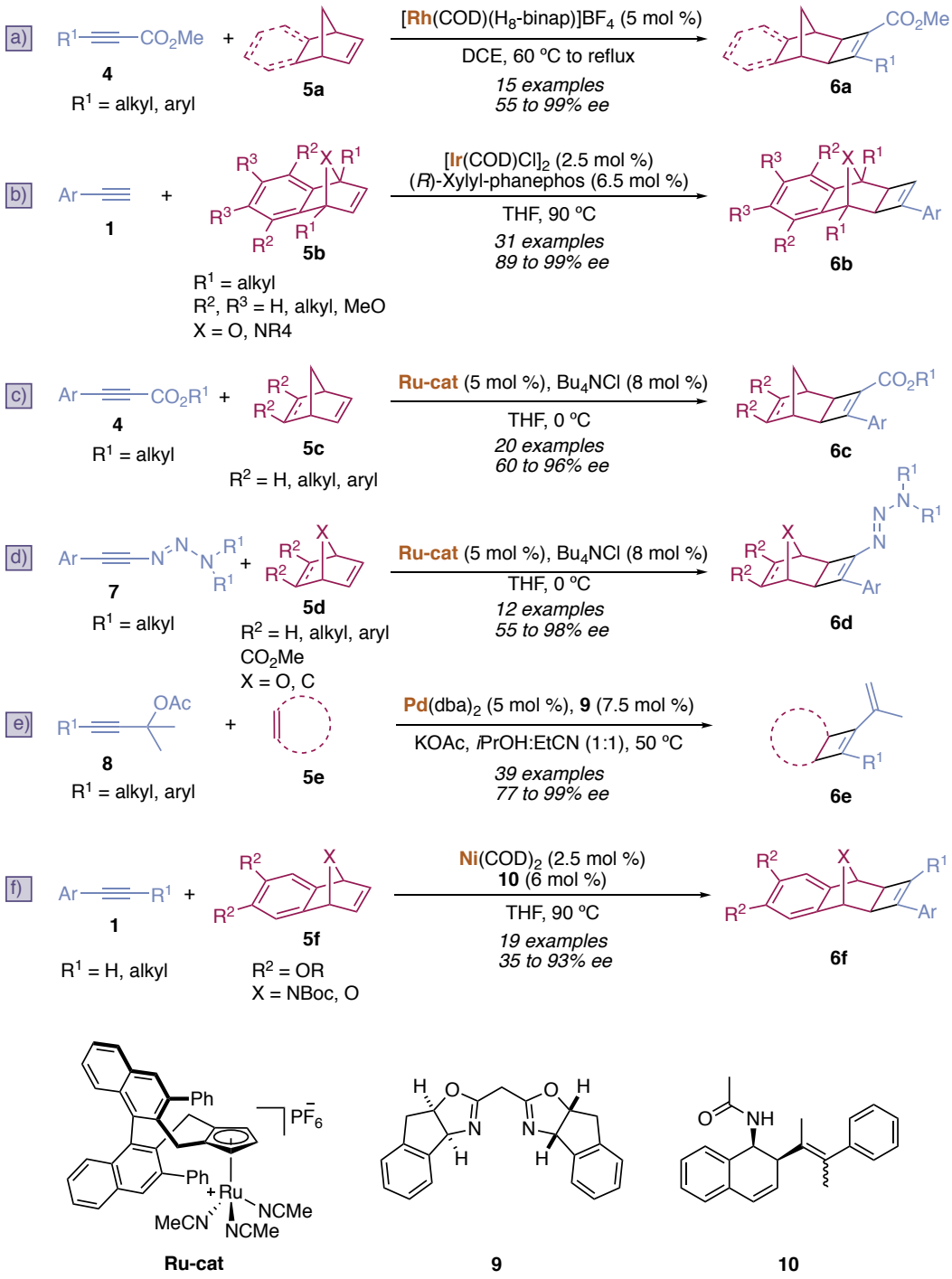

Scheme 3. Reported methods for enantioselective transition metal-catalyzed [2+2] cycloaddition.

Enantioselective chiral Lewis acid catalyzed synthesis of cyclobutenes: [2+2] cycloaddition of alkynes with alkenes

In 2004, a single example of an enantioselective [2+2] cycloaddition leading to enantioenriched bicyclic cyclobutene **6g** was reported as key step of the total synthesis of (+)-tricycloclavulone (Scheme 4).[9] The same strategy was later employed for the enantioselective

total synthesis of (+)-precapnelladiene (Scheme 4).[16] This protocol was limited to thioacetylene **11** and 2-alkoxycarbonyl-2-cycloalken-1-one **12** as substrates. Other alkynes counterparts led to the formation of the corresponding bicyclic cyclobutenes in low yield and low enantioselectivities.[17]

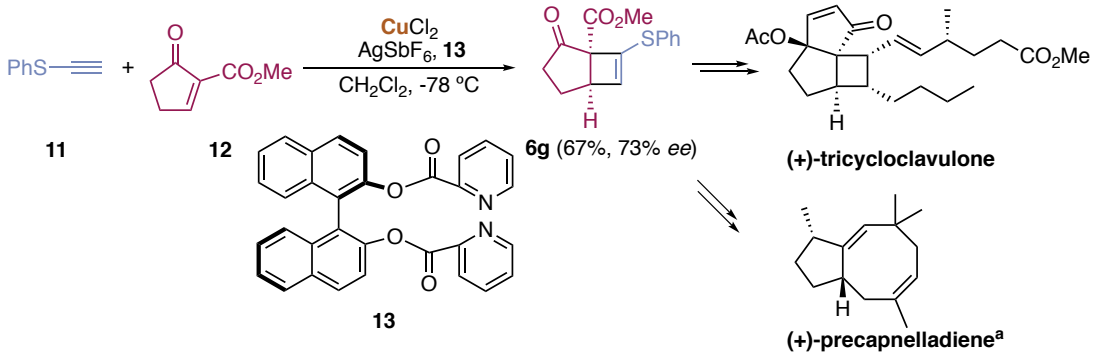

Scheme 4. Enantioselective Cu-catalyzed [2+2] cycloaddition and application to the total synthesis of natural products. [a] (+)-Precapnelladiene was synthetized from the opposite enantiomer of the shown cyclobutene **6g**.

The original Ficini reaction gives access to aminocyclobutenes *via* a thermal stepwise [2+2] cycloaddition of ynamines with cyclic enones.[18] In 2011, Mezzetti and co-workers demonstrated that the enantioselective catalytic approach can be performed using less polarized ynamides derivatives **14** to inhibit the thermal background reaction (Scheme 5a).[19] However, the scope of the transformation was restricted to the use of cyclopentenone β-keto ester **12**. Key for the success of this reaction is the chiral cationic ruthenium complex (**Ru-cat2**), which was proposed to stabilize the enolate intermediate. Later, the substrate scope was expanded using highly reactive cyclic α-alkylidene β-oxo imides **15** and chiral copper(II) catalysts (Scheme 5b).[20] Moreover, the versatility of the obtained aminocyclobutenes **6i** was proved by further transformation of the imide group.

The last type of chiral Lewis acid catalyzed [2+2] cycloaddition uses electron poor alkynones **17** and polarized electron-rich alkenes **18** as substrates (Scheme 6). Only a few examples with moderate enantiomeric excesses were first reported as part of a more detailed work about [4+2] cycloaddition reactions, in which terminal propiolamide **17a** reacted with cyclic electron rich

16 Takenaka, Y.; Ito, H.; Iguchi, K. *Tetrahedron* **2006**, *63*, 510–513.

17 Takenaka, Y.; Ito, H.; Hasegawa, M.; Iguchi, K. *Tetrahedron* **2006**, *62*, 3380–3388.

18 Ficini, J. *Tetrahedron* **1976**, *32*, 1449–1486.

19 (a) Schotes, C.; Mezzetti, A. *Angew. Chem. Int. Ed.* **2011**, *50*, 3072–3074. (b) Schotes, C.; Bigler, R.; Mezzetti, A. *Synthesis* **2012**, *44*, 513–526.

20 Enomoto, K.; Oyama, H.; Nakada, M. *Chem. –Eur. J.* **2015**, *21*, 2798–2802.

dienes and enol silyl ethers **18a** to build bicyclic cyclobutenes **6j** in the presence of chiral cupper catalysts (Scheme 6a).[21] A more recent report described the formation of strained cyclobutenes **6k** from both terminal and internal alkynones **17b** and cyclic enol silyl ethers **18b** using chiral *N,N´*-dioxide **20**-Zn(Tf$_2$)$_2$ as catalyst (Scheme 6b).[22]

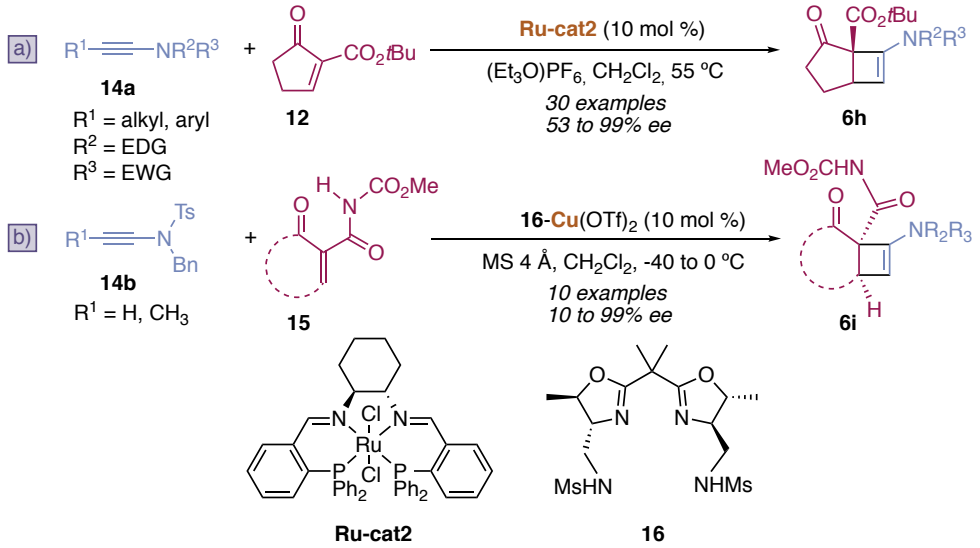

Scheme 5. Enantioselective Ficini reaction.

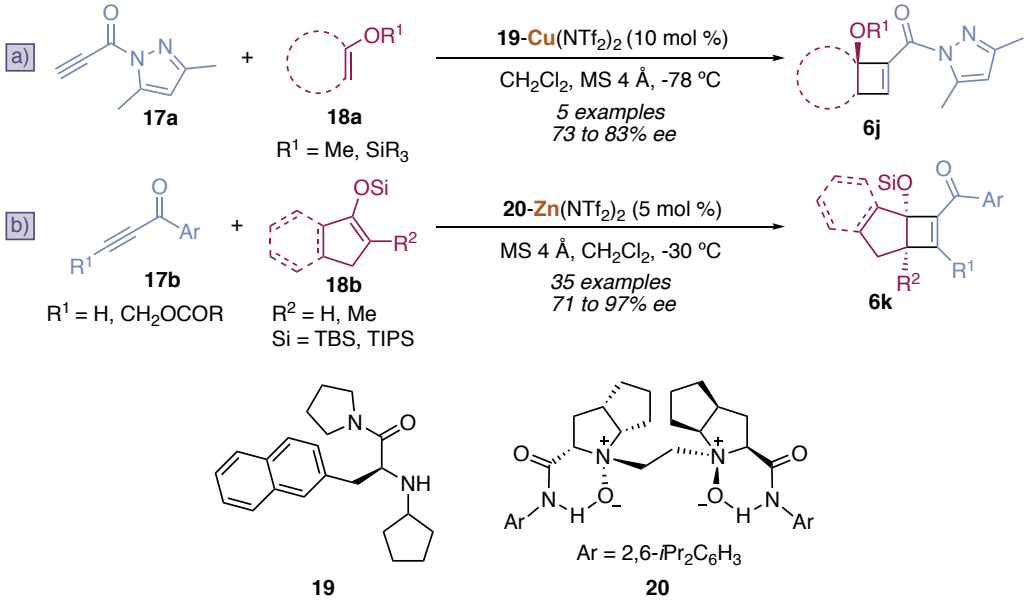

Scheme 6. Enantioselective [2+2] cycloaddition between polarized electron rich alkenes and electron poor alkynes.

21 Ishihara, K.; Fushimi, M. *J. Am. Chem. Soc.* **2008**, *130*, 7532–7533.

22 Kang, T.; Ge, S.; Lin, L.; Lu, Y.; Liu, X.; Feng, X. *Angew. Chem. Int. Ed.* **2016**, *55*, 5541–5544.

Enantioselective [2+2] photocycloaddition

Chiral sensitizers have been used to induce enantioselectivity in photochemical reactions since the 60's.[23] In this strategy, the chiral environment is provided by constant contact of the substrate with the chiral sensitizer in the excitation step. For intramolecular transformations, high levels of enantioinduction can only be achieved if the reaction of the sensitizer-substrate complex with the non-associated reagent takes places faster than the dissociation of the sensitizer-substrate complex.

Using a chiral triplet sensitizer (**23**), Bach and co-workers reported the first catalytic intermolecular [2+2] photocycloaddition that gives rise to bicyclic enantioenriched cyclobutenes **6l** (Scheme 7).[24] The reaction takes place between acetylenedicarboxylates **21** and 2-pyridones **22**, the latter are anchored in the excitation step to the chiral catalyst through two hydrogen bonds (Scheme 7).

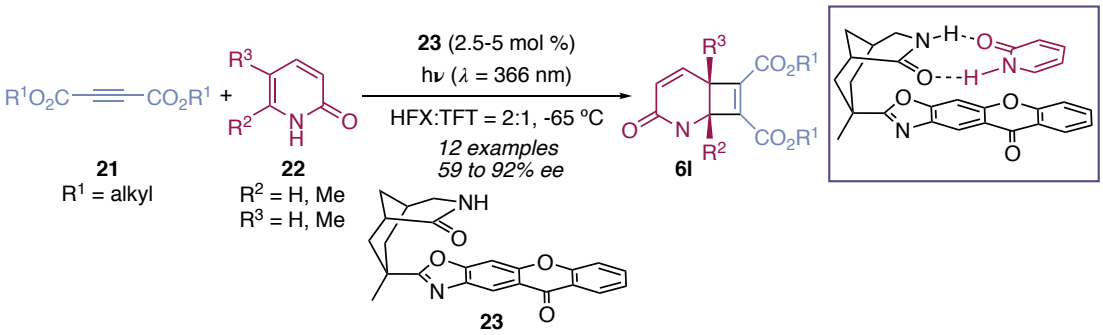

Scheme 7. Enantioselective intermolecular [2+2] photocycloaddition and proposed model for enantioface differentiation.

Gold(I)-Catalyzed Synthesis of Racemic Cyclobutenes

As explained in the general introduction, intermolecular gold(I)-catalyzed transformations are more challenging than intramolecular reactions. The use of two independent unsaturated partners results in the binding competition of both substrates to the gold(I) center. Additionally, alkenes can be dimerized and/or polymerized in the presence of gold catalysts.

Despite the initial difficulties, the first gold(I)-catalyzed intermolecular [2+2] cycloaddition of terminal alkynes **1** with non-cyclic alkenes **2** that leads to cyclobutenes **3** in a regioselective manner was reported by our group in 2010 (Scheme 8).[8] Key for the success of this reaction was the use of sterically crowded cationic gold(I) complex **A**. The [2+2] cycloaddition

23 (a) Hammond, G. S.; Cole, R. S. *J. Am. Chem. Soc.* **1965**, *87*, 3256–3257. (b) Murov, S.L.; Cole, R. S. Hammond, G. S. *J. Am. Chem. Soc.* **1968**, *90*, 2957–2958.

24 Maturi, M. M.; Bach, T. *Angew. Chem. Int. Ed.* **2014**, *53*, 7661–7664.

required aryl alkynes to reach good levels of reactivity. Regarding the alkene, di- and trisubstituted electron rich alkenes were the most efficient substrates. Further studies demonstrated that replacing SbF_6^- by BAr_4^{F-} as the counterion led to a significant increase in the yield in most cases.[25] In addition, aryl 1,3-butadiynes[26] and 1,3-enynes[27] also react with alkenes to form selectively cyclobutenes. With respect to 1,3-dienes, the selective cycloaddition of the most electron rich double bond leads to the formation of only one cyclobutene in most cases.[27]

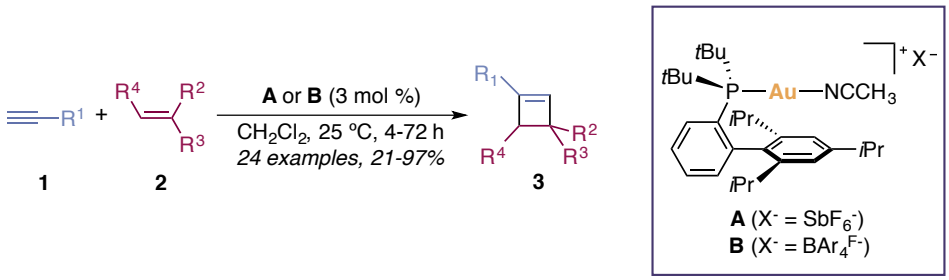

Scheme 8. Synthesis of cyclobutenes *via* gold(I)-catalyzed [2+2] cycloaddition.

Surprisingly, under the same conditions some *ortho*-substituted aryl alkynes react with alkenes to form 1,3-dienes **24** together with cyclobutenes **3** (Scheme 9).[26] The product distribution was dependent on the substitution pattern of the substrates and deuteration experiments confirmed that the alkene fragmentation products **24** result from a formal insertion of the alkyne carbons into the alkene carbons.

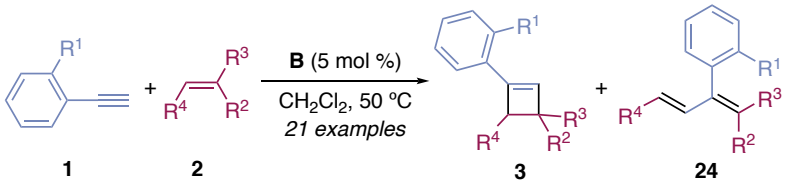

Scheme 9. Cycloaddition *vs.* rearrangement in the gold(I)-catalyzed reaction of *ortho*-substituted aryl alkynes and alkenes.

Cyclobutenes **3** can be transformed into a variety of products (Scheme 10).[27] Specifically, 1,3-dienes **25** can be produced by thermal conrotatory opening (Scheme 10, top right). The ring strain can also be liberated by oxidative cleavage obtaining 1,4-dicarbonyl compounds **26** (Scheme 10, bottom right). In addition, 2,3-dihydrofurans **27** can be formed through cyclobutene epoxidation followed by epoxide opening (Scheme 10, top left). Cyclobutenes **3**

25 Homs, A.; Obradors, C.; Leboeuf, D.; Echavarren, A. M. *Adv. Synth. Catal.* **2014**, *356*, 221–228.

26 de Orbe, M. E.; Amenós, L.; Kirillova, M. S.; Wang, Y.; López-Carrillo, V.; Maseras, F.; Echavarren, A. M. *J. Am. Chem. Soc.* **2017**, *139*, 10302–10311.

27 de Orbe, M. E.; Echavarren, A. M. *Eur. J. Org. Chem.* **2018**, *22*, 2740–2752.

can undergo a formal [4+1] cycloaddition with gold(I) carbenes generated by retro-Buchner reaction of cycloheptatriene **28** (Scheme 10, bottom left).[28] This transformation has been proposed to proceed through an initial cyclopropanation followed by a bond cleavage cascade process to yield spiro compound **29**.

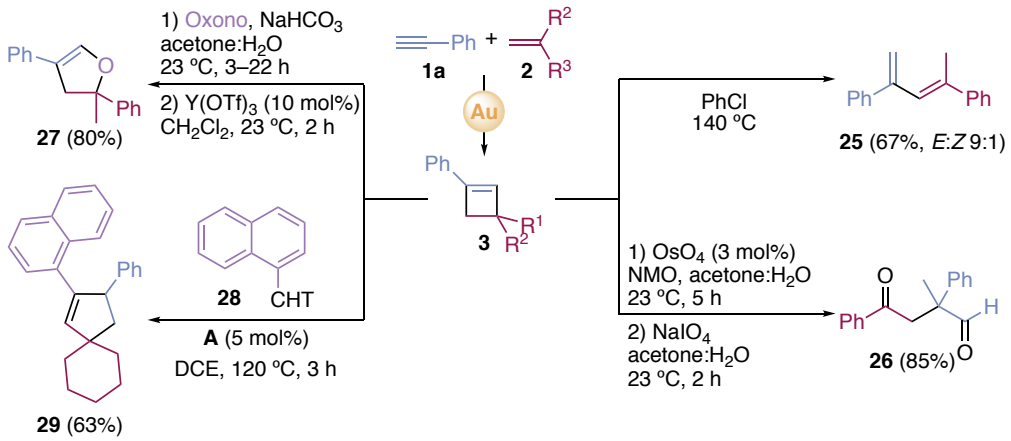

Scheme 10. Derivatization of cyclobutenes.

Experimental mechanistic studies were consistent with an associative ligand exchange between (η^2-alkene)gold(I) complex **30** and alkyne **1a** to generate complex **31** as the rate-determining step (Scheme 11). The electrophilic addition of (η^2-alkyne)gold(I) complexes **31** to alkene **2a** then forms cyclopropyl gold(I) carbenes **32**, similar to intermediates **9** involved in the cyclization of 1,6-enynes (Scheme 3, General Introduction). Cyclopropyl gold(I) carbenes **32** then undergo ring expansion leading to (η^2-cyclobutene)gold(I) complexes **33** that after a final associative ligand exchange liberate cyclobutene **3a**. As a side reaction, complexes **31** are in equilibrium with alkynylgold(I) complexes **34**, which can react with another molecule of the starting gold(I) complexes **A-B** to form non-catalytically active σ,π-digold(I) alkyne complexes **35**. Low temperature ^{31}P NMR studies revealed that complexes **30** and **35** were the only two long-living species of the catalytic cycle and the ratio between these two resting states was found to be highly counterion dependent. Formation of σ,π-digold(I) alkyne **35** was less favored with BAr_4^{F-} among all the counterions studied and consequently, the concentration of catalytically active species **30** was higher. Thus, it was proposed that complex **B** bearing BAr_4^{F-} as counterion is a more efficient catalyst for this transformation, most likely, simply due to the lower basicity of the bulkier BAr_4^{F-} anion.

28 Wang, Y.; Muratore, M. E.; Rong, Z.; Echavarren, A. M. *Angew. Chem. Int. Ed.* **2014**, *53*, 14022–14026.

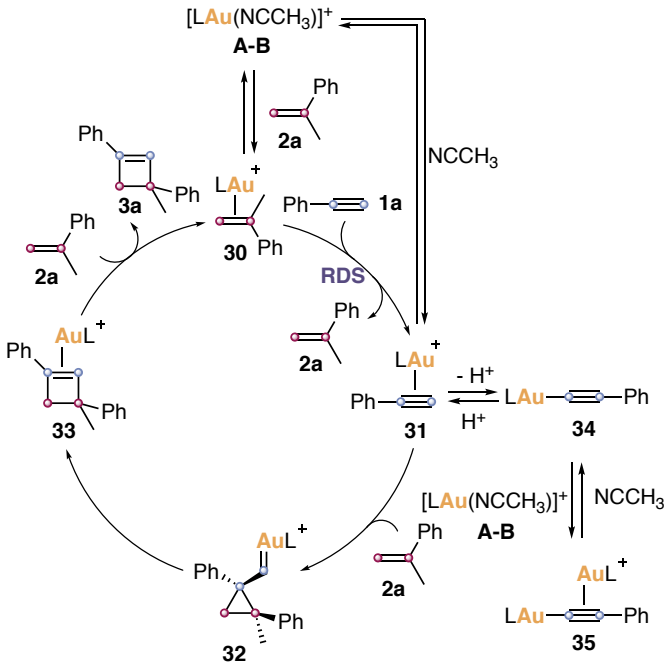

Scheme 11. Proposed mechanism for gold(I)-catalyzed [2+2] cycloaddition.

Based on DFT calculations (Scheme 12), the pathways that lead to the formation of both cyclobutenes (**3**) and 1,3-dienes (**24**) begin with the associative ligand exchange between (η^2-alkene)gold(I) complexes **30** and the alkyne (**1**) to form the moderately less stable (η^2-alkyne)gold(I) complexes **31**. Intermediates **32** and **36** can be generated by *anti*- or *syn*-attack of the alkene to **31**. These cyclopropyl gold(I) carbenes are in equilibrium due to C1–C2 rotation through ring opened gold(I) intermediates **37**. The evolution of complexes **32** to further intermediates involved in the formation of the products proceeds *via* lower energy barriers than for **36** and thus, the formation of products **3** and **24** is most likely to go through the evolution of **32**. Therefore, intermediates **32** can give rise to (η^2-cyclobutene)gold(I) complexes **33**, which after formal deauration afford cyclobutenes **3**. In the case of *ortho*-substituted alkynes, gold(I) carbenes **32** are also in equilibrium with the cyclopropyl-type intermediates **38** through C2 migration, which undergo ring opening to generate (η^2-1,3-diene)gold(I) complexes **39**. In general, the activation energies of the rearrangements of cyclopropyl gold(I) carbenes **32** do not differentiate much. Therefore, as observed experimentally, the reaction outcome can vary greatly depending on small changes in the substitution pattern of the substrates. For simplicity, the deaurations in the generation of **3** and **24** are shown as a dissociative process, although these transformations take place by associative ligand exchange steps.

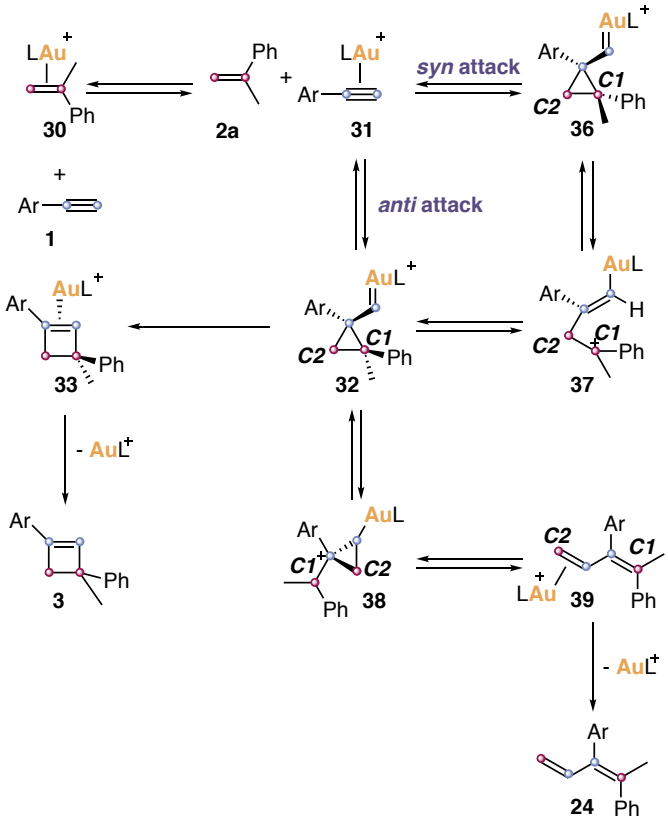

Scheme 12. Pathways for the formation of cyclobutenes and 1,3-dienes.

In a subsequent work, the groups of Gao and Zhang reported an intermolecular gold(I)-catalyzed [2+2] cycloaddition using aryl chloroalkynes **40** instead of terminal aryl alkynes **1**.[29] An important aspect of this methodology is the use of unactivated mono- and disubstituted alkenes **41** as reaction counterpart (Scheme 13). Furthermore, the corresponding chlorocyclobutenes **42** can be easily transformed into more complex structures **43** through cross-coupling reactions of the Csp^2–Cl bond (Scheme 13).

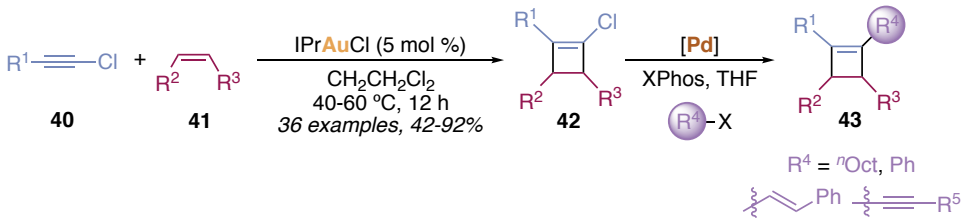

Scheme 13. Intermolecular [2+2] gold(I)-catalyzed cycloaddition using aryl chloroalkynes and subsequent derivatization.

29 Bai, Y.-B.; Luo, Z.; Wang, Y.; Gao, J.-M.; Zhang, L. *J. Am. Chem. Soc.* **2018**, *140*, 5860–5865.

Intermolecular Enantioselective Gold(I) Catalysis of Alkynes

Asymmetric gold(I) catalysis based on alkyne activation have only been successfully achieved for intramolecular transformations.[30] The complexity of the enantioinduction increases when linear alkynes and alkenes react in an intermolecular fashion (Figure 2). In this context, the outer-sphere enantio-determining step implies the discrimination between the prochiral faces of an alkene, which is located away from the chiral ligand. The difficulty of inducing enantioselectivity in this type of processes can be considered as a particular example of enantioselective electrophilic additions to alkenes.[31] In the case of gold(I) catalysis, the electrophile that reacts with the alkenes is generated *in situ* by coordination of the alkyne to the chiral metal complex.

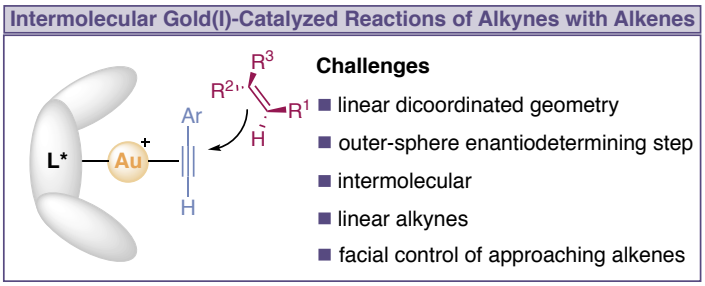

Figure 2. Challenges for the intermolecular gold(I)-catalyzed reactions of alkynes with alkenes.

Previous to the findings that will be discussed in this chapter,[32] only a single example of gold(I)-catalyzed enantioselective intermolecular [2+2] cycloaddition was published to build cyclobutene **3a** with very low enantioselectivity (65:35 *er*) using an axially chiral imidazoisoquinolin-2-ylidene as ancillary ligand (Scheme 14).[33]

---

30 (a) Wang, Y.; Lackner, A. D.; Toste, F. D. *Acc. Chem. Res.* **2014**, *47*, 889–901. (b) Zi, W.; Toste, F. D. *Chem. Soc. Rev.* **2016**, *45*, 4567–4589. (c) Li, Y.; Li, W.; Zhang, J. *Chem. –Eur. J.* **2017**, *23*, 467–512.

31 Leading references: (a) Snyder, S. A.; Tang, Z.-Y.; Gupta, R. *J. Am. Chem. Soc.* **2009**, *131*, 5744–5745. (b) Denmark, S. E.; Jaunet, A. *J. Am. Chem. Soc.* **2013**, *135*, 6419−6422. (c) Denmark, S. E.; Hartmann, E.; Kornfilt, D. J. P.; Wang, H. *Nat. Chem.* **2014**, *6*, 1056–1064. (d) Denmark, S. E.; Carson, N. *Org. Lett.* **2015**, *17*, 5728–5731. (e) Cresswell, A. J.; Eey, S. T.-C.; Denmark, S. E. *Angew. Chem. Int. Ed.* **2015**, *54*, 15642–15682. (f) Hu, D. X.; Seidl, F. J.; Bucher, C.; Burns, N. Z. *J. Am. Chem. Soc.* **2015**, *137*, 3795–3798. (g) Landry, M. L.; Hu, D. X.; McKenna, G. M.; Burns, N. Z. *J. Am. Chem. Soc.* **2016**, *138*, 5150–5158. (h) Denmark, S. E.; Ryabchuk, P.; Burk, M. T.; Gilbert, B. B. *J. Org. Chem.* **2016**, *81*, 10411–10423. (i) Samanta, R. S.; Yamamoto, H. *J. Am. Chem. Soc.* **2017**, *139*, 1460–1463.

32 García-Morales, C.; Ranieri, B.; Escofet, I.; Obradors, C.; López-Suárez, L.; Konovalov, A. I.; Echavarren, A. M. *J. Am. Chem. Soc.* **2017**, *139*, 13628–13631.

33 Grande-Carmona, F.; Iglesias-Sigüenza, J.; Álvarez, E.; Díez, E.; Fernández, R.; Lassaletta, J. M. *Organometallics* **2015**, *34*, 5073–5080.

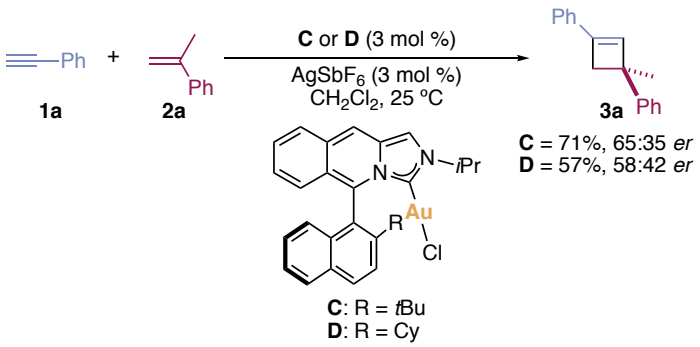

Scheme 14. Attempts for enantioselective gold(I)-catalyzed [2+2] cycloaddition.

Very recently, the enantioselective gold(I)-catalyzed intermolecular [4+2] annulation of *tert*-butyl propiolate (**44**) and non-activated alkenes **2** was reported using a bimetallic gold(I) catalyst bearing atropoisomeric bidentate phosphine DM-Segphos (Scheme 15).[34]

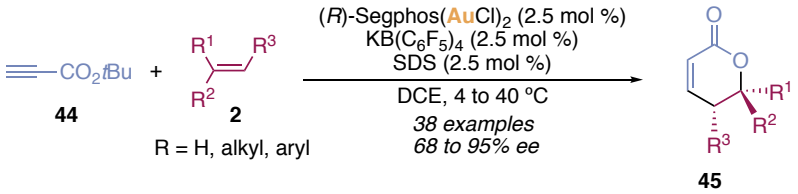

Scheme 15. Asymmetric gold(I)-catalyzed intermolecular [4+2] annulation.

34 Kim, H.; Choi, S. Y.; Shin, S. *Angew. Chem. Int. Ed.* **2018**, *130*, 13314–13318.

Objectives

The asymmetric synthesis of cyclobutenes is a particularly appealing synthetic endeavor giving their potential as synthetic intermediates in the synthesis of enantioenriched cyclobutanes, which are promising scaffolds for drug discovery.[35] In the last decade, catalytic enantioselective intermolecular [2+2] cycloadditions between alkynes and alkenes have been stablished as a straightforward method to access enantioenriched cyclobutenes.[10-**Error! Bookmark not defined.**] However, in most of these strategies, highly polarized substrates are required, and thus, the choice of substrates is limited.

Our group has shown the versatility of the intermolecular gold(I)-catalyzed [2+2] cycloaddition of terminal non-polarized alkynes with alkenes to access racemic cyclobutenes.[8,25-27] Recently, the synthetic potential of this reaction has been demonstrated through the facile derivatization of the cyclobutenes to a variety of different products.[27] Nevertheless, achieving high level of enantiocontrol for this transformation is still a significant challenge,[33] mainly because the enantio-determining step involves facial control of an approaching alkene located away from the chiral environment.

In this context, we aimed to develop a general enantioselective synthesis of cyclobutenes **3** by intermolecular gold(I)-catalyzed [2+2] cycloaddition (Scheme 16). Initial attempts pointed towards the use of chiral non-C_2 symmetrical Josiphos as suitable ligands to induce enantioselectivity in this transformation.[36]

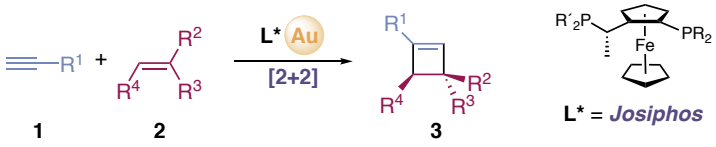

1 2 3

Scheme 16. Enantioselective gold(I)-catalyzed [2+2] cycloaddition of alkynes with alkenes.

35 (a) Vilaine, J. P.; Thollon, C.; Villenueve, N.; Pegion, J. L. *Eur. Heart J. Suppl.* **2003**, *5*, G26–G35. (b) Bakemore, D.C.; Bryans, J. S.; Carnell, P.; Carr, C. L.; Chessun, N. E. A.; Field, M. J.; Kinsella, N.; Osborne, S. A.; Warren, A. N.; Williams, S. C. Bioorg. Med. *Chem. Lett.* **2010**, *20*, 461–464.

36 Initial studies were performed by Dr. Laura López-Suárez and Imma Escofet.

Results and Discussion

Reaction Optimization

Initially, *ca.* 70 chiral ligands for the synthesis of cyclobutene **3a** were screened using high-throughput experimentation (HTE) methods by Dr. Laura López-Suárez and Imma Escofet.[36,37] Although the vast majority of chiral ligands led to **3a** with enantioselectivities lower than 60:40 *er*, the breakthrough was achieved using Josiphos ligands family (Figure 3). Among them, the best result was obtained using ligand (*S*,*R*P)-**L7**.

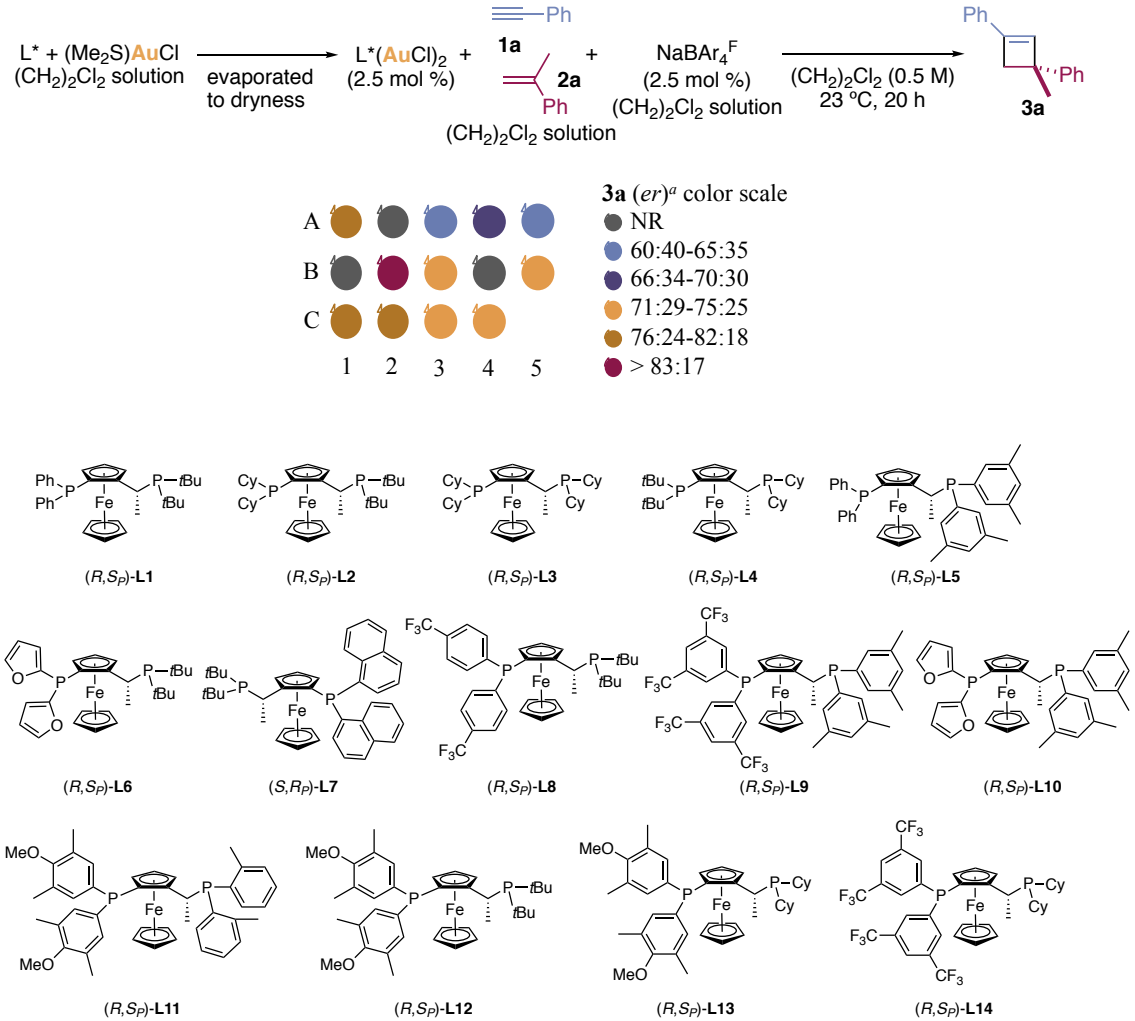

Figure 3. Josiphos HTE screening for the enantioselective [2+2] cycloaddition. [a]*er* of **3a** determined by UPC2 (Chiralpack ID, CH_3CN 15%). A1: **L1**, A2: **L2**, A3: **L3**, A4: **L4**, A5: **L5**, B1: **L6**, B2: **L7**, B3: **L8**, B4: **L9**, B5: **L10**, C1: **L11**, C2:**L12**, C3:**L13**, C4: **L14**.

37 All the ligands and complexes tested can be found in the supporting information of *J. Am. Chem. Soc.* **2017**, *139*, 13628–13631.

Josiphos ligands are chiral non-C_2 symmetrical diphosphines bearing a ferrocenyl backbone and different side chains (Figure 3), which were discovered at the former Ciba-Geigy, actual Novartis, by serendipity.[38] From the beginning, the catalytic tests were highly successful and soon they became privileged ligands in asymmetric homogeneous catalysis.[39] They are extremely modular and tunable by simple variation of the two substituents at the phosphorous atoms. So far, only the (R,S_P)/(S,R_P)-Josiphos enantiomers, but not the corresponding diastereomers, had found a general application in enantioselective metal catalysis.

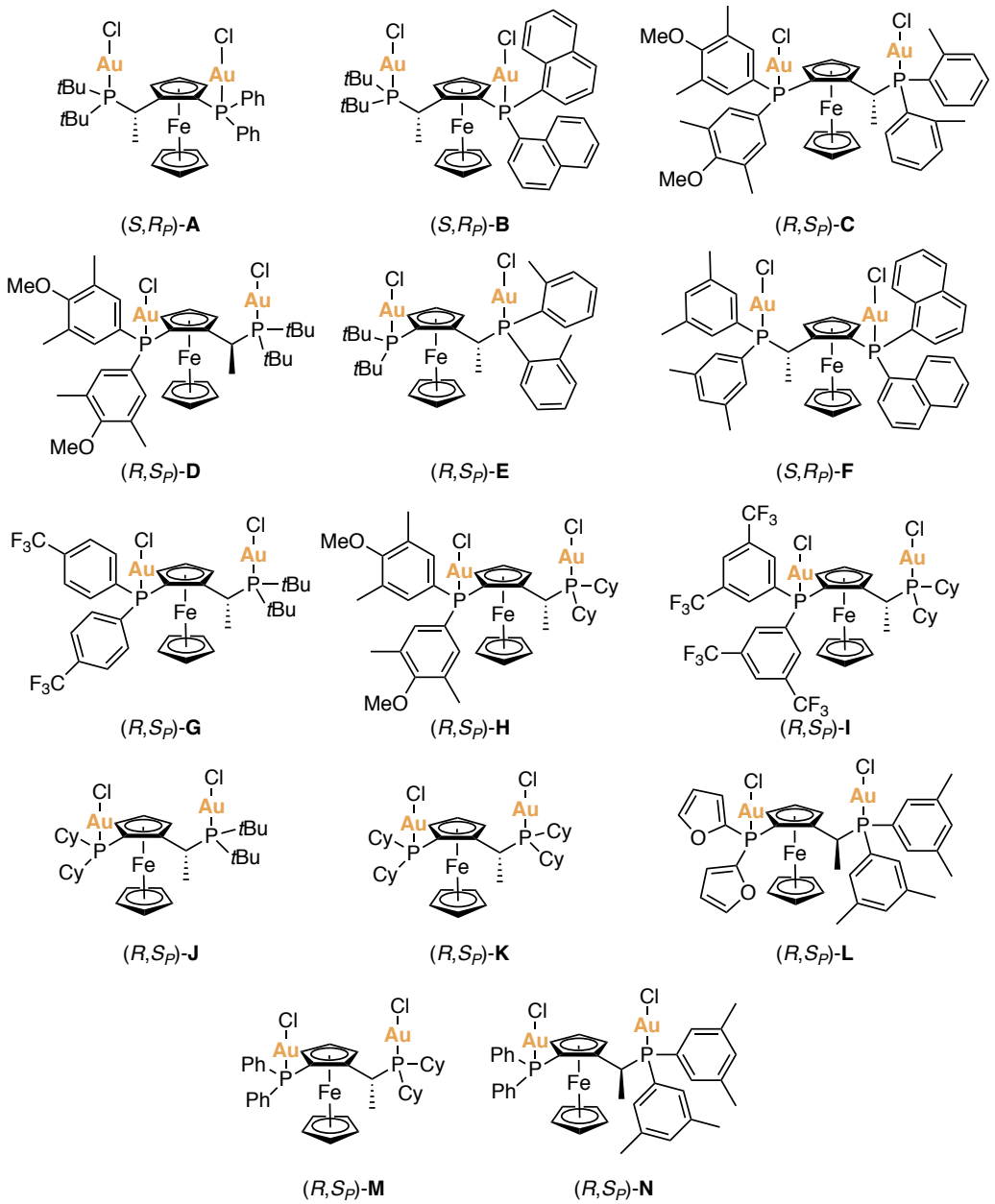

Figure 4. Josiphos digold(I) complexes.

38 Togni, A. *Chimia International Journal for Chemistry*, **1996**, *50*, 86–93.

39 Blaser, H.-U. *Topics Catal.* **2002**, *19*, 1–26.

Due to reproducibility issues regarding reactivity and enantioselectivity, high throughput techniques (HTE) were abandoned for further optimizations. To this end, we isolated a new family of digold(I) complexes bearing chiral Josiphos ligands with different sterically and electronically features to be tested as precatalysts for the enantioselective [2+2] cycloaddition at laboratory scale (Figure 4).

At the outset of our investigations, dichloroethane, $NaBAr_4^F$ and 2:1 ratio of **2a**:**1a** were chosen as initial conditions for further optimization to be consistent with the results obtained using HTE (Table 1). Considering that activation of neutral gold(I) chloride complexes **A**-**N** was done in situ by addition of $NaBAr_4^F$, all the reactions were set up following the guidelines to minimize the formation of less reactive chloride bridges digold(I) complexes,[40] which means that complex (*S*,*R*$_P$)-**B**, alkyne **1a** and alkene **2a** were dissolved in dichloroethane before adding solid $NaBAr_4^F$.

Extensive alkene oligomerization prevented the formation of cyclobutene when complexes (*R*,*S*$_P$)-**F**, (*S*,*R*$_P$)-**J**, (*R*,*S*$_P$)-**K**, (*R*,*S*$_P$)-**L** and (*S*,*R*$_P$)-**N** were employed as precatalysts (Table 1, entries 6, 10-12 and 14). Cyclobutene **3a** was isolated in low yields with precatalysts (*S*,*R*$_P$)-**A**, (*R*,*S*$_P$)-**C**, (*R*,*S*$_P$)-**D**, (*R*,*S*$_P$)-**E,** (*R*,*S*$_P$)-**G**, (*R*,*S*$_P$)-**I** and (*R*,*S*$_P$)-**M** (Table 1, entries 1, 3-5, 7, 9, 13), whereas complex (*R*,*S*$_P$)-**H** led to **3a** in 45% yield but low enantioselectivity (66:34 *er*). In agreement with the HTE results, the highest enantioselectivity was achieved with complex (*R*,*S*$_P$)-**B** (Table 1, entry 2). Fortunately, no alkene oligomerization was detected under these conditions and thus, reactivity was also superior for this complex. On the base of these results, further optimization was performed with complex (*S*,*R*$_P$)-**B** bearing two bulky naphthyl groups bound to one phosphorous.

As explained in the introduction, the counterion effect was found to be crucial in the racemic version of this transformation.[25] Bearing this in mind, an extensive screening of chloride scavengers was performed. Initially, common silver salts with non-coordinating counterions were tested. No cyclobutene **3a** was formed using $AgSbF_6$ or $AgPF_6$ (Table 2, entries 1-2), whereas **3a** was obtained in low yield but good levels of enantioselectivity with $AgBF_4$ (Table 2, entry 3). The use of silver salts with coordinating counterions also led to negative results (Table 2, entries 5-6). At this point, we envisaged that the presence of silver and/or the corresponding counterions of the salts could be hampering the gold(I)-catalyzed [2+2] cycloaddition. The silver effect was discarded by using sodium salts bearing the same anions (Table 2, entries 7-8), which were not suitable activators either. Knowing that the tested counterions have a negative effect on the reactivity, we came back to chloride scavengers

40 Homs, A.; Escofet, I.; Echavarren, A. M. *Org. Lett.* **2013**, *15*, 5782–5785.

bearing less basic bulky counterions to prevent alkyne deprotonation and further catalyst deactivation by generation of σ,π-digold(I) alkyne complexes **10** (Scheme 10). As already observed, $NaBAr_4^F$ drove the formation of **3a** in 66% yield and 84:16 *er*. Furthermore, a lithium salt bearing a similar fluorinated boron-based anion led to a similar result. Collectively, these results indicate the importance of the bulkiness and low basicity of the counterion to form catalytically active species. Lately, the possibility of inducing chirality by a chiral counterion was studied. However, as expected, the chiral phosphate was not a suitable counterion for the activation of alkyne **1a** (Table 2, entry 11). Relying on these results, $NaBar_4^F$ (2.5 mol %) was chosen to continue the optimization.

Table 1. Precatalyst screening for the formation of **3a** at laboratory scale.

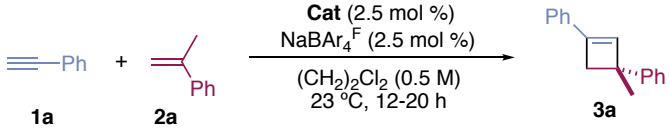

Entry[a]	Catalyst	**3a** Yield (%)[b]	**3a** *er* (%)[c]
1	(*R*,*S*P)-**A**	13	78:22
2	(*R*,*S*P)-**B**	66	84:16
3	(*R*,*S*P)-**C**	10	82:18
4	(*R*,*S*P)-**D**	10	80:20
5	(*S*,*R*P)-**E**	9	82:18
6	(*R*,*S*P)-**F**	0	-
7	(*R*,*S*P)-**G**	16	69:31
8	(*R*,*S*P)-**H**	45	66:34
9	(*R*,*S*P)-**I**	13	72:28
10	(*S*,*R*P)-**J**	0	-
11	(*R*,*S*P)-**K**	0	-
12	(*R*,*S*P)-**L**	0	-
13	(*R*,*S*P)-**M**	19	71:29
14	(*S*,*R*P)-**N**	0	-

[a]**2a/1a** = 2:1, **1a** (0.1 mmol). [b]Isolated yield. [c]Enantiomeric ratio determined by UPC2 (Chiralpak ID, CH_3CN 15%).

As explained in the general introduction, the use of cationic gold(I) complexes that do not need *in situ* activation is highly recommended for gold(I) catalysis (General Introduction, Scheme

1).[40] However, attempts to generate monocationic species from (S,R_P)-**B** with $NaBAr_F^4$ in the presence of labile ligands such as acetonitrile, benzonitrile or more coordinating 1,3,5-trimethoxybenzonitrile were unsuccessful. The coordination of the labile ligands to gold(I) was not detected by NMR in any of the cases. In fact, the same NMR spectra were obtained in every experiment and furthermore, matched the spectra recorded when (S,R_P)-**B** and $NaBAr_F^4$ were mixed in 1:1 ratio. Unfortunately, the low crystallinity of the obtained species prevented their full characterization. In view of this structural limitation, we decided to continue generating monocationic species *in situ* by chloride abstraction.

Table 2. Chloride scavenger screening for the formation of **3a**.

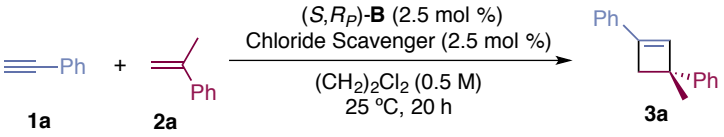

1a **2a** **3a**

Entry[a]	Chloride Scavenger	**3a** Yield (%)[b]	**3a** *er*[c]
1	$AgSbF_6$	-[d]	-
2	$AgPF_6$	-[d]	-
3	$AgBF_4$	23	84:16
4	$AgNTf_2$	-[d]	-
5	AgOBz	-[d]	-
6	AgOPNB	-[d]	-
7	$NaSbF_6$	-[d]	-
8	$NaBF_4$	-[d]	-
9	$NaBAr_4^F$	66	84:16
10	$Li[B(C_6F_5)_4]$	52	84:16
11[f]	AgX	-[d]	-

[a]**2a**/**1a** = 2:1, **1a** (0.1 mmol). [b]Isolated yield. [c]Enantiomeric ratio determined by UPC2. [d]No cyclobutene **3a** was formed. [f]Chlorobenzene.

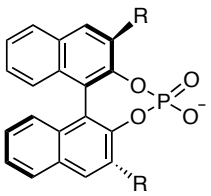

X (R = 2,4,6-*i*Pr_3-C_6H_2)

As expected, coordinating solvents suppressed catalytic activity (Table 3, entries 1-2), whereas the use of highly non-polar solvents led to **3a** in low yields and enantioselectivities (Table 3,

entries 3-4). In general, chlorinated solvents were superior in terms of enantioselectivity and conversion (Table 3, entries 5-9). On the other hand, fluorinated solvents decreased reactivity maintaining good levels of enantiomeric ratios. To select a chlorinated solvent, the reaction was carried out at 0 ºC (Table 3, entries 12-16). The best combination for enantioselectivity, reactivity and reaction time was obtained with chlorobenzene, which was chosen for further optimization (Table 3, entry 14).

Table 3. Solvent optimization for the [2+2] cycloaddition between **1a** and **2a**.

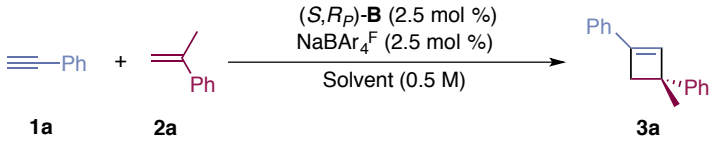

1a **2a** **3a**

Entry[a]	Solvent	T (ºC)	t (h)	**3a** Yield (%)[b]	**3a** *er* (%)[c]
1	THF	25	20	-	-
2	MeOH	25	20	-	-
3	Hexane	25	20	6	52:48
4	Toluene	25	20	10	75:25
5	$(CH_2)_2Cl_2$	25	20	66	84:16
6	$CHCl_3$	25	20	77	86:14
7	Chlorobenzene	25	20	76	86:14
8	1,1,2,2-Tetrachloroethane	25	20	77	83:17
9	1,1,2-Trichloroethane	25	20	71	83:17
10	Perfluorohexane	25	20	40	83:17
11	2,2,2-Trifluoroethanol	25	20	40	80:20
12	1,2-Dichlorobenzene	0	25	61	83:17
13	$(CH_2)_2Cl_2$	0	24	55	88:12
14	Chlorobenzene	0	24	63	88:12
15	$CHCl_3$	0	40	43	87:13
16	1,1,2-Trichloroethane	0	40	76	87:13

[a]**2a/1a** = 2:1**, 1a** (0.1 mmol). [b]Isolated yield. [c]Enantiomeric ratio determined by UPC2.

Maintaining constant all the previous optimized conditions (Table 4, entry 1), the impact of other parameters was studied. However, none of these new variations affected enantioselectivity (Table 4). Regarding yield, no erosion was found doubling the amount of

$NaBAr_4^F$ (Table 4, entry 2), while increasing catalyst loading had a detrimental effect (Table 4, entry 3). More diluted conditions or inverse order of addition impacted reaction time negatively (Table 4, entries 4-6).

Table 4. Further optimization studies for the [2+2] cycloaddition between **1a** and **2a**.

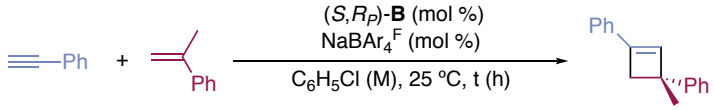

1a **2a** **3a**

Entry[a]	(S,R_P)-**B** (mol %)	$NaBar_4^F$ (mol %)	**2a**/**1a**	(M)	t (h)	**3a** Yield (%)[b]	**3a** *er*[c]
1	2.5	2.5	2	0.5	20	76	84:16
2	2.5	5	2	0.5	20	78	84:16
3	5	5	2	0.5	20	59	84:16
4	2.5	2.5	2	0.25	40	66	84:16
5	2.5	2.5	2	0.1	72	45	84:16
6[d]	2.5	2.5	2	0.5	48	71	84:16

[a]**1a** (0.3 mmol). [b]Isolated yield. Average of two runs. [c]*er* determined by UPC2. [d]((S,R_P)-**B** + $NaBAr_4^F$) + (**1a** + **2a**).

Table 5. Temperature optimization for the [2+2] cycloaddition between **1a** and **2a**.

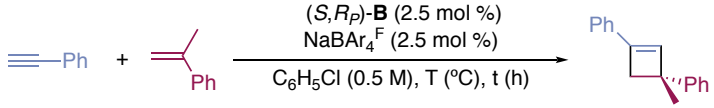

1a **2a** **3a**

Entry[a]	(S,R_P)-**B** (mol %)	$NaBar_4^F$ (mol %)	**2a**/**1a**	T (°C)	t (h)	**3a** Yield (%)[b]	**3a** *er*[c]
1	2.5	2.5	2	25	20	76	84:16
2	2.5	2.5	2	0	24	63	88:12
3	2.5	2.5	2	−10	24	62	89:11
4[e]	2.5	2.5	2	−20	72	46	90:10
5[e]	2.5	2.5	4	−20	72	49	90:10
6[e]	5	5	2	−20	20	37	90:10
7[f]	2.5	2.5	2	−20	48	70	90:10

[a] **1a** (0.3 mmol). [b] Isolated yield. Average of two runs. [c] *er* determined by UPC2. [d] ((S,R_P)-**B** + $NaBAr_4^F$) + (**1a** + **2a**). [e] Oligomerization of **2a**. [f] Slow addition of **2a**.

The best level of enantioselectivity was achieved by lowering the temperature from 25 to -20 ºC (Table 5, entries 1-4). However, oligomerization of **2a** competed with formation of **3a** at -20 ºC (Table 5, entry 4). To favor [2+2] cycloaddition, the amount of alkene (Table 5, entry 5) or catalyst loading (Table 5, entry 6). We were happy to see that the problem could be solved by adding slowly alkene **2a** to the mixture over a 12 h period (Table 5, entry 7).

Scope of Enantioselective Gold(I)-Catalyzed [2+2] Cycloaddition

With the optimal conditions in hand, we next explored the substrate generality of this transformation.

Terminal alkynes with 1,1-disubstituted alkene 2a

Regarding the alkyne, the cycloaddition reaction proceeds satisfactorily with aryl alkynes bearing electron rich substituents in *para* and *meta* position (**3b,c,d,g,h**) (Scheme 17). Halides in *para* were also well tolerated to form cyclobutenes (**3e-f**) in excellent enantioselectivities but moderate yields, while 3-ethynylthiophene led to cyclobutene **3i** in good yield and moderate enantiomeric ratio. The absolute configuration of **3f** was determined by X-ray diffraction as *R*.

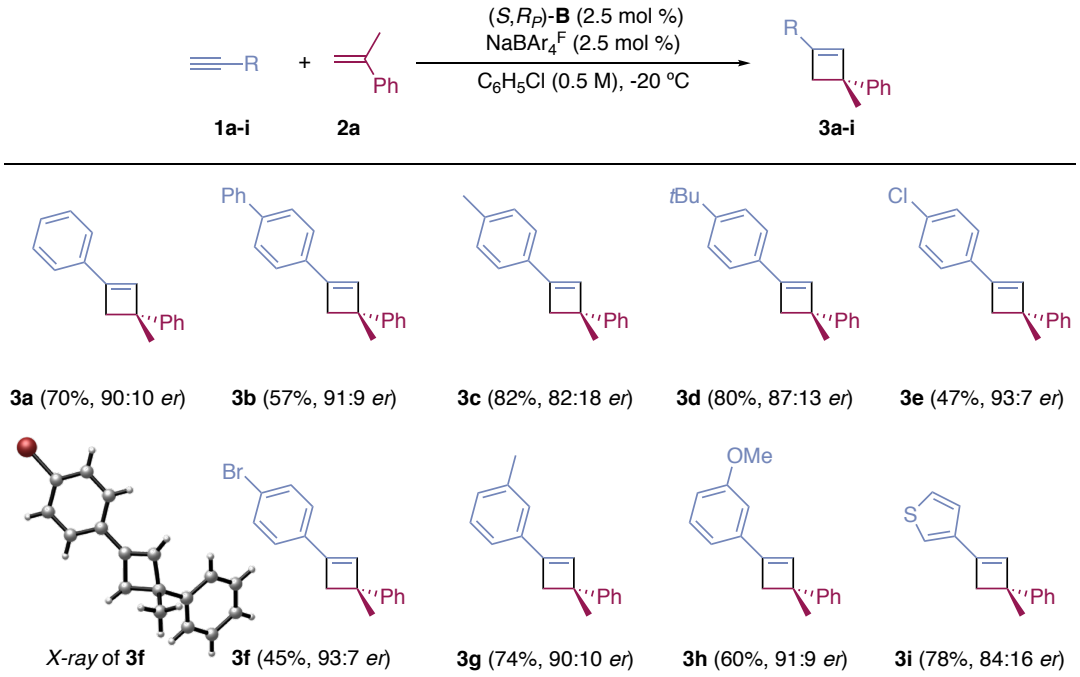

Scheme 17. Synthesis of cyclobutenes **3a-i**.

Under the same conditions, cyclobutenes **3j** and **3k** were isolated in good yields but low enantiomeric ratio (Table 6, entries 1-2). *meta*-Substituted aryl alkynes bearing halides or ester led to cyclobutenes **3l-o** in excellent enantioselectivities but very low yields (Table 6, entries 3-6). Even though cyclopropyl alkyne was a good substrate for the racemic version, no

cyclobutene was detected under the enantioselective protocol, which highlights the importance of the aryl moiety in the alkyne (Table 5, entry 7).

Table 6. Less reactive alkynes or alkynes leading to poor enantioselectivities.

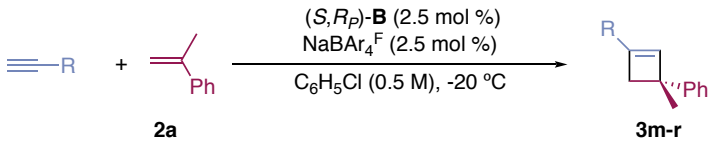

2a **3m-r**

Entry	R	Product	**3** yield (%)[a]	**3** *er*[b]
1	*p*-$MeOC_6H_4$	**3j**	87	73:27
2	2-thienyl	**3k**	61	77:23
3	*m*-FC_6H_4	**3l**	19	91:9
4	*m*-BrC_6H_4	**3m**	9	90:10
5	*m*-ClC_6H_4	**3n**	9	90:10
6	*m*-HOC_6H_4	**3o**	17	86:14
7	cyclopropyl	-	-	-

[a]Isolated yield. [b]*er* determined by UPC2.

1,1-Disbustituted alkenes with alkyne 1a

Regarding 1,1-disubstituted alkenes, the rate of alkene addition has to be tuned on an individual basis. Alkene oligomerization was not a problem for *para*-substituted α-methyl styrenes bearing alkyl and halides, and thus, the alkene was added in one pot. These alkenes gave cyclobutenes **3p-u** in good enantioselectivities and yields (Scheme 18). The rest of alkenes required slow addition. Ethyl-substituted styrene provided cyclobutene **3v** in good yield and moderate enantiomeric ratio (Scheme 18). However, simple styrene or 1,1-dialkyl substituted alkenes resulted in a significant loss of enantioselectivity, as shown in the case of **3w** and **3x** (Scheme 18). Poor enantio-discrimination was observed when the aryl moiety was located far away from the double bond (**3y**) (Scheme 18).

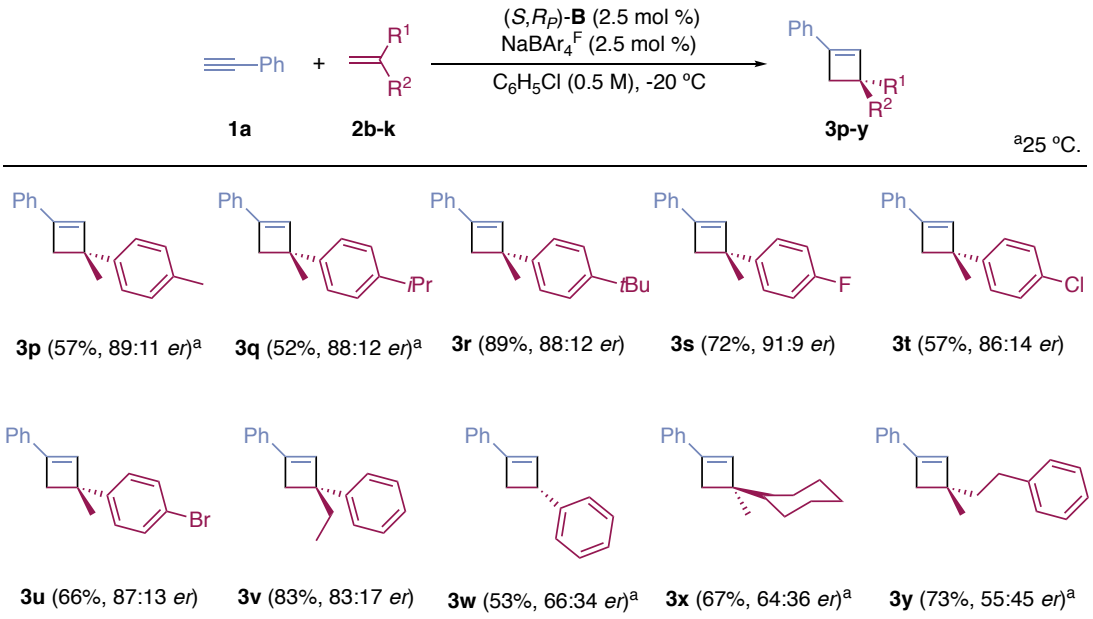

Scheme 18. Synthesis of cyclobutenes **3p-y**.

Table 7. Unsuccessful alkenes.

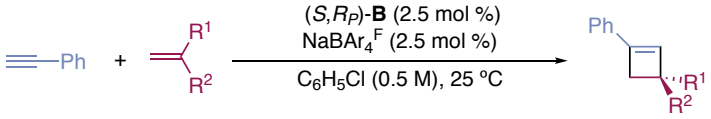

Entry	Alkene	Outcome	Entry	Alkene	Outcome
1	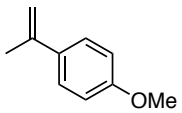	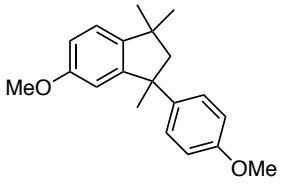	6	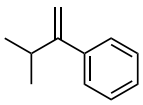	Complex mixture
2	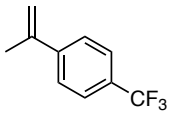	No reaction	7	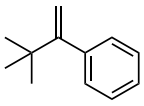	Complex mixture
3	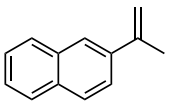	No reaction	8		No reaction
4	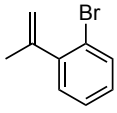	Complex mixture	9	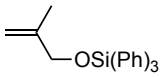	No reaction
5	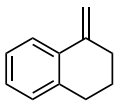	Complex mixture	10	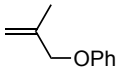	No reaction

Highly electron rich alkenes, such as *p*-methoxy-α-methylstyrene, suffered acid-catalyzed dimerization and oligomerization under the reaction conditions (Table 7, entry 1). Electron poor substituents in the aryl fragment resulted in no reaction or complex mixtures (Table 7, entries 2 and 3). These results highlight the importance of the electronics of the α-methylstyrene derivatives for the [2+2] cyloaddition. Complex mixtures were obtained with *o*-bromo-α-methylstyrene (table 7, entry 4), bicyclic alkene (Table 7, entry 5) and alkenes with bulkier alkyl substituents (Table 7, entries 6-7). Furthermore, the lack of reactivity with 1,1-dialkyl alkene, allyl ether and allyl silyl ether (Table 7, entries 8-10) highlights the relevance of the aryl substituent in the alkene.

Combinations of successful alkynes and alkenes

Cyclobutenes **3z-aj** were prepared in high enantioselectivities combining alkynes **1b-i** and alkenes **2c-d,g** (Scheme 19). As for **3f**, the absolute configuration of **3aa** was determined by X-ray diffraction as *R*. By analogy, the absolute configuration of all cyclobutenes was assigned as *R*.

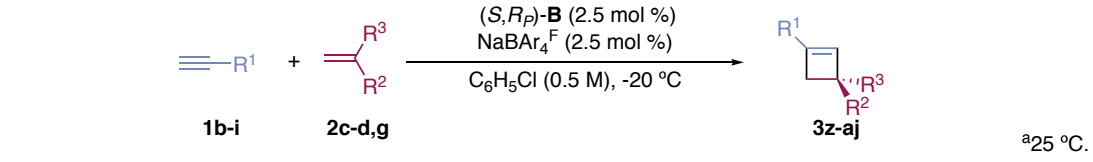

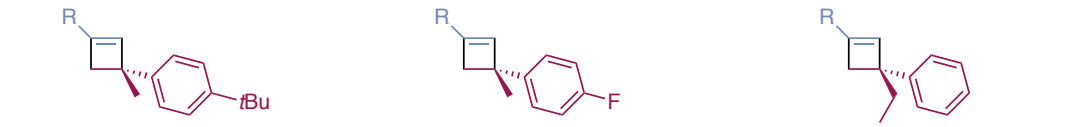

3z: R = *p*-*t*BuC$_6$H$_4$ (63%, 89:11 *er*)
3aa: R = 3-thienyl (56%, 94:6 *er*)

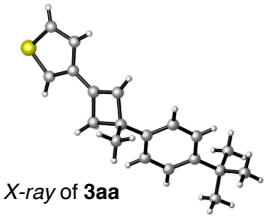

X-ray of **3aa**

3ab: R = *p*-*t*BuC$_6$H$_4$ (85%, 87:13 *er*)
3ac: R = *p*-ClC$_6$H$_4$ (37%, 91:9 *er*)
3ad: R = *p*-BrC$_6$H$_4$ (84%, 88:12 *er*)[a]
3ae: R = *m*-MeOC$_6$H$_4$ (40%, 89:11 *er*)
3af: R = 3-thienyl (85%, 86:14 *er*)

3ag: R = *p*-ClC$_6$H$_4$ (92%, 88:12 *er*)
3ah: R = *p*-BrC$_6$H$_4$ (81%, 85:15 *er*)
3ai: R = *m*-MeOC$_6$H$_4$ (88%, 89:11 *er*)
3aj: R = 3-thienyl (87%, 83:17 *er*)

Scheme 19. Synthesis of cyclobutenes **3z-aj**.

Biscyclobutenes

Biscyclobutenes **3ak-al** were also obtained with high enantioselectivities from dialkynes or dialkenes as reaction counterparts by twofold cycloaddition (Figure 5). The corresponding meso derivatives were obtained as minor products in these reactions (20-30% yields). In particular, 1,4-diethynylbenzene reacted with 4-fluoro-α-methyl-styrene to yield **3ak** in excellent enantioselectivity but low yield. At 25 ºC, 1,3-diethynylbenzene yielded biscyclobutene **3al** in excellent enantiomeric ratio but only 15% yield. Regarding dialkenes,

excellent enantioselectivities and moderate yields were obtained with both 1,3- and 1,4-diisopropenylbenzene (**3am-ap**).

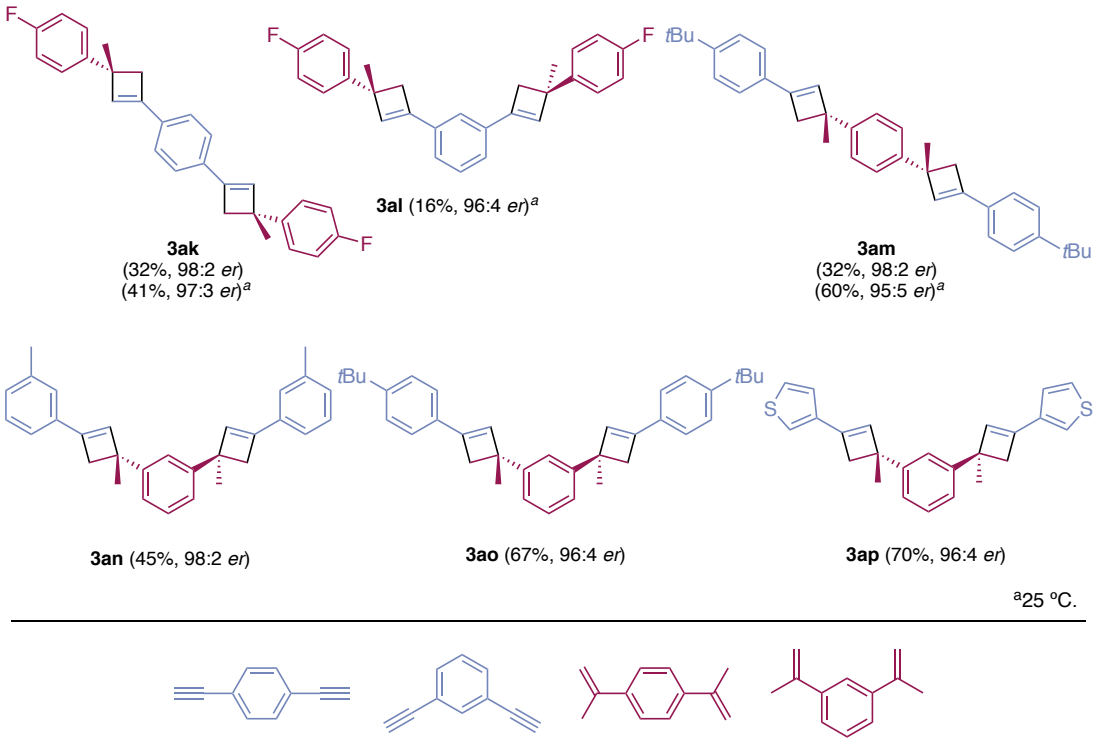

Figure 5. Synthesis of biscyclobutenes **3ak-ap**.

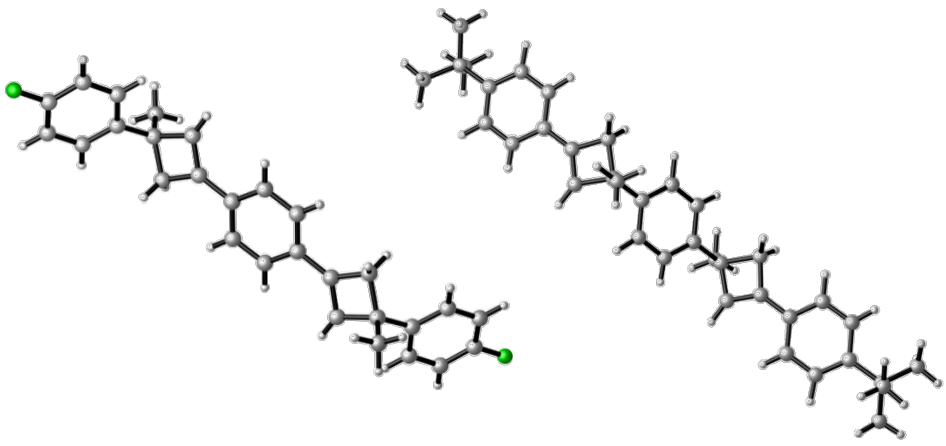

Figure 6. X-ray structures of biscyclobutenes **3ak** (left) and **3am** (right).

1,7-Enyne [2+2] cycloaddition

We also tested our optimized enantioselective protocol in the gold(I)-catalyzed [2+2] cycloaddition of 1,7-enyne **46**. However, tricyclic compound **47** was formed in good yield, although with very low enantioselectivity (Scheme 20). It is worth noting that no aryl groups are attached either to the alkyne or the alkene of 1,7-enyne **46** and we have previously found that aryl substituents in the intermolecular [2+2] are key to obtain good levels of chiral induction.

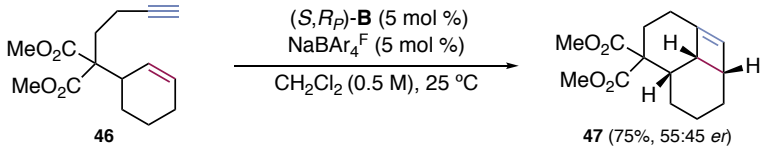

Scheme 20. Gold(I)-catalyzed intermolecular [2+2] cycloaddition of 1,7-enyne **46**.

1,1,2-Trisubstituted alkenes

The gold(I)-catalyzed [2+2] cycloaddition of 1,1,2-trisubstituted alkenes **2l-n** with terminal alkynes has been reported[8,25,26] and, under asymmetric gold(I) catalysis, would lead to the construction of tertiary stereocenters. Guided by our previous results, we applied our protocol to assembly quaternary stereocenters in cyclobutenes to these suitable substrates. However, complex (S,R_P)-**B** led to the formation of cylobutenes **3aq-as** in low enantiomeric and diastereomeric ratio (Scheme 21). Gratifyingly, these latter cyclobutenes were obtained with good enantioselectivities using precatalyst (R,S_P)-**F** (Scheme 21). The only difference between the two complexes is the substituents at the phosphorous bound to the stereogenic center of the ligand, which slightly modifies the steric and electronic nature of the catalyst.

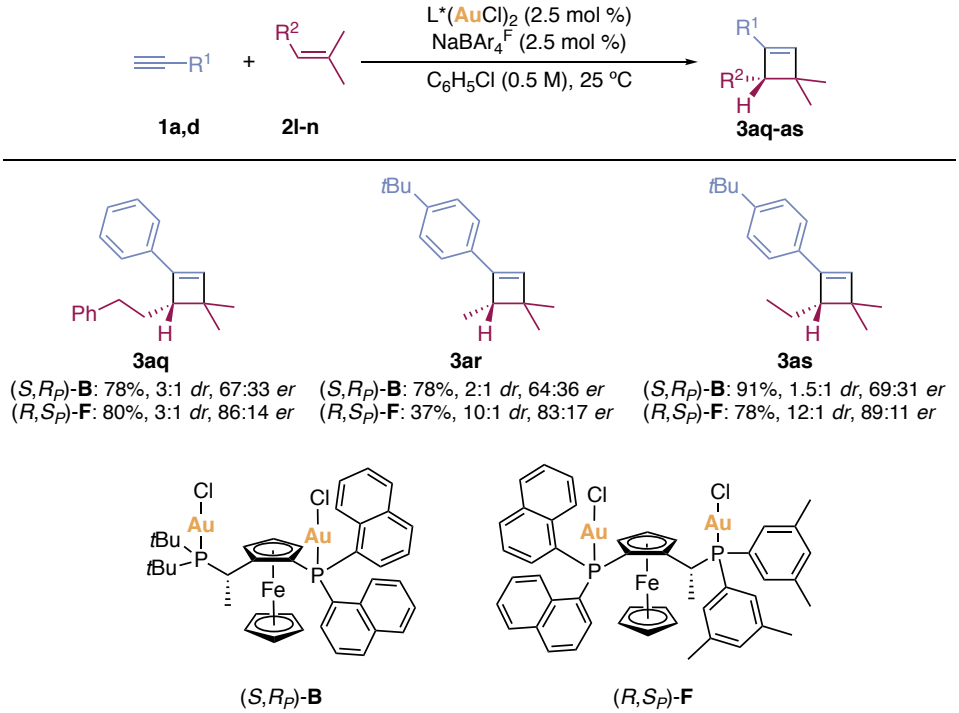

Scheme 21. Catalysts comparison for 1,1,2-trisubstituted alkenes.

Therefore, the cycloaddition of trisubstituted alkenes **2l-n** with terminal alkynes was carried out with catalyst (R,S_P)-**F** at -20 ºC. The reaction proceeds satisfactorily with aryl alkynes bearing substituents in *para* position and trialkyl substituted alkenes. Under these conditions, 1,3,3,4-tetrasubstituted cyclobutenes **3at-ba** were obtained in good yields and moderate to excellent regioselectivities, being 1,2,4,4-tetrasubstituted cyclobutenes formed as minor

regioisomers in most of the cases (Scheme 22). The enantioselectivities were on the same range to those obtained with 1,1-disusbtituted alkenes using catalyst (*S,R*$_P$)-**B**. It is worth noting that only alkynes with heavy substituents were used to minimize volatility issues.

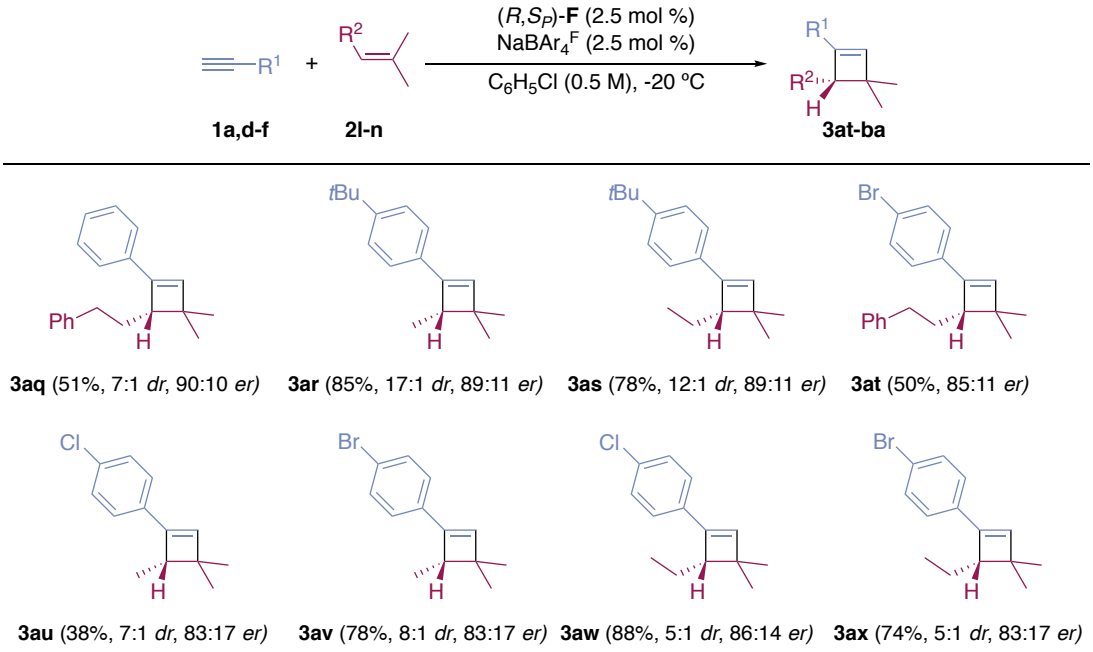

Scheme 22. Synthesis of cyclobutenes **3aq-ax**.

The enantioselective gold(I)-catalyzed [2+2] cycloaddition of (2-methylpropenyl)benzene (**2o**) and electron rich alkynes **1** led to cyclobutenes **3ay-bc** in excellent enantioselectivities but very low yields (Table 8, entries 1-4). Regarding the alkyne, the enantio-induction was eroded using *meta*-MeO phenyl alkyne with alkene **2l** (Table 8, entry 5).

Table 8. Other, less successful, enantioselective [2+2] cycloadditions.

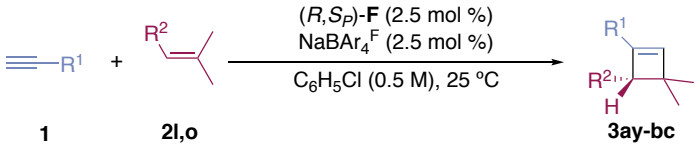

entry	R^1	R^2	Product	**3** yield (%)[a]	**3** *dr*	**3** *er*[b]
1	Ph	Ph	**3ay**	17	9:1	85:15
2	*p*-*t*BuC$_6$H$_4$	Ph	**3az**	16	13:1	86:14
3	3-thienyl	Ph	**3ba**	26	5:1	85:15
4	*m*-MeOC$_6$H$_4$	Ph	**3bb**	20	7:1	78:22
5	*m*-MeOC$_6$H$_4$	C$_2$H$_4$Ph	**3bc**	72	-	76:24

[a]Isolated yield. [b]*er* determined by UPC2.

Asymmetric synthesis of rumphellaone A

To demonstrate the utility of the asymmetric cyclobutene synthesis, a second-generation synthesis of rumphellaone A was developed in our laboratory by Dr. Beatrice Ranieri and Dr. Carla Obradors (Scheme 23). A previous diastereoselective total synthesis of this natural occurring cyclobutane was achieved in 12 steps by a gold(I)-catalyzed [2+2] macrocyclization of a 1,10-enyne (General Introduction, Scheme 5).[23] In this new synthesis, the key intermolecular [2+2] cycloaddition of **1a** with trisubstituted alkene **2p** was best performed in the presence of catalyst (*R*,S_P)-**F** to furnish cyclobutene **3bd** in 70% yield and 91:9 *er* (Scheme 23). Cyclobutene **3bd** was then converted into rumphellaone A in 8 steps.[32,Error! Bookmark not defined.]

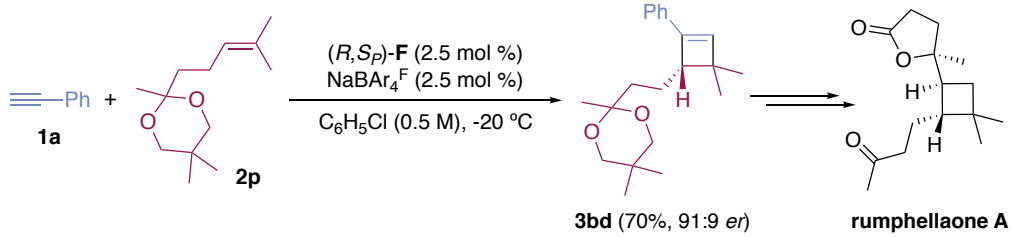

Scheme 23. Intermolecular gold(I)-catalyzed enantioselective [2+2] cycloaddition as key step for the total synthesis of rumphellaone A.

Mechanistic Investigations

Monogold complexes

Precatalyst (*S*,R_P)-**B** poses two gold(I) centers. To gain insight into the role of both metal centers in the enantioselective [2+2] cycloaddition, monogold complex (*S*,R_P)-**O** bearing the same ligand but only a gold center coordinated to the trialkyl phosphine was synthetized and used as precatalyst (Scheme 24). After 72 h, only traces of racemic cyclobutene **3a** were formed, presumably as a result of the formation of inactive dimeric species after chloride abstraction. To probe this hypothesis, complex (*S*,R_P)-**O·BH$_3$**, in which the naked phosphorous is coordinated to BH_3, was prepared and tested as precatalyst in the formation of **3a**. As for unprotected (*S*,R_P)-**O**, only traces of racemic product were formed using complex (*S*,R_P)-**O·BH$_3$** as precatalyst (Scheme 24).

However, by themselves, these observations are not sufficient to unambiguously exclude the formation of dimeric, or oligomeric, inactive species after chloride abstraction. Therefore, the reactivity of complexes (*S*,R_P)-**O** and (*S*,R_P)-**O·BH$_3$** in the well-known cycloisomerization of 1,6-enyne **48** was studied. Both complexes catalyzed the transformation of 1,6-enyne **48** to the expected cycloisomerized products (Scheme 25), which excludes the formation of inactive

gold(I) dimers after chloride abstraction.[41] Therefore, all these results indicate that the presence of (naphtyl)$_2$P–AuCl moiety in (*S,R*$_P$)-**B** is essential for the [2+2] cycloaddition reaction to proceed both in good yields and enantioselectivities.

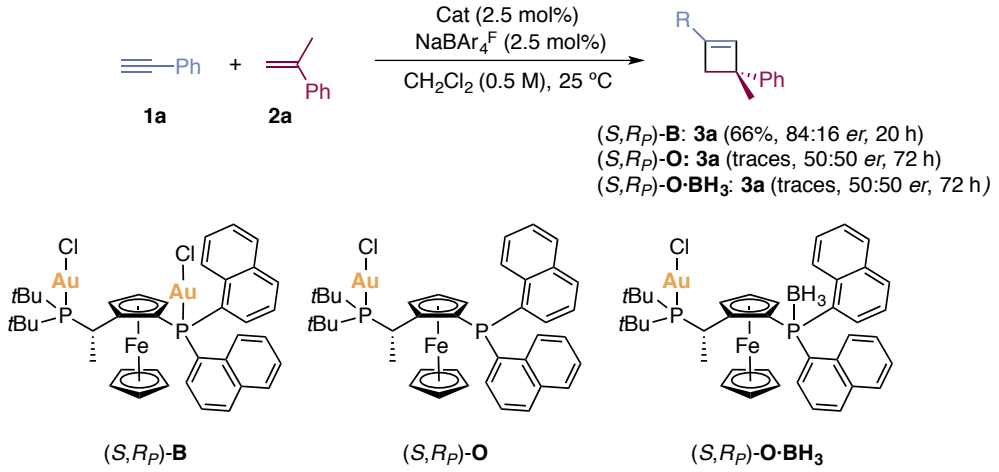

Scheme 24. Monogold complexes (*S,R*$_P$)-**O** and (*S,R*$_P$)-**O·BH$_3$** as precatalysts in the cycloaddition of alkyne **1a** and alkene **2a**.

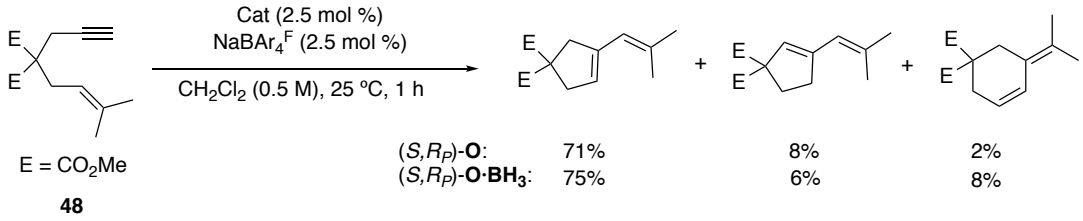

Scheme 25. Monogold complexes (*S,R*$_P$)-**O** and (*S,R*$_P$)-**O·BH$_3$** as precatalysts in the cycloisomerization of 1,6-enyne **48**.

Chloride abstraction

In the optimal reaction conditions, the gold to chloride scavenger ratio is 2:1. Therefore, in principle, there would be only enough NaBAr$_F^4$ to generate a monocationic species. To gain insight into which chloride is being abstracted, the cycloaddition of **3a** was followed by ^{31}P NMR, which show that the resonances corresponding to *t*BuP suffer an upfield shift, while the signals of NaphtylP remain unchanged.

To prove the formation of monocationic species, we studied the impact of the NaBAr$_4^F$ to (*S,R*$_P$)-**B** ratio in the [2+2] cycloaddition of **1a** with **2a** (Figure 7). The conditions used in our optimized method are represented as a pink line in Figure 6 (2.5 mol % of NaBAr$_4^F$). When the amount of NaBAr$_4^F$ was doubled (5 mol %), the yield of cyclobutene **3a** increased by 10%

41 Nieto-Oberhuber, C.; Muñoz, M. P.; Buñuel, E.; Nevado, C.; Cárdenas, D. J.; Echavarren, A. M. *Angew. Chem. Int. Ed.* **2004**, *43*, 2402–2406.

(grey line). However, when the amount of $NaBAr_4^F$ was further increased to 10 mol %, the reaction stopped after 1 h (green line). A closer analysis to this experiment showed that alkene **2a** was fully consumed in 1 h not only to form cyclobutene **3a** but also dimers and oligomers as side products. These results suggest that chemoselectivity towards the formation of cyclobutene **3a** decreases when the amount of $NaBAr_4^F$ is higher than 5 mol %.

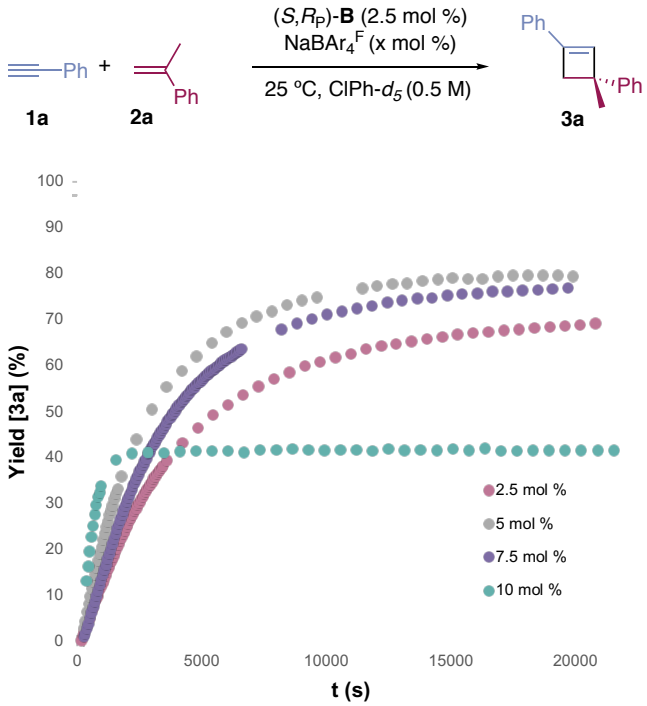

Figure 7. ^{1}H NMR monitoring of the [2+2] cycloaddition reaction changing the amount of $NaBAr_4^F$ and keeping **1a** (0.2 mmol), **2a** (0.4 mmol) and (*S,R*$_P$)-**B** (0.005 mmol) constant.

$NaBAr_4^F$ is not completely soluble in PhCl-d_5 and is less efficient than silver salts in the abstraction of chloride from gold centers. Therefore, to be sure of the gold to chloride scavenger ratio being used in our experiments, we activated (*S,R*$_P$)-**B** (2.5 mol %) with a silver salt bearing a bulky non-basic fluorinated counterion (Table 9). In these cases, the reactivity drastically changed when the amount of silver salt was doubled from 2.5 to 5 mol % (Table 9, entries 4-5), which indicates that when both chlorides are being abstracted, the resulting dicationic species is not active in the [2+2] cycloaddition.

Taken together, these results suggest that under the optimized conditions just one chloride is being abstracted from (*S*,*R*$_P$)-**B** by $NaBAr_4^F$ to generate monocationic digold(I) complexes, which are the catalytically active species in the [2+2] cycloaddition.

Table 9. [2+2] Cycloaddition reaction of **1a** and **2a** modifying chloride scavenger.

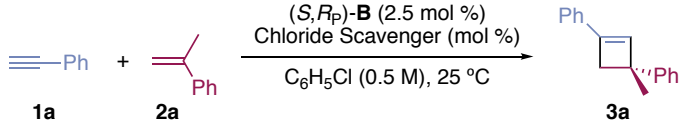

1a **2a** **3a**

Entry[a]	Chloride Scavenger	mol %	**3a** Yield (%)[b]	*er*[c]
1	$NaBAr_4^F$	2.5	76	84:16
2	$NaBAr_4^F$	5	78	86:14
3	$NaBAr_4^F$	10	40	85:15
4	$Ag\{Al[OC(CF_3)_3]_4\}$	2.5	65	84:16
5	$Ag\{Al[OC(CF_3)_3]_4\}$	5	-	-

[a]**1a** (0.3 mmol). **2a**:**1a** = 1:2. [b]Isolated yield. [c]*er* determined by UPC2.

Kinetics studies

The rate law or rate equation of a chemical reaction is an expression that indicates how the reaction rate depends on the concentration of the reactants. A generalized rate law for the reaction of A, B and C to give product P can be described as follow:

$$A + B + C \longrightarrow P$$

$$rate = \frac{d[P]}{dt} = k[A]^a[B]^b[C]^c$$

Equation 1. General rate equation.

where [A], [B], [C] and [P] are the concentration of the species in M, the exponents are the partial kinetic orders and k is the rate constant in s^{-1}.

For a complex reaction, the kinetic order is highly dependent upon the location of the rate-determining step in the mechanism. Only reaction steps that occur prior to or during the rate-determining step can be detected during kinetic studies. Therefore, the partial kinetic order of the different reactants provides information exclusively on the role of these reactants in the mechanism before or during the rate-limiting step.

In our case, the [2+2] cycloaddition of **1a** with **2a** is slow and significant competing pathways take place as the reaction proceeds. Therefore, we turned to initial-rate kinetics method to calculate the kinetic order of the [2+2] cycloaddition. Specifically, we followed the reaction to 5% formation of **3a** by ^{1}H NMR in PhCl-d_5 at 25 ºC modifying the initial amounts of **1a**, **2a** and **catalyst**. All these experiments were conducted with (*S,R*$_P$)-**B** and $NaBAr_4^F$ in a ratio of 1:1. For simplicity, this mixture will be named as **catalyst** (Scheme 26).

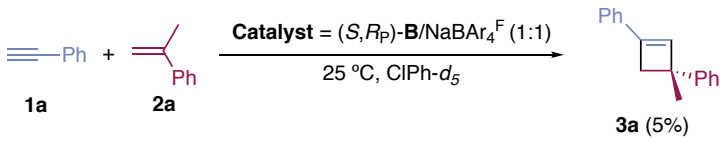

Scheme 26. Enantioselective [2+2] cycloaddition of **1a** and **2a**.

First, based on Equation 2, we represented [**3a**] (M) (until 5%) *vs.* time (s) varying the initial concentration of one reactant while keeping constant the rest of reactants (for **1a**: Figure 8, **2a**: Figure 9 and **catalyst**: Figure 10). Each line is related to a specific set of conditions, and thus, the slope of each line corresponds to the initial rate under the used conditions.

$$rate_0 = \frac{d[\mathbf{3a}]_{5\%}}{dt} \Rightarrow d[\mathbf{3a}]_{5\%} = rate_0 \cdot dt$$

Equation 2. Where $rate_0$: initial rate in M/s; $d[\mathbf{3a}]_{5\%}$: concentration of **3a** at time = t until 5% yield in molarity (M) and dt: time in seconds (s) at every measurement.

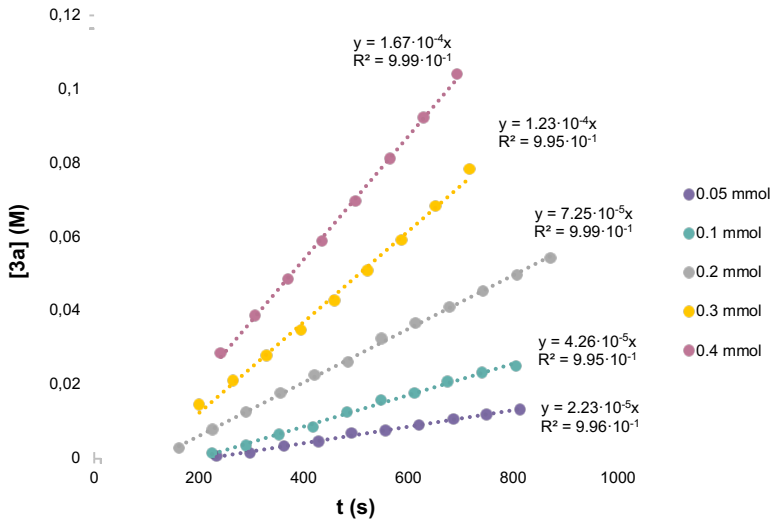

Figure 8 ^{1}H NMR monitoring of the [2+2] cycloaddition reaction changing the amount of **1a** and keeping **2a** (0.4 mmol), (*S,R*$_P$)-**B** (0.005 mmol) and $NaBAr_4^F$ (0.005 mmol) constant until **3a** was formed in 5%.

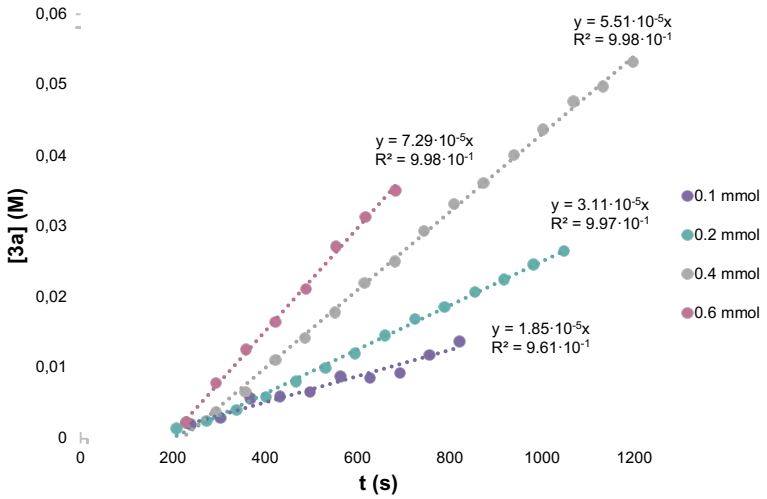

Figure 9. ^{1}H NMR monitoring of the [2+2] cycloaddition reaction changing the amount of **2a** and keeping **1a** (0.2 mmol), (*S,R*$_P$)-**B** (0.005 mmol) and NaBAr$_4^F$ (0.005 mmol) constant until **3a** was formed in 5%.

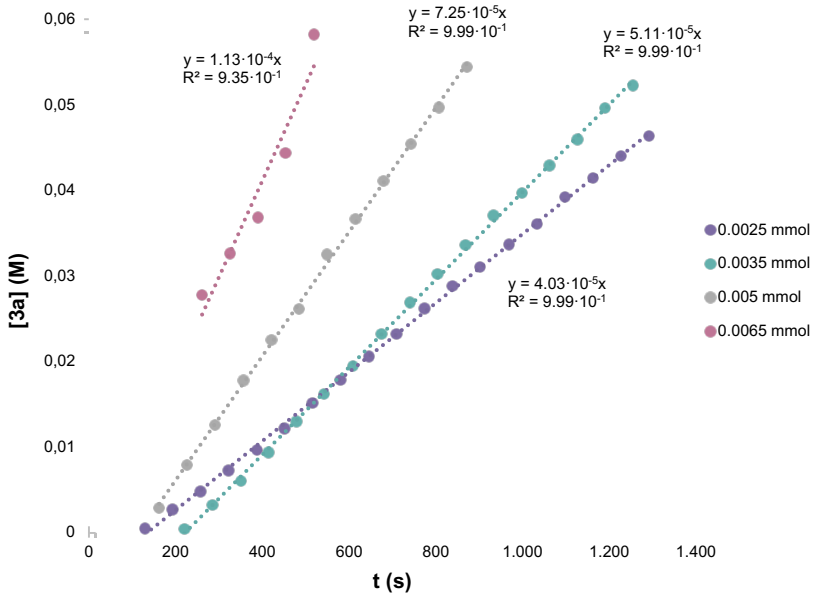

Figure 10. ^{1}H NMR monitoring of the [2+2] cycloaddition reaction changing the amount of (*R,S*$_P$)-**B** and NaBAr$_4^F$ (1:1) and keeping **1a** (0.2 mmol) and **2a** (0.4 mmol) constant until **3a** was formed in 5%.

To determine the kinetic order with respect to alkyne **1a**, we applied Equation 3. A straight line was obtained by plotting ln[initial rate]$_{\mathbf{1a}}$ *vs.* ln[**1a**]$_0$, whose slope corresponds to the kinetic order of alkyne **1a** (Figure 11). The same procedure was repeated to calculate the partial kinetic orders of alkene **2a** and **catalyst** (Figure 11).

$$initial\ rate = k[\mathbf{1a}]^a[\mathbf{2a}]^b[\mathbf{Catalyst}]^c$$

$$if\ [\mathbf{2a}]\ and\ [\mathbf{catalyst}]\ are\ constant$$

$$initial\ rate_{\mathbf{1a}} = k'[\mathbf{1a}]_0^a \quad \Rightarrow \ln[initial\ rate_{\mathbf{1a}}] = aln[\mathbf{1a}]_0 + lnk'$$

Equation 3. Where initial rate$_{\mathbf{1a}}$: initial rates calculated varying [**1a**] and maintaining constant [**2a**] and [**catalyst**]; [**1a**]$_0$: initial concentration of **1a** for every initial rate$_{\mathbf{1a}}$ measured and a: partial kinetic order of alkyne **1a**.

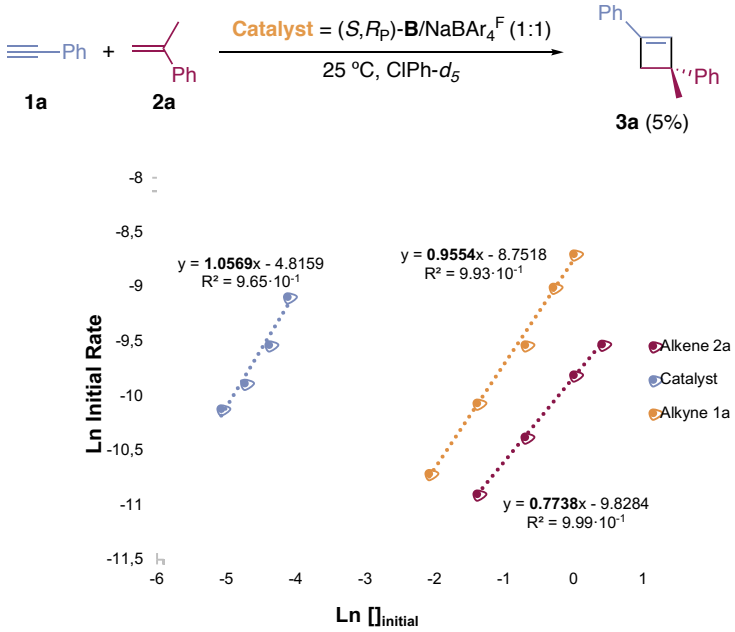

Figure 11. Order of the reagents in the enantioselective [2+2] cycloaddition between **1a** and **2a** with precatalyst (*S,R*$_P$)-**B** and NaBAr$_4^F$.

The rate equation for the intermolecular enantioselective gold(I)-catalyzed [2+2] cycloaddition of alkyne **1a** and alkene **2a** is shown in Equation 4. In the range of applied concentrations, the [2+2] cycloaddition reaction exhibited first order kinetic dependence on alkyne **1a** and alkene **2a**. The reaction also showed a first order dependence on the catalyst concentration when complex (*R,S*$_P$)-**B** and NaBAr$^F_4$ were mixed in 1:1 ratio. However, alone, these observations are not sufficient to determine the rate-limiting step of this transformation. Based on mechanistic studies performed for the racemic version (Schemes 11 and 12),[25,26] both ligand exchange and electrophilic addition could be rate-determining steps for this reaction.

$$rate = \frac{d[\mathbf{3a}]}{dt} = k_{obs}[\mathbf{1a}][\mathbf{2a}][\mathbf{Catalyst}]$$

Equation 4. Rate equation of the cycloaddition of **1a** and **2a** with precatalyst (*S,R*$_P$)-**B** and NaBAr$_4^F$.

Evaluation of substituent effects: Hammett plot studies

More in-depth analysis of the structure of the highest energy transition state of a reaction is obtained from studies of substituent effects using linear free energy relationships (LFER). A LFER relates the activation free energy change induced by a substituent with a parameter that describes the electron donating or electron withdrawing characteristics of the substituent.

The Hammett plot method, which is the most common LFER, is a general approach for examining changes in charge during a reaction. This method describes how reaction mechanisms vary as a function of the electronic changes induced by substituents. In this analysis, the substituents are only placed meta and para to eliminate possible steric effects. The original parameters scale, sigma (σ), measures the aptitude of substituents to influence the acidity of benzoic acid *via* inductive effects (Scheme 26). A substituent parameter was defined using Equation 5 for each substituent (X). A different set of sigma values is necessary for each position on the benzoic acid (σ_{para} and σ_{meta}).

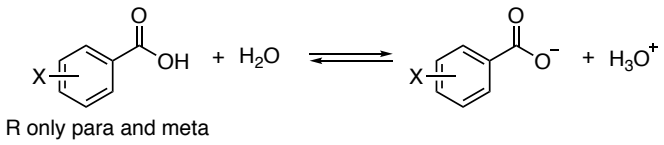

Scheme 26. Acid-base equilibrium of benzoic acid.

$$\log\left(\frac{K_X}{K_H}\right) = \sigma_X$$

Equation 5. Mathematical definition of substituent parameter σ_R. Where K_X: acid-base equilibrium constant for the reaction with substituent R; K_H: acid-base equilibrium constant for the R = H; σ_X = substituent parameter for substituent R.

To include resonance effects, two different parameter scales were developed. The sigma$^+$ scale (σ^+) is based upon the heterolysis (S_N1) reaction of *para*-substituted phenyldimethyl chloromethane, and it is suitable for groups that stabilizes positive charge *via* resonance in the transition state (Scheme 27a). The sigma$^-$ scale (σ^-) is based upon the ionization of *para*-substituted phenols and considers the stabilization of negative charge *via* resonance (Scheme 27b).

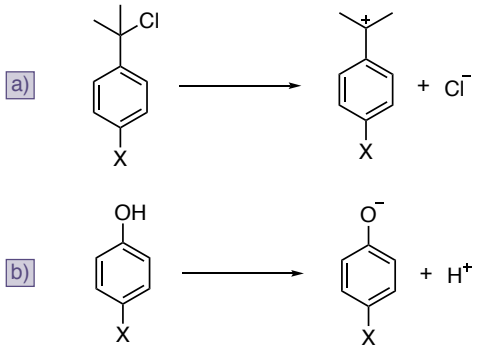

Scheme 27. Reactions in which σ^+ (a) and σ^- (b) are based on.

To determine how a reaction responds to substituents, we use the Hammett relationship (Equation 6) for kinetics analysis. Experimentally, the plot of $\log(k_X/k_H)$ *vs.* σ_X (or σ^+ or σ^-) gives the rho value (ρ). The latter provides information about the change in charge during the rate-determining step. If the value is positive ($\rho > 0$), the reaction is creating negative charge. Hence, if ρ is negative ($\rho < 0$), a positive charge is being built during the reaction.

$$\log\left(\frac{k_X}{k_H}\right) = \rho\sigma_X$$

Equation 6. Hammett relationship. Where k_X: reaction rate with substituent R; k_H: reaction rate with R = H; ρ: rho value; σ_X = substituent parameter for substituent R.

To obtain further information about the rate-limiting step of the [2+2] cycloaddition, we decided to examine Hammett correlations for reactions of alkyne **1a** with *para*-substituted-α-methyl styrenes **2a-h**. Such a study would shed light into the electronic effects in the rate-determining step, which would allow us to distinguish between a ligand exchange or an electrophilic addition as the slowest step of this cycloaddition. The substituent was modified in para for the alkene counterparts. This choice was guided by the involvement of the alkene in both potential rate-limiting steps. It is worth highlighting that the [2+2] cycloaddition does not proceed with *para*-substituted-α-methyl styrenes bearing highly electron rich or electron poor substituents (Table 7, entries 1-2), which limited the choice of viable substrates for this study.

Conditions and parameters similar to previous experiments for initial-rate kinetics were employed (Table 10). Therefore, the rate constants were calculated applying Equation 2 to the corresponding data until cyclobutenes **3a,s-x,bh** were formed in 5% yield.

Initially, the log (k_x/k_H) values were plotted *vs.* σ_{para}. However, the Hammett plot was not linear (Figure 12). As explained, σ_{para} values do not include effects for direct resonance stabilization. Considering that cationic gold(I) intermediates are usually highly stabilized by resonance, we

plotted log (k_x/k_H) *vs.* σ^+_{para}. Gratifyingly, a Hammett plot for the series of *para*-substituted α-methyl styrenes **2a-h** showed linear correlations with σ^+ constants for two different sets within the series, one for R = Me, *i*Pr, *t*Bu and cyclopropyl (ρ = +7.05, R^2 = 0.99) and the other one for R = F, H, Cl, and Br (ρ = -2.32, R^2 = 0.97) (Figure 13). The abrupt difference in the ρ values is indicative of a change in the catalytic turnover-limiting step as a function of substituents.

Table 10. Hammett plot data.

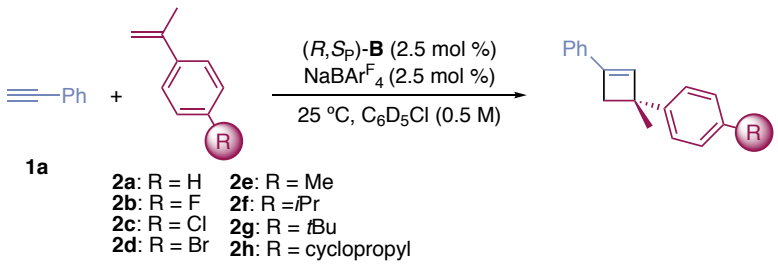

Entry	Alkene	R	σ_p^{42}	σ_p^{+42}	k_x (s^{-1})	log (k_x/k_H)
1	**2d**	Br	0.23	0.15	$3.25\cdot10^{-5}$	$-3.48\cdot10^{-1}$
2	**2c**	Cl	0.23	0.11	$3.34\cdot10^{-5}$	$-3.37\cdot10^{-1}$
3	**2a**	H	0	0	$7.25\cdot10^{-5}$	0
4	**2b**	F	0.06	-0.07	$9.52\cdot10^{-5}$	$-1.18\cdot10^{-1}$
5	**2g**	*t*Bu	-0.20	-0.26	$1.31\cdot10^{-4}$	$-2.57\cdot10^{-1}$
6	**2f**	*i*Pr	-0.15	-0.28	$8.89\cdot10^{-5}$	$8.86\cdot10^{-2}$
7	**2e**	Me	-0.17	-0.31	$6.73\cdot10^{-5}$	$-3.22\cdot10^{-2}$
8	**2h**	Cyclopropyl	-0.21	-0.41	$1.13\cdot10^{-5}$	$-8.07\cdot10^{-1}$

42 Hansch, C.; Leo, A.; Taft, R. W. *Chem. Rev.* **1991**, *91*, 165–195.

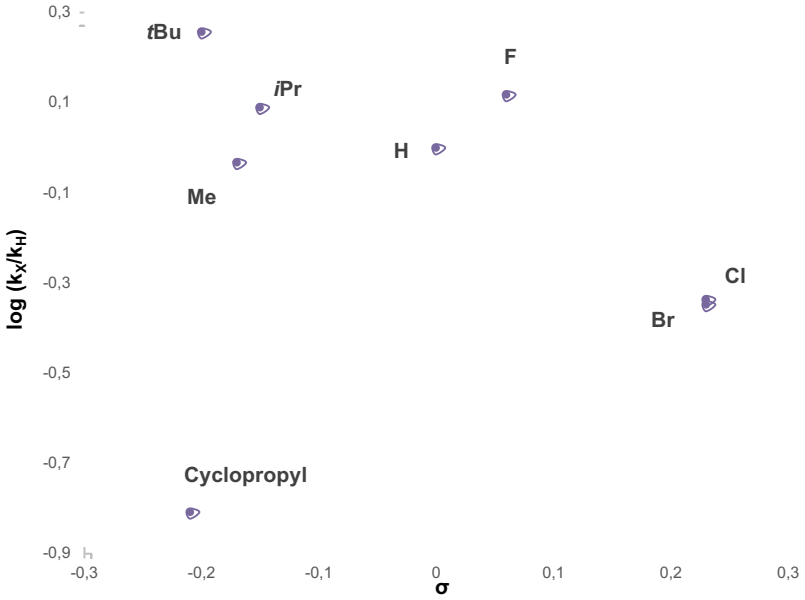

Figure 12. Hammett plot for individual kinetics using σ values.

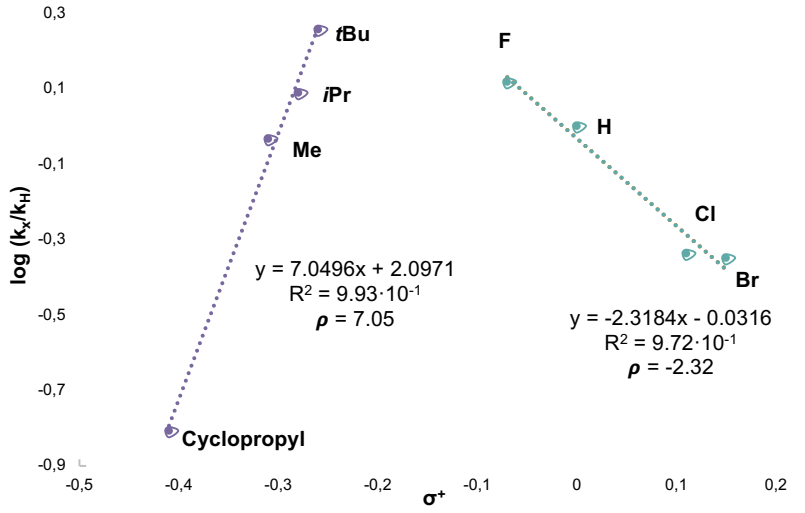

Figure 13. Hammett plot for individual kinetics using σ^+ values.

Full mechanistic picture

The mechanistic framework adopted to elaborate our mechanistic proposal is based on the reaction pathway originally proposed for the racemic [2+2] cycloaddition of alkynes with alkenes (Schemes 11 and 12) together with all the mechanistic investigations outlined in this chapter.[8,25,26]

In our proposal (Schemes 28 and 29), the first step is the associative ligand substitution by abstraction of just one chloride from the *t*BuPAuCl fragment of (*S*,R_P)-**B** by $NaBAr_4^F$ concerted with coordination of alkene **2** to gold(I) to generate (η^2-alkene)gold(I) complex **30**, which is in equilibrium with (η^2-alkyne)gold(I) intermediate **31**. Then, an alkene electrophilic addition generates the corresponding cyclopropyl gold(I) carbene **32**, which undergoes ring expansion to finally give rise to the enantioenriched cyclobutene **3a**.

The observation of a highly positive ρ value for *para*-alkyl substituted alkenes **2g-h** in an alkene electrophilic addition is seemingly puzzling, although it can be explained considering that in these cases the turnover limiting step is the ligand exchange between (η^2-alkene)gold(I) complex **30** and alkyne **1a** to form (η^2-alkyne)gold(I) complex **31** and free alkene **2**, which experiences a decrease in positive charge (Scheme 28). Indeed, we have shown before that the associative ligand exchange is the slowest step in the [2+2] cycloaddition reaction with mononuclear gold(I) complexes (Scheme 10).[25] For less electron-rich alkenes **2a-d** the formation of (η^2-alkene)gold(I) complex **30** is less favored, and therefore the observed negative ρ value is a result of the build-up of positive charge at the most substituted carbon of the alkene **2** in a turn-over limiting Markovnikov-type addition of electrophilic (η^2-alkyne)gold(I) complex **31** (Scheme 29). This mechanistic scenario is also consistent with the fact that *para*-methoxy α-methyl styrene suffered acid-catalyzed dimerization and oligomerization under the reaction conditions (Table 7, entry 1). In this case, the equilibrium between complex **30** and **31** is strongly shifted towards **30**, which can further react with another molecule of alkene **2**. Conversely, *para*-CF_3 α-methyl styrene was recovered unreacted, since the activation barrier for the electrophilic addition is too high in this case (Table 7, entry 2).

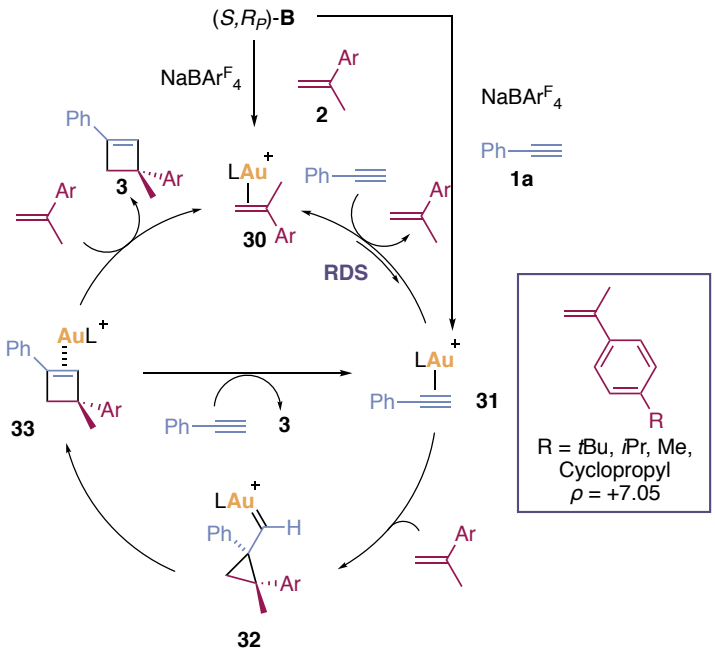

Scheme 28. Mechanism proposal for electron-rich *para*-alkyl-α-methylstyrene alkenes. Rate limiting step associative ligand exchange between (η^2-alkene)gold(I) complex **30** and phenylacetylene **1a** to (η^2-alkyne)gold(I) complex **31**.

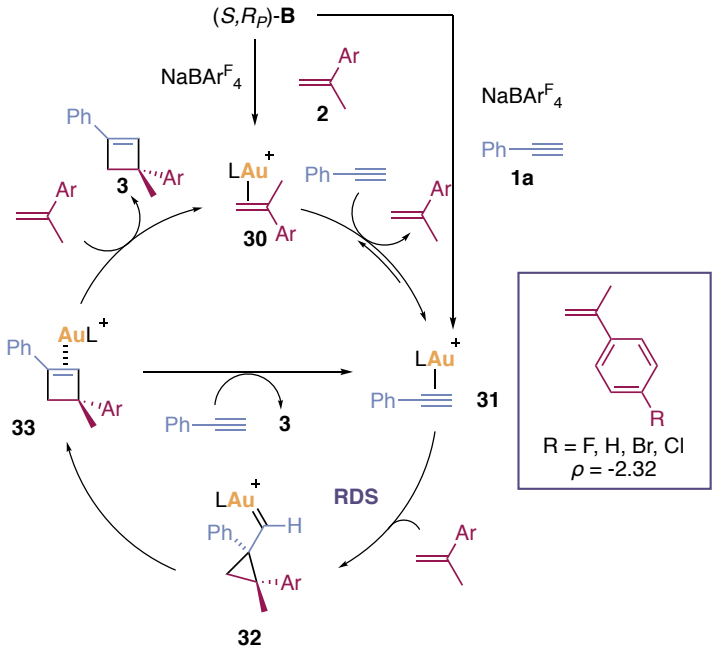

Scheme 29. Mechanism proposal for moderate electron-poor *para*-substituted α-methylstyrene alkenes. Rate limiting step Markovnikov-type addition of electrophilic (η^2-alkyne)gold(I) complex **31** to alkene **2**.

Enantioinduction Model

Aurophilic interactions have been claimed to be crucial for chiral transfer for digold(I) complexes.[43] However, in the solid state, the two gold(I) centers of (*S,R*$_P$)-**B** and (*S,R*$_P$)-**F** are *anti*-oriented with respect to each other and aurophilic interactions were not observed (Figure 14).

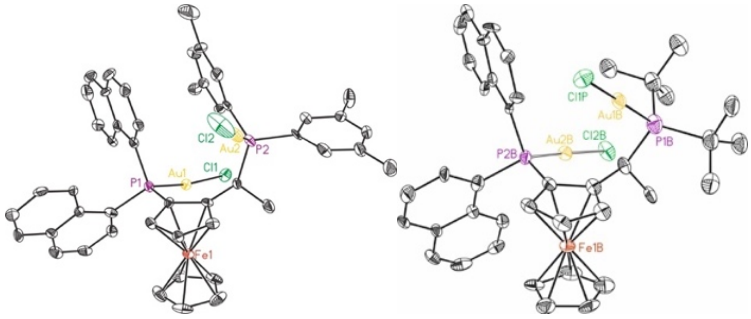

Figure 14. X-ray crystal structures of (*S,R*$_P$)-B (left) and (*S,R*$_P$)-F (right).

To design a model for the asymmetric induction in the intermolecular gold(I)-catalyzed [2+2] cycloaddition of 1,1-disubstituted alkenes and alkynes, DFT calculations were performed by Dr. Andrey I. Konovalov.[44] For the sake of completeness, relevant analysis to develop the enantioinduction model will be outlined in this chapter.

The lowest transition states for electrophilic addition of **31** to alkene **2a** are stabilized by π-stacking between two phenyl rings of the substrates (**1a** and **2a**) (Figure 15). Apparently, this face-to-face π-stacking plays an important role in enantiomeric discrimination, which is consistent with the fact that the use of alkenes without aromatic groups leads to lower enantioselectivities (Scheme 18, **3y-z**). The calculated energy difference between the lowest transition states that lead to (*S*)- and (*R*)-**3a** ($\Delta\Delta G^{\ddagger}_{S\text{-}R}$ = 0.7-1.1 kcal·mol^{-1}, depending on the method)[45] is in good agreement with experimentally derived value of $\Delta\Delta G^{\ddagger}_{S\text{-}R} \approx 1$ kcal·mol^{-1}.

To further explore the factors that lead to the relative destabilization of **TS*S*** *vs.* **TS*R***, Hirshfeld surface analysis was performed.[46] On Figure 16, the blue points depict the shape of the

43 (a) Widenhoefer, R. A. *Chem. –Eur. J.* **2008**, *14*, 5382–5391. (b) Sengupta, S.; Shi, X. *ChemCatChem*, **2010**, *2*, 609–619. (c) Pradal, A.; Toullec, P. Y.; Michelet, V. *Synthesis*, **2011**, 1501–1514. (d) Wang, Y. M.; Lackner, A. D.; Toste, F. D. *Acc. Chem. Res.*, **2014**, *47*, 889–901. (e) Zi, W.; Toste, F. D. *Chem. Soc. Rev.* **2016**, *45*, 4567–4589. (f) Li, Y.; Li, W.; Zhang, J. *Chem. –Eur. J.* **2017**, *23*, 467–512.

44 Calculations were performed at PCM(PhCl)-BP86-D3, SDD(Au, Fe), 6-31G(d) (C, H, P, Cl) level of theory.

45 Calculation at PCM(PhCl)-BP86-D3, SDD (Au, Fe), 6-31G(d) (C, H, P, Cl) level gives $\Delta\Delta G^{\ddagger}_{S\text{-}R}$ = 0.7 kcal·mol^{-1}. Calculation with M06-D3/BS2//BP86-D3/BS1 level gives $\Delta\Delta G^{\ddagger}_{S\text{-}R}$ = 1.1 kcal·mol^{-1}.

46 Spackman, M. A.; Jayatilaka, D. *CrystEngComm* **2009**, *11*, 19–32.

intramolecular surface between the ligand framework and the reaction center of the catalytic system in **TS*S***, whereas the red points display the region of elevated electron density, where weak van der Waals forces dominate in the overall interaction energy. Examination of the calculated surface revealed a direct intramolecular contact between α-methylstyrene **2a** and one of the naphthyl groups of the ligand, which is absent in **TS*R***, which might be responsible for the preferred formation of the (*R*)-cyclobutene **3a**.

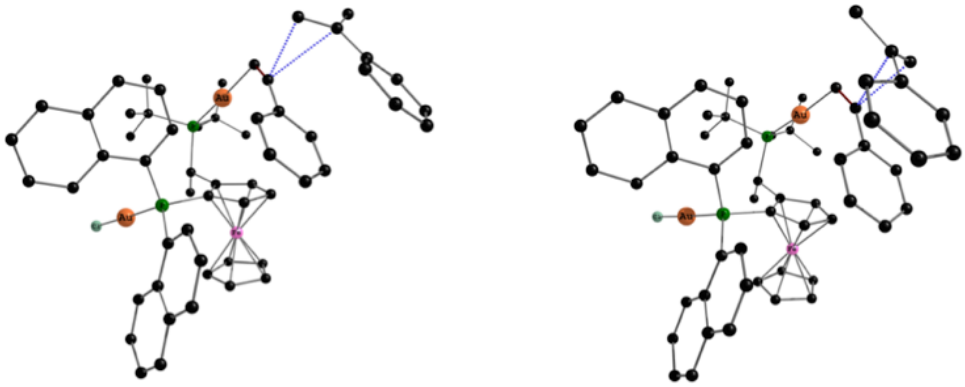

TS*R* (0.0 kcal·mol^{-1}) **TS*S*** (0.7-1.1 kcal·mol^{-1})

Figure 15. The lowest cyclopropanation transition states. Hydrogen atoms omitted for clarity.

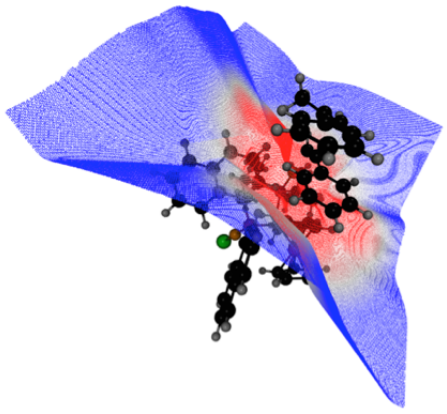

Figure 16. The color-mapped Hirshfeld surface for TS_S.

We further employed the Rediced Density Gradient (RDG) analysis,[47] which allows distinguishing weak interaction types based on the analysis of the residual electron density ρ(r) between molecular fragments. The left plot in Figure 17 shows a significant repulsion between $(naphthyl)_2P$ moiety and the reaction center. Unexpectedly, analysis of the RDG isosurface also revealed a strong repulsion between $(naphthyl)_2P$–AuCl and the methine hydrogen atom in the α-position to the Cp-ring of the ferrocenyl moiety (Figure 17, right).

47 Johnson, E. R.; Keinan, S.; Mori-Sánchez, P.; Contreras-García, J.; Cohen, A. J.; Yang, W. *J. Am. Chem. Soc.* **2010**, *132*, 6498−6506.

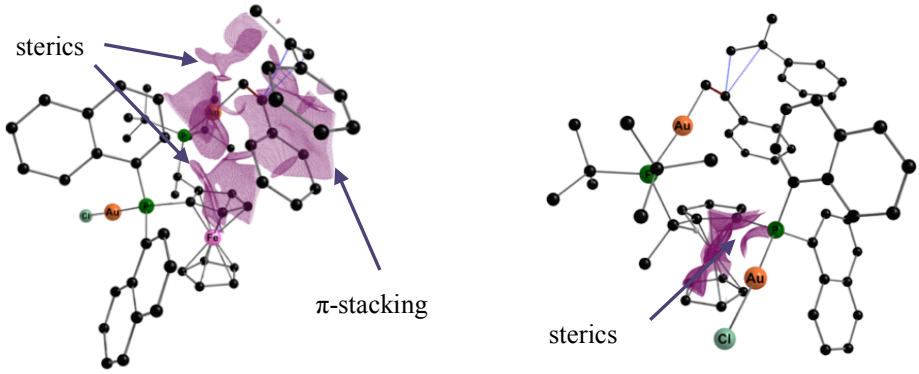

Figure 17. RDG isosurfaces (cut off = 0.6) for TS*S*. All hydrogen atoms but one which suffers from the steric repulsion coming from AuCl (right) are omitted for clarity.

Finally, we investigated the possibility of the cyclopropyl-gold(I) carbene isomerization from **32a** to **32a-iso**.[26] Despite the overcrowded steric environment, such a possibility was indeed found. However, ring expansion from cyclopropyl gold(I) carbene **32a** to form intermediate **33a**, which leads to the formation of cyclobutene **3a** product, was computed to be much more facile (Scheme 30). Among other things, the fact that $\Delta G^{\ddagger}_{exp}$ (8.1 kcal·mol^{-1}) << $\Delta G^{\ddagger}_{iso}$ (17.2 kcal·mol^{-1}) means that, once established, the stereocenter retains its configuration until the end of the catalytic cycle.

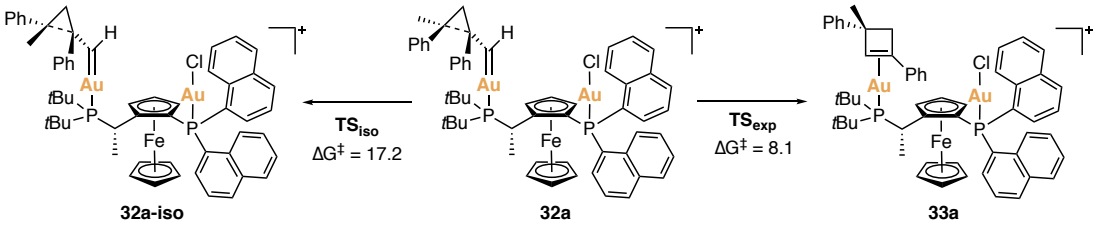

Scheme 30. Evolution of the (*R*)-cyclopropyl-gold(I) carbene intermediate 32a in the calculated reaction mechanism of [2+2] cycloaddition. Free energies in Kcalmol^{-1}.[48]

All these results support a mechanistic scenario in which the asymmetric induction is set up during the key electrophilic addition of (η^2-alkyne)gold(I) complex **31** to alkene **2a** (Figure 14). The combination of stabilizing π-stacking and unfavorable steric effects between the approaching alkene and the naphthyl rings of the ligand, together with a strong C–H – AuCl repulsion between the (naphthyl)$_2$P–AuCl and the methine hydrogen atom in the α-position to the Cp-ring of the ferrocenyl moiety rise the energy of the **TS*S*** transition state *vs*. **TS*R***. Furthermore, calculations of the corresponding transition states without the second AuCl on (naphthyl)$_2$P resulted in the complete loss of stereoselectivity, in agreement with the

48 Due to the convergence problems, the isomerization transition state and the corresponding energies were calculated at PBE0-D3/BS2//PBE0-D3/BS1 level of theory.

experimental data using complex (S,R_P)-**O** (Scheme 23), which highlights the importance of the (naphthyl)$_2$PAuCl moiety in the asymmetric induction.

Conclusions

We have developed a general synthesis of enantioenriched cyclobutenes by intermolecular gold(I)-catalyzed [2+2] cycloaddition of terminal alkynes with 1,1-disubstituted alkenes using Josiphos digold(I) catalysts. This protocol was applied to the reaction of aryl alkynes with α-ethyl styrenes, which led to cyclobutenes and biscyclobutenes with moderate to good enantioselectivities (82:18-94:6 *er*) (Scheme 31, right). Modification in the substituents of the Josiphos ligand allowed the expansion of the scope to non-aromatic 1,1,2-trisubstituted alkenes (Scheme 31, left).

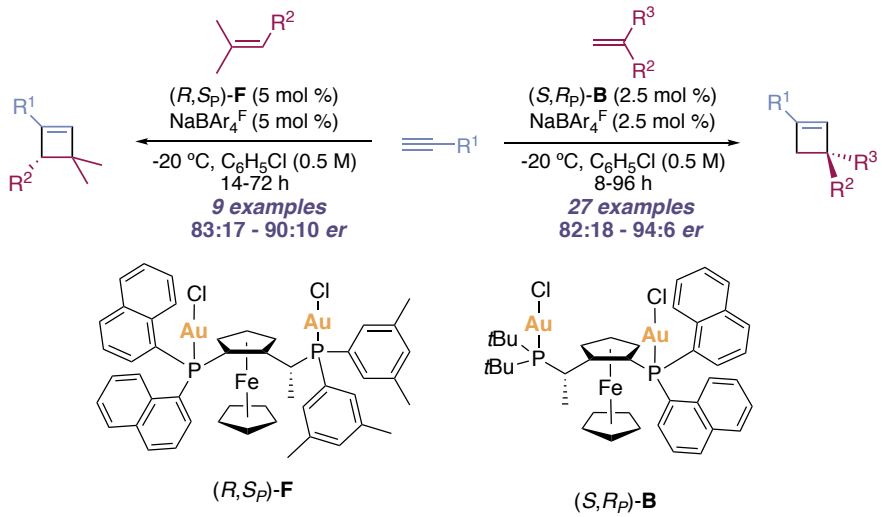

Scheme 31. Intermolecular enantioselective gold(I)-catalyzed [2+2] cycloaddition.

Our mechanistic studies indicate that only one of the gold(I) centers is directly involved in the activation of the alkyne, although the second one is required to induce the enantioselectivity. Our work also reveals that both ligand exchange and electrophilic addition can be turnover-limiting steps in this catalytic cycloaddition (Scheme 32).

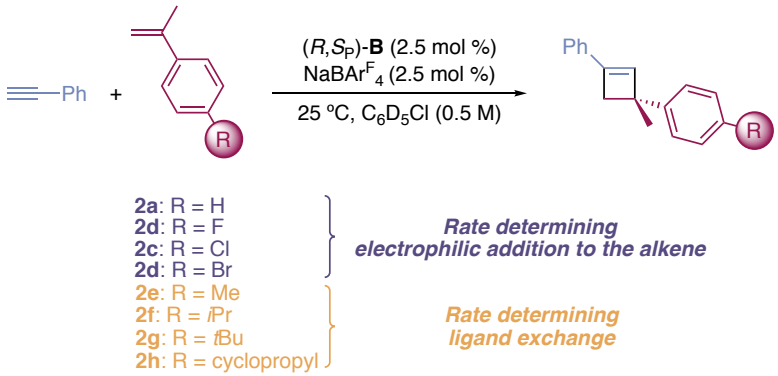

Scheme 32. Substituent dependence of the turnover-limiting steps in the intermolecular enantioselective gold(I)-catalyzed [2+2] cycloaddition.

Experimental Section

General Methods

The synthesis of gold(I) complexes was carried out under argon using solvents dried by passing through an activated alumina column on a PureSolv^{TM} solvent purification system. The cycloaddition reactions were done using HPLC solvents under air. Thin layer chromatography was carried out using TLC aluminium sheets coated with 0.2 mm of silica gel (Merck GF_{234}) using UV light as the visualizing agent and a solution of vanillin as stain. Reactions were followed using a GCMS apparatus or by TLC. Chromatographic purifications were carried out using flash grade silica gel (SDS Chromatogel 60 ACC, 40-60 μm) or automated flash chromatographer CombiFlash Companion. Preparative TLC was performed on 20 cm × 20 cm silica gel plates (2.0 mm or 1.0 mm thick, Analtech).

NMR data were recorded in deuterated solvents at 23 ºC on a Bruker Advance 400 Ultra Shield (400 MHz for ^{1}H, 100 MHz for ^{13}C, 162 MHz for ^{31}P and 376 MHz for ^{19}F), Bruker 500 Ultrashield (500 MHz for ^{1}H, 125 MHz for ^{13}C and 202 MHz for ^{31}P) apparatus and Bruker 300 Ultrashield (300 MHz for ^{1}H and 75 MHz for ^{13}C). Chemical shifts (δ) are reported in parts per million (ppm) and referenced to residual solvent or tetramethylsilane. Coupling constants (J) are reported in Hertz (Hz). Mass Spectra were recorded on a Waters LCT Premier Spectrometer (ESI) and Bruker Daltonics Autoflex (MALDI) spectrometers. Specific rotation [α] was determined using a polarimeter Jasco P1030. Elemental analyses were performed on a LECO CHNS 932 micro-analyzer at the Universidad Complutense de Madrid. Melting points were determined using a Büchi melting point apparatus. Single crystal X-ray diffraction data were recorded on a Bruker Kappa APEX II DUO diffractometer equipped with an APPEX 2 4K CCD area detector, a Microsource with Mo_{ka} radiation and an Oxford Cryostream 700 low temperature device (T = −173ºC).

Ligands **L1-L14**, $(Me_2S)AuCl$, $NaBAr_4^F$, alkynes and alkenes were purchased from commercial sources and used without further purification.

Synthetic Procedures and Analytical Data

General procedure for the synthesis of Josiphos gold(I) chloride complexes

$(Me_2S)AuCl$ was added to a solution of the corresponding phosphine in dry CH_2Cl_2 (0.09 M) under argon at 25 ºC. The solution was left stirring for 1 h and then concentrated under vacuum. The crude was purified by precipitation adding pentane or Et_2O to a CH_2Cl_2 solution of the crude or by flash column chromatography on silica gel.

Complex (S,R_P)-A

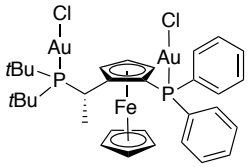

The digold chloride complex was synthesized according to the general procedure from (S,R_P)-**L1** (50 mg, 0.09 mmol) and $(Me_2S)AuCl$ (55 mg, 0.19 mmol). An orange solid was obtained in 72% yield (65 mg, 0.65 mmol) after recrystallization from a solution of CH_2Cl_2 with pentane.

mp 245-247 °C $[\alpha]_D = -58.2°$ (c = 0.32, 25 ºC), **^{1}H NMR** (400 MHz, $CDCl_3$) δ 7.88 – 7.78 (m, 2H), 7.77 – 7.67 (m, 2H), 7.60 – 7.45 (m, 5H), 7.45 – 7.39 (m, 1H), 4.82 (bs, 1H), 4.66 (bs, 1H), 4.38 – 4.21 (m, 1H), 4.16 (bs, 1H), 4.13 (s, 5H), 2.14 (dd, J (^{1}H-^{31}P) = 10.9, J = (^{1}H-^{1}H) 7.6 Hz, 3H), 1.53 (d, J (^{1}H-^{31}P) = 14.7 Hz, 9H), 0.99 (d, J (^{1}H-^{31}P) = 14.7 Hz, 9H). **^{13}C NMR** (100 MHz, $CDCl_3$) δ 135.4 (d, J (^{13}C-^{31}P) = 14.7 Hz), 133.8 (d, J (^{13}C-^{31}P) = 13.9 Hz), 132.4 (d, J (^{13}C-^{31}P) = 2.6 Hz), 131.9 (d, J (^{13}C-^{31}P) = 2.7 Hz), 130.4 (d, J (^{13}C-^{31}P) = 56.8 Hz), 130.0 (d, J (^{13}C-^{31}P) = 12.1 Hz), 129.4 (d, J (^{13}C-^{31}P) = 56.7), 129.0 (d, J (^{13}C-^{31}P) = 12.2 Hz), 102.1 (dd, J (^{13}C-^{31}P) = 16.6, 9.3 Hz), 73.9 (dd, J (^{13}C-^{31}P) = 6.7, 6.6 Hz), 72.5 (d, J (^{13}C-^{31}P) = 5.9 Hz), 72.0 (d, J (^{13}C-^{31}P) = 8.1 Hz), 71.0, 65.4 (dd, J (^{13}C-^{31}P) = 73.1, 2.5 Hz), 38.6 (d, J (^{13}C-^{31}P) = 18.1 Hz), 37.9 (d, J (^{13}C-^{31}P) = 23.5 Hz), 32.0 (d, J (^{13}C-^{31}P) = 5.1 Hz), 31.3 (dd, J (^{13}C-^{31}P) = 20.2, 4.9 Hz), 29.5 (d, J (^{13}C-^{31}P) = 4.7 Hz), 24.1 (d, J (^{13}C-^{31}P) = 3.1 Hz). **^{31}P NMR** (162 MHz, $CDCl_3$) δ 90.00, 23.89. **HRMS** (MALDI) calculated for $C_{32}H_{40}Au_2{}^{35}Cl_2{}^{56}FeP_2$ (M^+): 1006.0663; found: 1006.0647. **Elemental Analysis** calculated for $C_{32}H_{40}Au_2Cl_2FeP_2$: C, 38.16; H, 4.00; found: C, 38.06; H, 3.85.

Complex (S,R_P)-B

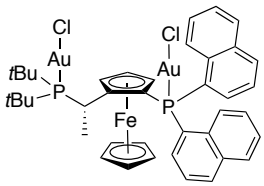

The digold chloride complex was synthesized according to the general procedure from (S,R_P)-**L7** (200 mg, 0.31 mmol) and $(Me_2S)AuCl$ (201 mg, 0.68 mmol, 2.2 equiv). The resulting solution was filtered through a Teflon disk, concentrated and layered with pentane. It was

allowed to stand in the fridge for 12 h. An orange solid was separated by decantation and washed with pentane (5 mL × 3). The orange solid was purified by flash column chromatography on silica gel (4:1 cyclohexane-ethyl acetate) and the product was obtained in 78% yield (269 mg, 0.25 mmol). X-ray quality crystals were obtained layering a solution of the mixture of complexes (*S*,R_P)-**B** and in (*S,R*$_P$)-**O** CH_2Cl_2 with hexane. NMR data for a mixture of conformers C1 and C2 in a ratio 70:30 (C1:C2) at 253K.

mp 228-229 ºC. **[α]$_D$** = + 83.9° (*c* = 0.09, $CHCl_3$, 25 ºC). **^{1}H NMR** (500 MHz, CD_2Cl_2, 253 K) δ 10.50 (C2, d, *J* = 8.6 Hz, 0.3H), 9.59 (C1, dd, *J* = 22.1, 7.2 Hz, 0.7H), 8.40 – 8.02 (C1 + C2, m, 4H), 8.02 – 7.70 (C1 + C2, m, 5H), 7.54 – 7.38 (C1 + C2, m, 2H), 7.35 (C1, ddd, *J* = 8.4, 6.9, 1.3 Hz, 1.4H), 7.19 (C2, t, *J* = 7.8 Hz, 0.6H), 5.12 (C2, bs, 0.3H), 5.02 (C1, bs, 0.7H), 4.72 (C2, bs, 0.3H), 4.67 (C1, bs, 0.7H), 4.62 – 4.52 (C1, m, 0.7H), 4.51 – 4.43 (C2, m, 0.3H), 4.40 (C1, bs, 0.7H), 4.03 (C1, s, 3H), 3.98 (C2, bs, 0.3H), 3.91 (C2, s, 2H), 2.23 (C1 + C2, dd, *J* = 11.0, 7.7 Hz, 3H), 1.62 (C1 + C2, d, *J* = 14.9 Hz, 9H), 1.00 (C1 +C2, m, 9H). **^{13}C NMR** (125 MHz, CD_2Cl_2, 253 K) δ 141.0 (C1 + C2), 140.7 (C1 +C2), 136.5 (C1 + C2), 135.4 (C1 +C2), 135.0 (C1 +C2), 134.8 – 134.4 (C1 +C2, m), 134.4 – 134.1 (C1 +C2, m), 133.9 – 133.8 (C2, m), 133.8 – 133.3 (C1, m), 133.2 (C1), 132.9 (C2), 132.3 (C1, d, *J* (^{13}C-^{31}P) = 12.7 Hz), 131.8 – 131.7 (C2, m), 129.9 (C1 + C2), 129.4 (C1 + C2), 128.1 – 127.8 (C1 + C2, m), 127.5 – 127.2 (C1 + C2, m), 127.0 (C2, d, *J* (^{13}C-^{31}P) = 12.0 Hz), 126.8 (C1, d, *J* (^{13}C-^{31}P) = 13.7 Hz), 126.2 (C2), 126.1 (C1), 125.6 – 125.5 (C1 + C2, m), 125.5 – 125.3 (C1 + C2, m), 125.3 – 125.1 (C1 +C2, m), 124.8 – 124.5 (C1 +C2, m), 104.11 – 101.72 (C1, m), 102.3 – 102.0 (C2, m), 76.6 – 76.1 (C2, m), 75.0 – 74.5 (C1, m), 72.6 – 72.1 (C1 + C2, m), 72.0 (C1, d, *J* = 8.1 Hz), 71.6 (C2, d, *J* (^{13}C-^{31}P) = 6.4 Hz), 71.3 (C1), 71.0 (C2), 66.9 (C2, d, *J* (^{13}C-^{31}P) = 80.27 Hz), 66.1 (C1, d, *J* (^{13}C-^{31}P) = 74.4 Hz), 38.9 – 37.8 (2C, C1 +C2, m), 32.0 (C1 +C2), 31.4 – 31.1 (C1, m), 31.0 – 30.9 (C2, m), 30.0 (C2), 29.6 (C1), 25.8 – 25.4 (C1 + C2, m). **^{31}P NMR** (202 MHz, $CDCl_3$, 253 K,) δ 89.42 (C2), 88.82 (C1), 23.26 (C1), −5.39 (C2). **HRMS** (ESI+) calculated for $C_{38}H_{52}Au_2Cl_2O_2FeP_2Na$ $(M+Na)^+$: 1145.1393; found: 1145.1365. **Elemental analysis** Anal. Calc. for $C_{40}H_{44}Au_2Cl_2FeP_2$, C, 43.38; H, 4.00; found: C, 43.59; H, 4.19.

Complex (*R*,*S*$_P$)-C

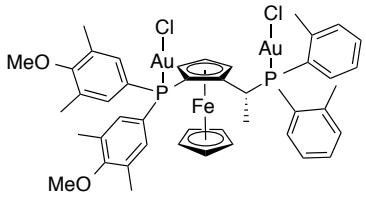

The digold chloride complex was synthetized according to the general procedure from (*R*,*S*$_P$)-**L11** (90 mg, 0.12 mmol) and $(Me_2S)AuCl$ (73.2 mg, 0.25 mmol). The desired complex was obtained as an orange solid in 89% yield (132 mg, 0.11 mmol) after flash column chromatography on silica gel (1:4 cyclohexane-CH_2Cl_2).

mp > 200 ºC. **[α]$_D$** = −102.4° (*c* = 0.10, $CHCl_3$, 25 ºC). **^{1}H NMR** (400 MHz, $CDCl_3$) δ 7.85-7.79 (m, 1H), 7.51 (dd, *J* (^{1}H-^{31}P) = 14.5, *J* (^{1}H-^{1}H) 7.7 Hz, 1H), 7.47-7.42 (m, 1H), 7.40-7.33 (m, 3H), 7.14-7.09 (m, 1H), 6.99-6.93 (m, 1H), 6.89 (d, *J* (^{1}H-^{31}P) = 13.4 Hz, 2H), 6.81 (t, *J* (^{1}H-^{1}H) = 7.8 Hz, 1H), 6.53 (dt, *J* (^{1}H-^{31}P) = 7.9, *J* (^{1}H-^{1}H) = 2.8 Hz, 1H), 5.31-5.28 (m, 2H), 4.60 (bs, 1H), 4.18 (bs, 1H), 4.03 (bs, 5H), 3.72 (s, 3H), 3.70 (s, 3H), 2.29 (s, 6H), 2.20 (s, 3H), 2.16 (s, 6H), 2.05 (dd, *J* (^{1}H-^{31}P) = 19.5, *J* (^{1}H-^{1}H) = 6.9 Hz, 3H), 1.85 (s, 3H). **^{13}C NMR** (100 MHz, $CDCl_3$) δ 160.2 (d, *J* (^{13}C-^{31}P) = 2.7 Hz), 159.9 (d, *J* (^{13}C-^{31}P) = 2.8 Hz), 141.8 (d, *J* (^{13}C-^{31}P) = 8.5 Hz), 141.6 (d, *J* (^{13}C-^{31}P) = 10.9 Hz), 136.4 (d, *J* (^{13}C-^{31}P) = 14.4 Hz), 135.1 (d, *J* (^{13}C-^{31}P) = 15.8 Hz), 133.4 (d, *J* (^{13}C-^{31}P) = 14.9 Hz), 132.9 (m), 132.2 (d, *J* (^{13}C-^{31}P) = 8.6 Hz), 132.0, 131.8 (m), 131.7, 131.6 (d, *J* (^{13}C-^{31}P) = 2.3 Hz), 131.2 (d, *J* (^{13}C-^{31}P) = 2.6 Hz), 127.1 (d, *J* (^{13}C-^{31}P) = 38.4 Hz), 127.0 (d, *J* (^{13}C-^{31}P) = 9.5 Hz), 126.6 (d, *J* (^{13}C-^{31}P) = 38.1 Hz), 125.7 (d, *J* (^{13}C-^{31}P) = 11.9 Hz), 125.6 (d, *J* (^{13}C-^{31}P) = 32.3 Hz), 125.0 (d, *J* (^{13}C-^{31}P) = 41.7 Hz), 96.1 (dd, *J* (^{13}C-^{31}P) = 17.1, 7.0 Hz), 73.2 (t, *J* (^{13}C-^{31}P) = 8.3 Hz), 72.3 (d, *J* (^{13}C-^{31}P) = 5.1 Hz), 71.2 (d, *J* (^{13}C-^{31}P) = 7.7 Hz), 70.9, 67.6 (dd, *J* (^{13}C-^{31}P) = 69.8, 2.9 Hz), 59.9, 59.6, 29.2 (dd, *J* (^{13}C-^{31}P) = 33.3, 4.6 Hz), 25.5 (d, *J* (^{13}C-^{31}P) = 8.1 Hz), 23.0 (d, *J* (^{13}C-^{31}P) = 8.2 Hz), 22.6 (d, *J* (^{13}C-^{31}P) = 11.0 Hz), 16.6, 16.5. **^{31}P{^{1}H} NMR** (162 MHz, $CDCl_3$) δ 36.60(bs), 20.96(s). **HRMS** (ESI+) calculated for $C_{44}H_{48}Au_2Cl_2O_2FeP_2Na$ $(M+Na)^+$: 1216.1080; found: 1216.1066. **Elemental analysis** calculated for $C_{44}H_{48}Au_2Cl_2O_2FeP_2.CH_2Cl_2$: C, 42.34; H, 4.06; found: C, 42.78; H, 4.06.

Complex (*R*,*S*$_P$)-D

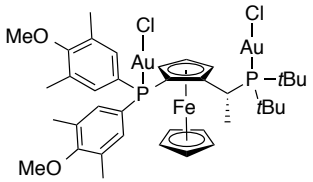

The digold chloride complex was synthetized according to the general procedure from (*R*,*S*$_P$)-L12 (89 mg, 0.14 mmol) and (Me_2S)AuCl (80 mg, 0.27 mmol). The desired complex was obtained as an orange solid in 72% yield (109 mg, 0.10 mmol) after flash column chromatography on silica gel (1:4 cyclohexane-CH_2Cl_2 to 100% CH_2Cl_2).

mp > 200 ºC. **[α]$_D$** = + 64.2° (*c* = 0.11, $CHCl_3$, 25 ºC). **^{1}H NMR** (400 MHz, $CDCl_3$) δ 7.45 (d, *J* (^{1}H-^{31}P) = 13.6 Hz, 2H), 7.29 (d, *J* (^{1}H-^{31}P) = 13.6 Hz, 2H), 4.88 – 4.82 (m, 1H), 4.66 – 4.59 (m, 1H), 4.18 – 4.07 (m, 7H), 3.77 (s, 3H), 3.67 (s, 3H), 2.33 (s, 6H), 2.31 (s, 6H), 2.19 (dd, *J* (^{1}H-^{31}P) = 11.1, *J* (^{1}H-^{1}H) = 7.6 Hz, 3H), 1.55 (d, *J* (^{1}H-^{31}P) = 15.5 Hz, 9H), 1.00 (d, *J* (^{1}H-^{31}P) = 14.8 Hz, 9H). **^{13}C NMR** (100 MHz, $CDCl_3$) δ160.4 (d, *J* (^{13}C-^{31}P) = 2.6 Hz), 160.2 (d, *J* (^{13}C-^{31}P) = 2.8 Hz), 135.8 (d, *J* (^{13}C-^{31}P) = 15.5 Hz), 134.0 (d, *J* (^{13}C-^{31}P) = 15.0 Hz), 132.7 (d, *J* (^{13}C-^{31}P) = 13.3 Hz), 132.0 (d, *J* (^{13}C-^{31}P) = 13.8 Hz), 125.4 (d, *J* (^{13}C-^{31}P) = 63.2 Hz), 124.5 (d, *J* (^{13}C-^{31}P) = 69.9 Hz), 102.8 – 101.9 (m), 74.5 (t, *J* (^{13}C-^{31}P) = 7.5 Hz), 72.6 (d, *J*

(^{13}C-^{31}P) = 6.1 Hz), 71.5 (d, *J* (^{13}C-^{31}P) = 8.3 Hz), 70.9, 67.0 - 66.3 (m), 60.0 , 59.8, 38.5 (d, *J* (^{13}C-^{31}P) = 18.4 Hz), 37.6 (d, *J* (^{13}C-^{31}P) = 23.4 Hz), 32.0 (d, *J* (^{13}C-^{31}P) = 5.1 Hz), 31.1 (dd, *J* (^{13}C-^{31}P) = 20.6, 4.5 Hz), 29.6 (d, *J* (^{13}C-^{31}P) = 4.8 Hz), 25.1 (d, *J* (^{13}C-^{31}P) = 2.9 Hz), 16.5, 16.4. **^{31}P{^{1}H} NMR** (162 MHz, $CDCl_3$) δ 91.09, 22.12. **HRMS** ESI(+) calculated for $C_{38}H_{52}Au_2Cl_2Na^{56}FeO_2P_2$ $(M+Na)^+$: 1145.1393; found: 1145.1365. **Elemental analysis** calculated for $C_{38}H_{52}Au_2Cl_2FeO_2P_2$: C, 40.63; H, 4.67; found: C, 40.26; H, 4.67.

Complex (*R*,*S*$_P$)-E

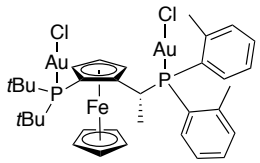

General procedure for the formation of digold chloride complexes afforded the desired complex as a crystalline orange solid in 71% yield (29.5 mg, 0.05 mmol) from the corresponding ligand (29.5 mg, 0.05 mmol) and $(Me_2S)AuCl$ (29.4 mg, 0.10 mmol) after precipitation with diethyl ether. The solid was separated by decantation and washed with 5 mL of dry diethyl ether (x3).

mp > 200 °C. **[α]$_D$** = + 76.4° (*c* = 0.1, $CHCl_3$, 25 ºC). **^{1}H NMR** (500 MHz, $CDCl_3$) δ 8.22 (bs, 1H), 7.47 - 7.38 (m, 2H), 7.33 - 7.28 (m, 2H), 7.25 - 7.21 (m, 1H), 7.18 - 7.14 (m, 1H), 6.97 - 6.91 (m, 1H), 5.67 - 5.63 (m, 1H), 4.94 - 4.83 (m, 1H), 4.59 - 4.55 (m, 1H), 4.54 (s, 4H), 4.47 (bs, 1H), 2.46 (s, 3H), 2.43 (bs, 3H), 1.86 (dd, *J* (^{1}H-^{31}P) = 20.0, 6.9 Hz, 3H), 1.78 (d, *J* = 16.1 Hz, 9H), 1.26 (d, *J* = 15.6 Hz, 9H). **^{13}C NMR** (125 MHz, $CDCl_3$) δ 142.5 (d, *J* (^{13}C-^{31}P) = 7.3 Hz), 142.2 (d, *J* (^{13}C-^{31}P) = 10.8 Hz), 133.1 (m), 132.9 (d, *J* (^{13}C-^{31}P) = 8.7 Hz), 132.5, 132.4, 131.5 (d, *J* (^{13}C-^{31}P) = 2.5 Hz), 127.4, 126.9, 126.8 (d, *J* (^{13}C-^{31}P) = 13.9 Hz), 125.6 (d, *J* (^{13}C-^{31}P) = 59.4 Hz), 125.3 (d, *J* (^{13}C-^{31}P) = 9.7 Hz), 96.28 (m), 74.4 (dd, *J* (^{13}C-^{31}P) = 15.1, 6.9 Hz), 73.22 (d, J (^{13}C-^{31}P) = 3.0 Hz), 72.1, 69.9 (d, *J* (^{13}C-^{31}P) = 6.4 Hz), 69.3 (dd, *J* (^{13}C-^{31}P) = 44.8, 8.3 Hz), 39.2 (d, *J* (^{13}C-^{31}P) = 29.0 Hz), 37.7 (d, *J* (^{13}C-^{31}P) = 29.4 Hz), 30.7 (d, *J* (^{13}C-^{31}P) = 5.7 Hz), 30.6 (d, *J* (^{13}C-^{31}P) = 5.7 Hz), 28.8 (m) 28.19 (d, *J* (^{13}C-^{31}P) = 7.3 Hz), 22.8, 22.7. **^{31}P{^{1}H} NMR** (203 MHz, $CDCl_3$) δ 59.70, 33.40 (bs). **HRMS (**MALDI+) Calc. for $C_{34}H_{44}Au_2Cl_2FeP_2$ $[M]^+$: 1034.0976 Found: 1034.1023 **Elemental analysis** Anal. Calc. for $C_{34}H_{44}Au_2Cl_2FeP_2$: C, 39.44; H, 4.53; found: C, 39.22; H, 4.53.

Complex (*R*,*S*$_P$)-F

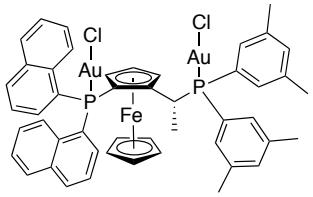

The digold chloride complex was synthetized according to the general procedure from the corresponding ligand (285 mg, 0.39 mmol) and $(Me_2S)AuCl$ (239 mg, 0.81 mmol). The

desired complex was obtained as an orange solid in 92% yield (429 mg, 0.36 mmol) after flash column chromatography on silica gel (9:1 to 3:2 cyclohexane-ethyl acetate).

mp 250-252 °C. **$[\alpha]_D$** = −99.5° (*c* = 0.15$_2$, 25 ºC). **^{1}H NMR** (500 MHz$_2$, 223 K) δ 10.51 (bd, *J* = 8.6 Hz, 1H, C1), 9.56 (dd, *J* (^{1}H-^{31}P) = 22.7, 7.3 Hz, 0.62H, C2), 8.39 (d, *J* = 8.5 Hz, 0.66H, C2), 8.17 – 7.85 (m, 9H), 7.80 – 7.77 (m, 1H), 7.63 (bd, *J* = 12.8 Hz, 2H), 7.54 – 7.12 (m, 14.8H), 7.06 – 7.01 (m, 1.6H), 6.88 – 6.84 (m, 0.54H, C2), 6.70 (s, 0.56H, C2), 6.54 – 6.49 (m, 1H, C1), 6.33 (s, 1H, C1), 5.57 – 5.55 (m, 1H, C1, C*H*P), 5.48 – 5.40 (m, 0.63H, C2, C*H*P), 5.19 (s, 1H, C1), 5.01 (s, 0.54H, C2), 4.73 (s, 1H, C1), 4.57 (s, 0.59H, C2), 4.45 (s, 0.54H, C2), 3.77 (s, 3.15H, C2), 3.58 (s, 4.45H, C1), 2.41 (s, 9.9H), 1.98 (s, 4.7H), 1.90 – 1.82 (m, 5H), 1.75 (s, 5H). **^{13}C NMR** (100 MHz$_2$) δ 139.2 (d, *J* (^{13}C-^{31}P) = 12.1 Hz, 2Cq), 138.4 (d, *J* (^{13}C-^{31}P) = 12.1 Hz, 2C2), 134.4 (d, *J* (^{13}C-^{31}P) = 7.6 Hz, Cq), 133.8 (d, *J* (^{13}C-^{31}P) = 2.6 Hz, CH), 133.7 (d, *J* (^{13}C-^{31}P) = 2.5 Hz, CH), 133.7 (Cq), 133.6 (CH), 132.2 (Cq), 132.1 (CH), 132.08 (CH), 131.9 (d, *J* (^{13}C-^{31}P) = 13.5 Hz, CH), 131.7 (d, *J* (^{13}C-^{31}P) = 2.5 Hz, CH), 131.5 (d, *J* (^{13}C-^{31}P) = 13.3 Hz, CH), 129.7 (d, *J* (^{13}C-^{31}P) = 1.8 Hz, CH), 129.2 (Cq), 128.9 (d, *J* (^{13}C-^{31}P) = 1.7 Hz, CH), 128.4 (Cq), 128.3 (Cq), 127.8, 127.7 (Cq), 127.4 (CH), 126.8 (d, *J* (^{13}C-^{31}P) = 17.8 Hz, CH), 126.4 (CH), 125.6 (d, *J* (^{13}C-^{31}P) = 11.3 Hz), 125.4 (d, *J* (^{13}C-^{31}P) = 11.2 Hz, CH), 125.1 (d, *J* (^{13}C-^{31}P) = 14.8 Hz, CH), 124.9 (d, *J* (^{13}C-^{31}P) = 14.6 Hz, CH), 96.5 (dd, *J* (^{13}C-^{31}P) = 16.7, 8.4 Hz, Cq, Cp), 73.8 (t, *J* (^{13}C-^{31}P) = 8.1 Hz, CH, Cp), 72.8 (d, *J* (^{13}C-^{31}P) = 5.4 Hz, CH, Cp,), 71.7 (d, *J* (^{13}C-^{31}P) = 8.0 Hz, CH, Cp), 70.8 (5CH, Cp), 68.2 (d, *J* (^{13}C-^{31}P) = 2.5 Hz, Cq. Cp), 67.5 (d, *J* (^{13}C-^{31}P) = 2.4 Hz, Cq, Cp), 31.8 – 30.8 (m, *C*HP), 23.6 (d, *J* (^{13}C-^{31}P) = 5.7 Hz, *C*H3P), 21.1 (2CH3), 20.6 (2CH3). **^{31}P{^{1}H} NMR** (202 MHz, CD_2Cl_2, 223 K) δ 54.41, 50.38, 22.97, −7.54. **HRMS (**ESI+) Calc. for $C_{48}H_{44}Au_2Cl_2FeP_2Na$ $[M+Na]^+$: 1225.0870 Found: 1225.0861 **Elemental analysis** Anal. Calc. for $C_{48}H_{44}Au_2Cl_2FeP_2$: C, 47.90; H, 3.69; found: C, 47.67; H, 3.63.

Complex (*S*,*R*$_P$)-F

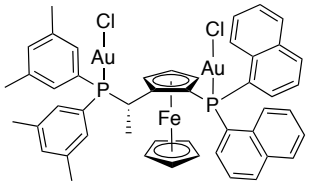

The digold chloride complex was synthetized according to the general procedure from the corresponding ligand (285 mg, 0.39 mmol) and (Me_2S)AuCl (239 mg, 0.81 mmol). The desired complex was obtained as an orange solid in 92% yield (429 mg, 0.36 mmol) after flash column chromatography on silica gel (9:1 to 3:2 cyclohexane-ethyl acetate). X-ray quality crystals were obtained layering a solution of the mixture of the complex in CH_2Cl_2 with methanol.

mp 266-268 °C. **[α]$_D$** = +88.38° (*c* = 0.15$_2$, 25 ºC). **HRMS** (ESI+) Calc. for $C_{48}H_{44}Au_2Cl_2FeP_2Na$ $[M+Na]^+$: 1225.0868 Found: 1225.0846 **Elemental analysis** Anal. Calc. for $C_{48}H_{44}Au_2Cl_2FeP_2$: C, 47.90; H, 3.69; found: C, 48.22; H, 3.79.

Complex *(S,R$_P$)*-O

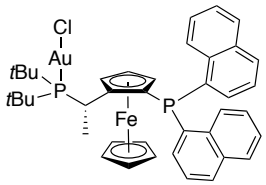

A solution of $(SMe_2)AuCl$ (18.3 mg, 0.06 mmol) in 10 mL of dry CH_2Cl_2 was added dropwise to a solution of (*S,R*$_P$)-**L7** (40 mg, 0.06 mmol) in 10 mL of dry CH_2Cl_2 under argon. It was stirred for 2 h at room temperature. The resulting solution was filtered through a Teflon disk, concentrated and layered with pentane. It was allowed to stand in the fridge for 12 h to give orange crystalline solid separated by decantation and washed with pentane (5mL × 3) (45 mg, 0.05 mmol, 87% yield). X-ray quality crystals were obtained layering a solution of the mixture of complexes (*S,R*$_P$)-**B** and (*S,R*$_P$)-**O** in CH_2Cl_2 with hexane.

mp 208-208 °C. **^{1}H NMR** (500 MHz, $CDCl_3$) δ 9.63 - 9.57 (m, 1H), 8.09 - 8.05 (m, 1H), 7.97 - 7.94 (m, 1H), 7.90 - 7.85 (m, 2H), 7.81 (ddd, ^3J (^{1}H-^{1}H) = 8.4, ^3J (^{1}H-^{1}H) = 6.8, 1.3 Hz, 1H), ^4J (^{1}H-^{31}P) = 7.79 - 7.74 (m, 3H), f, 7.56 (ddd, ^3J (^{1}H-^{1}H) = 6.9, ^3J (^{1}H-^{1}H) = 5.0, ^4J (^{1}H-^{31}P) = 1.3 Hz, 1H), 7.36 - 7.31 (m, 2H), 7.20 (ddd, ^3J (^{1}H-^{1}H) = 8.4, ^3J (^{1}H-^{1}H) = 6.9, ^4J (^{1}H-^{31}P) = 1.4 Hz, 1H), 4.74 - 4.71 (m, 1H), 4.62 (t, ^3J (^{1}H-^{1}H) = 2.6 Hz, 1H), 4.35 - 4.32 (m, 1H), 4.01 - 3.88 (m, 1H), 3.58 (s, 5H), 2.17 (dd, ^3J (^{1}H-^{31}P) = 11.3, ^3J (^{1}H-^{1}H) = 7.6 Hz, 3H), 1.57 (d, ^3J (^{1}H-^{31}P) = 14.6 Hz, 9H), 0.95 (d, ^3J (^{1}H-^{31}P) = 14.6 Hz, 9H). **^{13}C NMR** (125 MHz, $CDCl_3$) δ 136.5 (d, J (^{13}C-^{31}P) = 27.2 Hz), 135.5 (d, J (^{13}C-^{31}P) = 7.5 Hz), 134.8 (d, J (^{13}C-^{31}P) = 2.7 Hz), 134.5 (dd, J (^{13}C-^{31}P) = 5.5, 0.8 Hz), 134.0 (dd, J (^{13}C-^{31}P) = 22.1, 2.1 Hz), 133.8 - 133.8 (m), 133.4 (d, J (^{13}C-^{31}P) = 4.5 Hz), 129.9, 129.2 (d, J (^{13}C-^{31}P) = 2.2 Hz), 128.9 , 128.6 (d, J (^{13}C-^{31}P) = 2.0 Hz), 127.4 , 126.7 , 126.5 (d, J (^{13}C-^{31}P) = 2.7 Hz), 126.5 , 126.2 (d, J (^{13}C-^{31}P) = 2.1 Hz), 125.9 , 125.7 (d, J (^{13}C-^{31}P) = 1.1 Hz) 125.7 , 125.5 , 103.7 (dd, J (^{13}C-^{31}P) = 30.3, 9.5 Hz), 74.1 , 71.8 (dd, J (^{13}C-^{31}P) = 6.1, 3.8 Hz), 71.4 (d, J (^{13}C-^{31}P) = 3.8 Hz), 71.1 , 69.6 , 38.4 (d, J (^{13}C-^{31}P) = 18.4 Hz), 37.5 (d, J (^{13}C-^{31}P) = 23.0 Hz), 32.0 (d, J (^{13}C-^{31}P) = 5.3 Hz), 30.8 (dd, J (^{13}C-^{31}P) = 21.4, 17.5 Hz), 29.6 (d, J (^{13}C-^{31}P)= 3.5 Hz), 24.2. **^{31}P{^{1}H} NMR** (203 MHz, $CDCl_3$) δ 89.50, -50.88 (bs). **HRMS** (MALDI+) Calc. for $C_{40}H_{44}AuClFeP_2$ $[M]^+$: 874.1622 Found: 874.1619 **Elemental analysis** Anal. Calc. for $C_{40}H_{44}AuClFeP_2 \cdot CH_2Cl_2$: C, 51.30; H, 4.38; found: C, 51.73; H, 4.91.

General procedure for the preparation of alkenes.

Procedure A: To a stirred suspension of methyltriphenylphosphonium bromide in dry diethyl ether under argon was slowly added *n*-BuLi (2.5 M) at 0 ºC. After 1 h, the corresponding ketone was added and the mixture was stirred at 25 ºC until full conversion. The solution was poured into water and extracted with diethyl ether (×3). The combined organic layers were dried over $MgSO_4$ and the volatiles were removed under reduced pressure at 20 ºC. Purification by flash column chromatography on silica gel (100% pentane) afforded the entitled compounds.

Procedure B: To a stirred suspension of isopropyltriphenylphosphonium iodide in dry THF under argon was slowly added *n*-BuLi (2.5 M) at 0 ºC. After 1 h, the corresponding ketone was added and the mixture was heating under reflux until full conversion. The solution was poured into water and extracted with diethyl ether (×3). The combined organic layers were dried over $MgSO_4$ and the volatiles were removed under reduced pressure at 20 ºC. Purification by flash column chromatography on silica gel (two in a row, 100% pentane) afforded the entitled compounds.

***p*-Chloro-α-methylstyrene**[49]

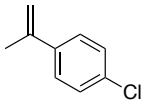

The title alkene was prepared following procedure A from methyltriphenylphosphonium bromide (9.0 g, 25.2 mmol), *n*BuLi (10.1 mL, 25.2 mmol) and 4-chloroacetophenone (3.2 g, 21 mmol). Colorless oil (1.1 g, 7.0 mmol, 33% yield).

^{1}H NMR (300 MHz, $CDCl_3$) δ 7.45 – 7.37 (m, 2H), 7.35 – 7.27 (m, 2H), 5.41 – 5.34 (m, 1H), 5.15 – 5.09 (m, 1H), 2.19 – 2.14 (m, 3H). **^{13}C NMR** (75 MHz, $CDCl_3$) δ 142.3, 139.8, 133.3, 128.5, 126.9, 113.1, 21.9. The physical data of the title alkene were identical to those previously reported.

***p*-Bromo-α-methylstyrene**[50]

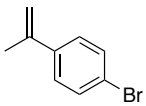

The title alkene was prepared following procedure A from methyltriphenylphosphonium bromide (6.4 g, 18 mmol), *n*BuLi (7.2 mL, 18 mmol) and 4-bromoacetophenone (3.0 g, 15 mmol). Colorless oil (744 mg, 3.75 mmol, 25% yield).

^{1}H NMR (400 MHz, $CDCl_3$) δ 7.49 – 7.43 (m, 2H), 7.38 – 7.30 (m, 2H), 5.42 – 5.33 (m, 1H), 5.12 (p, J = 1.5 Hz, 1H), 2.14 (bs, 3H). **^{13}C NMR** (101 MHz, $CDCl_3$) δ 142.3, 140.2, 131.4,

49 Gupton, J. T.; Layman, W. J. *JOC*, **1987**, *52*, 3683–3686.

50 Fryszkowka, A.; Fisher, K.; Gardiner, J. M.; Stephens, G. M. *JOC*, **2008**, *11*, 4295–4298.

127.3, 121.5, 113.2, 21.8. The physical data of the title alkene were identical to those previously reported.

***p-i*Propyl-α-methylstyrene**

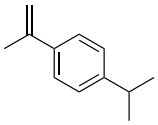

The title alkene was prepared following procedure A from methyltriphenylphosphonium bromide (8.6 g, 24 mmol), *n*BuLi (9.6 mL, 24 mmol) and 4-isopropylacetophenone (3.2 g, 20 mmol). Colorless oil (1.2 g, 7.4 mmol, 37% yield).

^{1}H NMR (400 MHz, $CDCl_3$) δ 7.49 – 7.43 (m, 2H), 7.27 – 7.22 (m, 2H), 5.41 – 5.38 (m, 1H), 5.09 (p, *J* = 1.5 Hz, 1H), 2.96 (hept, *J* = 6.9 Hz, 1H), 2.20 (dd, *J* = 1.5, 0.8 Hz, 3H), 1.31 (d, *J* = 6.9 Hz, 6H). **^{13}C NMR** (126 MHz, $CDCl_3$) δ 148.2, 143.2, 138.9, 126.4, 125.6, 111.8, 33.9, 24.1, 22.0.

***p-tert*-Butyl-α-methylstyrene**[51]

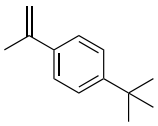

The title alkene was prepared following procedure A from methyltriphenylphosphonium bromide (11.6 g, 32.5 mmol), *n*BuLi (13 mL, 32.5 mmol) and 4-*tert*-butylacetophenone (4.8 g, 27 mmol). Colorless oil (3.1 g, 17.6 mmol, 65% yield).

^{1}H NMR (300 MHz, $CDCl_3$) *δ* 7.50 – 7.32 (m, 4H), 5.38 (dq, *J* = 1.5, 0.8 Hz, 1H), 5.07 (p, *J* = 1.5 Hz, 1H), 2.17 (dd, *J* = 1.5, 0.8 Hz, 3H), 1.35 (s, 9H). **^{13}C NMR** (75 MHz, $CDCl_3$) *δ* 150.5, 143.1, 138.4, 125.3, 125.3, 111.8, 34.6, 31.5, 21.9. The physical data of the title alkene were identical to those previously reported.

2-Phenyl-1-butene[52]

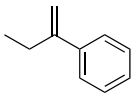

The title alkene was prepared following procedure A from methyltriphenylphosphonium bromide (15.93 g, 44.6 mmol), *n*BuLi (17.9 mL, 44.7 mmol) and propiophenone (5.0 g, 37.3 mmol). Colorless oil (3.45 g, 26.1 mmol, 70% yield).

^{1}H NMR (300 MHz, $CDCl_3$) *δ* 7.57 – 7.46 (m, 2H), 7.45 – 7.34 (m, 3H), 5.39 (dt, *J* = 1.6, 0.8 Hz, 1H), 5.17 (q, *J* = 1.6 Hz, 1H), 2.62 (qdd, *J* = 7.4, 1.6, 0.8 Hz, 2H), 1.21 (t, *J* = 7.4 Hz, 3H).

51 Gerst, M.; Ruechardt, C. *Tetrahedron Lett*., **1993**, *34*, 7733–7736.

52 Emer, E.; Brown, J. M.; Gouverneur, V. *Angew. Chem. Int. Ed.* **2014**, *52*, 4181–4185.

^{13}C NMR (75 MHz, $CDCl_3$) δ 150.2, 141.7, 128.4, 127.4, 126.1, 111.1, 28.2, 13.1. The physical data of the title alkene were identical to those previously reported.

2-Cyclohexyl-1-propene[53]

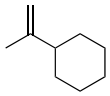

The title alkene was prepared following procedure A from methyltriphenylphosphonium bromide (16.9 g, 47.4 mmol), *n*BuLi (19 mL, 47.4 mmol) and 1-cyclohexylethan-1-one (5.0 g, 39.6 mmol). Colorless oil (2.8 g, 22.6 mmol, 57% yield).

^{1}H NMR (300 MHz, $CDCl_3$) δ 4.60 – 4.56 (m, 2H), 1.85 – 1.64 (m, 6H), 1.63 (t, J = 1.2 Hz, 3H), 1.30 – 1.00 (m, 5H). **^{13}C NMR** (75 MHz, $CDCl_3$) δ 151.2, 108.0, 45.8, 32.2, 26.9, 26.6, 21.0. The physical data of the title alkene were identical to those previously reported.

(4-Methylpent-3-en-1-yl)benzene[54]

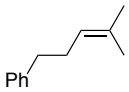

The title alkene was prepared following procedure B from isopropyltriphenylphosphonium bromide (6.4 g, 14.8 mmol), *n*BuLi (10.7 mL, 26.8 mmol) and 1-cyclohexylethan-1-one (1.8 g, 13.4 mmol). Colorless oil (456 mg, 2.8 mmol, 21% yield).

^{1}H NMR (500 MHz, $CDCl_3$) δ 7.30 – 7.24 (m, 2H), 7.21 – 7.12 (m, 3H), 5.21 – 5.13 (m, 1H), 2.67 – 2.58 (m, 2H), 2.35 – 2.24 (m, 2H), 1.68 (s, 3H), 1.56 (s, 3H).**^{13}C NMR** (126 MHz, $CDCl_3$) δ 142.6, 132.3, 128.6, 128.4, 125.8, 123.9, 36.3, 30.2, 25.8, 17.8. The physical data of the title alkene were identical to those previously reported.

***p*-Cyclopropyl-α-methylstyrene**

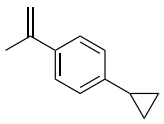

The title alkene was prepared following procedure A from methyltriphenylphosphonium bromide (7.0 g, 19.5 mmol), *n*BuLi (7.8 mL, 19.5 mmol) and 1-(4-cyclopropylphenyl)-ethanone (2.4 g, 15 mmol). Colorless oil (1.5 g, 9.1 mmol, 61% yield).

^{1}H NMR (500 MHz, $CDCl_3$) δ 7.49 – 7.28 (m, 2H), 7.14 – 6.93 (m, 2H), 5.41 – 5.30 (m, 1H), 5.10 – 4.99 (m, 1H), 2.17 (s, 3H), 1.99 – 1.85 (m, 1H), 1.06 – 0.91 (m, 2H), 0.80 – 0.65 (m, 2H). **^{13}C NMR** (126 MHz, $CDCl_3$) δ 143.5, 143.1, 138.5, 125.6, 125.5, 111.6, 22.0, 15.3, 9.4.

53 Young, P. C.; Hadfield, M. S.; Arrowsmith, L.; Macleod, K. M.; Mudd, R. J.; Jordan-Hore, J. A.; Lee, A. *Org. Lett.* **2012**, *14*, 898–901.

54 Schevenels, F. T.; Shen, M.; Snyder, S. A. *Org. Lett.*, **2017**, *19*, 2–5.

General procedure for the enantioselective gold(I)-catalyzed [2+2] cycloaddition of alkynes with alkenes.

Unless otherwise stated, cyclobutenes were prepared following procedure A, B or C.

Procedure A

Alkyne (0.3 mmol) and alkene (0.05 mmol) were added to a solution of (S,R_P)-**B** (2.5 mol %) in chlorobenzene (0.5 M), followed by the addition of $NaBAr_4^F$ (2.5 mol %) at -20 ºC. Alkene (0.55 mmol) was added slowly to the mixture over 1-12 h. The reaction was quenched adding a drop of NEt_3 when no alkyne was observed by GCMS or TLC. Purification by flash column chromatography or preparative TLC (silica gel) afforded the corresponding cyclobutenes.

Procedure B

Alkyne (0.3 mmol) and alkene (1.2 mmol) were added to a solution of (S,R_P)-**B** (2.5 mol %) in chlorobenzene (0.5 M) followed by the addition of $NaBAr_4^F$ (2.5 mol %) to the resulting solution at -20 ºC. The reaction was quenched adding a drop of NEt_3 when no alkyne was observed by GCMS or TLC. Purification by flash column chromatography or preparative TLC (silica gel) afforded the corresponding cyclobutenes.

Procedure C

Alkyne (0.3 mmol) and alkene (1.8 mmol) were added to a solution of (R,S_P)-**F** (5 mol %) in chlorobenzene (0.5 M) followed by the addition of $NaBAr_4^F$ (5 mol %) to the resulting solution at -20 ºC. The reaction was quenched adding a drop of NEt_3 when no alkyne was observed by GCMS or TLC. Purification by flash column chromatography or preparative TLC (silica gel) afforded the corresponding cyclobutenes.

The physical data for cyclobutenes **3a, c, e-g**[25] and **3h-i**[8] are identical to those previously reported.

Table 11. Remaining data for reported cyclobutenes **3a, c, e-i**.

Entry[a]	Cyclobutene	Procedure	$[\alpha]_D$ ($degcm^2g^{-1}$)	Yield (%)[a]	*er*[b]
1	**3a**	A	−34.3 (c = 0.23, $CHCl_3$, 27 ºC)	70	90:10
2	**3c**	A	−48.5 (c = 1, $CHCl_3$, 26 ºC)	82	82:18
3	**3e**	A	−65.7 (c = 0.95, $CHCl_3$, 27 ºC)	47	93:7
4	**3f**	B	−55.0 (c = 1, $CHCl_3$, 27 ºC)	45	93:7
5	**3g**	A	−48.5 (c = 1, $CHCl_3$, 26 ºC)	74	90:10
6	**3h**	A	−61.7 (c = 0.75, $CHCl_3$, 27 ºC)	60	91:9
7	**3i**	A	−10.3 (c = 0.55, $CHCl_3$, 26 ºC)	78	84:16

[a] Isolated yield. Average of two runs. [b] Enantiomeric ratio determined by UPC2.

(*R*)-3-Phenyl-1-[(1,1'-diphenyl)-4-yl]-3-methyl-cyclobut-1-ene (3b)

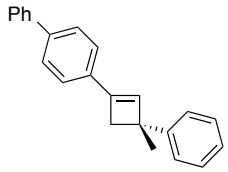

Cyclobutene **3b** was synthetized following procedure A, from (1,1'-biphenyl-4-yl)-acetylene (0.15 mmol, 27 mg) and α-methylstyrene (0.3 mmol, 35mg, 39 μL). The reaction time was 72 h. The crude was purified by silica gel flash column chromatography using pentane as eluent to afford **3b** as a white solid (25 mg, 0.086 mmol, 57% yield), 91:9 *er*.

mp 140.7-143.8 °C, $[\alpha]_D = -61.8$ ° (*c* = 1, $CHCl_3$, 25 ºC). **^{1}H NMR** (300 MHz, $CDCl_3$) δ 7.65 – 7.57 (m, 4H), 7.51 – 7.40 (m, 6H), 7.40 – 7.31 (m, 3H), 7.25 – 7.18 (m, 1H), 6.78 (s, 1H), 3.03 (d, *J* = 12.5 Hz, 1H), 2.96 (d, *J* = 12.5 Hz, 1H), 1.67 (s, 3H). **^{13}C NMR** (75 MHz, $CDCl_3$) δ 147.7, 143.5, 140.8, 140.5, 134.0, 133.7, 128.8, 128.2, 127.4, 127.1, 127.0, 125.9, 125.7, 125.1, 46.1, 44.4, 27.6. **HRMS** (APCI+) Calc. for $C_{23}H_{21}$ $[M+H]^+$: 297.1638 Found: 297.1652.

(*R*)-3-Phenyl-1-*p*-*tert*butylphenyl-3-methylcyclobut-1-ene (3d)

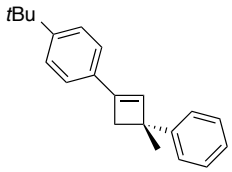

Cyclobutene **3d** was synthetized following procedure A, from 4-*tert*-butylphenylacetylene (0.3 mmol, 47.5 mg, 53 μL) and α-methylstyrene (0.6 mmol, 70.9 mg, 78 μL). The reaction time was 30 h. The crude was purified by silica gel flash column chromatography using pentane as eluent to afford **3d** as a colorless oil (66 mg, 0.240 mmol, 80% yield), 87:13 *er*.

$[\alpha]_D = -48.5$ ° (*c* = 1, $CHCl_3$, 26 ºC). **^{1}H NMR** (300 MHz, $CDCl_3$) δ 7.42 – 7.27 (m, 8H), 7.21 – 7.14 (m, 1H), 6.66 (s, 1H), 2.94 (d, *J* = 12.5 Hz, 1H), 2.88 (d, *J* = 12.5, 1H), 1.61 (s, 3H), 1.31 (s, 9H). **^{13}C NMR** (75 MHz, $CDCl_3$) δ 151.1, 147.9, 143.8, 133.1, 132.2, 128.2, 126.0, 125.8, 125.4, 124.5, 46.0, 44.5, 34.8, 31.4, 27.6. **HRMS** (APCI+) Calc. for $C_{20}H_{21}$ $[M-CH_3]^+$: 261.1638 Found: 277.1951.

(*R*)-3-Phenyl-1-*p*-tolyl-3-methylcyclobut-1-ene (3p)

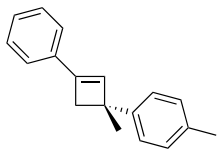

Cyclobutene **3p** was synthetized following procedure B at 25 ºC, from phenylacetylene (0.3 mmol, 31 mg, 33 μL) and α-methyl-*p*-methylstyrene (1.2 mmol, 159 mg, 0.175 μL). The reaction time was 24 h. The crude was purified by silica gel flash column chromatography using pentane as eluent to afford **3p** as a white solid (40 mg, 0.171 mmol, 57% yield), 89:11 *er*.

mp 57-59 °C, **[α]$_D$** = −31.6 ° (*c* = 1, $CHCl_3$, 25 ºC). **^{1}H NMR** (400 MHz, CD_2Cl_2) *δ* 7.44 – 7.38 (m, 2H), 7.37 – 7.24 (m, 5H), 7.18 – 7.13 (m, 2H), 6.73 (s, 1H), 2.96 (d, *J* = 12.5 Hz, 1H), 2.91 (d, *J* = 12.5 Hz, 1H), 2.35 (s, 3H), 1.67 – 1.60 (m, 3H). **^{13}C NMR** (100 MHz, CD_2Cl_2) *δ* 145.3, 144.3, 135.7, 135.4, 134.6, 129.3, 128.9, 128.3, 126.3, 125.1, 46.2, 44.7, 28.1, 21.3. **HRMS** (APCI+) Calc. for $C_{18}H_{19}$ $[M+H]^+$: 235.1481 Found: 235.1476.

(*R*)-1-Isopropyl-4-(1-methyl-3-phenylcyclobut-2-en-1-yl)benzene (3q)

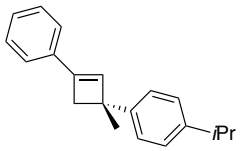

Cyclobutene **3q** was synthetized following procedure B at 25 ºC, from phenylacetylene (0.2 mmol, 20.4 mg) and *p*-*i*propyl-α-methylstyrene (0.4 mmol, 64.1 mg). The reaction time was 3 h. The crude was purified by silica gel flash column chromatography using pentane as eluent (two columns in a row) to give **3q** as a colorless oil (27 mg, 0.104 mmol, 52% yield), 88:12 *er*.

[α]$_D$ = −28.6 ° (*c* = 1.00, $CHCl_3$, 26 ºC). **^{1}H NMR** (500 MHz, $CDCl_3$) *δ* 7.43 – 7.36 (m, 2H), 7.36 – 7.30 (m, 4H), 7.29 – 7.23 (m, 1H), 7.22 – 7.16 (m, 2H), 6.72 (s, 1H), 2.97 (d, *J* = 12.4 Hz, 1H), 2.94 – 2.87 (m, 2H), 1.63 (s, 3H), 1.25 (d, *J* = 6.9 Hz, 6H). **^{13}C NMR** (126 MHz, $CDCl_3$) *δ* 146.3, 145.1, 143.9, 135.0, 134.2, 128.4, 127.9, 126.3, 125.9, 124.7, 45.8, 44.5, 33.8, 27.6, 24.2. **HRMS** (ESI+) Calc. for $C_{20}H_{23}$ $[M+H]^+$: 263.1794 Found: 263.1792.

(*R*)-3-*p*-*tert*-Butylphenyl-1-phenyl-3-methylcyclobut-1-ene (3r)

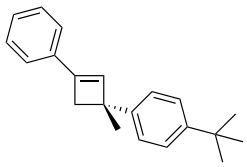

Cyclobutene **3r** was synthetized following procedure B at 25 ºC, from phenylacetylene (0.3 mmol, 33 μL) and 2-methyl-2-(4-*tert*-butyl)ethene (1.2 mmol, 209 mg). The reaction time was 20 h. The crude was purified by silica gel flash column chromatography using pentane as eluent to give **3r** as a white solid (74 mg, 0.267 mmol, 89% yield), 88:12 *er*.

mp 79-84 °C, **[α]$_D$** = −24.0 ° (*c* = 0.45, $CHCl_3$, 25 ºC). **^{1}H NMR** (400 MHz, $CDCl_3$) *δ* 7.43 – 7.39 (m, 2H), 7.38 – 7.33 (m, 6H), 7.30 – 7.26 (m, 1H), 6.74 (s, 1H), 2.99 (d, *J* = 12.4 Hz, 1H), 2.91 (d, *J* = 12.4 Hz, 1H), 1.65 (s, 3H), 1.34 (s, 9H). **^{13}C NMR** (75 MHz, $CDCl_3$) *δ* 148.6, 144.7, 143.9, 134.9, 134.2, 128.4, 127.9, 125.7, 125.1, 124.7, 45.7, 44.4, 34.5, 31.6, 27.5. **HRMS** (APCI+) Calc. for $C_{21}H_{25}$ $[M+H]^+$: 277.1951 Found: 277.1948.

(*R*)-3-*p*-Fluorophenyl-1-phenyl-3-methylcyclobut-1-ene (3s)

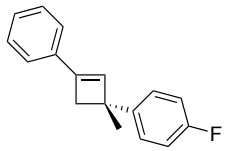

Cyclobutene **3s** was synthetized following procedure A, from phenylacetylene (0.3 mmol, 30.6 mg, 33 μL) and 2-(4-fluorophenyl)-1-propene (0.6 mmol, 82 mg, 81 μL). The reaction time was 40 h. The crude was purified by silica gel flash column chromatography using pentane as eluent to afford **3s** as a colorless oil (51 mg, 0.216 mmol, 72% yield), 91:9 *er*.

[α]$_D$ = −59.9 ° (*c* = 0.5, $CHCl_3$, 27 ºC). **^{1}H NMR** (300 MHz, $CDCl_3$) *δ* 7.50 – 7.34 (m, 6H), 7.34 – 7.28 (m, 1H), 7.12 – 6.96 (m, 2H), 6.73 (s, 1H), 3.00 – 2.92 (m, 2H), 1.66 (s, 3H). **^{13}C NMR** (75 MHz, $CDCl_3$) *δ* 161.2 (d, *J* (^{13}C-^{19}F) = 243.5 Hz), 144.1, 143.5 (d, *J* (^{13}C-^{19}F) = 3.1 Hz), 134.7, 133.6, 128.5, 128.1, 127.5 (d, *J* (^{13}C-^{19}F) = 7.8 Hz), 124.7, 114.9 (d, *J* (^{13}C-^{19}F) = 21.1 Hz), 45.6, 44.5, 27.7. **^{19}F{^{1}H} NMR** (376 MHz, $CDCl_3$) *δ* -117.94. **HRMS** (APCI+) Calc. for $C_{17}H_{16}F$ $[M+H]^+$: 239.1231 Found: 239.1226.

(*R*)-1-Chloro-4-(1-methyl-3-phenylcyclobut-2-en-1-yl)benzene (3t)

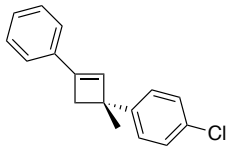

Cyclobutene **3t** was synthetized following procedure B, from phenylacetylene (0.2 mmol, 20.4 mg) and *p*-chloro-α-methylstyrene (0.4 mmol, 61 mg). The reaction time was 12 h. The crude was purified by silica gel flash column chromatography using pentane as eluent to give **3t** as a white solid (49.7 mg, 0.192 mmol, 98% yield), 86:14 *er*.

mp 61.8-63.5 °C, **[α]$_D$** = −35.4 ° (*c* = 1.00, $CHCl_3$, 26 ºC). **^{1}H NMR** (500 MHz, $CDCl_3$) *δ* 7.42 – 7.39 (m, 2H), 7.38 – 7.32 (m, 4H), 7.31 – 7.27 (m, 3H), 6.69 (s, 1H), 2.93 (s, 2H), 1.63 (s, 3H). **^{13}C NMR** (126 MHz, $CDCl_3$) *δ* 146.3, 144.2, 134.6, 133.4, 131.6, 128.5, 128.3, 128.1, 127.5, 124.8, 45.7, 44.5, 27.4. **HRMS** (ESI+) Calc. for $C_{17}H_{16}Cl$ $[M+H]^+$: 255.0935 Found: 255.0943.

(*R*)-1-Bromo-4-(1-methyl-3-phenylcyclobut-2-en-1-yl)benzene (3u)

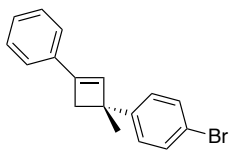

Cyclobutene **3u** was synthetized following procedure B, from phenylacetylene (0.2 mmol, 20.4 mg) and *p*-bromo-α-methylstyrene (0.4 mmol, 79 mg). The reaction time was 12 h. The crude was purified by silica gel flash column chromatography using pentane as eluent to give **3u** as a white solid (31 mg, 0.104 mmol, 52% yield), 87:13 *er*.

mp 68.7-71.5 °C, **[α]$_D$** = −25.0 ° (*c* = 1.00, $CHCl_3$, 26 ºC). **^{1}H NMR** (400 MHz, Chloroform-*d*) δ 7.47 – 7.43 (m, 2H), 7.42 – 7.39 (m, 2H), 7.36 (ddd, *J* = 7.9, 6.7, 0.9 Hz, 2H), 7.32 – 7.26

(m, 3H), 6.69 (s, 1H), 2.93 (s, 2H), 1.63 (s, 3H). **^{13}C NMR** (101 MHz, Chloroform-*d*) δ 146.8, 144.2, 134.6, 133.3, 131.3, 128.5, 128.1, 127.9, 124.8, 119.6, 45.7, 44.4, 27.4. **HRMS** (ESI+) Calc. for $C_{17}H_{16}Br$ $[M+H]^+$: 299.0430 Found: 299.0422.

(*R*)-3-Phenyl-1-phenyl-3-ethylcyclobut-1-ene (3v)

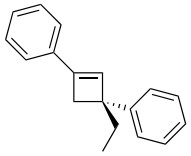

Cyclobutene **3v** was synthetized following procedure A, from phenylacetylene (0.3 mmol, 30.6 mg, 33 μL) and 2-phenyl-1-butene (0.6 mmol, 79 mg). The reaction time was 96 h. The crude was purified by silica gel column chromatography using pentane as eluent to give **3v** as a colorless oil (58 mg, 0.25 mmol, 83% yield), 83:17 *er*.

[α]$_D$ = −78.6 º (*c* = 1, $CHCl_3$, 26 ºC). **^{1}H NMR** (300 MHz, $CDCl_3$) *δ* 7.49 – 7.43 (m, 2H), 7.43 – 7.35 (m, 6H), 7.34 – 7.22 (m, 2H), 6.91 (s, 1H), 3.00 (m, 2H), 2.08 (dq, *J* = 13.3, 7.4 Hz, 1H), 1.90 (dq, *J* = 13.3, 7.4 Hz, 1H), 0.91 (t, *J* = 7.4 Hz, 3H). **^{13}C NMR** (75 MHz, $CDCl_3$) *δ* 146.3, 144.5, 134.8, 131.7, 128.4, 128.0, 127.9, 126.9, 125.7, 124.7, 50.7, 42.4, 34.4, 10.4. **HRMS** (APCI+) Calc. for $C_{18}H_{19}$ $[M+H]^+$: 235.1481 Found: 235.1474.

(*R*)-3-Cyclohexyl-1-phenyl-3-methylcyclobut-1-ene (3w)

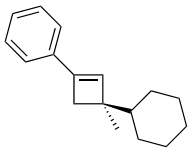

Cyclobutene **3w** was synthetized following procedure B at 25 ºC, from phenylacetylene (0.3 mmol, 30.6 mg, 33 μL) and 2-cyclohexyl-1-propene (1.2 mmol, 149 mg). The reaction time was 24 h. The crude was purified by silica gel flash column chromatography (two in a row, first using pentane and then using cyclohexane as eluents), to give **3w** as a colorless oil (46 mg, 0.201 mmol, 67% yield), 64:36 *er*.

[α]$_D$ = + 8.3 ° (*c* = 0.3, $CHCl_3$, 25 ºC). **^{1}H NMR** (300 MHz, $CDCl_3$) *δ* 7.39 – 7.28 (m, 4H), 7.26 – 7.19 (m, 1H), 6.51 (s, 1H), 2.58 (d, *J* = 12.5 Hz, 1H), 2.33 (d, *J* = 12.5 Hz, 1H), 1.86 – 1.59 (m, 5H), 1.49 – 0.96 (m, 6H), 1.16 (s, 3H). **^{13}C NMR** (75 MHz, $CDCl_3$) *δ* 143.1, 136.1, 135.4, 128.4, 127.5, 124.4, 46.5, 46.0, 40.0, 28.7, 28.5, 27.0, 27.0, 26.8, 20.4. **HRMS** (APCI+) Calc. for $C_{17}H_{23}$ $[M]^+$: 227.1794 Found: 227.1787.

(*R*)-3-Phenyl-1-phenyl-cyclobut-1-ene (3x)

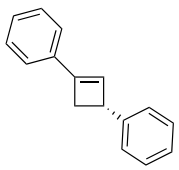

Cyclobutene **3x** was synthetized following procedure A at 25ºC, from phenylacetylene (0.3 mmol, 31 mg, 33 µL) and styrene (1.2 mmol, 125 mg, 138 µL). The reaction time was 72 h. The crude was purified by silica gel column chromatography using pentane as eluent to afford **3x** as a colorless oil (33 mg, 0.160 mmol, 53% yield), 66:34 *er*.

[α]$_D$ = + 4.4 ° (*c* = 0.25, $CHCl_3$, 27 ºC). **^{1}H NMR** (500 MHz, $CDCl_3$) δ 7.45 – 7.41 (m, 2H), 7.38 – 7.34 (m, 2H), 7.33 – 7.26 (m, 5H), 7.24 – 7.19 (m, 1H), 6.55 (d, *J* = 1.3 Hz, 1H), 4.02 (dt, *J* = 4.9, 1.5 Hz, 1H), 3.32 (dd, *J* = 12.8, 4.8 Hz, 1H), 2.67 (dd, *J* = 12.8, 1.9 Hz, 1H). **^{13}C NMR** (125 MHz, $CDCl_3$) δ 146.6, 143.9, 134.6, 129.8, 128.5, 128.5, 128.0, 126.9, 126.4, 124.8, 43.1, 38.6. **HRMS** (APCI+) Calc. for $C_{16}H_{13}$ $[M]^+$: 205.1012 Found: 205.1009.

(*R*)-3-*p*-*tert*-Butylphenyl-1-*p*-*tert*-butylphenyl-3-methylcyclobut-1-ene (3z)

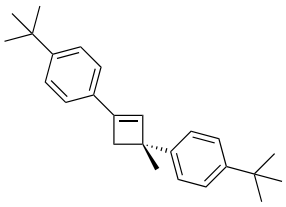

Cyclobutene **3z** was synthetized following procedure B, from 4-*tert*-butylphenylacetylene (0.3 mmol, 47 mg) and *p*-tert-butyl-α-methylstyrene (1.2 mmol, 209 mg). The reaction time was 40 h. The crude was purified by silica gel flash column chromatography using pentane as eluent to give **3u** as a white solid (63 mg, 0.189 mmol, 63% yield), 89:11 *er*. X-ray quality crystals were obtained by slow evaporation of a CH_2Cl_2 solution of **3z**.

mp 51-54 °C, **[α]$_D$** = −23.6 ° (*c* = 1, $CHCl_3$, 25 ºC). **^{1}H NMR** (300 MHz, $CDCl_3$) δ 7.44 – 7.33 (m, 8H), 6.69 (s, 1H), 2.99 (d, *J* = 12.5 Hz, 1H), 2.90 (d, *J* = 12.5 Hz, 1H), 1.66 (s, 3H), 1.40 – 1.32 (m, 18H). **^{13}C NMR** (75 MHz, $CDCl_3$) δ 151.0, 148.5, 144.8, 143.8, 133.5, 132.3, 125.7, 125.4, 125.1, 124.5, 45.6, 44.6, 34.8, 34.5, 31.6, 31.5, 27.4. **HRMS** (APCI+) Calc. for $C_{25}H_{33}$ $[M+H]^+$: 333.2577 Found: 333.2563.

(*R*)-3-*p*-*tert*-Butylphenyl-1-(thiophen-3-yl)-3-methylcyclobut-1-ene (3aa)

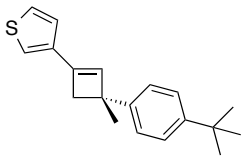

Cyclobutene **3aa** was synthetized following procedure B, from 3-ethynylthiophene (0.3 mmol, 32.4 mg) and *p*-*tert*-butyl-α-methylstyrene (1.2 mmol, 209 mg). The reaction time was 24 h. The crude was purified by silica gel flash column chromatography using pentane as eluent to give **3v** as a white solid (47.2 mg, 0.167 mmol, 56% yield), 94:6 *er*. X-ray quality crystals were obtained by slow evaporation of a CH_2Cl_2 solution of **3aa**.

mp 107-110 °C, **[α]$_D$** = + 11.3 ° (*c* = 1.00, $CHCl_3$, 25 ºC). **^{1}H NMR** (300 MHz, $CDCl_3$) δ 7.40 – 7.32 (m, 4H), 7.29 (dd, *J* = 5.1, 2.2 Hz, 1H), 7.22 (dd, *J* = 5.1, 1.2 Hz, 1H), 7.16 (dd, *J* = 2.9, 1.2 Hz, 1H), 6.50 (s, 1H), 2.97 (d, *J* = 12.5 Hz, 1H), 2.89 (d, *J* = 12.5 Hz, 1H), 1.65 (s, 3H),

1.34 (s, 9H). **^{13}C NMR** (75 MHz, $CDCl_3$) δ 148.6, 144.7, 139.3, 138.0, 133.1, 126.0, 125.6, 125.1, 125.1, 121.0, 46.8, 45.2, 34.5, 31.6, 27.6. **HRMS** (APCI+) Calc. for $C_{19}H_{23}S$ $[M+H]^+$: 283.1515 Found: 283.1515.

(*R*)-3-*p*-Fluorophenyl-1-*p*-*tert*butylphenyl-3-methylcyclobut-1-ene (3ab)

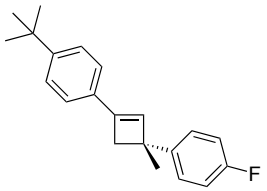

Cyclobutene **3ab** was synthetized following procedure B, from 4-*tert*-butylphenylacetylene (0.3 mmol, 47.5 mg, 53 µl) and methyl-2-(4-fluoro)-ethene (1.2 mmol, 163 mg). The reaction time was 20 h. The crude was purified by silica gel flash column chromatography using pentane as eluent to obtain **3ab** as a yellowish oil (74.7 mg, 0.254 mmol, 85% yield), 87:13 *er*.

$[\alpha]_D$ = −49.4 ° (*c* = 1.00, $CHCl_3$, 25 ºC). **^{1}H NMR** (300 MHz, $CDCl_3$) δ 7.45 – 7.33 (m, 6H), 7.06 – 6.97 (m, 2H), 6.66 (s, 1H), 2.95 – 2.89 (m, 2H), 1.64 (s, 3H), 1.36 (s, 9H). **^{13}C NMR** (101 MHz, $CDCl_3$) δ 161.2 (d, J (^{13}C-^{19}F) = 243.5 Hz), 151.3, 143.9, 143.6 (d, J (^{13}C-^{19}F) = 3.1 Hz), 132.9, 132.0, 127.4 (d, J (^{13}C-^{19}F) = 7.7 Hz), 125.4, 124.5, 114.9 (d, J (^{13}C-^{19}F) = 21.1 Hz), 45.5, 44.7, 34.8, 31.4, 27.6. **^{19}F NMR** (376 MHz, $CDCl_3$) δ −118.04 . **HRMS** (APCI+) Calc. for $C_{21}H_{24}F$ $[M+H]^+$: 295.1857 Found: 295.1852.

(*R*)-3-*p*-Fluorophenyl-1-*p*-chlorophenyl-3-methylcyclobut-1-ene (3ac)

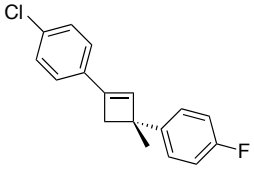

Cyclobutene **3ac** was synthetized following procedure B, from 4-chlorophenylacetylene (0.3 mmol, 41 mg) and 2-methyl-2-(4-fluorophenyl)-ethene (1.2 mmol, 163 mg, 162 µl). The reaction time was 72 h. The crude was purified by silica gel flash column chromatography using cyclohexane as eluent to obtain **3ac** as a white solid (30 mg, 0.111 mmol, 37% yield), 91:9 *er*.

m.p. 59.9-63.0 °C, **$[\alpha]_D$** = −68.0 ° (*c* = 1, $CHCl_3$, 26 ºC).**^{1}H NMR** (400 MHz, $CDCl_3$) δ 7.36 – 7.31 (m, 2H), 7.31 (s, 4H), 7.04 – 6.96 (m, 2H), 6.69 (s, 1H), 2.93 – 2.86 (m, 2H), 1.61 (s, 3H). **^{13}C NMR** (101 MHz, $CDCl_3$) δ 161.3 (d, J (^{13}C-^{19}F) = 243.8 Hz), 143.2 (d, J (^{13}C-^{19}F) = 3.2 Hz), 143.0, 134.3, 133.8, 133.2, 128.7, 127.4 (d, J (^{13}C-^{19}F) = 7.9 Hz), 126.1, 115.0 (d, J (^{13}C-^{19}F) = 21.0 Hz), 45.7, 44.4, 27.7. **^{19}F{^{1}H} NMR** (376 MHz, $CDCl_3$) δ −117.79. **HRMS** (APCI+) Calc. for $C_{17}H_{15}ClF$ $[M+H]^+$: 273.0841 Found: 273.0836.

(*R*)-3-*p*-Fluorophenyl-1-*p*-bromophenyl-3-methylcyclobut-1-ene (3ad)

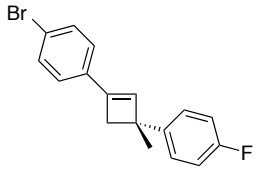

Cyclobutene **3ad** was synthetized following procedure B at 25 ºC, from 4-bromophenylacetylene (0.3 mmol, 54.3 mg) and 2-methyl-2-(4-fluoro)-ethene (1.2 mmol, 163 mg). The reaction time was 12 h. The crude was purified by silica gel flash column chromatography (two in a row) using pentane as eluent to obtain **3ad** as a white solid (80 mg, 0.252 mmol, 84% yield), 88:12 *er*.

m.p. 77.1-80.2 °C, **[α]$_D$** = −48.7 ° (*c* = 1, $CHCl_3$, 26 ºC). **^{1}H NMR** (400 MHz, $CDCl_3$) δ 7.49 – 7.42 (m, 2H), 7.35 – 7.28 (m, 2H), 7.26 – 7.21 (m, 2H), 7.03 – 6.95 (m, 2H), 6.70 (s, 1H), 2.86 - 2,93 (m, 2H), 1.60 (s, 3H). **^{1}H{^{19}F} NMR** (400 MHz, $CDCl_3$) δ 7.48 – 7.43 (m, 2H), 7.34 – 7.29 (m, 2H), 7.25 – 7.21 (m, 2H), 7.02 – 6.97 (m, 2H), 6.70 (s, 1H), 2.86 – 2.93 (m, 2H), 1.60 (s, 3H). **^{13}C NMR** (100 MHz, $CDCl_3$) δ 161.3 (d, *J* (^{13}C-^{19}F) = 243.8 Hz), 143.2 (d, *J* (^{13}C-^{19}F) = 3.1 Hz), 143.0, 134.5, 133.6, 131.6, 127.4 (d, *J* (^{13}C-^{19}F) = 7.9 Hz), 126.4, 122.0, 115.0 (d, *J* (^{13}C-^{19}F) = 21.0 Hz), 45.7, 44.4, 27.7. **^{19}F NMR** (376 MHz, $CDCl_3$) δ −117.81. **HRMS** (APCI+) Calc. for $C_{17}H_{15}BrF$ $[M+H]^+$: 317.0336 Found: 317.0325.

(*R*)-3-*p*-Fluoro-phenyl-1-(3-methoxyphenyl) -3-methylcyclobut-1-ene (3ae)

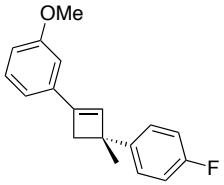

Cyclobutene **3ae** was synthetized following procedure B, from 3-metoxyphenylacetylene (0.3 mmol, 39.6 mg) and 2-methyl-2-(4-fluoro)-ethene (1.2 mmol, 163 mg, 162 µl). The reaction time was 72 h. The crude was purified by silica gel flash column chromatography using pentane: CH_2Cl_2 (9:1) as eluent to obtain **3ae** as a yellowish oil (32 mg, 0.120 mmol, 40% yield), 89:11 *er*.

[α]$_D$ = −32.4 ° (*c* = 0.59, $CHCl_3$, 26 ºC). **^{1}H NMR** (400 MHz, $CDCl_3$) δ 7.38 – 7.32 (m, 2H), 7.31 – 7.24 (m, 1H), 7.05 – 6.96 (m, 3H), 6.94 – 6.92 (m, 1H), 6.84 (ddd, *J* = 8.2, 2.6, 1.0 Hz, 1H), 6.70 (s, 1H), 3.84 (s, 3H), 2.96 – 2.87 (m, 2H), 1.63 (s, 3H). **^{13}C NMR** (100 MHz, $CDCl_3$) δ 161.2 (d, *J* (^{13}C-^{19}F) = 243.6 Hz), 159.89, 144.0, 143.4 (d, *J* (^{13}C-^{19}F) = 3.0 Hz), 136.1, 134.1, 129.6, 127.5 (d, *J* (^{13}C-^{19}F) = 7.8 Hz), 117.4, 114.9 (d, *J* (^{13}C-^{19}F) = 21.1 Hz), 113.9, 110.0, 55.4, 45.5, 44.6, 27.6. **^{19}F NMR** (376 MHz, $CDCl_3$) δ −117.95. **HRMS** (ESI+) Calc. for $C_{18}H_{18}FO$ $[M+H]^+$: 269.1336 Found: 269.1343.

(*R*)-3-Phenyl-1-(thiophen-3-yl) -3-methylcyclobut-1-ene (3af)

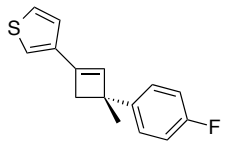

Cyclobutene **3af** was synthetized following procedure B, from 3-ethynylthiophene (0.3 mmol, 32 mg) and 2-methyl-2-(4-fluoro)-ethene (1.2 mmol, 163 mg). The reaction time was 20 h. The crude was purified by silica gel flash column chromatography using pentane as eluent to obtain **3af** as a white solid (62 mg, 0.252 mmol, 85% yield), 86:14 *er*.

m.p. 71.2-74.1 ºC, $[\alpha]_D$ = −27.3 ° (*c* = 1.00, $CHCl_3$, 26 ºC). **^{1}H NMR** (400 MHz, $CDCl_3$) δ 7.39 – 7.33 (m, 2H), 7.31 (dd, J = 5.0, 2.9 Hz, 1H), 7.23 (dd, J = 5.0, 1.2 Hz, 1H), 7.18 (dd, J = 2.9, 1.2 Hz, 1H), 7.06 – 6.98 (m, 2H), 6.47 (s, 1H), 2.92 (s, 2H), 1.64 (s, 3H). **^{13}C NMR** (100 MHz, $CDCl_3$) δ 161.2 (d, J (^{13}C-^{19}F) = 243.5 Hz), 143.5 (d, J (^{13}C-^{19}F) = 3.3 Hz), 139.5, 137.7, 132.5, 127.4 (d, J (^{13}C-^{19}F) = 7.8 Hz), 126.1, 125.1, 121.3, 114.9 (d, J (^{13}C-^{19}F) = 21.0 Hz), 46.6, 45.3, 27.7. **^{19}F NMR** (376 MHz, $CDCl_3$) δ −117.90. **HRMS** (ESI+) Calc. for $C_{15}H_{14}S$ $[M+H]^+$: 245.0795 Found: 245.0805.

(*R*)-3-Phenyl-1-*p*-chlorophenyl-3-ethylcyclobut-1-ene (3ag)

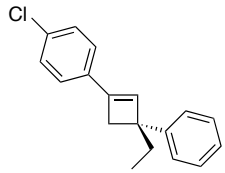

Cyclobutene **3ag** was synthetized following procedure B, from 4-chlorophenylacetylene (0.3 mmol, 41 mg) and 2-phenyl-1-butene (1.2 mmol, 159 mg). The reaction time was 72 h. The crude was purified by silica gel flash column chromatography using pentane as eluent to give **3ag** as a yellowish oil (74 mg, 0.275 mmol, 92% yield), 88:12 *er*.

$[\alpha]_D$ = −56.4 ° (*c* = 0.86, $CHCl_3$, 27 ºC). **^{1}H NMR** (400 MHz, $CDCl_3$) δ 7.35 – 7.29 (m, 8H), 7.25 – 7.18 (m, 1H), 6.85 (s, 1H), 2.93 (s, 2H), 2.02 (dq, J = 13.4, 7.4 Hz, 1H), 1.85 (dq, J = 13.4, 7.4 Hz, 1H), 0.85 (t, J = 7.4 Hz, 3H). **^{13}C NMR** (100 MHz, $CDCl_3$) δ 146.0, 143.5, 133.6, 133.3, 132.5, 128.6, 128.1, 126.9, 126.0, 125.8, 50.9, 42.3, 34.4, 10.3. **HRMS** (APCI+) Calc. for $C_{18}H_{18}Cl$ $[M+H]^+$: 269.1092 Found: 269.1084.

(*R*)-3-Phenyl-1-*p*-bromophenyl-3-ethylcyclobut-1-ene (3ah)

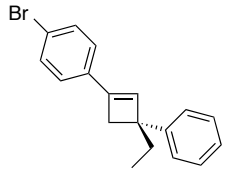

Cyclobutene **3ah** was synthetized following procedure B at 25 ºC, from 4-bromophenylacetylene (0.3 mmol, 54 mg) and 2-phenyl-1-butene (1.2 mmol, 159 mg). The reaction time was 24 h. The crude was purified by silica gel flash column chromatography

using pentane as eluent to give **3ah** as a colorless oil (76 mg, 0.243 mmol, 81% yield), 85:15 *er*.

[α]$_D$ = −60.5 ° (*c* = 1.00, $CHCl_3$, 25 ºC). **^{1}H NMR** (300 MHz, $CDCl_3$) *δ* 7.49 – 7.36 (m, 2H), 7.33 – 7.25 (m, 4H), 7.24 – 7.13 (m, 3H), 6.83 (s, 1H), 2.88 (s, 2H), 1.97 (dq, *J* = 13.4, 7.4 Hz, 1H), 1.80 (dq, *J* = 13.4, 7.4 Hz, 1H), 0.80 (t, *J* = 7.4 Hz, 3H). **^{13}C NMR** (100 MHz, $CDCl_3$) *δ* 146.0, 143.5, 133.7, 132.7, 131.6, 128.1, 126.9, 126.3, 125.8, 121.8, 50.9, 42.2, 34.3, 10.3. **HRMS** (APCI+) Calc. for $C_{18}H_{18}Br$ $[M+H]^+$: 313.0586 Found: 313.0598.

(*R*)-3-Phenyl-1-(3-methoxyphenyl)-3-ethylcyclobut-1-ene (3ai)

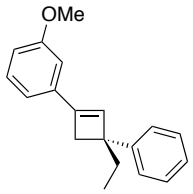

Cyclobutene **3ai** was synthetized following procedure B, from 3-metoxyphenylacetylene (0.3 mmol, 39.6 mg) and 2-phenyl-1-butene (1.2 mmol, 159 mg). The reaction time was 72 h. The crude was purified by silica gel flash column chromatography using 9:1 pentane-CH_2Cl_2 as eluent to give **3ai** as a yellowish oil (70.1 mg, 0.265 mmol, 88% yield), 89:11 *er*.

[α]$_D$ = −86.9 ° (*c* = 1.00, $CHCl_3$, 27 ºC). **^{1}H NMR** (400 MHz, $CDCl_3$) *δ* 7.41 – 7.35 (m, 4H), 7.34 – 7.29 (m, 1H), 7.29 – 7.23 (m, 1H), 7.08 – 7.05 (m, 1H), 7.01 – 6.98 (m, 1H), 6.91 (s, 1H), 6.90 – 6.86 (m, 1H), 3.88 (s, 3H), 3.04 – 2.93 (m, 2H), 2.08 (dq, *J* = 13.2, 7.4 Hz, 1H), 1.91 (dq, *J* = 13.2, 7.4 Hz, 1H), 0.91 (t, *J* = 7.4 Hz, 3H). **^{13}C NMR** (100 MHz, $CDCl_3$) *δ* 159.7, 146.2, 144.4, 136.2, 132.1, 129.4, 127.9, 126.8, 125.6, 117.3, 113.7, 109.9, 55.3, 50.6, 42.3, 34.3, 10.3. **HRMS** (ESI+) Calc. for $C_{19}H_{21}O$ $[M+H]^+$: 265.1587 Found: 265.1596.

(*R*)-3-Phenyl-1-(thiophen-3-yl)-3-ethylcyclobut-1-ene (3aj)

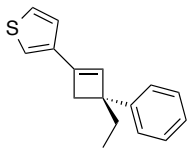

Cyclobutene **3aj** was synthetized following procedure B, from 3-ethynylthiophene (0.3 mmol, 32.4 mg) and 2-phenyl-1-butene (1.2 mmol, 159 mg). The reaction time was 72 h. The crude was purified by silica gel flash column chromatography using pentane as eluent to give **3aj** as a yellowish oil (63 mg, 0.261 mmol, 87% yield), 83:17 *er*.

[α]$_D$ = −29.2 ° (*c* = 1.00, $CHCl_3$, 26 ºC). **^{1}H NMR** (500 MHz, $CDCl_3$) *δ* 7.35 – 7.32 (m, 4H), 7.29 (dd, *J* = 5.0, 2.9 Hz, 1H), 7.24 – 7.19 (m, 2H), 7.17 (dd, *J* = 2.9, 1.2 Hz, 1H), 6.62 (s, 1H), 2.93 (s, 2H), 2.03 (dq, *J* = 13.4, 7.4 Hz, 1H), 1.87 (dq, *J* = 13.4, 7.4 Hz, 1H), 0.86 (t, *J* = 7.4 Hz, 5H). **^{13}C NMR** (100 MHz, $CDCl_3$) *δ* 146.3, 140.0, 137.9, 130.6, 128.0, 126.9, 126.0, 125.7, 125.1, 121.1, 51.8, 43.2, 34.4, 10.4. **HRMS** (ESI+) Calc. for $C_{16}H_{17}S$ $[M+H]^+$: 241.1045 Found: 241.1043.

1,4-Bis-((*R*)-3-(4-fluorophenyl)-3-methylcyclobut-1-en-1-yl)benzene (3ak)

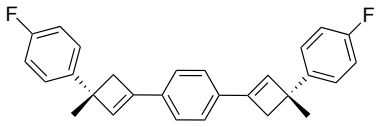

Biscyclobutene **3ak** was synthetized following procedure A with 5 mol% of **(***S*,R_P)-**B** and $NaBAr_4^F$, from 1,4-diethynylbenzene (0.3 mmol, 37.8 mg) and 2-methyl-2-(4-fluoro)-ethene (1.8 mmol, 245 mg) at 25 ºC. The crude was purified by silica gel flash column chromatography using a mixture of 10:1 pentane-CH_2Cl_2 as eluent to give **3ak** as a white solid (48.8 mg, 0.122 mmol, 41% yield, 28% meso), 97:3 *er*. **3ak** could also be prepared at −20 ºC (38.2 mg, 0.096 mmol, 32% yield, 21% meso), 98:2 *er*. X-ray quality crystals were obtained by slow diffusion of methanol over a CH_2Cl_2 solution of **3ak**.

NMR spectroscopy signals are overlapped for the meso form and the enantiomers.

mp 152-158 °C, **[α]$_D$** = −91.7 ° (*c* = 0,48, $CHCl_3$, 24 ºC). **^{1}H NMR** (300 MHz, $CDCl_3$) δ 7.46 – 7.28 (m, 8H), 7.11 – 6.89 (m, 4H), 6.70 (s, 2H), 2.92 (s, 4H), 1.62 (s, 6H). **^{13}C NMR** (75 MHz, $CDCl_3$) δ 161.2 (d, J (^{13}C-^{19}F) = 243.7 Hz), 143.7, 143.5 (d, J (^{13}C-^{19}F) = 3.2 Hz), 134.2, 133.9, 127.5 (d, J (^{13}C-^{19}F) = 7.7 Hz), 124.8, 114.9 (d, J (^{13}C-^{19}F) = 20.9 Hz), 45.7, 44.5, 27.8. **^{19}F NMR** (376 MHz, $CDCl_3$) δ −117.91. **HRMS** (APCI+) Calc. for $C_{28}H_{25}F_2$ $[M+H]^+$: 399.1919 Found: 399.1914.

1,4-Bis-((*R*)-3-(4-(*tert*-butyl)phenyl)-1-methylcyclobut-2-en-1-yl)benzene (3am)

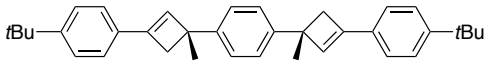

Biscyclobutene **3am** was synthetized following procedure B with 5 mol % of (*S*,R_P)-**B** and $NaBAr^F_4$, from 4-*tert*-butylphenylacetylene (0.9 mmol, 142 mg) and 1,4-diisocraticpropenylbenzene (0.3 mmol, 47.5 mg) at 25 ºC. The crude was purified by silica gel flash column chromatography using a mixture of 19:1 pentane-CH_2Cl_2 as eluent to give **3am** as a white solid (86 mg, 0.181 mmol, 60% yield, 32% meso), 95:5 *er*. **3am** could also be prepared at −20 ºC (46 mg, 0.097 mmol, 32% yield, 22% meso), 98:2 *er*. X-ray quality crystals were obtained by slow diffusion of pentane over a CH_2Cl_2 solution of **3am**. Enantiomers (e) and Meso (m).

mp 183-187 °C, **[α]$_D$** = −24.1 ° (*c* = 0.37, $CHCl_3$, 24 ºC). **^{1}H NMR** (400 MHz, $CDCl_3$) δ 7.39 – 7.37 (m, 1H) (e + m), 7.36 (s, 3H) (e + m), 7.37 – 7.35 (m, 7H) (e + m), 7.33 – 7.32 (m, 1H) (e + m), 6.66 (bs, 2H) (e + m), 3.06 – 2.90 (m, 2H) (e + m), 2.87 (d, J = 12.4 Hz, 2H) (e + m), 1.62 (s, 6H) (e + m), 1.32 (s, 18H) (e + m). **^{13}C NMR** (100 MHz, $CDCl_3$) δ 151.0 (e + m), 145.2 (e + m), 143.8 (e + m), 133.4 (m), 133.4 (e), 132.3 (e + m), 125.7 (e + m), 125.4 (e + m), 124.5 (e + m), 45.7 (e + m), 44.6 (e + m), 34.8 (e + m), 31.4 (e + m), 27.5 (e + m). **HRMS** (APCI+) Calc. for $C_{36}H_{43}$ $[M+H]^+$: 475.3359 Found: 475.3360.

1,3-Bis-((*R*)-1-Methyl-3-(*m*-tolyl)cyclobut-2-en-1-yl)benzene (3an)

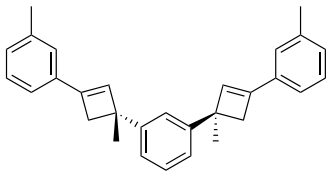

Biscyclobutene **3an** was synthetized following procedure A with 5 mol % of (*S*,R_P)-**B** and $NaBAr_4^F$, from 3-ethynyltoluene (0.9 mmol, 105 mg) and 1,3-diisoprenylbenzene (0.3 mmol, 47.5 mg). The reaction time was 14 h. The crude was purified by silica gel flash column chromatography using from 97:3 to 95:5 pentane-CH_2Cl_2 as eluent to give **3an** as a yellowish oil (52.4 mg, 0.134 mmol, 45% yield, 23% meso), 98:2 *er*. Enantiomers (e) and Meso (m). **[α]$_D$** = −35.8 ° (*c* = 0.43, $CHCl_3$, 25 ºC). **^{1}H NMR** (400 MHz, $CDCl_3$) *δ* 7.46 -7.42 (m, 1H) (e + m), 7.35 – 7.25 (m, 9H) (e + m), 7.15 – 7.10 (m, 2H) (e + m), 6.78 (s, 1.5H) (e), 6.77 (s, 0.5H) (m), 3.09 – 3.00 (m, 2H) (e + m), 2.98 – 2.92 (m, 2H) (e + m), 2.40 (s, 6H) (e + m), 1.68 (s, 6H) (e + m). **^{13}C NMR** (100 MHz, $CDCl_3$) *δ* 147.7 (e), 147.7 (m), 144.0 (e + m), 138.0 (e + m), 134.9 (e + m), 133.8 (m), 133.8 (e), 128.7 (e + m), 128.4 (e + m), 128.0 (e + m), 125.4 (e + m), 123.4 (e), 123.39 (m), 121.9 (e + m), 46.3 (e + m), 44.5 (e), 44.4 (m), 28.1 (m), 28.1 (e) , 21.52 (e + m). **HRMS** (APCI+) Calc. for $C_{30}H_{31}$ $[M+H]^+$: 391.2420 Found: 391.2415.

1,3-Bis-((*R*)-3-(4-(*tert*-Butyl)phenyl)-1-methylcyclobut-2-en-1-yl)benzene (3ao)

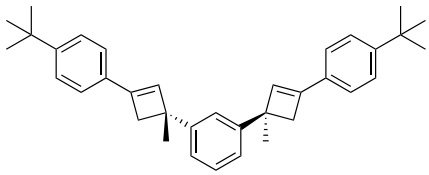

Biscyclobutene **3ao** was synthetized following procedure A with 5 mol % of (*S*,R_P)-**B** and $NaBAr_4^F$, from 4-*tert*-butylphenylacetylene (0.9 mmol, 142 mg) and 1,3-diisoprenylbenzene (0.3 mmol, 47.5 mg). The reaction time was 12 h. The reaction crude was purified by silica gel flash column chromatography using a 19:1 pentane-CH_2Cl_2 as eluent to give **3ao** as a white solid (94.8 mg, 0.200 mmol, 67% yield, 27% meso), 96:4 *er*. Enantiomers (e) and meso (m). **mp** 72-77 °C, **[α]$_D$** = −42.3 ° (*c* = 0.48, $CHCl_3$, 25 ºC). **^{1}H NMR** (400 MHz, $CDCl_3$) *δ* 7.45 – 7.42 (m, 2H) (e + m), 7.43 – 7.39 (m, 6H) (e + m), 7.39 – 7.37 (m, 1H) (e + m), 7.33 – 7.24 (m, 3H) (e + m), 6.75 – 6.72 (m, 2H) (e + m), 3.07 – 2.99 (m, 2H) (e + m), 2.97 – 2.91 (m, 2H) (e + m), 1.67 (s, 6H) (e + m), 1.38 (s, 18H) (e + m). **^{13}C NMR** (100 MHz, $CDCl_3$) *δ* 151.0 (e + m), 147.8 (e), 147.7 (m), 143.8 (e + m), 133.2 (m), 133.2 (e), 132.3 (e + m), 127.9 (e + m), 125.4 (e + m), 124.6 (e + m), 123.4 (e + m), 123.4 (e + m), 46.3 (e + m), 44.6 (e), 44.5 (m), 34.8 (e + m), 31.5 (e + m), 28.0 (m), 28.0 (e). **HRMS** (APCI+) Calc. for $C_{36}H_{43}$ $[M+H]^+$: 475.3359 Found: 475.3367.

1,3-Bis-((*R*)-1-Methyl-3-(thiophen-3-yl)cyclobut-2-en-1-yl)benzene (3ap)

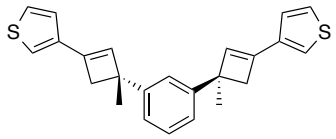

Cyclobutene **3ap** was synthetized following procedure A with 5 mol % of (*S*,R_P)-**B** and $NaBAr_4^F$, from 3-ethynylthiophene (0.9 mmol, 97 mg) and 1,3-diisoprenylbenzene (0.3 mmol, 47.5 mg). The reaction time was 72 h. The crude was purified by silica gel flash column chromatography using a mixture of 19:1 pentane-CH_2Cl_2 as eluent to give **3ap** as a white solid (78.9 mg, 0.211 mmol, 70% yield, 26% meso), 96:4 *er*. Enantiomers (e) and Meso (m).

mp 69-74 °C, **[α]$_D$** = −3.1 ° (*c* = 0.12, $CHCl_3$, 25 ºC). **^{1}H NMR** (400 MHz, $CDCl_3$) *δ* 7.38 – 7.36 (m, 1H) (e + m), 7.31 – 7.26 (m, 3H) (e + m), 7.25 – 7.20 (m, 4H) (e + m), 7.16 (dd, *J* = 2.9, 1.2 Hz, 2H) (e + m), 6.53 (s, 1.5H) (e), 6.52 (s, 0.5H) (m), 3.03 – 2.95 (m, 2H) (e + m), 2.93 – 2.87 (m, 2H) (e + m), 1.64 (s, 6H) (e + m). **^{13}C NMR** (100 MHz, $CDCl_3$) *δ* 147.7 (e), 147.7 (m), 139.3 (e + m), 138.0 (e + m), 132.84 (m), 132.79 (e), 128.0 (e + m), 126.0 (e + m), 125.2 (e + m), 123.4 (e + m), 123.3 (e + m), 121.1 (e + m), 47.4 (e + m), 45.2 (e), 45.1 (m), 28.2 (m), 28.1 (e). **HRMS** (APCI+) Calc. for $C_{24}H_{23}S_2$ $[M+H]^+$: 375.1236 Found: 375.1237.

(*S*)-(2-(4,4-Dimethyl-2-phenylcyclobut-2-en-1-yl)ethyl)benzene (3aq)

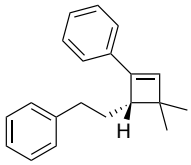

Cyclobutene **3aq** was synthetized following procedure C, from phenylacetylene (0.3 mmol, 30.6 mg) and (4-methylpent-3-en-1-yl)benzene (0.6 mmol, 96 mg). The reaction time was 36 h. The crude was purified by silica gel flash column chromatography using pentane as eluent to give **3aq** as a colorless oil 7:1 mixture of regioisomers (40.2 mg, 0.153 mmol, 51% yield), 90:10 *er*. Major regioisomer (Mr), minor regioisomer (mr).

[α]$_D$ = −2.3 ° (*c* = 0.6, $CHCl_3$, 23 ºC). **^{1}H NMR** (500 MHz, $CDCl_3$) *δ* 7.39 – 7.35 (m, 0.3H, mr), 7.33 – 7.27 (m, 5.60H, Mr + mr), 7.25 – 7.17 (m, 4.6H Mr + mr), 6.33 (d, *J* = 1.3 Hz, 0.15H, mr), 6.31 (s, 1H, Mr), 2.84 – 2.75 (m, 2.15H Mr + mr), 2.75 – 2.71 (m, 0.15H, mr), 2.67 (ddd, *J* = 14.2, 10.2, 6.7 Hz, 1H, Mr), 2.44 (dd, *J* = 9.6, 4.8 Hz, 0.15H, mr), 2.16 – 2.07 (m, 1H, Mr), 1.91 (ddt, *J* = 13.2, 9.0, 6.3 Hz, 0.15H, mr), 1.80 (dtd, *J* = 14.2, 10.4, 4.9 Hz, 1H, Mr), 1.69 (dtd, *J* = 13.2, 9.6, 6.3 Hz, 0.15H, mr), 1.41 (s, 0.45H, mr), 1.32 (s, 0.45H, mr), 1.29 (s, 3H, Mr), 1.25 (s, 3H, Mr). **^{13}C NMR** (126 MHz, $CDCl_3$) *δ* 145.8 (Mr), 142.9 (mr), 142.8 (Mr), 136.5 (Mr), 134.9 (Mr), 128.6 (mr), 128.5 (mr), 128.5 (Mr), 128.5 (Mr), 128.4 (Mr), 128.1 (mr), 127.5 (mr), 127.4 (Mr), 125.9 (Mr), 125.8 (mr), 125.4 (mr), 125.2 (Mr), 51.6 (mr), 51.5 (Mr), 43.1 (Mr), 35.3 (Mr), 34.9 (mr), 32.2 (mr), 31.4 (Mr), 28.0 (Mr), 26.8 (mr), 22.1 (Mr), 21.6 (mr). Some signals from the minor regioisomer are missing. **HRMS** (APCI+) Calc. for $C_{20}H_{23}$ $[M+H]^+$: 263.1794 Found: 263.1796.

(*S*)-1-(*tert*-Butyl)-4-(3,3,4-trimethylcyclobut-1-en-1-yl)benzene (3ar)

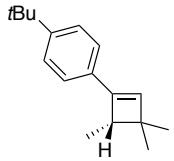

Cyclobutene **3ar** was synthetized following procedure C, from 4-*tert*-butylphenylacetylene (0.3 mmol, 47.5 mg) and 2-methylbut-2-ene (1.8 mmol, 126 mg). The reaction time was 36 h. The crude was purified by silica gel flash column chromatography using pentane as eluent to give **3ar** as a colorless oil 17:1 mixture of regioisomers (58.4 mg, 0.255 mmol, 85% yield), 89:11 *er*. Major regioisomer (Mr), minor regioisomer (mr).

[α]$_D$ = +10.8 ° (*c* = 0.9, $CHCl_3$, 23 ºC). **^{1}H NMR** (500 MHz, $CDCl_3$) δ 7.36 – 7.32 (m, 2H, Mr), 7.31 – 7.27 (m, 2H, Mr), 6.28 (s, 1H, Mr), 6.23 (d, *J* = 1.3 Hz, 0.06H, mr), 2.79 (q, *J* = 7.1 Hz, 1H, Mr), 1.31 (s, 9H, Mr), 1.21 – 1.17 (m, 6H, Mr), 1.09 (s, 3H, Mr). **^{13}C NMR** (126 MHz, $CDCl_3$) δ 150.5 (Mr), 146.9 (Mr), 135.2 (Mr), 132.2 (Mr), 125.4 (mr), 125.4 (Mr), 125.1 (mr), 124.9 (Mr), 46.1 (Mr), 45.6 (mr), 42.4 (Mr), 42.3 (mr) 34.8 (Mr), 31.8 (mr), 31.6 (mr), 31.5 (Mr), 27.5 (Mr), 26.5 (mr), 21.9 (Mr), 21.7 (mr), 14.6 (mr), 14.3 (Mr). Some signals from the minor regioisomer are missing. **HRMS** (APCI+) Calc. for $C_{17}H_{25}$ $[M+H]^+$: 229.1951 Found: 229.1949.

(*S*)-1-(*tert*-Butyl)-4-(4-ethyl-3,3-dimethylcyclobut-1-en-1-yl)benzene (3as)

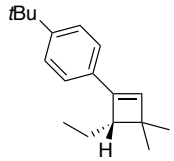

Cyclobutene **3as** was synthetized following procedure C, from 4-*tert*-butylphenylacetylene (0.3 mmol, 47.5 mg) and 2-methylpent-2-ene (1.8 mmol, 151 mg) at 0 ºC. The reaction time was 36 h. The crude was purified by silica gel flash column chromatography using pentane as eluent to give **3as** as a colorless oil 12:1 mixture of regioisomers (56.0 mg, 0.234 mmol, 78% yield), 89:11 *er*. Major regioisomer (Mr), minor regioisomer (mr).

[α]$_D$ = −16.4° (c = 0.7, $CHCl_3$, 24 ºC). **^{1}H NMR** (400 MHz, $CDCl_3$) δ 7.41 – 7.37 (m, 2H, Mr), 7.36 – 7.31 (m, 2H, Mr), 6.38 (d, *J* = 1.3 Hz, 0.9H, mr), 6.30 (s, 1H, Mr), 2.69 (dd, *J* = 10.6, 4.1 Hz, 1H, Mr), 1.92 – 1.81 (m, 1H, Mr), 1.57 – 1.47 (m, 1H, Mr), 1.36 (s, 9H, Mr), 1.29 (s, 3H, Mr), 1.22 (s, 3H, Mr), 1.05 (t, *J* = 7.4 Hz, 3H, Mr). **^{13}C NMR** (101 MHz, $CDCl_3$) δ 152.9 (Mr), 150.4 (Mr), 145.9 (Mr), 135.6 (Mr), 132.4 (Mr), 129.9 (mr), 128.8 (mr), 127.4 (mr), 125.4 (mr), 125.3 (Mr), 125.1 (mr), 125.0 (Mr), 53.9 (mr), 53.9 (Mr), 45.8 (mr), 43.0 (Mr), 34.8 (mr), 31.5 (Mr), 28.2 (Mr), 26.9 (mr), 23.1 (mr), 22.5 (Mr), 21.9 (Mr), 21.5 (mr), 13.6 (Mr), 12.8 (mr). Some signals from the minor regioisomer are missing. **HRMS** (+) Calc. for $C_{18}H_{27}$ $[M+H]^+$: 243.2107 Found: 243.2103.

(*S*)-1-Bromo-4-(3,3-dimethyl-4-phenethylcyclobut-1-en-1-yl)benzene (3at)

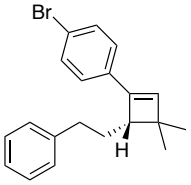

Cyclobutene **3at** was synthetized following procedure C, from 4-bromophenylacetylene (0.1 mmol, 18.1 mg) and (4-methylpent-3-en-1-yl)benzene (0.2 mmol, 32.1 mg). The reaction time was 20 h. The crude was purified by silica gel flash column chromatography using pentane as eluent to give **3at** as a colorless oil >99:1 mixture of regioisomers (17.2 mg, 0.05 mmol, 50% yield), 85:15 *er*.

[α]$_D$ = −17.0 ° (*c* = 0.1, $CHCl_3$, 24 ºC). **^{1}H NMR** (500 MHz, $CDCl_3$) *δ* 7.43 – 7.39 (m, 1H), 7.31 – 7.26 (m, 1H), 7.22 – 7.18 (m, 1H), 7.17 – 7.13 (m, 1H), 6.31 (s, 0H), 2.76 (td, *J* = 10.7, 4.3 Hz, 1H), 2.67 – 2.58 (m, 0H), 2.08 – 1.98 (m, 0H), 1.78 (dtd, *J* = 14.1, 10.4, 4.9 Hz, 0H), 1.27 (s, 1H), 1.23 (s, 1H). **^{13}C NMR** (126 MHz, $CDCl_3$) *δ* 144.8, 142.6, 137.4, 133.8, 131.6, 128.5, 128.5, 126.8, 125.9, 121.2, 51.4, 43.3, 35.2, 31.3, 27.9, 21.9. **HRMS** (APCI+) Calc. for $C_{20}H_{22}Br$ $[M+H]^+$: 341.0899 Found: 339.0735.

(*S*)-1-Chloro-4-(3,3,4-trimethylcyclobut-1-en-1-yl)benzene (3au)

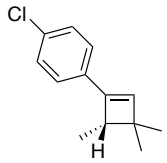

Cyclobutene **3au** was synthetized following procedure C, from 4-chlorophenylacetylene (0.3 mmol, 41 mg) and 2-methylbut-2-ene (1.8 mmol, 126 mg). The reaction time was 24 h. The crude was purified by silica gel flash column chromatography using pentane as eluent to give **3au** as a colorless oil 6:1 mixture of regioisomers (23.6 mg, 0.114 mmol, 38% yield), 83:17 *er*. Major regioisomer (Mr), minor regioisomer (mr).

[α]$_D$ = +15.0 ° (*c* = 0.06, $CHCl_3$, 24 ºC). **^{1}H NMR** (500 MHz, $CDCl_3$) *δ* 7.27 – 7.26 (m, 2H, Mr), 7.26 (s, 2H, Mr), 6.32 (s, 1H, Mr), 6.27 (d, *J* = 1.3 Hz, 0.16H, mr), 2.77 (q, *J* = 7.2 Hz, 1H, Mr), 1.21 (s, 3H, Mr), 1.17 (d, *J* = 7.2 Hz, 3H, Mr), 1.10 (s, 3H, Mr). **^{13}C NMR** (126 MHz, $CDCl_3$) *δ* 145.9 (Mr), 140.0 (mr), 136.5 (Mr), 133.1 (Mr), 132.8 (mr), 131.4 (Mr), 128.6 (mr), 128.5 (Mr), 128.2 (mr), 127.1 (mr), 126.5 (mr), 126.3 (Mr), 46.0 (Mr), 42.5 (Mr), 27.2 (Mr), 26.2 (mr), 22.8 (mr), 21.6 (Mr), 19.8 (mr), 18.6 (mr), 14.2 (mr), 13.9 (Mr). Some signals from the minor regioisomer are missing. **HRMS** (APCI+) Calc. for $C_{13}H_{14}Cl$ $[M+H]^+$: 205.0779 Found: 205.0779.

(*S*)-1-bromo-4-(3,3,4-trimethylcyclobut-1-en-1-yl)benzene (3av)

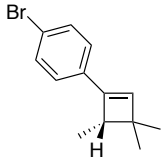

Cyclobutene **3av** was synthetized following procedure C, from 4-bromophenylacetylene (0.3 mmol, 54.3 mg) and 2-methylbut-2-ene (1.8 mmol, 126 mg). The reaction time was 24 h. The crude was purified by silica gel flash column chromatography using pentane as eluent to give **3av** as a colorless oil 8:1 mixture of regioisomers (58.9 mg, 0.234 mmol, 78% yield), 83:17 *er*. Major regioisomer (Mr), minor regioisomer (mr).

[α]$_D$ = +7.9 ° (c = 0.5, $CHCl_3$, 24 ºC). **^{1}H NMR** (500 MHz, $CDCl_3$) δ 7.45 – 7.40 (m, 2.24H, Mr + mr), 7.21 – 7.17 (m, 2.24H, Mr + mr), 6.34 (s, 1H, Mr), 6.29 (d, J = 1.3 Hz, 0.12H, mr), 2.78 (q, J = 7.2 Hz, 1H, Mr), 2.46 (qd, J = 7.1, 1.3 Hz, 0.12H, mr), 1.34 (s, 0.36H, mr), 1.22 (s, 0.36H, mr), 1.21 (s, 3H, Mr), 1.17 (d, J = 7.1 Hz, 3H, Mr), 1.10 (s, 3H, Mr), 1.07 (d, J = 7.2 Hz, 0.36H, mr). **^{13}C NMR** (126 MHz, $CDCl_3$) *δ* 146.0 (Mr), 136.9 (Mr), 133.7 (Mr), 131.7 (mr), 131.6 (Mr), 126.9 (mr), 126.8 (Mr), 121.1 (Mr), 46.1 (Mr), 42.6 (Mr), 27.3 (Mr), 21.7 (Mr), 21.5 (mr), 14.3 (mr), 14.1 (Mr). Some signals from the minor regioisomer are missing. **HRMS** (APCI+) Calc. for $C_{13}H_{14}Br$ $[M-H]^+$: 249.0273 Found: 249.0270.

(*S*)-1-Chloro-4-(4-ethyl-3,3-dimethylcyclobut-1-en-1-yl)benzene (3aw)

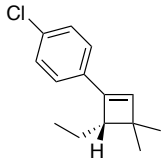

Cyclobutene **3aw** was synthetized following procedure C, from 4-chlorophenylacetylene (0.3 mmol, 41 mg) and 2-methylpent-2-ene (1.8 mmol, 151 mg) at 0 ºC. The reaction time was 36 h. The formation of 1,3-diene was observed in the crude in a ratio of 10:2:1 (Mr:mr:1,3-diene).**Error! Bookmark not defined.** The crude was purified by silica gel flash column chromatography using pentane as eluent to give **3aw** as a colorless oil 4:1 mixture of regioisomers (58.0 mg, 0.264 mmol, 88% yield), 86:14 *er*. Major regioisomer (Mr), minor regioisomer (mr).

[α]$_D$ = −28.5 ° (c = 0.03, $CHCl_3$, 24 ºC). **^{1}H NMR** (500 MHz, $CDCl_3$) *δ* 7.28 – 7.23 (m, 5H, Mr + mr), 6.36 (d, *J* = 1.3 Hz, 0.25H, mr), 6.28 (s, 1H, Mr), 2.62 (dd, *J* = 10.6, 4.1 Hz, 1H, Mr), 2.32 – 2.24 (m, 0.25H, mr), 1.83 – 1.70 (m, 1.25H, Mr + mr), 1.51 – 1.40 (m, 1.25H, Mr + mr), 1.37 (s, 0.75H, mr), 1.26 (s, 0.25H), 1.25 (s, 3H, Mr), 1.16 (s, 3H, Mr), 1.02 – 0.94 (m, 3.75H, Mr + mr). **^{13}C NMR** (101 MHz, $CDCl_3$) *δ* 151.8 (mr), 145.0 (Mr), 137.1 (Mr), 133.6 (Mr), 132.9 (Mr), 129.1 (mr), 128.7 (mr), 128.6 (Mr), 126.6 (mr), 126.6 (Mr), 54.0 (mr), 53.8 (Mr), 43.2 (Mr), 28.0 (Mr), 26.7 (mr), 22.9 (mr), 22.3 (Mr), 21.8 (Mr), 21.3 (mr), 14.2 (mr), 13.4 (Mr), 12.8 (mr). Some signals from the minor regioisomer are missing. **HRMS** (APCI+) Calc. for $C_{14}H_{16}Cl$ $[M+H]^+$: 219.0935 Found: 219.0928.

(*S*)-1-Bromo-4-(4-ethyl-3,3-dimethylcyclobut-1-en-1-yl)benzene (3ax)

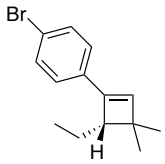

Cyclobutene **3ax** was synthetized following procedure C, from 4-bromophenylacetylene (0.3 mmol, 54.3 mg) and 2-methylpent-2-ene (1.8 mmol, 151 mg) at 25 ºC. The reaction time was 36 h. The formation of 1,3-diene was observed in the crude in a ratio of 10:2:1 (Mr:mr:1,3-diene). The crude was purified by silica gel flash column chromatography using pentane as eluent to give **3ax** as a colorless oil 5:1 mixture of regioisomers (61.7 mg, 0.234 mmol, 78% yield), 83:17 *er*. Major regioisomer (Mr), minor regioisomer (mr).

[α]$_D$ = −5.0 ° (c = 0.7, $CHCl_3$, 24 ºC). **^{1}H NMR** (400 MHz, $CDCl_3$) δ 7.45 – 7.39 (m, 2H, Mr), 7.24 – 7.20 (m, 0.4H, mr), 7.20 – 7.15 (m, 2H, Mr), 6.38 (d, *J* = 1.4 Hz, 0.2H, mr), 6.30 (s, 1H, Mr), 2.63 (dd, *J* = 10.5, 4.2 Hz, 1H, Mr), 2.31 – 2.23 (m, 0.2H, mr), 1.82 – 1.69 (m, 1.2H, Mr + mr), 1.52 – 1.40 (m, 1.2H, Mr + mr), 1.37 (s, 0.6H, mr), 1.26 (s, 0.2H, mr), 1.25 (s, 3H, Mr), 1.16 (s, 3H, Mr), 1.03 – 0.95 (m, 3.60H, Mr + mr). **^{13}C NMR** (75 MHz, $CDCl_3$) δ 145.1 (Mr), 137.4 (Mr), 134.0 (Mr), 131.7 (mr), 131.5 (Mr), 126.9 (mr), 126.9 (Mr), 121.1 (Mr), 53.8 (Mr), 43.2 (Mr), 28.0 (Mr), 22.3 (Mr), 21.7 (Mr), 13.4 (Mr). Some signals from the minor regioisomer are missing. **HRMS** (APCI+) Calc. for $C_{14}H_{18}Br$ $[M+H]^+$: 265.0586 Found: 265.0581.

(*R*)-1-cyclopropyl-4-(1-methyl-3-phenylcyclobut-2-en-1-yl)benzene (3be)

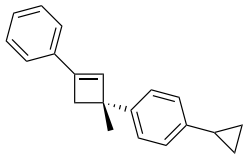

Cyclobutene **3be** was synthetized following procedure B at 25 ºC, from phenylacetylene (0.2 mmol, 20.4 mg) and *p*-Cyclopropyl-α-methylstyrene (0.4 mmol, 63.3 mg). The reaction time was 14 h. The crude was purified by silica gel flash column chromatography using pentane as eluent to give **3be** together with 5-cyclopropyl-3-(4-cyclopropylphenyl)-1,1,3-trimethyl-2,3-dihydro-1*H*-indene (**49**) coming from the alkene dimerization as a colorless oil, 2.6:1 (**3be**:**49**). Yield was calculated by ^{1}H NMR using diphenylmethane as internal standard (20% yield), 87:13 *er*.

[α]$_D$ = Could not be determined due to the impossibility of isolating a pure sample of **3be**. NMR listed as a mixture of **3be** and **49** (2.6:1).**^{1}H NMR** (500 MHz, $CDCl_3$) δ 7.44 – 7.40 (m, 2H, **3be**), 7.39 – 7.34 (m, 2H, **3be**), 7.34 – 7.28 (m, 3H, **3be**), 7.13 – 7.09 (m, 1.2H, **49**), 7.08 – 7.05 (m, 2H, **3be**), 7.03 – 6.96 (m, 1.2H, **49**), 6.86 (d, *J* = 1.7 Hz, 0.4H, **49**), 6.74 (s, 1H, **3be**), 2.97 (d, *J* = 12.4 Hz, 1H, **3be**), 2.92 (d, *J* = 12.4 Hz, 1H, **3be**), 2.39 (d, *J* = 13.0 Hz, 0.4H, **49**), 2.19 (d, *J* = 13.0 Hz, 0.4H, **49**), 1.98 – 1.83 (m, 1.8H, **3be** + **49**), 1.69 (s, 1.2H, **S1**), 1.65 (s, 3H, **3be**), 1.35 (s, 1.2H, **49**), 1.06 (s, 1.2H, **49**), 0.99 – 0.91 (m, 3.6H, **3be** + **49**), 0.75 –

0.66 (m, 3.6H, **3be** + **49**). **^{13}C NMR** (126 MHz, $CDCl_3$) δ 149.7 (**49**), 149.2 (**49**), 148.3 (**49**), 144.9 (**3be**), 143.9 (**3be**), 142.5 (**49**), 141.4 (**3be**), 141.0 (**49**), 134.9 (**3be**), 134.1 (**3be**), 128.4 (**3be**), 127.9 (**3be**), 126.8 (**49**), 125.9 (**3be**), 125.6 (**3be**), 125.3 (**49**), 124.7 (**3be**), 124.6 (**49**), 122.4 (**49**), 59.7 (**S3a**), 50.5 (**49**), 45.8 (**49**), 44.5 (**3be**), 42.6 (**49**), 31.0 (**49**), 30.9 (**49**), 30.7 (**49**), 27.6 (**3be**), 25.0 (**49**), 15.6 (**49**), 15.6 (**3be**), 15.1 (**49**), 9.4 (**49**), 9.2 (**49**), 9.2 (**49**), 9.1 (**3be**), 9.1 (**3be**). Some signals from **49** are missing. **HRMS** (ESI+) Calc. for $C_{20}H_{21}$ $[M+H]^+$: 261.1638 Found: 261.1640.

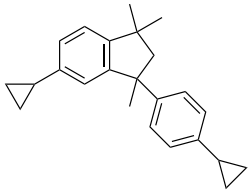

49

Crystallographic Data

Complex (S,R_P)-A

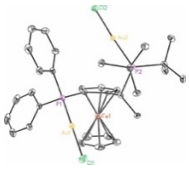

Table 12. Crystal data and structure refinement for complex (S,R_P)-**A**. Absolute configuration was determined.

Depostion number at CCDC	**CCDC 1563807**	
Identification code	mo_CG341c_0m	
Empirical formula	C64 H80 Au4 Cl4 Fe2 P4	
Formula weight	2014.52	
Temperature	100(2) K	
Wavelength	0.71073 Å	
Crystal system	Orthorhombic	
Space group	P2(1)2(1)2(1)	
Unit cell dimensions	a = 8.6631(2)Å	a= 90°.
	b = 11.5159(3)Å	b = 90°.
	c = 33.5456(9)Å	g = 90°.
Volume	3346.62(15) $Å^3$	
Z	2	
Density (calculated)	1.999 Mg/m^3	
Absorption coefficient	9.449 mm^{-1}	
F(000)	1920	
Crystal size	0.20 x 0.20 x 0.10 mm^3	
Theta range for data collection	1.214 to 35.010°.	
Index ranges	-12<=h<=7,-15<=k<=18,-36<=l<=53	
Reflections collected	28510	
Independent reflections	13019[R(int) = 0.0225]	
Completeness to theta =35.010°	92.4%	
Absorption correction	Multi-scan	
Max. and min. transmission	0.452 and 0.359	
Refinement method	Full-matrix least-squares on F^2	
Data / restraints / parameters	13019/ 0/ 359	
Goodness-of-fit on F^2	1.084	
Final R indices [I>2sigma(I)]	R1 = 0.0237, wR2 = 0.0476	
R indices (all data)	R1 = 0.0260, wR2 = 0.0536	
Flack parameter	x =-0.010(3)	
Largest diff. peak and hole	1.916 and -1.234 e.$Å^{-3}$	

Complex (S,R_P)-B and (S,R_P)-G

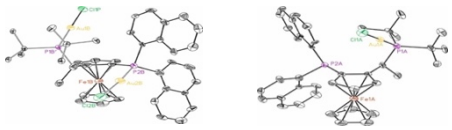

Table 13. Crystal data and structure refinement for IE-JosiPhosMAuCl2. Absolute configuration was determined. The crystal was formed for a mixture of (S,R_P)-**O** and (S,R_P)-**B**, 9:1.

Depostion number at CCDC	**CCDC 1563811**	
Identification code	IE-JosiPhosMAuCl2	
Empirical formula	C40.40 H44.80 Au1.10 Cl1.90 Fe P2	
Formula weight	932.17	
Temperature	100(2) K	
Wavelength	0.71073 ≈	
Crystal system	Orthorhombic	
Space group	P2(1)2(1)2(1)	
Unit cell dimensions	a = 14.788(3)≈	a= 90º.
	b = 18.134(4)≈	b = 90º.
	c = 28.447(6)≈	g = 90º.
Volume	7629(3) ≈^{3}	
Z	8	
Density (calculated)	1.623 Mg/m^3	
Absorption coefficient	4.849 mm^{-1}	
F(000)	3699	
Crystal size	0.20 x 0.20 x 0.20 mm^3	
Theta range for data collection	2.246 to 26.373∞.	
Index ranges	-18<=h<=18,-22<=k<=22,-35<=l<=34	
Reflections collected	43920	
Independent reflections	15132[R(int) = 0.0737]	
Completeness to theta =26.373∞	99.0%	
Absorption correction	Multi-scan	
Max. and min. transmission	0.444 and 0.342	
Refinement method	Full-matrix least-squares on F^2	
Data / restraints / parameters	15132/ 405/ 985	
Goodness-of-fit on F^2	1.151	
Final R indices [I>2sigma(I)]	R1 = 0.0511, wR2 = 0.0781	
R indices (all data)	R1 = 0.0959, wR2 = 0.1000	
Flack parameter	x =-0.017(9)	
Largest diff. peak and hole	1.535 and -1.150 e.≈$^{-3}$	

Complex (S,R_P)-F

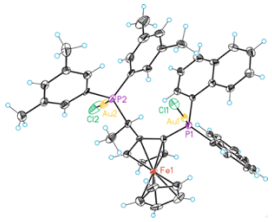

Table 14. Crystal data and structure refinement for complex (S,R_P)-**F**. Absolute configuration was determined.

Depostion number at CCDC	**CCDC 1563812**	
Identification code	mo_BR688_0m	
Empirical formula	C48.50 H45 Au2 Cl3 Fe P2	
Formula weight	1245.92	
Temperature	100(2) K	
Wavelength	0.71073 Å	
Crystal system	Monoclinic	
Space group	P2(1)	
Unit cell dimensions	a = 10.7462(8)Å	a= 90°.
	b = 10.3072(9)Å	b = 90.695(4)°.
	c = 20.126(3)Å	g = 90°.
Volume	2229.1(4) $Å^3$	
Z	2	
Density (calculated)	1.856 Mg/m^3	
Absorption coefficient	7.172 mm^{-1}	
F(000)	1202	
Crystal size	0.25 x 0.15 x 0.12 mm^3	
Theta range for data collection	1.012 to 30.049°.	
Index ranges	-15<=h<=12,-13<=k<=14,-27<=l<=27	
Reflections collected	22601	
Independent reflections	10444[R(int) = 0.0437]	
Completeness to theta =30.049°	89.4%	
Absorption correction	Empirical	
Max. and min. transmission	0.480 and 0.282	
Refinement method	Full-matrix least-squares on F^2	
Data / restraints / parameters	10444/ 60/ 547	
Goodness-of-fit on F^2	1.018	
Final R indices [I>2sigma(I)]	R1 = 0.0408, wR2 = 0.0883	
R indices (all data)	R1 = 0.0496, wR2 = 0.0940	
Flack parameter	x =-0.026(6)	
Largest diff. peak and hole	2.077 and -1.053 $e.Å^{-3}$	

(*R*)-3-*p*-Bromophenyl-1-phenyl-3-methylcyclobut-1-ene (3f)

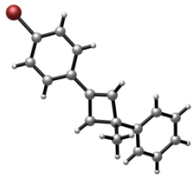

Table 15. Crystal data and structure refinement for **3f**. Absolute configuration was determined.

Depostion number at CCDC	**CCDC 1563806**	
Identification code	CG-3-104	
Empirical formula	C17 H15 Br	
Formula weight	299.20	
Temperature	100(2) K	
Wavelength	0.71073 Å	
Crystal system	Monoclinic	
Space group	P2(1)	
Unit cell dimensions	a = 6.0054(7)Å	a= 90°.
	b = 31.426(4)Å	b = 90.918(7)°.
	c = 7.3514(10)Å	g = 90°.
Volume	1387.2(3) $Å^3$	
Z	4	
Density (calculated)	1.433 Mg/m^3	
Absorption coefficient	2.943 mm^{-1}	
F(000)	608	
Crystal size	0.20 x 0.20 x 0.20 mm^3	
Theta range for data collection	2.592 to 28.280°.	
Index ranges	-8<=h<=8,-41<=k<=41,-9<=l<=9	
Reflections collected	20099	
Independent reflections	6327[R(int) = 0.0810]	
Completeness to theta =28.280°	98.9%	
Absorption correction	Multi-scan	
Max. and min. transmission	0.591 and 0.455	
Refinement method	Full-matrix least-squares on F^2	
Data / restraints / parameters	6327/ 1/ 327	
Goodness-of-fit on F^2	1.174	
Final R indices [I>2sigma(I)]	R1 = 0.0791, wR2 = 0.1903	
R indices (all data)	R1 = 0.0864, wR2 = 0.1934	
Flack parameter	x =0.020(12)	
Largest diff. peak and hole	2.703 and -1.993 e.$Å^{-3}$	

3-*p-tert*-Butylphenyl-1-*p-tert*butylphenyl-3-methylcyclobut-1-ene (3z)

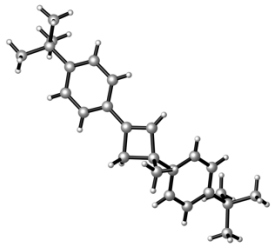

Table 16. Crystal data and structure refinement for **3z**.

Depostion number at CCDC	**CCDC 1563808**	
Identification code	CG3_49	
Empirical formula	C25 H32	
Formula weight	332.50	
Temperature	100(2) K	
Wavelength	0.71073 Å	
Crystal system	Monoclinic	
Space group	P2(1)	
Unit cell dimensions	a = 10.1094(6)Å	α= 90°.
	b = 6.1675(4)Å	β = 91.584(6)°.
	c = 16.2477(12)Å	γ = 90°.
Volume	1012.66(12) $Å^3$	
Z	2	
Density (calculated)	1.090 Mg/m^3	
Absorption coefficient	0.061 mm^{-1}	
F(000)	364	
Crystal size	0.15 x 0.10 x 0.04 mm^3	
Theta range for data collection	2.344 to 30.190°.	
Index ranges	-12<=h<=14,-8<=k<=8,-21<=l<=21	
Reflections collected	13423	
Independent reflections	5030[R(int) = 0.0717]	
Completeness to theta =30.190°	89.3%	
Absorption correction	Multi-scan	
Max. and min. transmission	0.998 and 0.768	
Refinement method	Full-matrix least-squares on F^2	
Data / restraints / parameters	5030/ 1/ 233	
Goodness-of-fit on F^2	1.044	
Final R indices [I>2sigma(I)]	R1 = 0.0703, wR2 = 0.1616	
R indices (all data)	R1 = 0.1045, wR2 = 0.1777	
Largest diff. peak and hole	0.422 and -0.286 $e.Å^{-3}$	

(*R*)-3-Phenyl-1-(thiophen-3-yl) -3-methylcyclobut-1-ene (3aa)

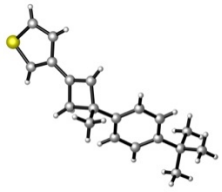

Table 17. Crystal data and structure refinement for **3aa**. Absolute configuration was determined.

Depostion number at CCDC	**CCDC 1563810**	
Identification code	CG-3-498-2a	
Empirical formula	C19 H22 S	
Formula weight	282.42	
Temperature	100(2) K	
Wavelength	0.71073 Å	
Crystal system	Monoclinic	
Space group	P2(1)	
Unit cell dimensions	a = 8.3202(3)Å	a= 90°.
	b = 6.0778(2)Å	b = 98.970(3)°.
	c = 16.2853(5)Å	g = 90°.
Volume	813.45(5) $Å^3$	
Z	2	
Density (calculated)	1.153 Mg/m^3	
Absorption coefficient	0.188 mm^{-1}	
F(000)	304	
Crystal size	0.15 x 0.1 x 0.04 mm^3	
Theta range for data collection	2.478 to 37.314°.	
Index ranges	-14<=h<=14,-10<=k<=10,-27<=l<=27	
Reflections collected	34968	
Independent reflections	8189[R(int) = 0.0455]	
Completeness to theta =37.314°	98.4%	
Absorption correction	Multi-scan	
Max. and min. transmission	0.993 and 0.764	
Refinement method	Full-matrix least-squares on F^2	
Data / restraints / parameters	8189/ 1/ 185	
Goodness-of-fit on F^2	1.037	
Final R indices [I>2sigma(I)]	R1 = 0.0473, wR2 = 0.1222	
R indices (all data)	R1 = 0.0581, wR2 = 0.1284	
Flack parameter	x =0.01(2)	
Largest diff. peak and hole	0.526 and -0.516 $e.Å^{-3}$	

1,4-Bis-[3-(4-fluorophenyl)-3-methylcyclobut-1-en-1-yl]benzene (3ak)

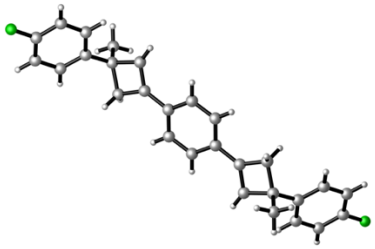

Table 18. Crystal data and structure refinement for **3ak**.

Depostion number at CCDC	**CCDC 1563805**	
Identification code	mo_CG30531_0m	
Empirical formula	C28 H24 F2	
Formula weight	398.47	
Temperature	100(2) K	
Wavelength	0.71073 Å	
Crystal system	Monoclinic	
Space group	C2/c	
Unit cell dimensions	a = 23.1418(14)Å	a= 90°.
	b = 5.7036(3)Å	b = 101.5997(19)°.
	c = 15.8393(10)Å	g = 90°.
Volume	2048.0(2) $Å^3$	
Z	4	
Density (calculated)	1.292 Mg/m^3	
Absorption coefficient	0.086 mm^{-1}	
F(000)	840	
Crystal size	0.15 x 0.05 x 0.01 mm^3	
Theta range for data collection	1.797 to 29.653°.	
Index ranges	-32<=h<=29,-7<=k<=7,-19<=l<=22	
Reflections collected	16858	
Independent reflections	2882[R(int) = 0.0482]	
Completeness to theta =29.653°	99.7%	
Absorption correction	Multi-scan	
Max. and min. transmission	0.999 and 0.915	
Refinement method	Full-matrix least-squares on F^2	
Data / restraints / parameters	2882/ 0/ 137	
Goodness-of-fit on F^2	1.159	
Final R indices [I>2sigma(I)]	R1 = 0.0710, wR2 = 0.1474	
R indices (all data)	R1 = 0.0920, wR2 = 0.1551	
Largest diff. peak and hole	0.421 and -0.351 $e.Å^{-3}$	

1,4-Bis-[3-(4-(*tert*-butyl)phenyl)-1-methylcyclobut-2-en-1-yl]benzene (3au)

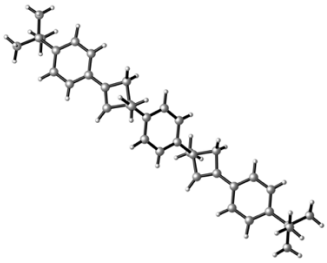

Table 19. Crystal data and structure refinement for **3au**.

Depostion number at CCDC	**CCDC 1563809**	
Identification code	CG-3-0574_P21	
Empirical formula	C36 H42	
Formula weight	474.69	
Temperature	100(2) K	
Wavelength	0.71073 Å	
Crystal system	Monoclinic	
Space group	P2(1)	
Unit cell dimensions	a = 15.4670(5)Å	a= 90°.
	b = 6.10912(17)Å	b= 115.627(4)°.
	c = 16.5386(5)Å	g = 90°.
Volume	1409.00(8) $Å^3$	
Z	2	
Density (calculated)	1.119 Mg/m^3	
Absorption coefficient	0.062 mm^{-1}	
F(000)	516	
Crystal size	0.2 x 0.15 x 0.1 mm^3	
Theta range for data collection	2.392 to 64.554°.	
Index ranges	-25<=h<=38,-11<=k<=12,-41<=l<=37	
Reflections collected	59815	
Independent reflections	28367[R(int) = 0.0334]	
Completeness to theta =64.554°	70.9%	
Absorption correction	Multi-scan	
Max. and min. transmission	0.994 and 0.765	
Refinement method	Full-matrix least-squares on F^2	
Data / restraints / parameters	28367/ 2/ 485	
Goodness-of-fit on F^2	0.725	
Final R indices [I>2sigma(I)]	R1 = 0.0422, wR2 = 0.1199	
R indices (all data)	R1 = 0.0581, wR2 = 0.1351	
Flack parameter	x =-4.3(10)	
Largest diff. peak and hole	0.591 and -0.306 e.$Å^{-3}$	

Chapter II: "Synthesis and Reactivity of Chloromethylgold(I) Carbenoids"

Introduction

Gold(I) Carbene Intermediates

Gold(I) carbenes (**1**) can be generated through different methods in catalytic transformations and have been proposed as key intermediates in many gold(I)-catalyzed reactions (Scheme 1).[1,2,3,4,5,6,7] Among these transformations, the cycloisomerization of 1,*n*-enynes **2** have attracted special attention to the synthetic community due to their versatility to access complex skeletons in an atom economical fashion (Scheme 1a).[1] Other examples include the cycloaddition of dialkyl compounds **3** to form gold vinylidene intermediates **2b** (Scheme 1b),[2] and the nucleophilic addition of *N*-oxides or sulfoxides to the electrophilic (η^2-alkyne)gold(I) complexes **4** (Scheme 1c).[3,4] In addition to reactions involving alkynes, transformations based on gold(I)-catalyzed decomposition of diazo compounds **5** (Scheme 1d)[5] and opening of

1 (a) López, S.; Herrero-Gómez, E.; Pérez-Galán, P.; Nieto-Oberhuber, C.; Echavarren, A. M. *Angew. Chem. Int. Ed.* **2006**, *45*, 6029–6032. (b) Taduri, B. P.; Sohel, S. M. A.; Cheng, H.-M.; Lin, G.-Y.; Liu, R.-S. *Chem. Commun.* **2007**, 2530–2532. (c) Escribano-Cuesta, A.; López-Carrillo, V.; Janssen, D.; Echavarren, A. M. *Chem. –Eur. J.* **2009**, *15*, 5646–5650. (d) Pérez-Galán, P.; Martin, N. J. A.; Campaña, A. G.; Cárdenas, D. J.; Echavarren, A. M. *Chem. Asian J.* **2011**, *6*, 482–486. (e) Brooner, R. E. M.; Brown, T.J.; Widenhoefer, R.A. *Angew. Chem. Int. Ed.* **2013**, *52*, 6259–6261.

2 (a) Ye, L.; Wang, Y.; Aue, D. H.; Zhang, L. *J. Am. Chem. Soc.* **2012**, *134*, 31–34. (b) Hashmi, A. S. K.; Braun, I.; Nösel, P.; Schädlich, J.; Wieteck, M.; Rudolph, M.; Rominger, F. *Angew. Chem. Int. Ed.* **2012**, *51*, 4456–4460. (c) Hashmi, A. S. K.; Wieteck, M.; Braun, I.; Rudolph, M.; Rominger, F. *Angew. Chem. Int. Ed.* **2012**, 51, 10633–10637. (d) Hansmann, M. M.; Rudolph, M.; Rominger, F.; Hashmi, A. S. K. *Angew. Chem. Int. Ed.* **2013**, *52*, 2593–2598. (e) Hansmann, M. M.; Rominger, F.; Hashmi, A. S. K. *Chem. Sci.* **2013**, *4*, 1552–1559.

3 (a) Shapiro, N.D.; Toste, F.D. *J. Am. Chem. Soc.* **2007**, *129*, 4160–4161. (b) Ye, L.; Cui, L.; Zhang, G.; Zhang, L. *J. Am. Chem. Soc.* **2010**, *132*, 3258–3259. (c) He, W.; Li, C.; Zhang, L. *J. Am. Chem. Soc.* **2011**, *133*, 8482–8485. (d) Noey, E. L.; Luo, Y.; Zhang, L.; Houk, K. N. *J. Am. Chem. Soc.* **2012**, *134*, 1078–1084. (e) Ji, K.; Zhang, L. *Org. Chem. Front.* **2014**, *1*, 34–38. (f) D. Vasu, H.-H. Hung, S. Bhunia, S. A. Gawade, A. Das, R.-S. Liu, *Angew. Chem. Int. Ed.* **2011**, *50*, 6911–6914. (g) Nçsel, P.; Nunes dos Santos Comprido, L.; Lauterbach, T.; Rudolph, M.; Rominger, F.; Hashmi, A. S. K. *J. Am. Chem. Soc.* **2013**, *135*, 15662–15666. (h) Shu, C.; Liu, R.; Liu, S.; Li, J.-Q.; Yu, Y.-F.; He, Q.; Lu, X.; Ye, L.-W. *Chem. Asian J.* **2015**, *10*, 91–95.

4 Schulz, J.; Jasíkovμ, L.; Skríba, A.; J. Roithová, J. *J. Am. Chem. Soc.* **2014**, *136*, 11513–11523.

5 (a) Fructos, M. R.; Belderrain, T. R.; de Frémont, P.; Scott, N. M.; Nolan, S. P.; Díaz-Requejo, M. M.; Pérez, P. J. *Angew. Chem. Int. Ed.***2005**, *44*, 5284–5288. (b) Prieto, A.; Fructos, M. R.; Díaz-Requejo, M. M.; Pérez, P. J.; Pérez-Galán, P.; Delpont, N.; Echavarren, A. M. *Tetrahedron* **2009**, *65*, 1790–1793. (c) Rivilla, I.; Gómez-Emeterio, B. P.; (d) Zhou, L.; Liu, Y.; Zhang, Y.; Wang, J. *Beilstein J. Org. Chem.* **2011**, *7*, 631–637.

cyclopropenes **6** (Scheme 1e)[6] have also been proposed to form these highly electrophilic species (**1d-e**). More recently, these intermediates (**1f**) have been invoked as key players in the retro-Buchner reaction of cycloheptatrienes **7** (Scheme 1f).[7]

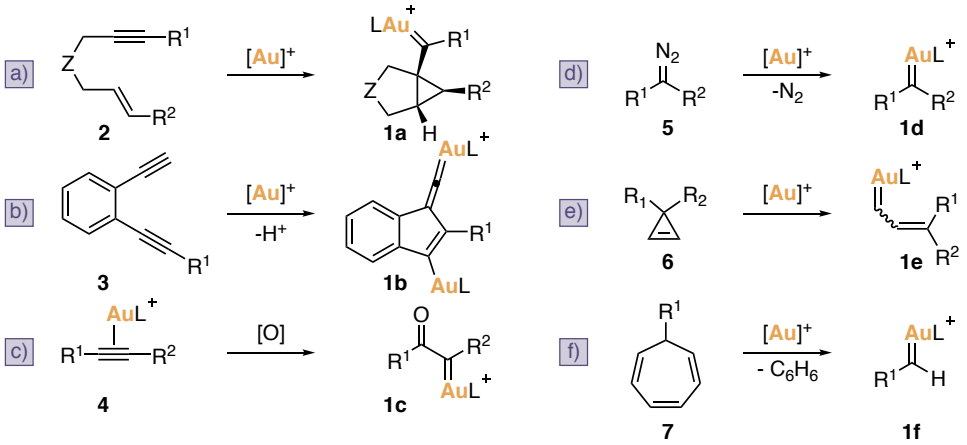

Scheme 1. Common methods for the generation of gold(I) carbenes in catalysis.

Despite the importance of gold(I) carbenes in catalysis, a debate is underway regarding the nature and the electronic structure of these intermediates. Some authors even reject their existence and propose that these species should be considered as gold(I)-stabilized carbocations. To clarify, both gold(I) carbenes and gold(I)-stabilized carbocations are just the same species represented in a different way by their extreme resonance forms (Scheme 2).[8,9]

6 (a) Hadfield, M. S.; Bauer, J. T.; Glen, P. E.; Lee, A.-L. *Org. Biomol. Chem.* **2010**, *8*, 4090–4095. (b) Li, C.; Zeng, Y.; Wang, J. *Tetrahedron Lett.* **2009**, *50*, 2956–2959. (c) Li, C.; Zeng, Y.; Zhang, H.; Feng, J.; Zhang, Y.; Wang, J. *Angew. Chem. Int. Ed.* **2010**, *49*, 6413–6417. (d) For a review on gold-catalyzed transformations of cyclopropenes, see: Miege, F.; Meyer, C.; Cossy, J. *Beilstein J. Org. Chem.* **2011**, *7*, 717–734.

7 (a) Solorio-Alvarado, C. R.; Wang, Y.; Echavarren, A. M. *J. Am. Chem.* Soc. **2011**, *133*, 11952–11955. (b) Wang, Y.; McGonigal, P. R.; Herlé, B.; Besora, M.; Echavarren, A. M. *J. Am. Chem. Soc.* **2014**, *136*, 801–809. (c) Lebœuf, D.; Gaydou, M.; Wang, Y.; Echavarren, A. M. *Org. Chem. Front.* **2014**, *1*, 759–764. (d) Wang, Y.; Muratore, M. E.; Rong, Z.; Echavarren, A. M. *Angew. Chem. Int. Ed.* **2014**, *53*, 14022–14026. (e) Herlé, B.; Holstein, P. M.; Echavarren, A. M. *ACS Catal.* **2017**, *7*, 3668–3675. (f) Yin, X.; Mato, M.; Echavarren, A. M. *Angew. Chem. Int. Ed.* **2017**, *56*, 14591–14595.

8 (a) Fürstner, A.; Morency, L. *Angew. Chem.* **2008**, *120*, 5108–5111. (b) Hashmi, A. S. K. *Angew. Chem. Int. Ed.* **2008**, *47*, 6754–6756. (c) Seidel, G.; Mynnot, R.; Fürstner, A. *Angew. Chem. Int. Ed.* **2009**, *48*, 2510–2513. (d) Echavarren, A. M. *Nat. Chem.* **2009**, 431–433.

9 Reviews on the topic: (a) Wang, Y.; Muratore, M. E.; Echavarren, A. M. *Chem. –Eur. J.* **2016**, *21*, 7332–7339. (b) Harris, R. J.; Widenhoefer, R. A. *Chem. Soc. Rev.* **2016**, *45*, 4533–4551.

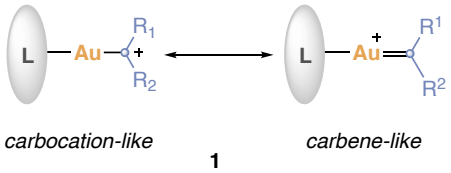

1

Scheme 2. Carbocation and carbene resonance forms used to represent gold(I) carbenes.

In 2009, a bonding model was proposed by Goddart and Toste to better understand the electronic structures of gold(I) carbenes **1**. Based on this proposal, both the ancillary ligand and the carbene moiety can donate their paired electrons to gold(I) forming a three-center-four-electron σ-hyperbond (Figure 1, left).[10] In these species, the gold center can also form π-bonds by backdonation of its electrons from filled *5d* orbitals to empty π-acceptor orbitals on the carbene moiety and the ancillary ligand (Figure 1, right).

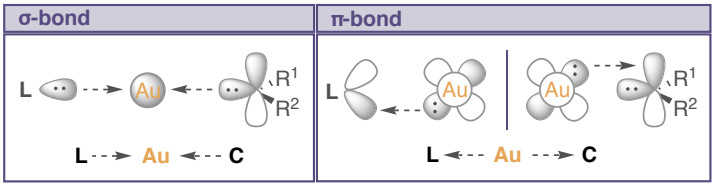

Figure 1. Bonding model of gold(I) carbenes.

Considering the competition of the ancillary ligand and the carbene moiety for the electron density of gold(I), the electronic nature of both fragments will play an important role in the gold(I)-carbon bond and the reactivity of a given gold(I) carbene (Figure 2). Regarding the carbene fragment (Figure 2, left), a decrease in the carbon-gold σ-bonding and an increase in gold-carbon π-bonding will lead to structures with more carbene-like character. Moreover, good σ-donating and poor π-acidic ancillary ligands will also increase the carbene-like character by increasing π-backdonation from gold to carbon (Figure 2, right).

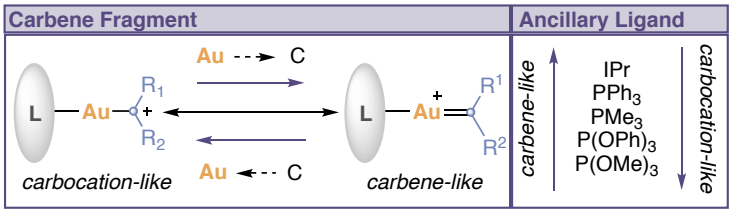

Figure 2. Fragment influence on the Au(I)-C bond of gold(I) carbenes.

Gold(I) carbenes (**1**) can be viewed as an extreme case of Fischer carbenes, which contain a π-donating group attached to the carbenic carbon atom that stabilizes the *p* empty orbital on

10 Benitez, D.; Shapiro, N. D.; Tkatchouk, E.; Wang, Y.; Goddard, W. A. 3rd, Toste, F. D. *Nat. Chem.* **2009**, *1*, 482–486.

the carbonic carbon through π-donation from one of the heteroatom electron lone pairs (Figure 3, left). As a consequence, the metal-to-carbon π-backdonation is weak, and thus, the carbon atom is positively charge and the carbene shows electrophilic character. In the case of gold, the most electronegative of all transition metals, the π-backdonation is low and the corresponding carbenes are highly electrophilic (Figure 3, right).

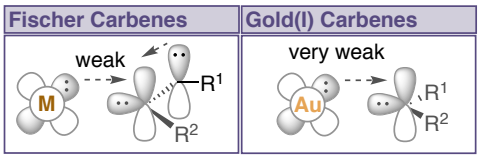

Figure 3. Relation between Fischer carbenes and gold(I) carbenes.

Beyond the theoretical bonding model, the extension of the π-backbonding interaction between gold(I) center and carbenic carbon atom in real intermediates is controversial. As explained before, this gold-to-carbon π-backdonation influences the relative contributions of carbene and carbocation resonances forms, and thus, the reactivity displayed by gold(I) carbenes (**1**). This lack of agreement about the contribution of gold-to-carbon π-backdonation in the stabilization of gold(I) carbenes can be understood by the absence of well-defined gold(I) carbenes intermediates (this subject will be discussed in detail in the introduction of chapter 3).[11,12]

In this Thesis manuscript, we represent gold-carbon bonds as double bonds in gold(I) carbenes. However, we advised the reader to bear in mind that gold(I) carbenes are better accounted as a continuum that ranges from metal-stabilized singlet carbenes with a bond order of two to metal-coordinated carbocations with a bond order of one.

Metal Carbenoids

---

11 Gold(I) carbenes isolated bearing stabilizing functional groups attached to the carbenic carbon: (a) Fañanás-Mastral, M.; Aznar, F. *Organometallics*, **2009**, *28*, 666–668. (b) Ung, G.; Bertrand, G. *Angew. Chem. Int. Ed.* **2013**, *52*, 11388–11391. (c) Brooner, R. E. M.; Widenhoefer, R. A. *Chem. Commun.* **2014**, *50*, 2420–2423. (d) Seidel, G.; Gabor, B.; Goddard, R.; Heggen, B.; Thiel, W.; Fürstner, A. *Angew. Chem. Int. Ed.* **2014**, *53*, 879–882. (e) Seidel, G.; Fürstner, A. *Angew. Chem. Int. Ed.* **2014**, *53*, 4807–4811. (f) Ciancaleoni, G.; Biasiolo, L.; Bistoni, G.; Macchioni, A.; Tarantelli, F.; Zuccaccia, D.; Belpassi, L. *Chem. –Eur. J.* **2015**, *21*, 2467–2473. (g) Wang, J.; Cao, X.; Lv, S.; Zhang, C.; Xu, S.; Shi, M.; Zhang, J. *Nature Comm.* **2017**, *8*, 14625–14635.

12 Gold(I) carbenes isolated without stabilizing functional groups attached to the carbenic carbon: (a) Hussong, M. W.; Rominger, F.; Krämer, P.; Straub, B. F. *Angew. Chem. Int. Ed.* **2014**, *53*, 9372–9375. (b) Harris, R. J.; Widenhoefer, R. A. *Angew. Chem. Int. Ed.* **2014**, *53*, 9369–9371. (c) Joost, M.; Estévez, L.; Mallet-Ladeira, S.; Miqueu, K.; Amgoune, A.; Bourissou, D. *Angew. Chem. Int. Ed.* **2014**, *53*, 14512–14516. (d) Zeineddine, A.; Rekhroukh, F.; Carrizo, E. D. S.; Mallet-Ladeira, S.; Miqueu, K.; Amgoune, A.; Bourissou, D. *Angew. Chem. Int. Ed.* **2018**, *57*, 1306–1310.

To stress the low gold-to-carbon π-backdonation in gold(I) carbenes intermediates of type **1**, some authors have recommended the use of the term gold(I) carbenoid to describe such species.[13]

In 1964, the term carbenoid was first stablished to refer to compounds that exhibit similar reactivity to carbenes not being free divalent CR_2 species.[14] Often, the term carbenoid has been used to describe organometallic species **8**, which are structurally related to metallocarbenes **9**. More precisely, they contain a sp^3 carbon bound both to a metal and to a good leaving group (**X**) (Scheme 3). After removal of the leaving group from species **8**, formal metallocarbenes **9** are generated, which can transfer the carbene moiety onto a substrate.

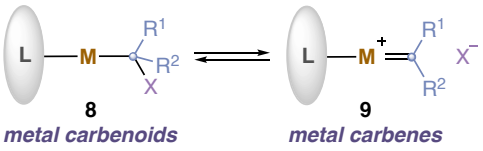

Scheme 3. Structural relationship between metal carbenoids **8** and carbenes **9**.

Recently, Pérez and co-workers have revised the use of the terms metal carbene and carbenoid in the metal catalyzed carbene transfer from diazo compounds to substrates such as alkenes and alkanes.[15] In these processes, a diazo compound can coordinate to the metal center through different atoms to generate intermediates **10**, **11** and **8** (Scheme 4). The coordination of the diazo compounds *via* the carbon atom generates intermediates **8**, which are metal carbenoids. Complexes **8** are different species than metal carbenes **9** but, at the same time, are the only productive species capable of generating metal carbenes by nitrogen exclusion as leaving group removal (Scheme 4).

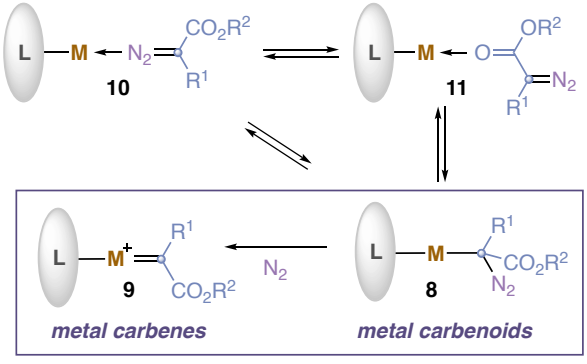

Scheme 4. Relevant intermediates for metal-diazo interaction.

13 Seidel, G.; Fürstner, A. *Angew. Chem. Int. Ed.* **2014**, *53*, 4807–4811.

14 Closs, G. L.; Moss, R. A. *J. Am. Chem. Soc.* **1964**, *86*, 4042–4053.

15 Caballero, A.; Pérez, P. J. *Chem. –Eur. J.* **2017**, *23*, 14389–14393.

Gold(I) Carbenoids

The first example of well-characterized gold(I) carbenoid was reported 30 years ago.[16] In this seminal work, the synthesis of chloromethylgold(I) complex **12a** used toxic and potentially explosive diazomethane (Scheme 5).[16a] In a more recent work, gold(I) carbenoid **12a** was prepared through a different method *via in situ* formation of [Mg(CH_2Cl)Cl] at low temperature (Scheme 5).[17] Gold(I) carbenoid **12a** was able to promote cyclopropanation of 3-cyclohexenol under harsh conditions in very low yield (Scheme 5). Furthermore, chloromethylgold(I) carbenoid **12a** react with KI, NaOMe and PPh_3 through leaving group exchange to form gold(I) carbenoids **12b-d** (Scheme 5).[17] Interestingly, iodomethylgold(I) carbenoid **12b** rapidly decomposes at room temperature yielding ethylene.[17]

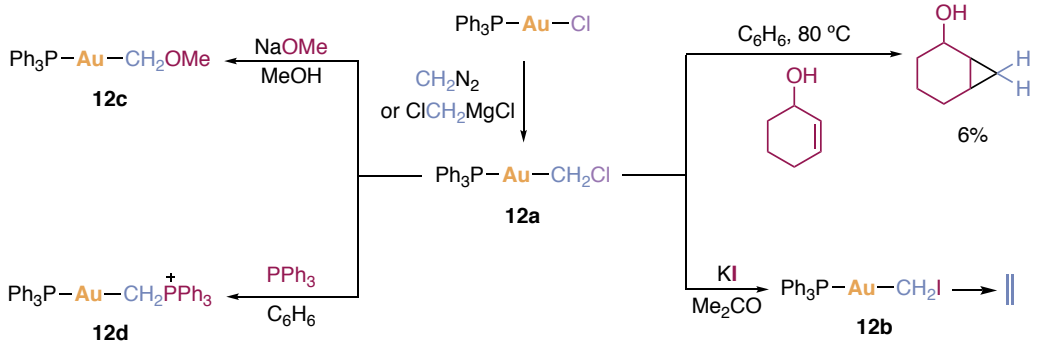

Scheme 5. Synthesis and reactivity of gold(I) carbenoid **12a**.

Other gold(I) carbenoids bearing different substituents at the Csp^3 bound to gold were prepared by different methods. Specifically, both $Ph_3PAuCCl_3$ (**12e**)[18] and $Ph_3PAuCCl_2CN$ (**12f**)[19] (Scheme 6) were obtained by treating complex $(Ph_3PAu)_3OBF_4$ in the presence of a base with $CHCl_3$ and $CHCl_2CN$ respectively. Additionally, the reaction of complex Me_3PAuCl with $LiCH_2SPh$ led to the stable phenylthiomethylgold(I) complex **12g** (Scheme 6).[17]

Scheme 6. Gold(I) carbenoids **12e-g**.

16 Nesmeyanov, A. N.; Perevalova, É. G.; Smyslova, E. I.; Dyadchenko, V. P.; Grandberg, K. I. *Russ. Chem. Bull.* **1977**, *26*, 2417–2419.

17 Steinborn, D.; Becke, S.; Herzog, R.; Günther, M.; Kircheisen, R.; Stoeckli-Evans, H.; Bruhn, C. *Z. Anarg. Allg. Chem.* **1998**, *624*, 1303–1307.

18 Perevalova, E. G.; Smyslova, E. I.; Grandberg, K. *I. Russ. Chem. Bull.* **1982**, *31*, 2506–2506.

19 Perevalova, E. G.; Struchkov, Y. T.; Dyadchenko, V. P.; Smyslova, E. I.; Slovokhotov, Y. L.; Grandberg, K. I. *Russ. Chem. Bull.* **1983**, *32*, 2529–2536.

Terminologically, we recommend to differentiate between gold(I) carbenes and gold(I) carbenoids that are, as explained, different species. Furthermore, we encourage to use the term gold(I) carbenes and not gold(I) carbenoids or gold(I) carbocations to refer to cationic gold(I) complexes in which the gold center is bounded to a CR_2 moiety.[9a,15]

Objectives

Despite the central role of gold(I) carbenes in gold catalysis,[1,2,3,4,5,6,7] few non-heteroatom-stabilized gold(I) carbene complexes have been characterized.[12] The reduced steric shielding provided by commonly used ligands and the intrinsically high electrophilicity exhibited by simple gold(I) carbenes preclude their isolation in condensed phase. The isolation of this type of compounds, or their functional equivalents, is therefore of great importance for the fundamental understanding of the reactivity of electrophilic gold carbenes.

Gold(I) complexes of the type [LAuCHRX], formally defined as gold(I) carbenoids,[9a,15] are, in principle, stable and chemically equivalents to their carbene counterparts, which would provide an attractive alternative to otherwise non-isolable gold(I) carbene species. To date however, very little is known about gold(I) carbenoids and their reactivity.[16,17] Furthermore, complexes of the type [LAuCH$_2$Cl] have been prepared using either toxic and potentially explosive diazomethane[16] or low temperature *in situ* formation of [Mg(CH$_2$Cl)Cl.[17]

In this context, we aimed to develop a convenient approach to easily and safely prepare gold(I) carbenoids and thus, explore their role as a stable source of gold(I) carbenes in solution (Scheme 7). In particular, we focused our attention on the synthesis and reactivity of chloromethylgold(I) complexes bearing bulky ligands.

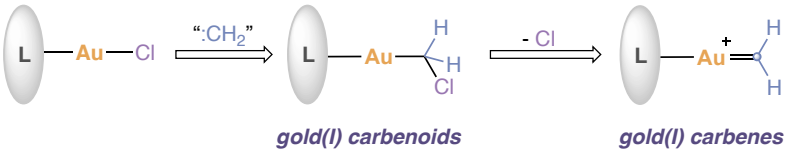

Scheme 7. Synthesis of gold(I) carbenoids and their possible role as precursors of gold(I) carbenes.

Results and Discussion

Synthesis of Chloromesitylgold(I) Carbenoids

As mentioned in the introduction of this chapter, chloromethylgold(I) complexes, [LAuCH_2Cl], have been prepared using either potentially hazardous diazomethane (CH_2N_2)[16] or low temperature *in situ* formation of [Mg(CH_2Cl)Cl],[17] and not much is known about their reactivity. Therefore, in order to have access to a variety of chloromethylgold(I) carbenoids, we began our investigations by developing a more convenient way to synthetize these complexes. To this end, we focused our attention on trimetylsilyldiazomethane. The latter has been extensively used as a safe alternative to diazomethane in the presence of methanol as co-solvent for the methyl esterification of carboxylic acids (Scheme 8, right).[20,21] The mechanism of this transformation has been recently studied and the reaction proceeds through the *in situ* methanol-promoted liberation of CH_2N_2.[22] Furthermore, in organometallic chemistry, a similar procedure for the *in situ* generation of CH_2N_2 from $TMSCHN_2$ in a mixture of H_2O/Acetone/DCM as solvent has been used for the synthesis of halogenomethylplatinum(II) complexes, [$L_2Pt(CH_2X)_2$] (Scheme 8, left).[23]

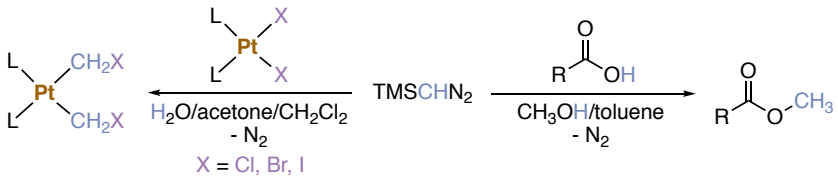

Scheme 8. $TMSCHN_2$ for the *in situ* generation of CH_2N_2

With this knowledge, a synthesis for gold(I) carbenoid **14a** was developed based on the methanol-promoted decomposition of tetramethylsilyldiazomethane (Table 1). The optimization of this method was performed by Mihai Raducan, Ekaterina S. Smirnova and Dr. Dirk Spigel and a short optimization table will be outlined here for the sake of completeness (Table 1). Initially, they found that the reaction of [JohnPhosAuCl] (**13a**) with $TMSCHN_2$ in benzene led to a complex mixture in which [JohnPhosAuCH_2Cl] (**14a**) was the major product (Table 1, entry 1). The addition of alcohols as proton sources had a positive impact in the chemoselectivity increasing the ratio of gold(I) carbenoid **14a** *vs.* other possible products (**15a**,

20 Original conditions for the use of $TMSCHN_2$ with CH_3OH/Toluene as solvents for methyl esterification: Hashimoto, N.; Aoyama, T.; Shioiri, T. *Chem. Pharm. Bull.* **1981**, *29*, 1475–1478.

21 For reviews of the use of $TMSCHN_2$, see: (a) Shioiri, T.; Aoyama, T. *Adv. Use Synthons Org. Chem.* **1993**, *1*, 51–101. (b) Podlech, J. *J. Prakt. Chem./Chem.-Ztg.* **1998**, *340*, 679–682. (c) Presser, A.; Hüfner, A. *Monatsh. Chem.* **2004**, *135*, 1015–1022.

22 Kühnel, E.; Laffan, D. D. P.; Lloyd-Jones, G. C.; Martínez del Campo, T.; Shepperson, I. R.; Slaughter, J. L. *Angew. Chem. Int. Ed.* **2007**, *46*, 7075–7078.

23 Bergamini, P.; Bortolini, O.; Costa, E.; Pringle, P. G. *Inorg. Chim. Acta*, **1996**, *252*, 33–37.

16a and other unknown products) (Table 1, entries 2-6). In particular, the addition of 10 equiv of methanol led to the formation of the desired complex **14a** in a selective manner (Table 1, entry 4).

Table 1. Optimization of the synthesis of [JohnPhosAuCH$_2$Cl] (**14a**).

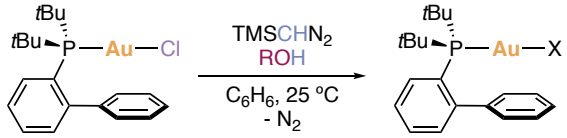

13a

14a (X = CH_2Cl)
15a (X = CH_2OR)
16a (X = OR)

Entry	ROH (equiv)	t (h)	Outcome (ratio of products)[c] **14a**:**15a**:**16a**:**13a**:unknown
1[a]	none	< 0.5	Complex mixture, **14a** major product
2[a]	CF_3CH_2OH (14)	0.5	42:9:29:3:17
3[b]	*t*BuOH (10)	96	63:0:3:27:7
4[b]	CH_3OH (10)	1	95:4:0:1:0
5[b]	EtOH (10)	3	93:1:0:2:4
6[b]	*i*PrOH (10)	3	78:0:0:11:11

[a] TMSCHN2 (2 equiv). [b] TMSCHN2 (1.2 equiv.). [c] Calculated by ^{1}H NMR.

With the previously optimized conditions,[Error! Bookmark not defined.] and in collaboration with Dr. Juan M. Sarria Toro, we prepared a new family of chloromethylgold(I) carbenoids **14** from the corresponding gold(I) chloride complexes **13** (Scheme 9). In particular, treatment of JohnPhos-type phosphines (**13a-b**), IPr carbene ligand (**13c**) and phosphite (**13d**) gold(I) chloride complexes with trimethylsilyldiazomethane in benzene solution in presence of methanol afforded gold carbenoids **14a** to **14d** within minutes as evidenced by the disappearance of the yellow color (Scheme 9).

Complexes **14a-c** could be easily purified by column chromatography on neutral aluminum oxide. Remarkably, gold(I) carbenoids **14a-c** can be stored indefinitely when protected from air and only decompose slowly when left under ambient conditions. However, complex **14d** bearing a less σ-donating phosphite as ancillary ligand was not stable in column chromatography and it had to be purified by filtration and precipitation. Furthermore, carbenoid **14d** decomposes even under inert conditions, and thus, no reliable yield could be calculated.

Molecular structures of complexes **14a**, **14b** and **14c** could be obtained and are shown in Figure 4. Measured Au–C1 distances are within the range of 2.058-2.088 Å (Table 2, entries 1-3, column 3) and, are close to the observed Au–C1 distance for the previously reported

PPh_3AuCH_2Cl complex (**12a**) (Table 2, entry 5, column 3).[17] On the other hand, C1–Cl distances (1.828-1.830 Å, Table 2, entries 1-3, column 4) are markedly longer than found in **12a** (1.681 Å, Table 2, entry 5, column 4)[17] and, in fact, are the longest among all 79 currently published crystal structures containing a $[MCH_2Cl]$ motif.[24] The longest previously reported C1–Cl distance in a (chloromethyl)metal fragment was found in a Rh(III) complex and measured 1.826 Å.[25] On the other hand, the Au–C1–Cl angles (110.3-111.1 º, Table 2, entries 1-3, column 5) are closer to the ideal tetrahedral angle as opposed to the majority of other structures in which the M–C1–Cl angle is found around 116 degrees. In particular, for the previously reported chloromethylgold(I) complex **12a**, this angle is 115.4 º.[17]

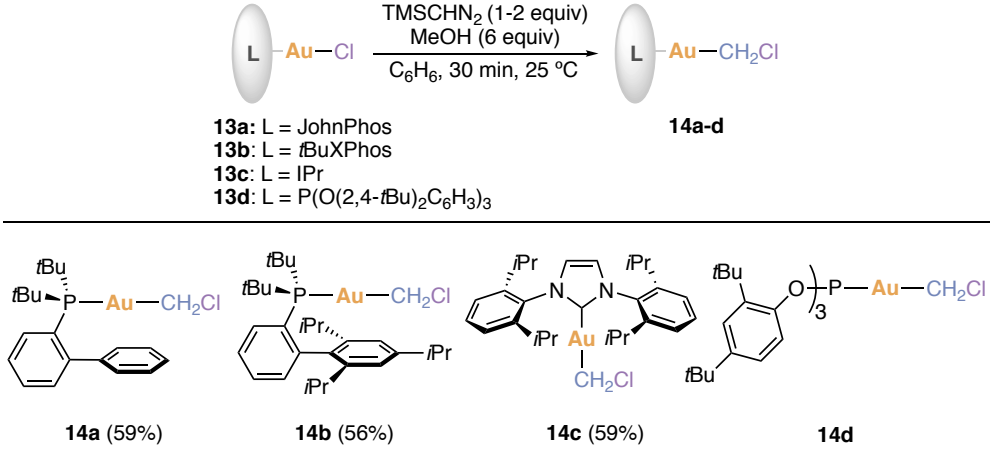

Scheme 9. Synthesis of chloromethylgold(I) carbenoids **14a-d**.

Table 2. Selected bond distances and angles from X-ray crystal structures and chemical shifts for the new gold(I) carbenoid complexes **14a-d** and the previously reported carbenoid **12a**.[17]

Entry	Complex	Au–C1 (Å)	C1–Cl (Å)	Au–C1–Cl (º)	H1 (ppm)[a]	C1 (ppm)[a]
1	**14a**	2.058	1.828	110.3	2.96	53.6
2	**14b**	2.088	1.829	111.1	2.94	53.9
3	**14c**	2.060	1.830	110.4	3.34	47.2
4	**14d**	-	-	-	3.63	47.2
5	**12a**[17]	2.088	1.681	115.4	3.90[b]	52.9[b]

[a] Chemical shift measured in CD_2Cl_2 at 25 ºC. [b] Chemical shift measured in CD_3Cl at 25 ºC.

Chemical shifts for the chloromethyl moiety (H1 and C1, Figure 4) are found between 2.94 and 3.63 ppm in ^1H NMR (Table 2, entries 1-4, column 6) and 47.2 and 53.9 ppm in ^{13}C NMR (Table 2, entries 1-4, column 7), in concordance with the chemical shifts reported for complex

24 Groom, C. R.; Bruno, I. J.; Lightfoot, M. P.; Ward, S. C. *Acta Crystallogr. Sect. B: Struct. Sci.* **2016**, *72*, 171–179.

25 Vetter, A. J.; Rieth, R. D.; Brennessel, W. W.; Jones, W. D. *J. Am. Chem. Soc.* **2009**, *131*, 10742–10752.

12a.[17] These results reflect the overall electron deficient character of these chloromethylgold(I) carbenoids.

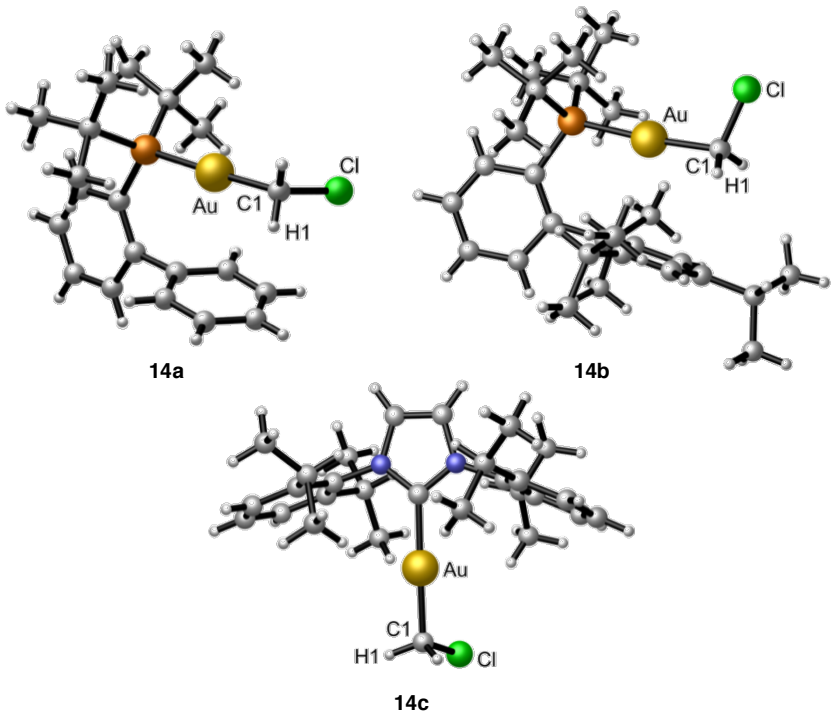

Figure 4. X-ray crystal structures of gold(I) carbenoids **14a-c**.

Activation of Chloromethylgold(I) Carbenoids with Chloride Scavengers

Ethylene formation

When solutions of complexes **14a-d** were treated with chloride scavengers possessing weakly coordinating counterions, *e.g.* TMSX and AgX (X = NTf_2^-, OTf^-, SO_3Me^-, $CF_3CO_2^-$), the conversion of **14a-d** to new gold(I) carbenoids of the type **15** could be detected in all cases (Scheme 10). Intermediates **15**, in which the chloride has been replaced by the counterion of the scavenger, bear a better leaving group than carbenoids **14a-d**. In fact, they are not stable in toluene-d_8 or CD_2Cl_2 at 25 ºC and decay over time giving rise to the formation of simple gold(I) salts **16** and ethylene (**17**) (Scheme 10). Analysis of the volatile products by GC-MS confirmed the identity of ethylene (**17**) and excluded the formation of any additional organic compounds.[26]

26 See experimental section for further details.

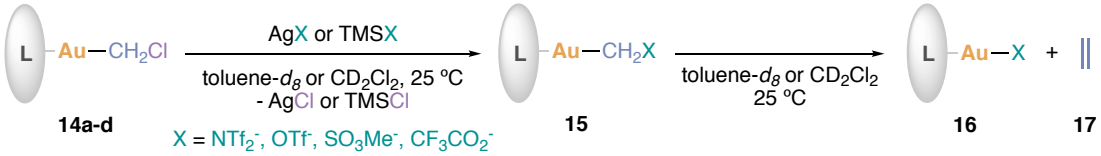

Scheme 10. General scheme for the activation of chloromethylgold(I) carbenoids **14a-d** with chloride scavengers possessing weakly coordinating counterions.

The reaction of complexes **14a-d** with $AgSbF_6$ did not afford the aforementioned intermediates **15**, in which the chloride would have been replaced by SbF_6^-. However, immediate conversion of the corresponding carbenoids **14a-d** into ethylene and gold(I) chlorides **13a-d** was observed (Scheme 11). These results highlight the poor coordinating ability of SbF_6^-.

Scheme 11. General scheme for the activation of chloromethylgold(I) carbenoids **14a-d** with $AgSbF_6$.

Even though ethylene (**17**) was detected along all the experiments, its signal could not be accurately integrated due to its rapid equilibration with the gas phase. For this reason, ethylene (**17**) was quantified by means of pressure measurements in a closed system at CIQSO, Universidad de Huelva, in Prof. Pedro J. Pérez Laboratory with the help of Dr. Manuel Romero Fructos-Vázquez. To perform these experiments we first analyzed the reaction of gold(I) carbenoid **14a** with TMSOTf in toluene at 25 ºC by NMR. Accordingly, after chloride abstraction, initial formation of species **15a** was detected and the latter was subsequently converted into gold(I) chloride **16a** and ethylene (**17**) (Figure 5). By means of pressure changes, a final yield of 60% of ethylene (**17**) could be calculated after 60 minutes under the aforementioned conditions (Figure 5).

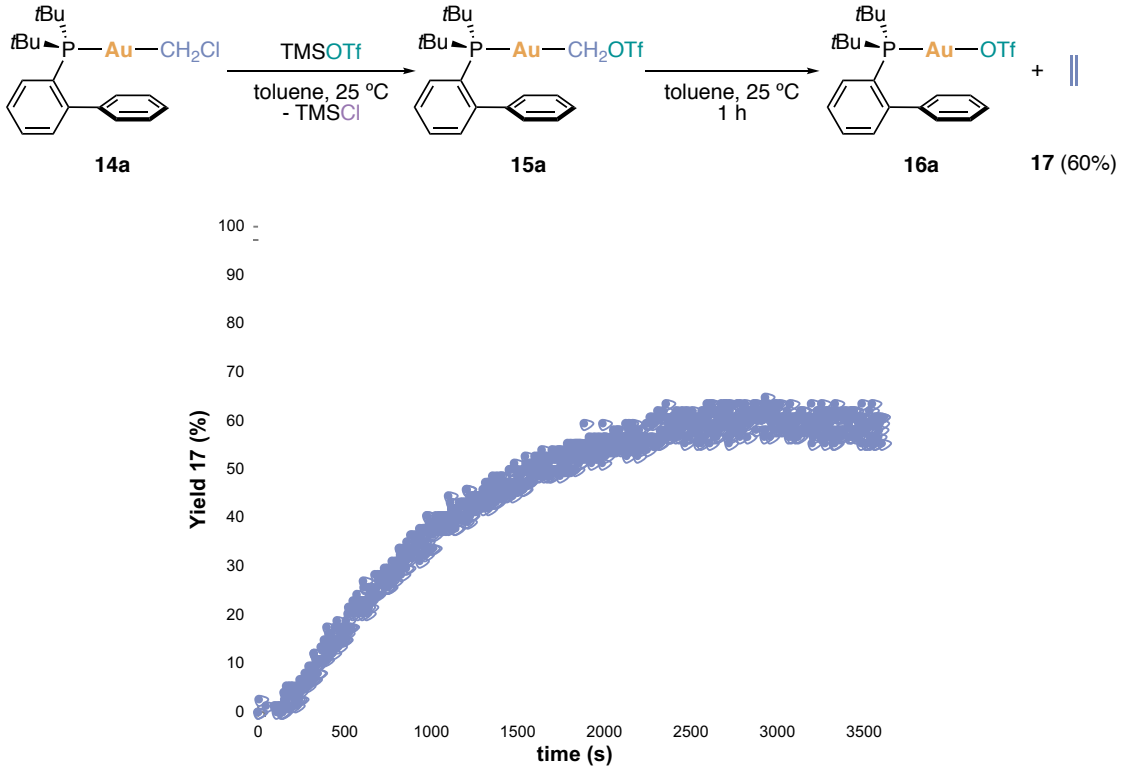

Figure 5. Ethylene evolution *vs.*time in the decay of gold(I) carbenoid **15a**.

Mechanistic investigations on ethylene formation

To gain further insight into the formation of ethylene, we prepared a monodeuterated carbenoid **14a-*d*$_1$** through our optimized route for the synthesis of chloromethylgold(I) carbenoids but using deuterated methanol as deuterium source (Scheme 12). The deuterium incorporation was calculated by ^{1}H NMR as 50% (**14a**:**14a-*d*$_1$** = 1:1) suggesting that methanol is not the only proton source in the synthesis of chloromethylgold(I) complexes *via* methanol-promoted decomposition of $TMSCHN_2$.

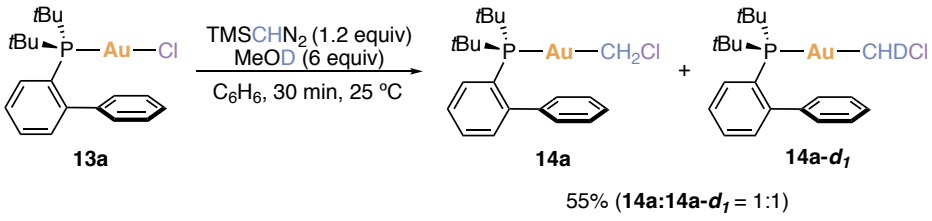

Scheme 12. Synthesis of partially monodeuterated **14-*d*$_1$** carbenoid.

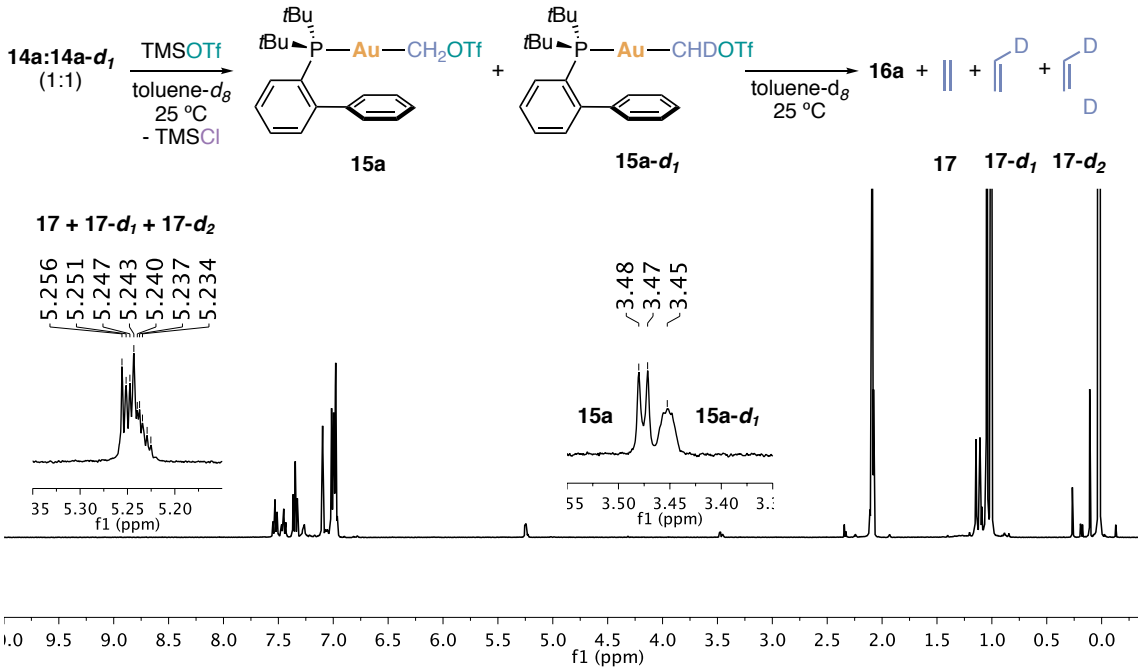

Figure 6. ^{1}H NMR spectra obtained after activation of complexes **14a**:**14a-*d*$_1$** with TMSOTf in toluene-d_8.

The ^{1}H NMR spectrum obtained upon chloride abstraction with TMSOTf on the partially monodeuterated mixture of carbenoids **14a**:**14a-*d*$_1$** (1:1) exhibits signals with characteristic deuterium couplings arising from the formation of the mono- and bi-deuterated ethylenes **17-*d*$_1$**[27] and **17-*d*$_2$**[28] alongside **17** (Figure 6). This result suggests a bimolecular ethylene formation *via* reaction of two molecules of carbenoid complex. However, by itself, this observation is not sufficient to unambiguously determine the reaction pathway.

We decided to perform kinetic studies on the ethylene formation to determine the partial order of carbenoid **14a** in this process. To this end, kinetic studies of the reaction of **14a** with an excess of AgOTf were performed by Dr. Juan M. Sarria Toro. Under these conditions, the reaction of carbenoid **14a** with AgOTf could be conveniently monitored by ^{1}H NMR to obtain accurate kinetic concentration profiles of carbenoid **14a**, triflate substituted species **15a** and the final gold salt **16a** varying the temperature.

The consumption of carbenoid **14a** at 278 K follows a first order decay as expected from the pseudo-first order conditions employed (Scheme 13, first step). Surprisingly, the subsequent decay of intermediate **15a** at 303 K into complex **16a** and ethylene (**17**) also follows a first

27 Reddy, G. S.; Goldstein, J. H. *J. Mol. Spectrosc.* **1962**, *8*, 475–484.

28 Chetcuti, M. J.; Chisholm, M. H.; Folting, K.; Haitko, D. A.; Huffman, J. C. *J. Am. Chem. Soc.* **1982**, *104*, 2138–2146.

order kinetic regime on complex **15a** (Scheme 13, second step), contrary to what would be expected for a dimerization process and the reported second order homocoupling of well-characterized methylidene complexes of Ta[29] and Re.[30,31]

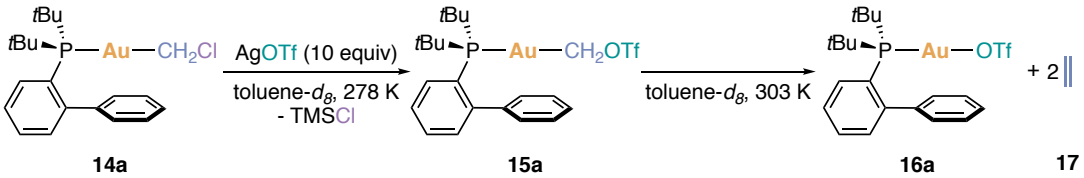

14a **15a** **16a** **17**

Scheme 13. Reaction of **14a** with excess AgOTf used for the determination kinetics order by ^{1}H-NMR.

The kinetically unusual formation of ethylene was examined on a model system by means of DFT calculations performed by Dr. Juan M. Sarria Toro. The main conclusions will be outlined here to fully understand the ethylene formation mechanism. These studies were performed using PMe_3 as ligand (Scheme 14).

Initially, an ionization (S_N1 dissociative-type) mechanism to generate cationic gold(I) carbene **IntI**, [$Me_3PAuCH_2^+$], was calculated (Scheme 14). However, even if species corresponding to cationic [JohnPhosAuCH$_2$]$^+$ could be experimentally detected upon ESI-MS of **14a**,[26] the formation of **IntI** in solution is unlikely as the energy required to generate this species from the corresponding neutral carbenoid **15b** is prohibitively high (70.9 kcalmol^{-1}). Instead, the formation of a neutral tricoordinated gold(I) carbene **IntII** from **15b** was located with an activation energy barrier of 31.1 kcalmol^{-1} (Scheme 14). This gold(I) carbene intermediate (**IntII**) could further react with another molecule of carbenoid **15b** to yield, after several steps, a dimer with two bridging methylene units (**IntIV**) from which, as proposed from Co[32] and Rh,[33] free ethylene (**17**) could be generated (Scheme 14). Since the formation of **IntII** (RDS according to the calculations) and the ethylene extrusion (according to the experiments) are both unimolecular reactions, the experimentally observed first order decay of **14a** can be rationalized in terms of our proposed mechanism. It is worth mentioning that no path for the formation of ethylene from two carbenoids **15b** could be located.

29 Schrock, R. R.; Sharp, P. R. *J. Am. Chem. Soc.* **1978**, *100*, 2389–2399.

30 Merrifield, J. H.; Lin, G. Y.; Kiel, W. A.; Gladysz, J. A. *J. Am. Chem. Soc.* **1983**, *105*, 5811–5819.

31 For further details see supporting information of *Angew. Chem. Int. Ed.* **2017**, *56*, 1859–1863.

32 Laws, W. J.; Puddephatt, R. J. *J. Chem. Soc., Chem. Commun.* **1984**, 116–117.

33 Saez, I. M.; Andrews, D. G.; Maitlis, P. M. *J. Organomet. Chem.* **1987**, *334*, C17–C19.

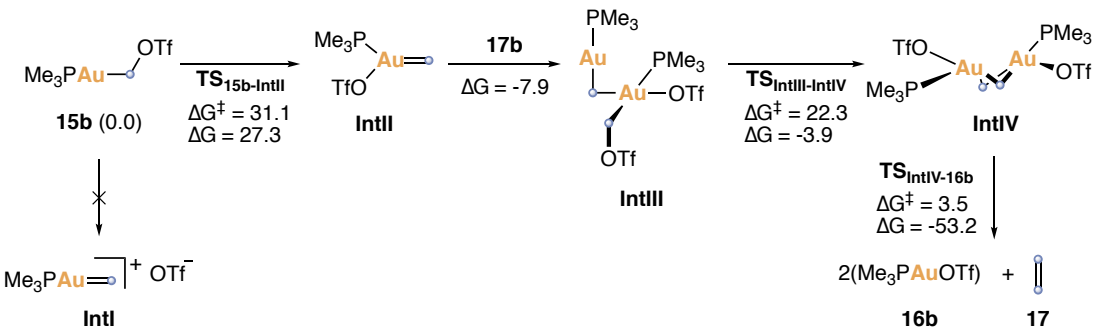

Scheme 14. Calculated reaction profile for the formation of ethylene on the model system. DFT calculations were performed at B3LYP-D3/6-31G(d,p) + SDD(f,g) on Au. Toluene was represented with the PCM. Free energies are in kcal·mol^{-1}.

Trapping with THF

Activation of **14a** with $AgSbF_6$ at -20 ºC in THF suppressed the formation of ethylene (**17**) and yielded instead a gold(I)-stabilized oxonium ylide **18** (Scheme 15). Trapping is irreversible and no ethylene (**17**) is formed even upon heating of the sample. Gold(I) complex **18** was characterized by X-ray crystal structure (Figure 7). The molecular structure of complex **18** shows a Au–C1 (2.065 Å) distance within the range of the previously characterized gold(I) carbenoids **14a-c** (Table 2). As expected, the new C1–O bond (1.517 Å) is markedly shorter than C1–Cl bonds in **14a-c** (Table 2). Furthermore, the Au–C1–O angle (109.0 º) corresponds to the ideal tetrahedral angle between two substituents around a sp^3 hybridized carbon.

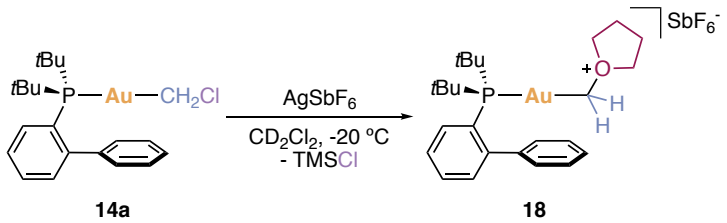

Scheme 15. Synthesis of gold(I)-stabilized oxonium ylide **18**.

Chemical shifts for the chloromethyl moiety (H1 and C1, Figure 7) are found at 4.66 ppm in ^{1}H NMR and 116.2 ppm in ^{13}C NMR, and are deshielded with respect to the signals for the same atoms in chloromethylgold(I) carbenoid **14a**.

Despite the lack of reactivity of complex **18**, its formation hinted at the possibility of an intermolecular trapping of the methylene moiety with a suitable substrate, which leads us to the next section.

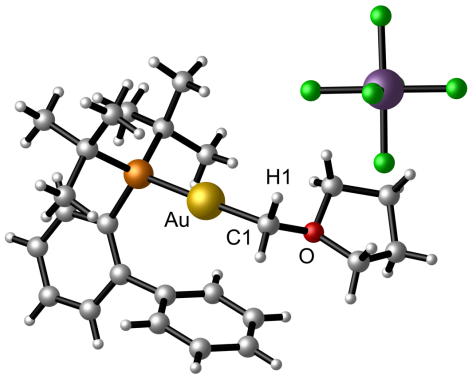

18

Figure 7. X-ray crystal structure of gold(I)-stabilized oxonium ylide **18**.

Cyclopropanation of alkenes

When the activation of carbenoids **14** was carried out in the presence of cyclic alkene **19** and **20**, methylene transfer to form cyclopropanes **21** and **22** alongside ethylene (**17**) was observed (Table 3).

Table 3. Gold(I)-promoted cyclopropanation of alkenes **19** and **20** *via* chloride abstraction of gold(I) carbenoids **14a,c-d**.

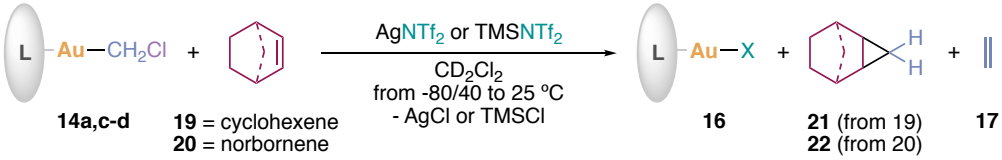

14a,c-d **19** = cyclohexene **20** = norbornene **16** **21** (from 19) **22** (from 20) **17**

Entry[a]	Complex	Chloride Scavenger	Yield **21** (%)[b]	Yield **22** (%)[b]
1	**14a**	$TMSNTf_2$	51	97
2		$AgNTf_2$	60	74
3	**14c**	$TMSNTf_2$	67	75
4		$AgNTf_2$	45	51
5	**14d**	$TMSNTf_2$	0	0
6		$AgNTf_2$	4	0

[a] **14** (0.017 mmol), **19** or **20** (20 equiv). [b] ^1H NMR yield calculated using diphenylmethane as internal standard.

In particular, complexes **14a** and **14c** could methylenate cyclohexene (**19**) and norbornene (**20**) yielding norcarene **21** and *exo*-tricyclo[3.2.1.$0^{2,4}$]octane **22** in moderate to good yields when the carbenoids were activated with either $AgNTf_2$ or $TMSNTf_2$ (Table 3, entries 1-4). These cyclopropanation reactions occur faster than ethylene (**17**) formation and at temperatures as low as -40 ºC. In the case of phosphite complex **14d**, only traces of cyclopropanes could be detected with cyclohexene (**19**) even after warming the samples to 25 ºC (Table 3, entries 5 and 6). These results show that good σ-donor and poor π-acceptor ligands attached to gold(I)

in **14a** and **14c** (JohnPhos-type phosphines and *N*-heterocyclic carbenes) stabilize carbene ligands as explained in the introduction of this chapter (Figure 2).

The possible reaction mechanisms leading to cyclopropanes were also examined by means of DFT calculations by Dr. Juan M. Sarria Toro. The main conclusions will be outlined here for the sake of completeness. As before, studies were performed using PMe_3 as ligand (Scheme 16).

Having previously excluded the possibility of a S_N1-type pathway to generate cationic gold(I) carbene **IntI** $[Me_3PAuCH_2]^+$ from gold(I) carbenoid **15b** (Scheme 14), other pathways had to be examined. Gratifyingly, cyclopropanation can alternatively occur *via* a three-centered transition state $\mathbf{TS_{20\text{-}22}}$ in analogy to the Simmons-Smith reaction[34] leading to $Me_3PAuOTf$ (**16b**) and cyclopropane **22** (Scheme 16). This pathway is energetically accessible and can be considered competent for the formation of cyclopropanes.

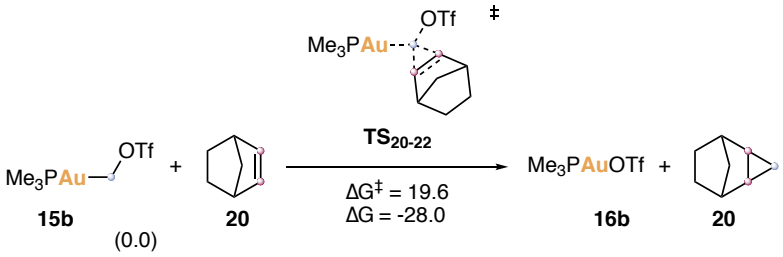

Scheme 16. Calculated reaction profile for the cyclopropanation of norbornene (**20**) on the model system. DFT calculations were performed at B3LYP-D3/6-31G(d,p) + SDD(f,g) on Au. Toluene was represented with the PCM. Free energies are in kcal·mol^{-1}.

Buchner reaction of benzene

The gold(I)-catalyzed Buchner reaction of benzene and toluene has been previously reported *via* gold(I)-catalyzed carbene transfer using diazomethane reagents.[35] Under the reported conditions, the corresponding cycloheptatrienes were formed in 25-40% yield together with the products arising from the formal insertion into the aromatic Csp^2-H bonds.[35]

34 (a) Nakamura, M.; Hirai, A.; Nakamura, E. *J. Am. Chem. Soc.* **2003**, *125*, 2341–2350. (b) Bernardi, F.; Bottoni, A.; Miscione, G. P. *J. Am. Chem. Soc.* **1997**, *119*, 12300–12305. (c) Fang, W.-H.; Phillips, D. L.; Wang, D.-Q.; Li, Y.-L. *J. Org. Chem.* **2002**, *67*, 154–160.

35 (a) Fructos, M. R.; Belderrain, T. R.; Frémont, P. de; Scott, N. M.; Nolan, S. P.; Díaz-Requejo, M. M.; Pérez, P. J. *Angew. Chem. Int. Ed.* **2005**, *44*, 5284–5288. (b) Prieto, A.; Fructos, M. R.; Díaz-Requejo, M. M.; Pérez, P. J.; Pérez-Galán, P.; Delpont, N.; Echavarren, A. M. *Tetrahedron* **2009**, *65*, 1790–1793.

Mechanistically, the Buchner reaction proceeds through initial methylenation to form norcaradiene derivatives followed by electrocyclic opening to yield cycloheptatrienes.[36]

During our experiments, we noticed that when the activation of gold(I) carbenoids **14** was performed in C_6D_6 as solvent, cycloheptatriene **23-*d*$_6$** was presumably detected by ^{1}H NMR and GC-MS. In order to avoid any structural misinterpretation, gold(I) carbenoid **14a** was activated with $TMSNTf_2$ in benzene at 25 ºC (Scheme 17). In this case, the formation of cycloheptatriene **23** could be confirmed by comparison of the ^{1}H NMR of the crude reaction with an authentic sample of **23**.

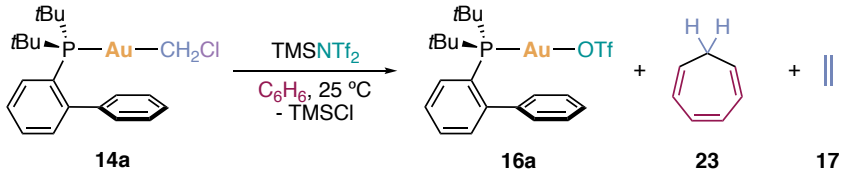

Scheme 17. Gold(I)-promoted Buchner reaction of benzene *via* activation of gold(I) carbenoid **14a**.

Table 4. Gold(I)-promoted Buchner reaction of C_6D_6 *via* chloride abstraction of gold(I) carbenoids **14a,c-d**.

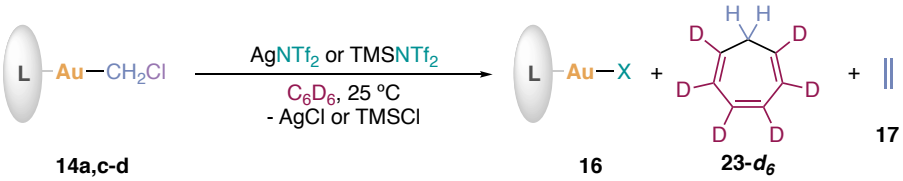

Entry[a]	Complex	Chloride Scavenger	Yield **23-*d*$_6$** (%)[b]
1	**14a**	$TMSNTf_2$	12
2		$AgNTf_2$	7
3	**14c**	$TMSNTf_2$	28
4		$AgNTf_2$	12
5	**14d**	$TMSNTf_2$	2
6		$AgNTf_2$	1

[a] **14** (0.017 mmol), **19** or **20** (20 equiv). [b] ^{1}H NMR yield calculated using diphenylmethane as internal standard.

To this end, we further analyzed the formation of **23-*d*$_6$** by gold(I)-promoted Buchner reaction. Particularly, cycloheptatriene **23-*d*$_6$** was formed in low yield alongside ethylene (**17**) when gold(I) carbenoids **14a** and **14c** were treated with $AgNTf_2$ or $TMSNTf_2$ at 25 ºC in C_6D_6 as solvent (Table 4, entries 1-4). Carbenoid **14d** yielded only traces of **23-*d*$_6$** (Table 4, entries 5-

36 Dzhemilev, U. M.; Dokichev, V. A.; Sultanov, S. Z.; Sadykov, R. A.; Tolstikov, G. A.; Nefedov, O. M. *Russ. Chem. Bull.* **1991**, *40*, 945–950.

6) in parallel with its low reactivity towards cyclopropanation (Table 3, entries 5-6). It is worth mentioning that, contrary to what has been published,[35] no product resulting from the formal aromatic C–H insertion was detected in these experiments.

Based on the latter results, it would be reasonable to expect that gold(I) carbenoids could also promote Buchner reaction of toluene. However, even if the mass corresponding to the potential cycloheptatrienes was detected by GC-MS, we were not able to assign unequivocally the signals to these products by ^{1}H NMR.

Synthesis of Chloro(phenyl)methylgold(I) Carbenoid

Gratifyingly, we found that the formation of gold(I) carbenoids is not limited to the formal insertion of diazomethane between the gold(I)-chloride bond. However, the reaction conditions have to be tuned to introduce substituents in the sp^3 carbon bound to the gold atom. To this end, reaction of phenyldiazomethane with [JohnPhosAuCl] (**13a**) provided complex **24** (Scheme 18).

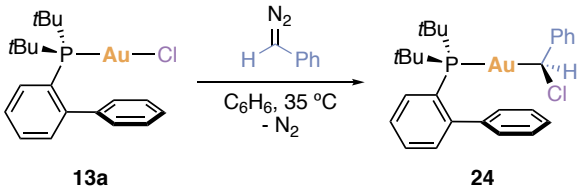

13a **24**

Scheme 18. Synthesis of chloro(phenyl)methylgold(I) carbenoid **24**.

Chloro(phenyl)methylgold(I) carbenoid **24** was not as stable as the previously prepared chloro(methyl)gold(I) complexes **14** and thus, it could not be purified by column chromatography and had to be stored under inert conditions in the glovebox. Due to the handling and final characteristics of complex **24**, an accurate determination of the reaction yield was not possible, however, conversion is complete as evidenced by ^{31}P NMR evaluation during the synthesis. In comparison with its chloromethyl analogs **14** (Table 2), complex **24** exhibits a similar Au–C1 bond (2.074 Å), a longer C1–Cl bond (1.838 Å) and a more acute Au–C1–Cl angle (106.7 º) in the solid state (Figure 8).

Activation of carbenoid complex **24** with TMSOTf in CD_2Cl_2 solution at 25 ºC showed complete consumption of **24** and formation of homocoupling products *cis*- and *trans*-stilbene **25** together with their cyclopropanation product 1,2,3-triphenylcyclopropane **26** among other not identified products (Scheme 19). Contrary to the reactivity pattern display by its chloro(methyl)gold(I) analogues **14**, the formation of a new carbenoid after substitution of the chloride by OTf was not detected by NMR at 25 ºC. This result suggests that in this case an undetected gold(I) carbene is responsible of the reactivity observed. Furthermore, the observed

reactivity closely resembles that previously reported cyclopropanation of stilbenes by gold carbenes generated *via* retro-Buchner reaction of cycloheptatrienes.[7a]

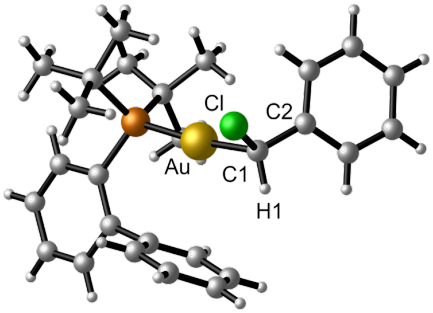

24

Figure 8. X-ray crystal structure of chloro(phenyl)methylgold(I) carbenoid **24**.

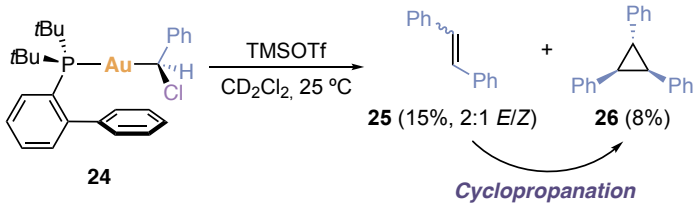

24

Scheme 19. Activation of complex **24** with TMSOTf. Yields determined by GC-FID.

Conclusions

In summary, we have developed a simple method for the preparation of well-defined chloromethylgold(I) carbenoids (**14**) by reaction of trimethylsilyldiazomethane with the corresponding gold(I) chloride precursors (**13**) in the presence of methanol (Scheme 20). Activation of these gold(I) carbenoids with a variety of chloride scavengers give rise to new gold(I) carbenoids bearing better leaving groups, which promote reactivity typical of metallocarbenes in solution, namely homocoupling to ethylene, alkene cyclopropanation and Buchner ring expansion of benzene (Scheme 20). Kinetic evidence, supported by DFT calculations, suggests the involvement of gold(I) carbenes with a trigonal planar geometry in the formation of ethylene. On the other hand, the cyclopropanation reaction probably occurs through a Simmons-Smith type mechanism.

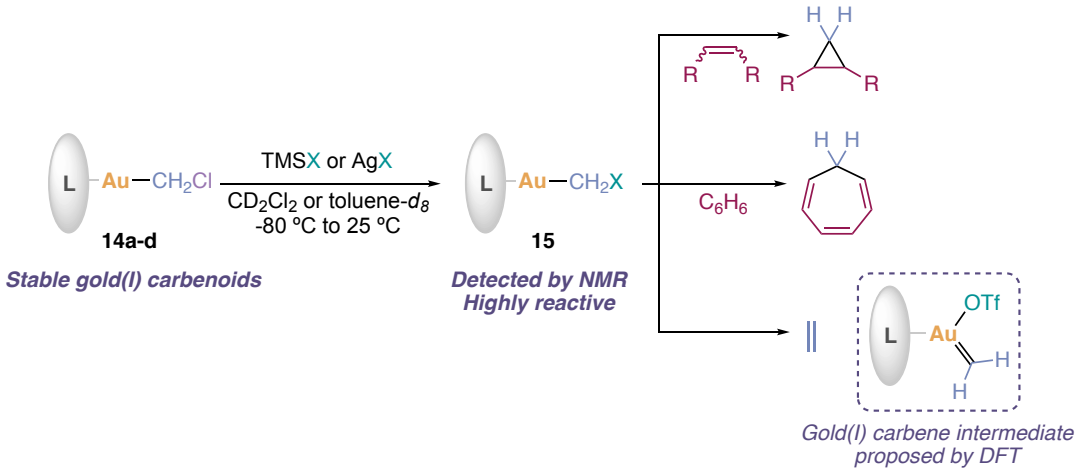

Scheme 20. Reactivity of chloromethylgold(I) carbenoids.

Chloro(phenyl)methylgold(I) carbenoid **24** has also been synthetized and, upon activation, promotes reactivity that resembles the gold(I)-catalyzed cyclopropanation *via* generation of carbenes through retro-Buchner reaction of cycloheptatrienes.

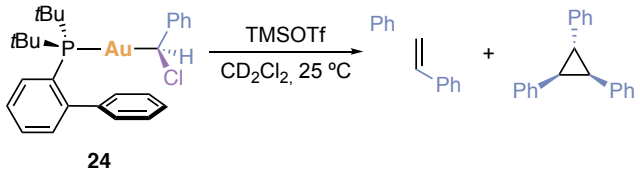

24

Scheme 21. Synthesis and reactivity of chloro(phenyl)methylgold(I) carbenoid **24**.

Experimental Section

General Methods

All reactions under a N_2 atmosphere were conducted after preparation in the glove box, reactions carried out under Ar atmosphere were performed using standard Schlenk techniques. Anhydrous solvents for synthesis were obtained by passing them through an activated alumina column on a PureSolvTM solvent purification system (Innovative Technologies, Inc., MA). Deuterated solvents were purchased from Sigma-Aldrich and, unless otherwise stated, distilled over a suitable drying agent (C_6D_6, toluene-d_8 and THF-d_8 over molten K, CD_2Cl_2 and $DCCl_3$ over CaH_2) under Ar before use. Analytical TLC was performed on precoated neutral aluminum oxide plates (0.2 mm thick, Gf234, Merck, Germany) and observed under UV light. Column chromatography was performed on neutral aluminum oxide Carlo Erba. NMR spectra were recorded either on a Bruker Avance 300, 400 or 500 Ultrashield instruments. Chemical shifts are reported in parts per million and referenced to residual solvent. Coupling constants (*J*) are reported in hertz (Hz). Mass spectra were recorded on a Water LCT Premier Spectrometer (ESI and APCI), on an Autoflex Bruker Daltonics (MALDI and LDI), or on an AgilentMSD-5975B (GC-MS).

2-(Di-*tert*-butylphosphino)biphenyl gold(I) chloride, 2-Di-*tert*-butylphosphino-2′,4′,6′-triisopropylbiphenyl gold(I) chloride, 1,3-Bis(2,6-diisopropylphenyl-imidazol-2-ylidene)gold(I) chloride, (Trimethylsilyl)diazomethane ($TMSCHN_2$) (2M in hexanes), Silver hexafluoroantimonate(VI), Silver bis(trifluoromethanesulfonyl)imide, Trimethylsilyl trifluoromethanesulfonate (TMSOTf), Trimethylsilyl trifluoroacetate ($TMSO_2CCF_3$), Trimethylsilyl mathanesulfonate ($TMSOSO_2CH_3$) and Norbornene were purchased from Sigma-Aldrich and used without further purification. Trimethylsilyl bis(trifluoromethanesulfonyl)imide ($TMSNTf_2$) was purchased from TCI and used without further purification. Cyclohexene was purchased from Acros and used without further purification

Unless otherwise stated, all other reagents were purchased from commercial sources and used without further purification.

Synthetic Procedures and Analytical Data

General procedure for the synthesis of chloromethylgold(I) chloride complexes

A solution of $TMSCHN_2$ (2 M in hexane, 1 to 2 equiv) was added to a solution of the corresponding gold chloride complex **13** (1 equiv) and MeOH (6 equiv) in anhydrous C_6H_6 (6 mL). After a few seconds, N_2 evolution started and it stopped after 30 min. The mixture was filtered through a small pad of silica gel in order to quench the excess $TMSCHN_2$ and rinsed three times with 2 mL of CH_2Cl_2. After evaporation of the volatiles in a rotary evaporator the complexes were purified by either recrystallization or column chromatography on neutral aluminum oxide. Single crystals suitable for X-ray diffraction were obtained by slow diffusion of pentane into a solution of the pure carbenoid compounds in CH_2Cl_2.

Gold(I) carbenoid 14a

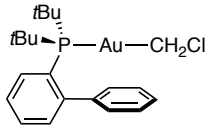

Gold(I) carbenoid **14a** was synthetized according to the general procedure from 2-(di-*tert*-butylphosphino)biphenyl gold(I) chloride **13a** (200 mg, 0.377 mmol), MeOH (91 μL, 2.26 mmol) and $TMSCHN_2$ (0.226 mL, 0.452 mmol). Complex **14a** was purified by column chromatography on neutral aluminum oxide using a pentane/CH_2Cl_2/acetonitrile (100:10:2) mixture as eluent. Yield: 120 mg (58.5 %) of **14a** as a white solid.

^{1}H NMR (400 MHz, CD_2Cl_2) δ 7.91 – 7.86 (m, 1H), 7.52 – 7.44 (m, 2H), 7.42 – 7.35 (m, 3H), 7.26 – 7.22 (m, 1H), 7.18 – 7.14 (m, 2H), 2.96 (d, $J_{H\text{-}P}$ = 3.6 Hz, 2H), 1.39 (d, $J_{H\text{-}P}$ = 14.5 Hz, 18H). **^{13}C NMR** (101 MHz, CD_2Cl_2) δ 150.67 (d, $J_{C\text{-}P}$ = 16.2 Hz), 143.98 (d, $J_{C\text{-}P}$ = 5.6 Hz), 135.58 (s), 133.27 (d, $J_{C\text{-}P}$ = 7.6 Hz), 130.56 (d, $J_{C\text{-}P}$ = 2.2 Hz), 130.08 (s), 129.22 (d, $J_{C\text{-}P}$ = 33.5 Hz), 128.63 (s), 127.43 (s), 127.17 (d, $J_{C\text{-}P}$ = 5.3 Hz), 53.58 (d, $J_{C\text{-}P}$ = 112.6 Hz, Au*C*H_2Cl), 37.63 (d, $J_{C\text{-}P}$ = 19.7 Hz), 31.31 (d, $J_{C\text{-}P}$ = 7.0 Hz). **^{31}P NMR** (162 MHz, CD_2Cl_2) δ 68.29 (s). **HRMS** (ESI+) Calculated for $C_{21}H_{29}AuPClNa$ $[M+Na]^+$: 567.1253 Found: 567.1274. **Elemental Analysis** for $C_{21}H_{29}AuClP$: C, 46.29; H, 5.37; found: C, 46.23; H, 5.21.

Gold(I) carbenoid 14a-*d*$_1$

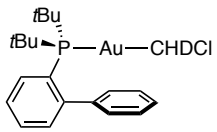

Gold(I) carbenoid **14a-*d*$_1$** was synthetized according to the general procedure from 2-(di-*tert*-butylphosphino)biphenyl gold(I) chloride **13a** (200 mg, 0.377 mmol), CD_3OD (91 μL, 2.26 mmol) and $TMSCHN_2$ (0.226 mL, 0.452 mmol). Complex **14a-*d*$_1$** was purified by column chromatography on neutral aluminum oxide using a pentane/CH_2Cl_2/acetonitrile (100:10:2) mixture as eluent. Yield: 113 mg (54.9%) of **14a-*d*$_1$** as a white crystalline solid.

^{1}H NMR (400 MHz CD_2Cl_2) δ 7.91 – 7.85 (m, 1H), 7.52 – 7.43 (m, 2H), 7.42 – 7.36 (m, 3H), 7.26 – 7.22 (m, 1H), 7.19 – 7.13 (m, 2H), 2.96 (d, J_{H-P} = 3.6 Hz, 2H), 2.94 (dt, J_{H-P} = 3.2, J_{H-D} = 1.4 Hz, 1H), 1.39 (d, J_{H-P} = 14.5 Hz, 18H). **^{13}C NMR** (101 MHz, CD_2Cl_2) δ 150.1 (d, J_{C-P} = 16.1 Hz), 143.4 (d, J_{C-P} = 5.7 Hz), 135.0, 132.7 (d, J_{C-P} = 7.7 Hz), 130.0 (d, J_{C-P} = 2.2 Hz), 129.5, 128.6 (d, J_{C-P} = 33.6 Hz), 128.0, 126.8, 126.6 (d, J_{C-P} = 5.3 Hz), 53.0 (d, J_{C-P} = 112.7 Hz), 52.9 (dt, J_{C-P} = overlapping, J_{C-D} = 21.8 Hz) (d, J_{C-P} = 19.6 Hz), 30.7 (d, J_{C-P} = 7.0 Hz). **^{31}P NMR** (162 MHz, CD_2Cl_2) δ 68.3 (s).

Gold(I) carbenoid 14b

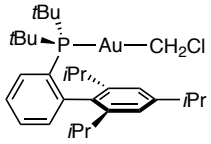

Gold(I) carbenoid **14b** was synthetized according to the general procedure from 2-(di-*tert*-butylphosphino)-2′,4′,6′-triisopropylbiphenyl gold(I) chloride **13b** (197 mg, 0.300 mmol), MeOH (73 μL, 1.80 mmol) and $TMSCHN_2$ (0.500 mL (0.6 M), 0.300 mmol). Complex **14b** was purified by column chromatography on neutral aluminum oxide using a pentane/CH_2Cl_2/acetonitrile (100:10:2) mixture as eluent. Yield: 112 mg (55.9 %) of **14b** as a white solid.

^{1}H NMR (400 MHz, CD_2Cl_2) δ 7.89 (m, 1H), 7.51 – 7.42 (m, 2H), 7.22 (m, 1H), 7.05 (m, 2H), 3.03 – 2.86 (m, 1H), 2.94 (d, J_{H-P} = 3.8 Hz, 2H), 2.40 (hept, J_{H-H} = 6.7 Hz, 2H), 1.41 (d, J_{H-P} = 14.4 Hz, 18H), 1.33 (d, J_{H-H} = 6.9 Hz, 6H), 1.27 (d, J_{H-H} = 6.8 Hz, 6H), 0.90 (d, J_{H-H} = 6.7 Hz, 6H). **^{13}C NMR** (101 MHz, CD_2Cl_2) δ 149.3 (s), 148.7 (d, J_{C-P} = 16.9 Hz), 147.0 (s), 138.2 (d, J_{C-P} = 4.3 Hz), 136.5 (s), 135.3 (d, J_{C-P} = 8.4 Hz), 131.6 (d, J_{C-P} = 31.2 Hz), 130.3 (d, J_{C-P} = 2.2 Hz), 126.8 (d, J_{C-P} = 5.4 Hz), 121.8 (s), 53.9 (d, J_{C-P} = 112.5 Hz), 38.3 (d, J_{C-P} = 20.1 Hz), 34.7 (s), 31.8 (d, J_{C-P} = 6.8 Hz), 31.4 (s), 26.4 (s), 24.6 (s), 23.3 (s). **^{31}P NMR** (162 MHz, CD_2Cl_2) δ 68.85 (s). **HRMS** (ESI+) Calculated for $C_{30}H_{47}AuPClNa$ $[M+Na]^+$: 693.2662 Found: 693.2688. **Elemental analysis** for $C_{30}H_{47}AuClP$: C, 53.69; H, 7.06; found: C, 53.69; H, 6.96.

Gold(I) carbenoid 14c

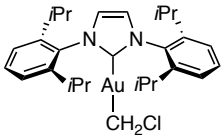

Gold(I) carbenoid **14c** was synthetized according to the general procedure from 1,3-bis(2,6-diisopropylphenyl)imidazole-2-ylidene gold(I) chloride **13c** (300 mg, 0.483 mmol), MeOH (117 μL, 2.90 mmol) and $TMSCHN_2$ (531 μL (2 M), 1.063 mmol). Complex **14c** was purified by column chromatography on neutral aluminum oxide using a pentane/EtOAc/acetonitrile (10:1:0.5) mixture as eluent. Yield: 180 mg (58.7 %) of **14c** as a white solid.

^{1}H NMR (300 MHz, CD_2Cl_2) δ 7.54 (t, J_{H-H} = 7.7 Hz, 2H), 7.34 (d, J_{H-H} = 7.7 Hz, 4H), 7.16 (s, 2H), 3.34 (s, 2H), 2.60 (hept, J_{H-H} = 7.0 Hz, 4H), 1.34 (d, J_{H-H} = 6.9 Hz, 12H), 1.22 (d, J_{H-H} = 6.9 Hz, 12H). **^{13}C NMR** (101 MHz, CD_2Cl_2) δ 195.2 (s), 146.5 (s), 135.1 (s), 130.8 (s), 124.5 (s), 123.6 (s), 47.2 (s), 29.3 (s), 24.7 (s), 24.2 (s). **HRMS** (ESI+) Calculated. for $C_{28}H_{39}AuClN_2$ $[M+H]^+$: 635.2462 Found: 635.2475. **Elemental Analysis** for $C_{28}H_{38}AuClN_2$: C, 52.96; H, 6.03; N, 4.41; found: C, 52.88; H, 6.09; N, 4.24.

Gold(I) carbenoid 14d

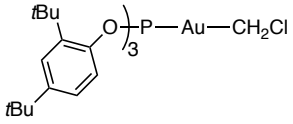

Gold(I) carbenoid **14d** was synthetized according to the general procedure from tris(2,4-di-*tert*-butylphenyl)phosphite gold(I) chloride **13d** (300 mg, 0.341 mmol), MeOH (83 μL, 2.05 mmol) and $TMSCHN_2$ (341 μL (2 M), 0.682 mmol) . Complex **14d** could not be purified by conventional means as it would immediately decompose in the column. After $TMSCHN_2$ was consumed (as evidenced by the disappearance of the yellow color) the solvents were removed under reduced pressure and the residue redissolved in anhydrous Et_2O (2 mL) and filtered through 2 HPLC filters into a Schlenk flask. Anhydrous *n*-hexane (5 mL) were added over the solution and the solvents removed under vacuum. The off-white solid thus obtained was used without further purification.

^{1}H NMR (500 MHz, CD_2Cl_2) δ 7.49 (dd, $J_{H,H}$ = 8.5, 1.5 Hz, 3H), 7.46 (dd, $J_{H,H}$ = 2.6, 1.1 Hz, 3H), 7.17 (dd, $J_{H,H}$ = 8.5, 2.6 Hz, 3H), 3.62 (d, $J_{H,P}$ = 5.7 Hz, 2H), 1.45 (s, 27H), 1.30 (s, 27H). **^{13}C NMR** (126 MHz, CD_2Cl_2) δ 148.4 (s), 148.1 (d, $J_{C,P}$ = 5.1 Hz), 139.7 (d, $J_{C,P}$ = 5.8 Hz), 125.9 (s), 124.5 (s), 119.8 (d, $J_{C,P}$ = 9.5 Hz), 49.1 (d, $J_{C,P}$ = 180.5 Hz), 35.6 (s), 35.1 (s), 31.7 (s), 30.8 (s). **^{31}P NMR** (202 MHz, CD_2Cl_2) δ 143.2 (s).

Synthesis of gold(I)-stabilized oxonium ylide 18

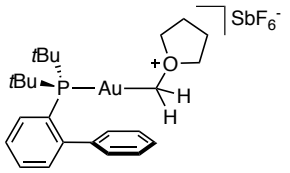

Complex **18** was obtained as the product of an NMR scale experiment as follows: A solution of silver hexafluoroantimonate (16.40 mg, 0.048 mmol) in 0.4 mL of CD_2Cl_2 was added to a solution of **14a** (20 mg, 0.037 mmol) and tetrahydrofuran (30.0 μL, 0.367 mmol) in 0.6 mL of CD_2Cl_2 contained in an NMR tube at -78 ºC. The mixture was well mixed at this temperature and transferred to the NMR instrument. The reaction was monitored by multinuclear NMR as it was warmed up from -78 ºC to -20 ºC. At this temperature total conversion of **14a** into **18** was observed. Single crystals suitable for X-ray diffraction were obtained by layering anhydrous *n*-hexane over the previously analyzed sample at -20 ºC under nitrogen atmosphere.

^{1}H NMR (500 MHz, -20 ºC, CD_2Cl_2) δ 7.86 (m, 1H), 7.55 – 7.48 (m, 2H), 7.44 – 7.33 (m, 3H), 7.23 (m, 1H), 7.19 – 7.13 (m, 2H), 4.66 (d, $J_{H\text{-}P}$ = 3.5 Hz, 2H), 4.34 – 4.26 (m, 4H), 2.27 – 2.20 (m, 4H), 1.37 (d, $J_{H\text{-}P}$ = 15.0 Hz, 18H). **^{13}C NMR** (126 MHz, -20 ºC, CD_2Cl_2) δ 149.5 (d, $J_{C\text{-}P}$ = 15.3 Hz), 143.9 (d, $J_{C\text{-}P}$ = 5.8 Hz), 135.1, 133.0 (d, $J_{C\text{-}P}$ = 7.6 Hz), 130.9 (d, $J_{C\text{-}P}$ = 2.3 Hz), 130.0, 128.6, 127.5 (d, $J_{C\text{-}P}$ = 38.8 Hz), 127.5 (d, $J_{C\text{-}P}$ = 5.9 Hz), 127.1, 116.2 (d, $J_{C\text{-}P}$ = 105.0 Hz), 87.5, 37.6 (d, $J_{C\text{-}P}$ = 21.6 Hz), 30.9 (d, $J_{C\text{-}P}$ = 6.6 Hz), 25.0. **^{31}P NMR** (202 MHz, -20 ºC, CD_2Cl_2) δ 64.4 (s).

Synthesis of chloro(phenyl)methylgold(I) carbenoid 24

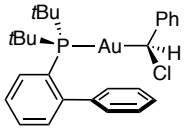

Phenyldiazomethane[37] (5 mL solution in benzene, approx. 1.8 mmol) was added directly over 2-(di-*tert*-butylphosphino)biphenyl gold(I) chloride **13a** (300 mg, 0.565 mmol) in a 25 mL Schlenk flask under Ar atmosphere (strict exclusion of oxygen and water are essential for the reproducibility of this reaction). The mixture was then stirred at 35 ºC while reaction progress was monitored by ^{31}P NMR. Once all the starting material has been consumed the heating was removed and the mixture concentrated to about 1 mL under reduced pressure. (**Attention!** Excess phenyldiazomethane is still present in the mixture, as evidenced by the intense red color, and a risk of explosion exists if all the solvent is removed). Anhydrous *n*-pentane (15 mL) is added over the mixture. The system is cooled down to -40 ºC with constant stirring for 30 minutes in order to induce precipitation of the product as a white solid. Filtration of the supernatant is performed with a cannula at -40 ºC. The product is washed with two portions of 2.5 mL anhydrous *n*-pentane at -40 ºC. The combined supernatant is treated with 1M HCl in MeOH until all the red color of the remaining phenyldiazomethane has faded and then safely discarded. The obtained white solid is dried on the high vacuum overnight at 0 ºC. Crystals suitable for X-ray measurement were obtained by storing a solution of complex **24** in a mixture of toluene and pentane in a ratio of about 1:10 in the freezer (-35 ºC) for several days. Due to the handling and final characteristics of the product an accurate determination of the reaction yield is not possible, however conversion is complete as evidenced by ^{31}P NMR evaluation during the synthesis.

^{1}H NMR (400 MHz, CD_2Cl_2) δ 7.90 – 7.85 (m, 1H), 7.57 – 7.36 (m, 4H), 7.25 – 7.19 (m, 3H), 7.16 (s, 2H), 7.15 (s, 2H), 7.09 – 7.05 (m, 1H), 6.96 (m, 1H), 4.04 (d, $J_{H\text{-}P}$ = 5.5 Hz, 1H), 1.42 (d, $J_{H\text{-}P}$ = 14.7 Hz, 9H), 1.30 (d, $J_{H\text{-}P}$ = 14.6 Hz, 9H). **^{13}C NMR** (100 MHz, CD_2Cl_2) δ 151.9 (d, $J_{C\text{-}P}$ = 2.6 Hz), 150.7 (d, $J_{C\text{-}P}$ = 16.3 Hz), 143.7 (d, $J_{C\text{-}P}$ = 5.7 Hz), 135.4 (s), 133.3 (d, $J_{C\text{-}P}$ =

37 Wulfman, D. S.; Yousefian, S.; White, J. M. *Synth. Commun.* **1988**, *18*, 2349–2352.

7.5 Hz), 130.6 (d, $J_{C\text{-}P}$ = 2.2 Hz), 130.1 (s), 130.0 (s), 128.8 (s), 128.7 (d, $J_{C\text{-}P}$ = 33.6 Hz), 128.6 (s), 128.2 (d, $J_{C\text{-}P}$ = 2.4 Hz), 128.0 (s), 127.6 (s), 127.2 (d, $J_{C\text{-}P}$ = 5.3 Hz), 124.3 (s), 76.0 (d, $J_{C\text{-}P}$ = 105.0 Hz), 37.6 (d, $J_{C\text{-}P}$ = 19.8 Hz), 37.5 (d, $J_{C\text{-}P}$ = 20.0 Hz), 31.3 (d, $J_{C\text{-}P}$ = 7.0 Hz), 31.1 (d, $J_{C\text{-}P}$ = 7.0 Hz). **^{31}P NMR** (162 MHz, CD_2Cl_2) δ 66.38 (s).

Quantification of ethylene

Ethylene formation was quantified using a ManontheMoonTech X102 Gas Evolution device (Figure 8) that monitors the gas evolution by measuring the pressure change *vs.*time in closed reaction systems at CIQSO, Universidad de Huelva, in Prof. Pedro J. Pérez group.

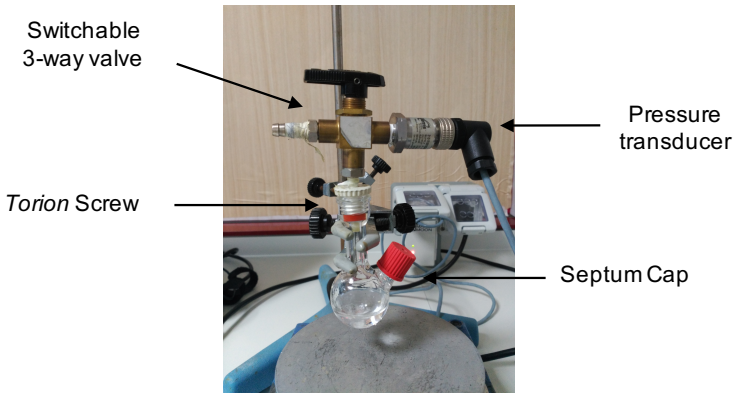

Figure 8. ManontheMoonTech X102 reaction flask.

Calibration method

In a glass ampule, toluene was saturated in ethylene by bubbling the gas through anhydrous toluene for 15 minutes. The reaction flask was connected to the switchable 3-way valve via the *Torion* screw and capped with the septum cap (Figure 8). The closed reaction flask was filled with ethylene gas and 5.0 ml of the previously saturated toluene. The reaction flask was connected to the pressure transducer and controlled until the pressure reading stabilized at 0.390-0.400 bar. Separately, a high-pressure reactor was charged with 1 bar of ethylene (total pressure = 1 bar + atmospheric pressure) and a known volume of gas was withdrawn using a Hamilton® SampleLock syringe. Ethylene was then injected to the ManontheMoonTech X102 reaction flask through the septum cap and the change in pressure was determined. Applying the gas ideal equation (Equation 1), the molar amount *n* of added ethylene was calculated which was then correlated to the observed change in pressure ΔP (bar).

$$PV = nRT \rightarrow n = \frac{PV}{RT}$$

Equation 1. Ideal gas equation, where: P = pressure of the gas, V = volume of the gas, n = moles of the gas, R = the ideal gas constant, T = the absolute temperature of the gas.

Table 5. Calibration of the pressure response to ethylene in toluene.

Entry	$V_{ethylene}$ (ml)	T (K)	$P_{ethylene}$ (bar)	$n_{ethyelene}$ (mmol)	ΔP (bar)
1	2.50	298	2	0.2	0.128
2	2.50	298	2	0.2	0.123
				Average: $\Delta P_{0.2\ mmol}$	0.125
3	1.25	298	2	0.1	0.071
4	1.25	298	2	0.1	0.077
				Average: $\Delta P_{0.1\ mmol}$	0.074

Ethylene quantification

The reaction flask was filled with toluene (5.0 mL, anhydrous and saturated in ethylene), **14a** and ethylene gas. Then, it was connected to the pressure transducer and controlled until the pressure reading stabilized at 0.390-0.400 bar. TMSOTf (2 equiv) was injected through the septum cap and the pressure change measured over time. The yield of ethylene at any time was calculated using Equation 2.

$$Yield\ (\%) = \frac{\Delta P_t}{\Delta P_{max}} * 100$$

Equation 2. Where: ΔP_t = pressure difference along the reaction. ΔP_{max} = maximum pressure change expected given the amount of **14a** used (see calibration).

Conditions A: **14a** (0.2 mmol, 109 mg), TMSOTf (0.4 mmol, 72 µL), ΔP_{max} = 0.074 bar.

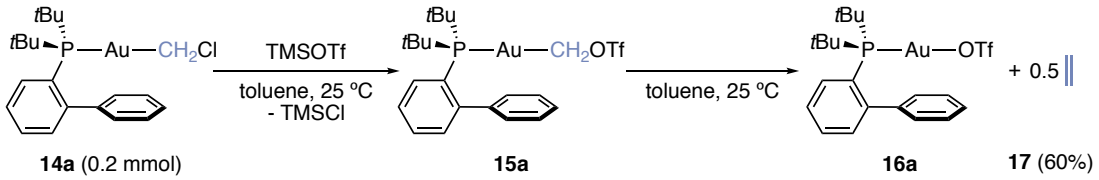

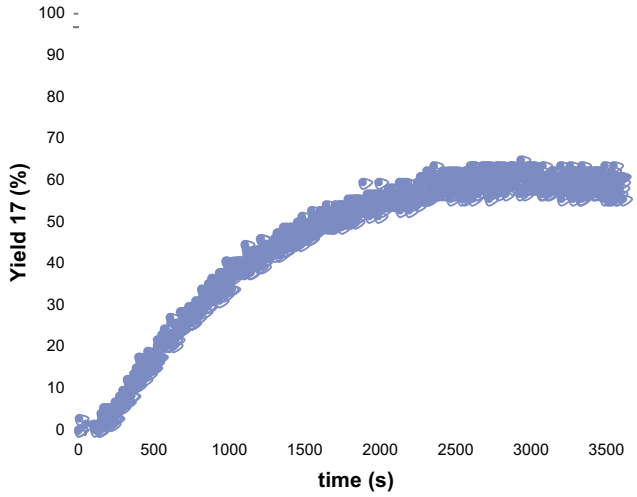

Figure 9. Yield of ethylene (**17**) over time for the reaction of **14a** (0.2 mmol) with TMSOTf.

Conditions B: **14a** (0.4 mmol, 218 mg), TMSOTf (0.8 mmol, 144 µL), ΔP_{max} = 0.125 bar.

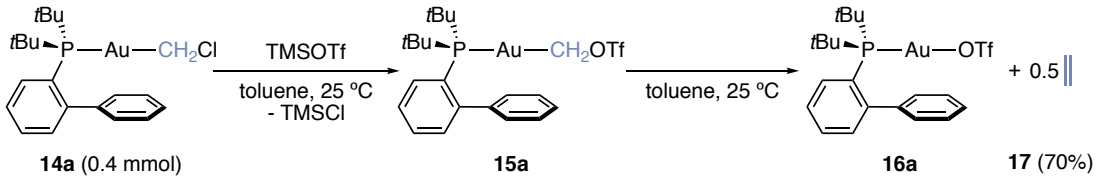

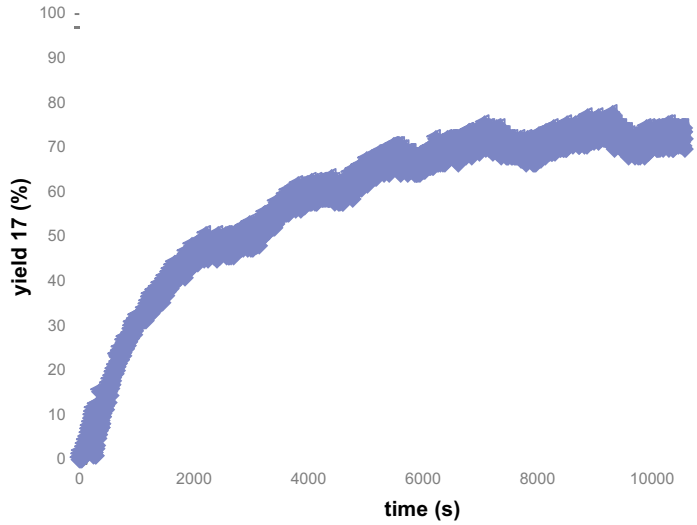

Figure 10. Yield of ethylene over time for the reaction of **14a** (0.4 mmol) with TMSOTf.

Gas phase analysis

In a closed reaction flask under argon, carbenoid **14a** (0.03 mmol, 16 mg) was dissolved in 0.5 mL of anhydrous toluene. In a glovebox, TMSOTf (0.06 mmol, 11 µL) was taken in a microsyringe and protected from air. Outside the glovebox TMSOTf was added over the solution. The mixture was then stirred at 25 ºC for 30 minutes. A Hamilton® SampleLock syringe was filled with 250 µL of gas from the gas phase of the reaction. The gas was injected in a GC-MS instrument. Ethylene (**17**) was detected as the only organic product in the gas phase.

Mass spectrometry of gold(I) carbenoid 14a: observation of gold(I) carbene

Mass Spectrum SmartFormula Report

Analysis Info

Analysis Name	W:\Data\160610\160610_CGJS190-1_RE3_01_10680.d	Acquisition Date	10/06/2016 14:29:32
Method	tune_low_hplc-exactas3min-noe.m	Operator	ICIQ
Sample Name	160610_CGJS190-1	Instrument / Ser#	micrOTOF 213750.10394
Comment	0.5 uL starting sol, MeOH injection, END PLATE. -700V		

Acquisition Parameter

Source Type	ESI	Ion Polarity	Positive	Set Nebulizer	1.2 Bar
Focus	Active			Set Dry Heater	180 °C
Scan Begin	50 m/z	Set Capillary	4500 V	Set Dry Gas	8.0 l/min
Scan End	2000 m/z	Set End Plate Offset	-700 V	Set Divert Valve	Source

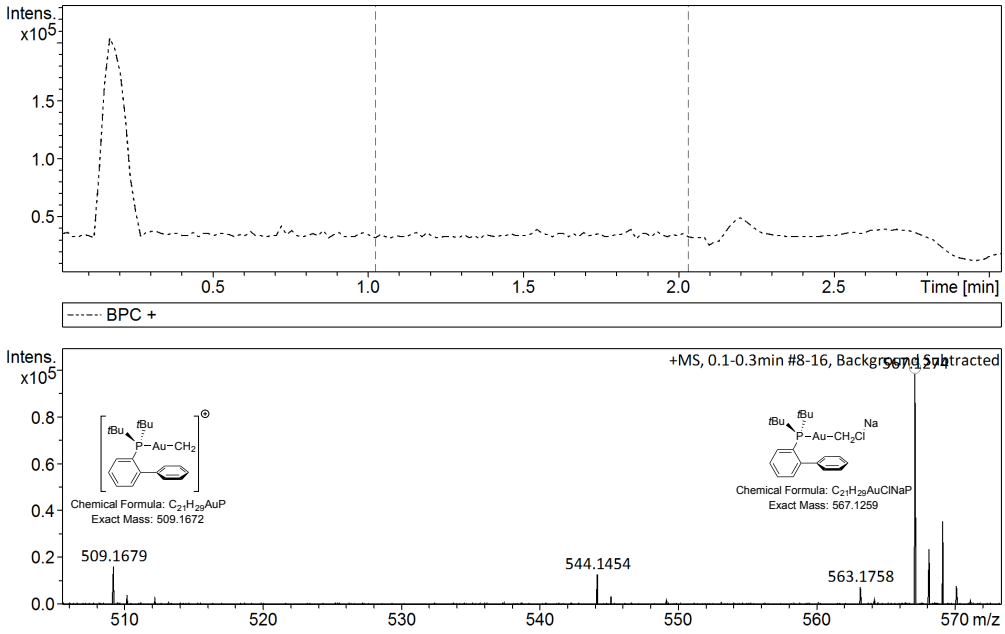

Crystallographic Data

Gold(I) carbenoid 14a

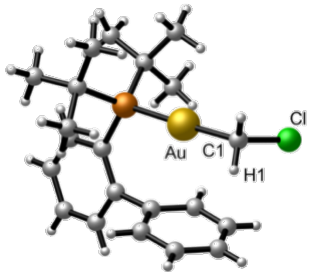

Table 6. Crystal data and structure refinement for complex **14a**.

Empirical formula	C42 H58 Au2 Cl2 P2	
Formula weight	1089.66	
Temperature	100(2) K	
Wavelength	0.71073 Å	
Crystal system	Triclinic	
Space group	P-1	
Unit cell dimensions	a = 10.4982(6) Å	α = 72.868(3) °.
	b = 13.6572(7) Å	β = 89.459(3) °.
	c = 15.1002(9) Å	γ = 88.404(3) °.
Volume	2068.1(2) $Å^3$	
Z	2	
Density (calculated)	1.750 Mg/m^3	
Absorption coefficient	7.320 mm^{-1}	
F(000)	1064	
Crystal size	0.20 x 0.20 x 0.10 mm^3	
Theta range for data collection	1.56 to1.56 °.	
Index ranges	-16 <=h<=16 ,-19 <=k<=21 ,0 <=l<=23	
Reflections collected	15820	
Independent reflections	13265 [R(int) = 0.0000]	
Completeness to theta =33.32 °	0.989 %	
Absorption correction	Empirical (TWINABS)	
Max. and min. transmission	0.5281 and 0.3222	
Refinement method	Full-matrix least-squares on F^2	
Data / restraints / parameters	15820 / 0 / 446	
Goodness-of-fit on F^2	1.032	
Final R indices [I>2sigma(I)]	R1 = 0.0729 , wR2 = 0.1911	
R indices (all data)	R1 = 0.0863 , wR2 = 0.2084	
Largest diff. peak and hole	11.419 and -6.610 $e.Å^{-3}$	

Gold(I) carbenoid 14b

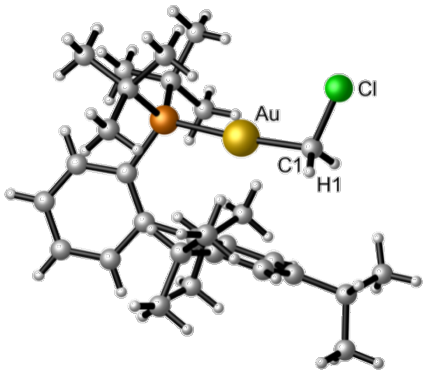

Table 7. Crystal data and structure refinement for complex **14b**.

Empirical formula	C30 H47 Au Cl P	
Formula weight	671.06	
Temperature	100(2) K	
Wavelength	0.71073 Å	
Crystal system	Monoclinic	
Space group	P2(1)/c	
Unit cell dimensions	a = 20.5365(8) Å	α 90.00 °.
	b = 8.9497(4) Å	β = 104.0760(10) °.
	c = 16.4737(6) Å	γ = 90.00 °.
Volume	2936.9(2) $Å^3$	
Z	4	
Density (calculated)	1.518 Mg/m^3	
Absorption coefficient	5.170 mm^{-1}	
F(000)	1352	
Crystal size	0.30 x 0.30 x 0.30 mm^3	
Theta range for data collection	1.02 to 29.95 °.	
Index ranges	-25 <=h<=26 ,-12 <=k<=11 ,-22 <=l<=16	
Reflections collected	30282	
Independent reflections	7571 [R(int) = 0.0611]	
Completeness to theta =29.95 °	0.888 %	
Absorption correction	Empirical	
Max. and min. transmission	0.224 and 0.212	
Refinement method	Full-matrix least-squares on F^2	
Data / restraints / parameters	7571 / 0 / 310	
Goodness-of-fit on F^2	1.071	
Final R indices [I>2sigma(I)]	R1 = 0.0512 , wR2 = 0.1431	
R indices (all data)	R1 = 0.0570 , wR2 = 0.1493	
Largest diff. peak and hole	5.340 and -3.785 $e.Å^{-3}$	

Gold(I) carbenoid 14c

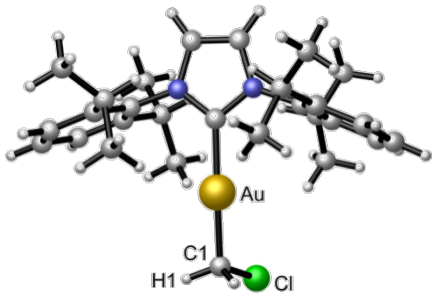

Table 8. Crystal data and structure refinement for complex **14c**.

Empirical formula	C28 H38 Au Cl N2	
Formula weight	635.02	
Temperature	100(2) K	
Wavelength	0.71073 Å	
Crystal system	Triclinic	
Space group	P-1	
Unit cell dimensions	a = 9.8883(11)Å	α= 88.838(3)°.
	b = 11.5073(13)Å	β = 88.638(3)°.
	c = 12.2747(14)Å	γ = 83.728(3)°.
Volume	1387.7(3) $Å^3$	
Z	2	
Density (calculated)	1.520 Mg/m^3	
Absorption coefficient	5.414 mm^{-1}	
F(000)	632	
Crystal size	0.30 x 0.20 x 0.20 mm^3	
Theta range for data collection	2.072 to 35.077°.	
Index ranges	-15<=h<=12,-14<=k<=18,-19<=l<=19	
Reflections collected	23948	
Independent reflections	11088[R(int) = 0.0177]	
Completeness to theta =35.077°	90.3%	
Absorption correction	Multi-scan	
Max. and min. transmission	0.411 and 0.337	
Refinement method	Full-matrix least-squares on F^2	
Data / restraints / parameters	11088/ 0/ 297	
Goodness-of-fit on F^2	1.073	
Final R indices [I>2sigma(I)]	R1 = 0.0190, wR2 = 0.0454	
R indices (all data)	R1 = 0.0216, wR2 = 0.0462	
Largest diff. peak and hole	2.151 and -1.303 e.$Å^{-3}$	

Complex 18

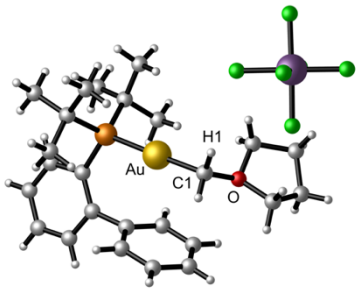

Table 9. Crystal data and structure refinement for complex **18.**

Empirical formula	C25 H37 Au F6 O P Sb	
Formula weight	817.23	
Temperature	100(2) K	
Wavelength	0.71073 Å	
Crystal system	Monoclinic	
Space group	P2(1)/n	
Unit cell dimensions	a = 13.6064(7)Å	α = 90°.
	b = 9.3096(5)Å	β = 105.7134(12)°.
	c = 23.0909(12)Å	γ = 90°.
Volume	2815.6(3) $Å^3$	
Z	4	
Density (calculated)	1.928 Mg/m^3	
Absorption coefficient	6.277 mm^{-1}	
F(000)	1576	
Crystal size	0.30 x 0.01 x 0.01 mm^3	
Theta range for data collection	1.832 to 34.453°.	
Index ranges	-20<=h<=21,-11<=k<=14,-28<=l<=36	
Reflections collected	42197	
Independent reflections	11560[R(int) = 0.0276]	
Completeness to theta =34.453°	97.2%	
Absorption correction	Multi-scan	
Max. and min. transmission	0.940 and 0.647	
Refinement method	Full-matrix least-squares on F^2	
Data / restraints / parameters	11560/ 0/ 322	
Goodness-of-fit on F^2	1.032	
Final R indices [I>2sigma(I)]	R1 = 0.0216, wR2 = 0.0432	
R indices (all data)	R1 = 0.0307, wR2 = 0.0456	
Largest diff. peak and hole	1.766 and -0.676 e.$Å^{-3}$	

Gold(I) carbenoid 24

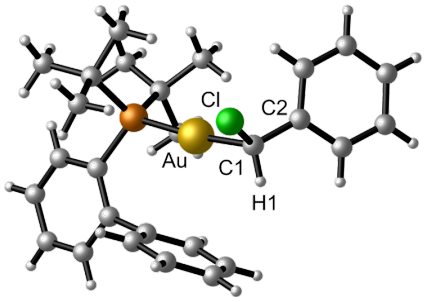

Table 10. Crystal data and structure refinement for complex **24**.

Empirical formula	C56.33 H68.67 Au2 Cl2 P2	
Formula weight	1272.55	
Temperature	100(2) K	
Wavelength	0.71073 Å	
Crystal system	Monoclinic	
Space group	P2(1)/n	
Unit cell dimensions	a = 20.8103(14)Å	α = 90°.
	b = 10.4355(6)Å	β = 103.897(2)°.
	c = 36.623(3)Å	γ = 90°.
Volume	7720.6(9) $Å^3$	
Z	6	
Density (calculated)	1.642 Mg/m^3	
Absorption coefficient	5.896 mm^{-1}	
F(000)	3772	
Crystal size	0.20 x 0.12 x 0.03 mm^3	
Theta range for data collection	1.033 to 27.349°.	
Index ranges	-20<=h<=26,-12<=k<=13,-47<=l<=40	
Reflections collected	53754	
Independent reflections	17186[R(int) = 0.0812]	
Completeness to theta =27.349°	98.299995%	
Absorption correction	Multi-scan	
Max. and min. transmission	0.843 and 0.385	
Refinement method	Full-matrix least-squares on F^2	
Data / restraints / parameters	17186/ 120/ 893	
Goodness-of-fit on F^2	0.941	
Final R indices [I>2sigma(I)]	R1 = 0.0598, wR2 = 0.1542	
R indices (all data)	R1 = 0.0883, wR2 = 0.1702	
Largest diff. peak and hole	5.522 and -2.700 e.$Å^{-3}$	

Chapter III: "Characterization of Mesityl Gold(I) Carbenes: Genuine Intermediates in the Retro-Buchner Reaction"

Introduction

As explained in the introduction of Chapter II, gold(I) carbenes have attracted great interest from the outset of the homogeneous gold catalysis era.[1] However, there is no a generally accepted manner to structurally describe them and, in particular, the degree of stabilization provided by the π-backdonation from gold(I) to the electron-deficient carbon is still ambiguous.[2,3] This lack of agreement between the chemical community can be understood because it was not until recently that examples of well-defined cationic gold(I) carbenes were spectroscopically and structurally characterized.

Characterized Gold(I) Carbenes

To be characterized, gold(I) carbenes require the presence of heteroatoms or highly conjugated systems at the carbene moiety and/or shielding ancillary ligands or bidentate phosphines at the metal center (Figure 1). In this section, we will review these stabilization strategies in detail and the structural and electronic nature of the corresponding isolated gold(I) carbenes.

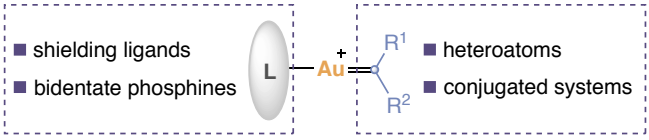

Figure 1. Stabilization strategies followed to isolate gold(I) carbenes.

As stated in Chapter II, we represent gold(I)-carbon bond as double bond in gold(I) carbenes by default. However, we advised the reader to bear in mind that gold(I) carbenes are better accounted as a continuum that ranges from metal-stabilized singlet carbenes with a bond order of two to metal-coordinated carbocations with a bond order of one. Further discussion about the main

1 (a) Fürstner, A. *Chem. Soc. Rev.* **2009**, *38*, 3208–3221. (b) Shapiro, N.; Toste, F. D. *Synlett* **2010**, 675–691. (c) Hashmi, A. S. K. *Angew. Chem. Int. Ed.* **2010**, *49*, 5232–5241. (d) Liu, L.-P.; Hammond, G. B. *Chem. Soc. Rev.* **2012**, *41*, 3129–3139. (e) Obradors, C.; Echavarren, A. M. *Acc. Chem. Res.* **2014**, *47*, 902–912. (f) Fensterbank, L.; Malacria, M. *Acc. Chem. Res.* **2014**, *47*, 953–965. (g) Dorel, R.; Echavarren, A. M. *Chem. Rev.* **2015**, *115*, 9028–9072. (h) Pflästerer, D.; Hashmi, A. S. K. *Chem. Soc. Rev.* **2016**, *45*, 1331–1367. (i) Echavarren, A. M.; Muratore; M.; López-Carrillo, V.; Escribano-Cuesta, A.; Huguet, N.; Obradors, C. *Org. React.* **2017**, *92*, 1.

2 (a) Fürstner, A.; Morency, L. *Angew. Chem. Int. Ed.* **2008**, *47*, 5030–5033. (b) Hashmi, A. S. K. *Angew. Chem. Int. Ed.* **2008**, *47*, 6754–6756. (c) Seidel, G.; Mynnot, R.; Fürstner, A. *Angew. Chem. Int. Ed.* **2009**, *48*, 2510–2513. (d) Benitez, D.; Shapiro, N. D.; Tkatchouk, E.; Wang, Y.; Goddard, W. A.; Toste, F. D. *Nat. Chem.* **2009**, *1*, 482–486. (e) Echavarren, A. M. *Nat. Chem.* **2009**, 431–433.

3 Reviews on the topic: (a) Wang, Y.; Muratore, M. E.; Echavarren, A. M. *Chem. –Eur. J.* **2015**, *21*, 7332–7339. (b) Harris, R. J.; Widenhoefer, R. A. *Chem. Soc. Rev.* **2016**, *45*, 4533–4551.

resonance forms of every characterized gold(I) carbene will also be outlined here when they provide relevant information.

For simplicity, we will refer sometimes to the carbenic carbon as C1 over this Chapter and it will be represented by a blue circle in the schemes.

Gold(I) carbenes stabilized by heteroatoms directly attached to the carbenic carbon

As explained in the introduction of Chapter II, Fisher carbenes contain a π-donating group attached to the carbenic carbon atom that stabilizes the *p* empty orbital on the electron-deficient carbenic carbon through π-donation from one of the electron lone pairs of the heteroatom. Gold(I) carbenes, regardless the substituents on the carbenic carbon, can be considered as an extreme case of Fisher carbenes. Guided by their similar electronic nature, the original stabilization strategy followed to detect gold(I) carbenes was based on attaching π-donating groups to the carbenic carbon.

In this context, the first characterization of a Fisher-type gold(I) carbene (**1**) was reported in the seminal work by Aumann almost 40 years ago (Scheme 1a).[4] Structurally, complex **1** bears an anionic ancillary ligand and the electron-deficient carbenic carbon is stabilized both by a dimethylamine substituent and a phenyl moiety directly attached to it. Furthermore, gold(I) carbene **1** was stable and the Au–C1 distance was 2.02 Å in the solid state. In 1990, neutral amino(thio)gold(I) carbene **2** was synthetized (Scheme 1b).[5] In this case, the carbenic carbon is directly bound to two π-donating groups and the Au–C1 distance measured in the solid state was 1.961 Å.

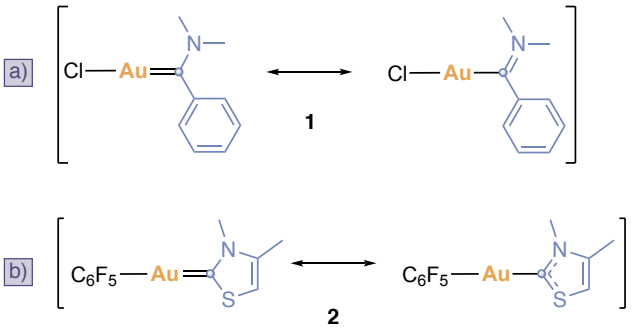

Scheme 1. Main resonance forms of gold(I) carbene (a) **1** and (b) **2**.

4 Schubert, U.; Ackermann, K.; Aumann, R. *Cryst. Struct. Commun.* **1982**, *11*, 591–594.

5 Raubenheimer, H. G.; Scott, F.; Roos, M; Otte, R. *J. Chem. Soc., Chem. Commun.* **1990**, 1722–1723.

A well-known method to access carbene complexes of late transition metals is based on the transfer of a carbene ligand from a metal complex to another metallic center.[6] In 2007, Fischer and co-workers reported a straightforward method to transfer pyrazoline-3-ylidene ligands from chromium complexes to gold(I) and gold(III).[7] Following this strategy, chlorogold(I) carbenes **3a-c**, which bear a N atom directly attached to the C1 and are further stabilized by a highly conjugated system, were prepared (Scheme 2). Complexes **3a-c** were stable and their structures could be confirmed by X-ray analysis for **3a** and **3b**. The Au–C1 distances, (**3a**: 1.981 Å; **3b**: 1.991 Å), are within the range of the previously reported neutral gold(I) carbenes. The absence of the conjugated system in the carbene fragment led to the formation of an unstable gold(I) carbene that could not be fully characterized.

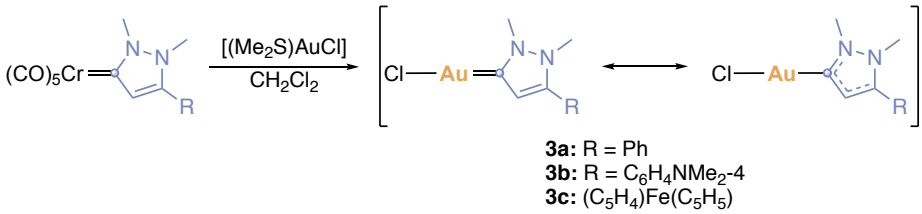

Scheme 2. Synthesis of chlorogold(I) carbenes **3a-c** and their main resonance forms.

The carbene transfer method from chromium(0) complexes to gold(I) was also employed to prepare cationic gold(I) carbenes with commonly used ancillary ligands in gold(I) catalysis (Scheme 3).[8,9,10,11] These gold(I) carbenes are supported either by IPr (**4a**[8] and **4f**[11]), Cy_3P (**4b**[8] and **4c**[9]) or JohnPhos (**4d**[10] and **4e**[11]). For all of them, C1 is directly attached to a methoxy group and, as a consequence, they are stable to air at room temperature and do not display any carbene-like reactivity. Thereby, complexes **4a**, **4c** and **4d** were characterized by X-ray diffraction analysis and the Au–C1 bond lengths (**4a**: 2.010 Å; **4c**: 2.1445 Å and **4d**: 2.032 Å), fall within the range of previously characterized Fisher-type gold(I) carbenes **1** to **3**. The C–O bonds (**4c**: 1.289 Å and **4d**: 1.285 Å) are notably contracted and are consistent with predominant contribution of the oxocarbenium resonance form.

---

6 For reviews on the topic: (a) Liu, S.-T.; Reddy, K. R. *Chem. Soc. Rev.* **1999**, *28*, 315–322. (b) Gómez-Gallego, M.; Mancheño, M. J.; Sierra, M. A. *Acc. Chem. Res.* **2005**, *3*, 44–53.

7 Kessler, F.; Szesni, N.; Maaß, C.; Hohberger, C.; Weibert, B.; Fischer, H. *J. Organomet. Chem.* **2007**, *692*, 3005–3018.

8 Fañanás-Mastral, M.; Aznar, F. *Organometallics* **2009**, *28*, 666–668.

9 Seidel, G.; Gabor, B.; Goddard, R.; Heggen, B.; Thiel, W.; Fürstner, A. *Angew. Chem. Int. Ed.* **2014**, *53*, 879–882.

10 Brooner, R. E. M.; Widenhoefer, R. A. *Chem. Commun.* **2014**, *50*, 2420–2423.

11 Carden, R. G.; Lam, N.; Widenhoefer, R. A. *Chem. –Eur. J.* **2017**, *23*, 17992–18001.

Widenhoefer and co-workers experimentally evaluated the electron-donor ability of LAu fragment in cationic gold(I) carbenes **4d**, **4e** and **4f**. For cyclopropyl(methoxy)gold(I) carbene complex **4d**, the authors proposed that the stabilizing ability of LAu fragment is similar to that of a cyclopropyl group. Through Hammett studies, they proposed that LAu fragments must be considered as strongly inductively electron donating and that π-backbonding represents a minor component of the total LAu–C1 electron donation in gold carbene complexes.

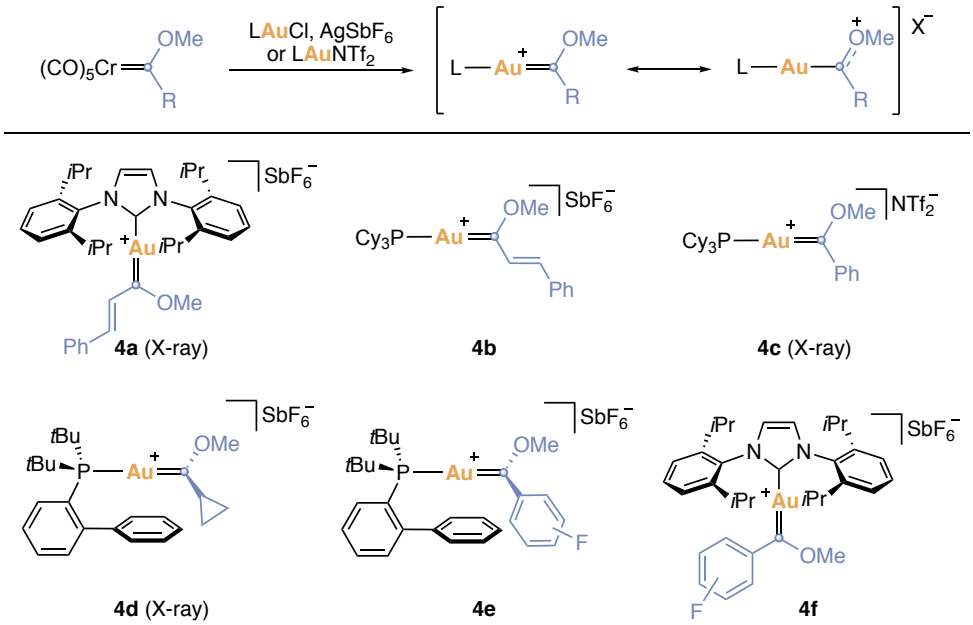

Scheme 3. Synthesis of gold(I) carbenes **4a-f** and main resonance forms.

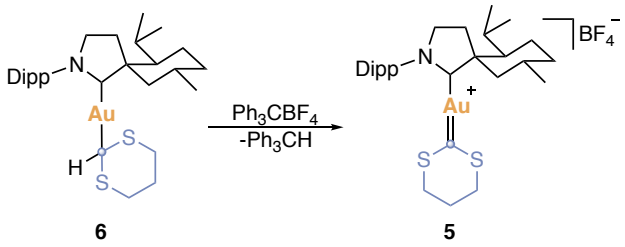

Scheme 4. Synthesis of gold(I) carbene **5**.

Biscarbene gold(I) complex **5** was prepared during an in-depth study on β- and α-hydride abstraction to gold(I) alkyl complexes **6**.[12] Thus, Bertrand and co-workers demonstrated that gold(I) carbene **5** could be cleanly generated after α-hydride abstraction from gold(I) dithianyl complex **6**. Gold(I) carbene **5** was stable due to the well-known stabilizing effect of heteroatoms linked to the carbenic carbon center (Scheme 4). Complex **5** was characterized by NMR and X-

12 Ung, G.; Bertrand, G. *Angew. Chem. Int. Ed.* **2013**, *52*, 11388–11391.

ray diffraction, however, the quality of the crystals was not good enough to determine the Au–C1 distance in the solid state.

The last family of Fischer-type gold(I) carbenes corresponds to complexes **7a-j**, which are stabilized by a pyrrolidine nitrogen and a secondary amine directly attached to C1 (Scheme 5).[13] Gold(I) carbenes **7a-j** were fully characterized by NMR and are stable at room temperature although no X-ray diffraction structure was obtained for any member of the family. The nitrogen cyclic carbene ligand was designed to properly measured the rotational barriers of C–N bond by NMR. From the obtained results, the authors concluded that the gold-to-C1 π-backdonation can be related to the rotational barriers of C–N bond. Furthermore, the rotational barriers calculated ($\Delta G^{\ddagger}_{C1-N}$ = 17.2-18.8 kcalmol^{-1}) suggests a strong double bond character in the C1–N bond and therefore, a strong stabilization from the organic fragment to the electron-deficient C1.

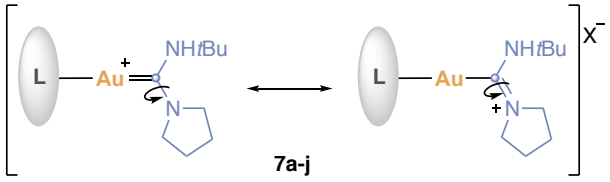

7a-j

$\Delta G^{\ddagger}_{C1-N}$ = 17.2 - 18.8 kcalmol^{-1}

L = Cl, Br, I, PPh_3, PCy_3, PAr^F, CN*t*Bu, Py, IPr, Ph

Scheme 5. Gold(I) carbenes **7a-j**.

All the mentioned Fischer-type gold(I) carbenes in this section (**1-7**) have in common the presence of stabilizing heteroatoms at the carbenic carbon center (C1, blue circle), and as a result, the carbene reactivity is reduced due to the excessive stabilization provided by them to the carbenic carbon that deprives the electrophilicity of the gold(I) carbene. Hence, the chemical knowledge acquired from these structures cannot be extrapolated to the invoked intermediates in gold(I) catalysis.

Diaryl gold(I) carbene complexes

To pursue an approach to prepare a diphenylcarbene gold(I) complex, Fürstner and co-workers relied on the already mentioned exceptional ability of chromium complexes to transfer the carbene ligand to gold.[14] At the outset of their investigations, the reaction of $Ph_2C{=}Cr(CO)_5$ with various $LAuNTf_2$ (L = Cy_3P, Me_3P, Ph_3P, IMes) was tested but the observation of a non-heteroatom stabilized gold(I) carbene failed (Scheme 6). To make the carbene stable enough to be characterized, they modified the carbene ligand in the chromium precursor adding two

13 Ciancaleoni, G.; Biasiolo, L.; Bistoni, G.; Macchioni, A.; Tarantelli, F.; Zuccaccia, D.; Belpassi, L. *Chem. – Eur. J.* **2015**, *21*, 2467–2473.

14 Seidel, G.; Fürstner, A. *Angew. Chem. Int. Ed.* **2014**, *53*, 4807–4811.

electron-rich methoxy substituents in the para position of the aryl groups. In this case, the carbene transfer to $Cy_3PAuNTf_2$ proceeded successfully at -50 ºC yielding a bright red gold(I) carbene complex (**8a**) (Scheme 6). Unlike gold(I) carbenes **1-7**, complex **8a** was only partially stable at room temperature even in the dark. Related to its partial instability, these authors found that complex **8a** was capable of promoting cyclopropanation of *p*-methoxystyrene at room temperature (Scheme 7).

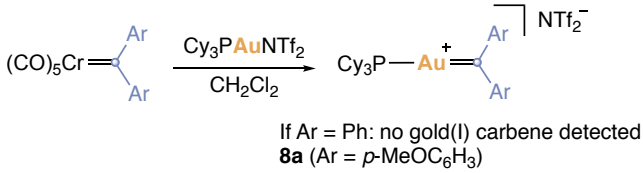

Scheme 6. Synthesis of gold(I) carbene **8a**.

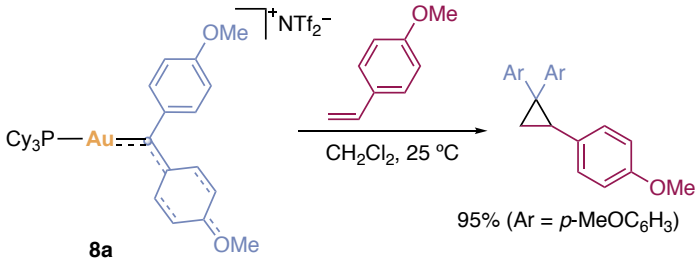

Scheme 7. Gold(I)-promoted cyclopropanation by **8a**.

The ancillary ligand is well-known to highly affect gold(I) catalysis. For a systematic study into how the nature of gold(I) carbenes can be affected by the ligand, the group of Fürstner prepared complexes **8b** and **8c** by other means (Figure 2).[15] Gold(I) carbenes **8a-c** were characterized by NMR and X-ray crystallography. Contrary to what expected, Au–C1 bond lengths fall into a rather narrow range (**8a**: 2.039 Å, **8b**: 2.028 Å and **8c**: 2.020 Å). Similar results were observed for the chemical shift for C1 (**8a**: 285 ppm, **8b**: 275 ppm and **8c**: 290 ppm). It is important to note that in all the cases, the carbene center is stabilized from an interaction with the aryl groups as evidenced by the shortened of the C1–Cipso (Figure 2). Furthermore, the C1–Cipso rotational barrier of **8a** was estimated as 8.4 kcalmol^{-1}. Based on these results, these authors proposed that the gold-to-carbon π-backdonation is not sufficient to stabilize complexes **8a-c** and thus, the contribution of the aryl rings is more important than the ancillary ligand in the stabilization of gold(I) carbenes.

15 Werlé, C.; Goddard, R.; Fürstner, A. *Angew. Chem. Int. Ed.* **2015**, *54*, 15452–15456.

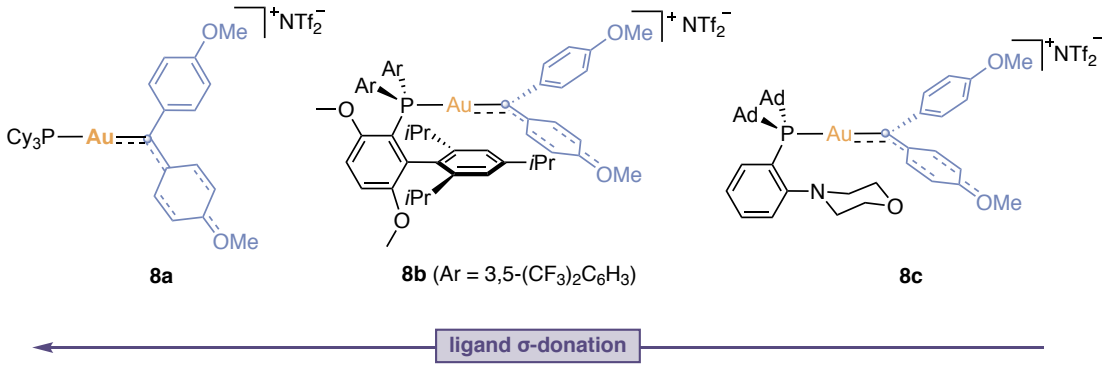

Figure 2. Comparison of gold(I) carbenes **8a-c**.

Recently, Fürstner and co-workers reported the synthesis of two new diaryl gold(I) carbene bearing dimethyl amine groups in the aryl moieties and IPr (**8d**) or XPhos (**8e**) as ancillary ligands (Figure 3).[16] Based on the shortened of C1–Cipso (1.433 Å) and C–N (1.359 Å) bonds for complex **8d** in the solid state, they proposed that the carbenic carbon is mainly stabilized again by the electron-rich aryl substituents.

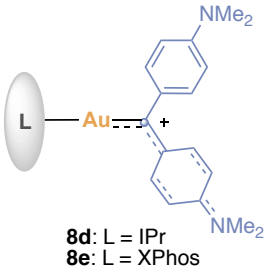

Figure 3. Structure of complexes **8d** and **8e**.

Non-heteroatom stabilized gold(I) carbenes

The aforementioned gold(I) carbenes include iminio, sulfonio or oxonio ylide-type ligands and their stabilization relies on the conjugation of heteroatoms to the electron-deficient carbenic carbon atom (C1).

In 2014, Widenhoefer and co-workers published the first gold(I) carbene complex that lacks stabilization from conjugated heteroatoms.[17] To impart greater stability, they exploited the potential aromatic stabilization of the cycloheptatrienylidene ligand, which would stabilize the charge by delocalization over the aromatic fragment. Complex **9** was prepared *via* hydride abstraction with triphenylcarbenium tetrafluoroborate from the neutral cycloheptatrienyl complex **10** (Scheme 8). Remarkably, complex **9** bears JohnPhos as ancillary ligand, which is a well-known ligand for gold(I)-catalyzed cycloisomerization of 1,*n*-enynes, and it was thermally stable and could be characterized both by NMR and X-ray diffraction. The authors proposed that the

16 Tskhovrebov, A. G.; Goddard, R.; Fürstner, A. *Angew. Chem. Int. Ed.* **2018**, *57*, 8089–8094.

17 Harris, J. R.; Widenhoefer, R. A. *Angew. Chem. Int. Ed.* **2014**, *53*, 9369–9371.

NMR data was consistent with a structure with major contribution of the aromatic canonical form **9a**. On the other hand, the X-ray data supported a minor contribution of the gold(I) carbene canonical form **9b**.

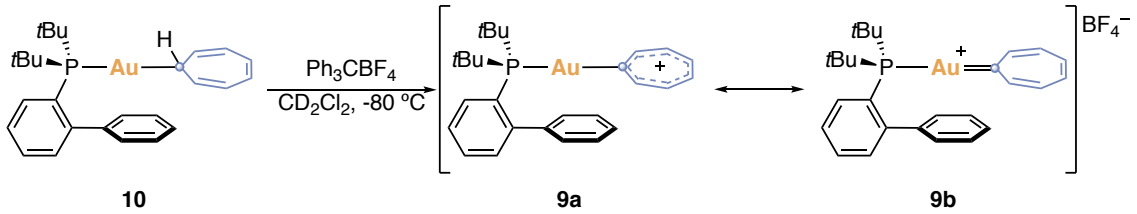

Scheme 8. Synthesis of gold(I) carbene **9** and main resonance forms.

Complex **9** was reactive towards reduction by mild hydride donors such as triethylsilane (Scheme 9, right) and also underwent oxidation in the presence of pyridine-*N*-oxide to form tropone (Scheme 9, left).

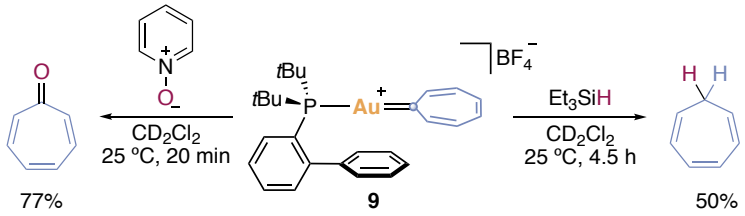

Scheme 9. Reactivity of gold(I) carbene **9**.

In parallel to the synthesis of complex **9**, Straub and co-workers reported the isolation of gold(I) carbene **12** by direct reaction of a gold(I) complex **11** and (dimesityl)diazomethane (Scheme 10)[18]. Complex **12** bears a large NHC ancillary ligand (IPr**) combined with a sterically demanding bimesityl carbene fragment. The extreme steric shielding of the carbene center provided by both the IPr** and the bimesityl ligand results in high water-, air-, and thermal stability of complex **12** and, therefore, this complex does not diplay any typical carbene reactivity.

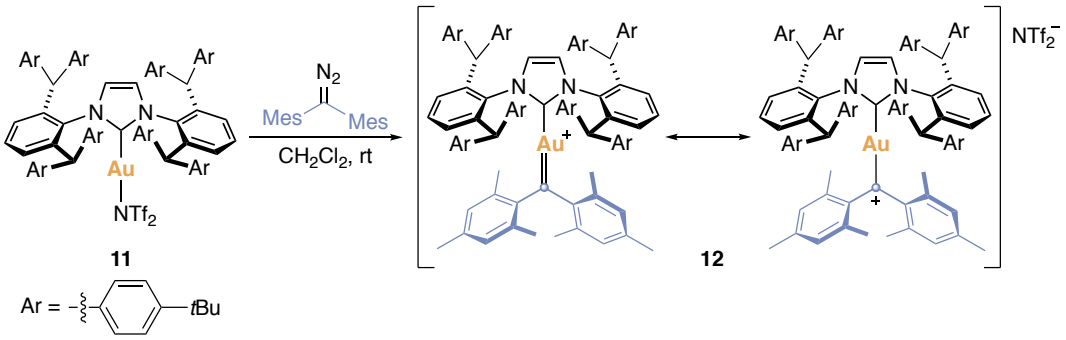

Scheme 10. Synthesis and main resonance forms of gold(I) carbene **12**.

18 Hussong, M. W.; Rominger, F.; Kräner, P.; Straub, B. F. *Angew. Chem. Int. Ed.* **2014**, *53*, 9372–9375.

In the solid state of **12**, the Au–C1 bond (2.014 Å) is slightly shorter than the Au–C(IPr**) bond (2.030 Å), which the authors attribute to "a significant but not predominant double bond character Au=C1".[18] Likewise, the bathocromic shift of the emerald-green gold(I) carbene **12** compared to the red-purple carbenium ion $[Mes_2CH]^+[HSO_4]^-$ further reinforces the participation of gold fragment in the stabilization of the positive charge. The analysis of the frontier orbitals revealed an antibonding σ interaction in the HOMO between a gold *5d* filled orbital and the sp^2 donor electron pair of the carbenic carbon atom. Guided by this later result, Straub proposed that the consideration of a third resonance form with a Au–C1 bond order of zero should be considered to explain the Au–C1 bond situation in gold(I) carbenes (Scheme 11).

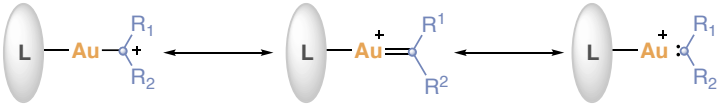

Scheme 11. Resonance forms invoked by Straub to describe the Au–C bond in gold(I) carbenes.

After several unsuccessful attempts,[9,14,17] Bourissou and co-workers isolated the first diphenyl gold(I) carbene using a bent *o*-carborane diphosphine ligand, which forces gold atom to rearrange to a trigonal-planar environment (Scheme 12).[19] Complex **13** was isolated as a thermally stable violet solid. The chemical shift of C1 (316.2 ppm) is at the upper range of the chemical shift for the previously reported gold(I) carbenes. In addition, the Au–C1 bond distance (1.984 Å) is slightly shorter than all other gold(I) carbenes reported. Also important is that the C1–Cipso bonds are not contracted and the phenyl rings are twisted, which suggest very weak π-interaction between the carbenic carbon and the phenyl groups.

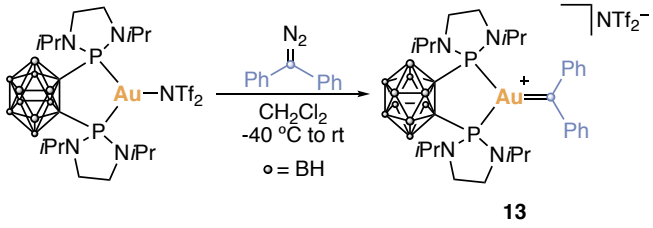

Scheme 12. Synthesis of gold(I) carbene **13**.

The Au–C1 bonding situation and the role of the $[(DPCb)Au]^+$ fragment on gold(I) carbene **13** were studied by DFT calculations. First, the analysis of the frontier orbitals revealed a bonding interaction between the d_{xz}(Au) and $2p^{\pi}$(C1) orbitals in the HOMO. Likewise, the NLMO related to the π-backdonation from gold-to-carbon is highly delocalized over C1 (88.0% d_{xz}(Au), 10.6% $2p^{\pi}$(C1)) (Figure 4). To better understand the role of gold-to-carbon π-backdonation in the

19 Joost, M.; Estévez, L.; Mallet-Ladeira, S.; Miqueu, K.; Amgoune, A.; Bourissou, D. *Angew. Chem. Int. Ed.* **2014**, *53*, 14512–14516.

stabilization of gold(I) carbenes, the authors also performed in-depth bonding analysis for gold(I) carbenes **9** and **12**. They observed that the respective molecular orbitals exhibit much less interaction between the vacant $2p^{\pi}$(C1) and the filled d_{xz}(Au) (Figure 4). Additionally, the computed charge transfer (estimated from the NBO charges) from the carbene to gold(I) for complexes **9** (0.35e$^-$), **12** (0.28e$^-$) and **13** (0.0 e$^-$) indicates that the bonding situation in the latter is unique. Based on all these data, the authors proposed that the bidentate ligand elevates the energy of the occupied *d* orbital of gold strengthening π-backdonation. The specific electronic properties of $[(DPCb)Au]^+$ fragment allowed the preparation of the first carbene complex (**13**) mainly stabilized by the gold fragment rather than by the carbene substituents.

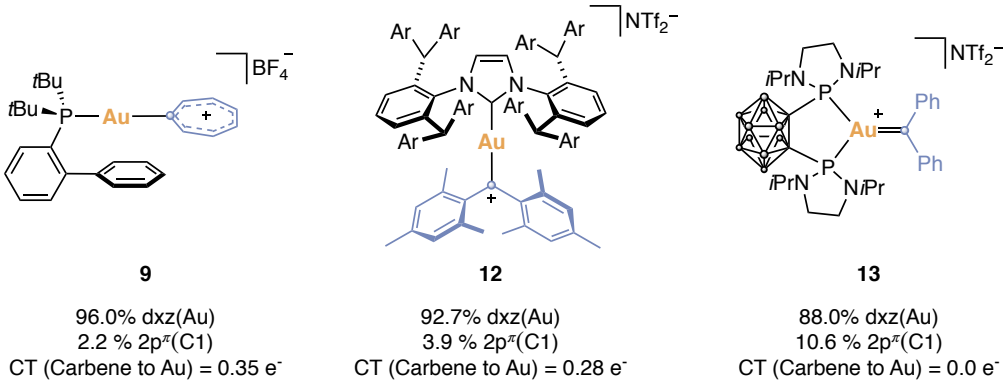

Figure 4. Bonding situation in gold(I) carbenes **9**, **12** and **13**. Percentages of the delocalization of the NLMO related to the π-backdonation from gold-to-carbon on different orbitals.

Hihgly electrophilic α-oxo gold(I) carbenes

After the pioneering work by the groups of Pérez and Nolan,[20] α-oxo gold(I) carbenes have been proposed as intermediates in gold(I) catalyzed cyclopropanation, X–H insertion, C–H insertion and other cycloadditions. However, their characterization has remained elusive due to the inherent electrophilicity of these complexes. Taking advantage of the unique electronic properties of the bent gold(I) fragment used to isolate complex **13**, Bourissou and co-workers were capable of characterizing the first α-oxo gold(I) carbene (**14**) (Scheme 13).[21] In this case, the resulting dark violet product was thermally unstable, although the authors were able to fully characterize it by NMR and X-ray analysis. In the solid state, the Au–C1 length (1.961 Å) is the shortest previously reported for a gold(I) carbene complex. Besides that, the phenyl ring is co-planar with the carbene center and the C1–Cipso bond is also slightly shortened, which indicate that the π-system of the

20 (a) Fructos, M. R.; Belderrain, T. R.; Frémont, P. de; Scott, N. M.; Nolan, S. P.; Díaz-Requejo, M. M.; Pérez, P. J. *Angew. Chem. Int. Ed.* **2005**, *44*, 5284–5288. (b) Frémont, P. de; Stevens, E. E.; Fructos, M. R.; Díaz-Requejo, M. M. Pérez, P. J., Nolan, S. P. *Chem. Commun.* **2006**, 2045–2047.

21 Zeineddine, A.; Rekhroukh, F.; Carrizo, E. D. S.; Mallet-Ladeira, S.; Miqueu, K.; Amgoune, A.; Bourissou, D. *Angew. Chem. Int. Ed.* **2018**, *57*, 1306–1310.

aryl collaborates in the stabilization of the electron deficient carbenic carbon C1. The bonding analysis of complex **14** shows significant contribution of the $2p^{\pi}$(C1) orbital in the NLMO associated to the π-backdonation (85.7% d_{xz}(Au), 12.1% $2p^{\pi}$(C1)). In addition, the charge transfer revealed a small electron transfer between the carbene moiety and gold fragment (-0.07 e^-). The bonding analysis of complex **14** reinforces the previously found observation that this bidentate phosphine enhances π-backdonation from gold(I)-to-carbon.

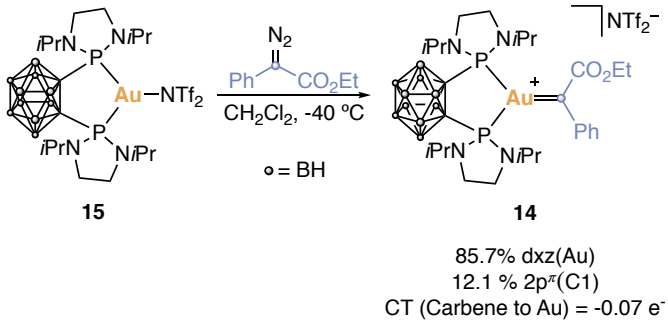

Scheme 13. Synthesis of gold(I) carbene **14** and bonding situation analysis for the Au–C1 bond. Percentages of the delocalization of the NLMO related to the π-backdonation from gold-to-carbon on different orbitals.

To determine if gold(I) carbene **14** could be considered as a real catalytic intermediate, the authors mixed complex **15** with diazocompound **16** in the presence of suitable substrates to generate gold(I) carbene **14** under catalytic conditions (Scheme 14).[21] As expected, this system was capable of catalyzing the cyclopropanation of styrene (Scheme 14, up), as well as the B-H (Scheme 14, middle) and O-H (Scheme 14, bottom) insertions into phosphine-borane and phenol, respectively.

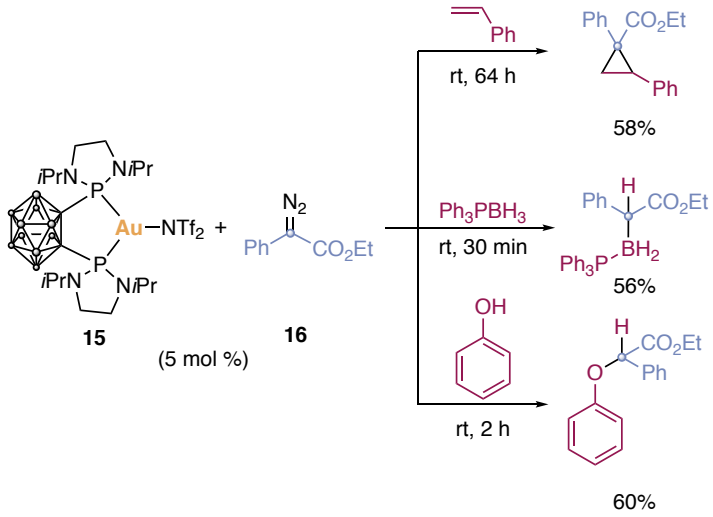

Scheme 14. Reactivity upon reaction of **15** with α-oxo diazocompound **16**.

IBO Analysis on Stabilization Effects

Considering the structures of gold(I) carbenes **1**-**4, 6**-**9**, **12** and **13** (the structures are shown along this chapter), it becomes clear that the organic fragments linked to the carbenic carbon play an important role in the stabilization of these complexes. In 2015, Hashmi and co-workers used the intrinsic bond orbital (IBO) method to dissect the role of carbene substituents for previously isolated gold(I) carbenes **4a**,[8] **8a**,[14] **9**,[17] and **13**.[22] This method describes orbitals in an intuitive way and allow to interpret chemical bonds in a straightforward manner.

Regarding complex **4a**, the IBO analysis revealed a strong covalent stabilization of the carbenic carbon *via* the O lone pair of the methoxy group directly attached to C1 (Figure 4). For complex **8a**, it was found that the π-systems of the electron rich aromatic rings stabilized the carbenic carbon to a large extent (Figure 5). Complex **9**, which lacks heteroatoms, is highly stabilized through aromaticity and thus, the three IBOs of the π-system (6 electrons) of the cycloheptatrienylidene ligand are equally distributed over the seven atoms (Figure 5). For the aforementioned complexes (**4a**, **8a**, and **9**), the filled *d* orbital of gold is mainly located at gold (94-95%), which suggests a low contribution of the gold-to-carbon π-backdonation in the carbene stabilization. For complex **13**, the gold-to-carbon π-backdonation has been proposed to be significant by NBO analysis.[19] Likewise, the IBO related to the filled *5d* orbital of gold supports this statement since the latter is only located 87% at gold. Nevertheless, even for complex **13**, it was proposed that the stabilization obtained from the π-system of the phenyl groups dominates the stabilization of carbenic carbon (Figure 5).

All these results led the group of Hashmi to conclude that the π-stabilization effects imparted by the carbene organic fragment is substantial and cannot be ignored.[22] In fact, they proposed that the carbene substituents play a more significant role in the stabilization than gold-to-carbon π-backdonation in gold(I) carbene complexes.

22 Comprimido, L. N. dos S.; Kein, J. M. N.; Knizia, G.; Kästner, J.; Hashmi, A. S. K. *Angew. Chem. Int. Ed.* **2015**, *54*, 10336–10340.

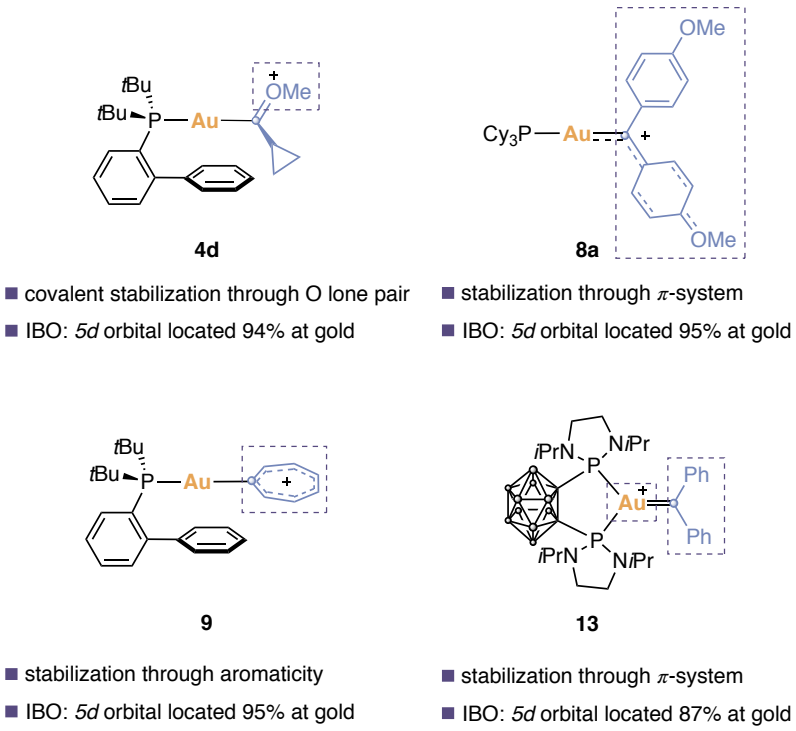

Figure 5. Stabilization effects in gold(I) carbenes based on IBO analysis.

Aryl Gold(I) Carbenes

As explained in the introduction of Chapter II, our group have developed a safe method to generate aryl gold(I) carbenes **17** *via* gold(I)-catalyzed retro-Buchner reaction of cycloheptatrienes **18** (Scheme 15).[23] In-depth investigations support that cycloheptatrienes **18** react with cationic gold(I) complexes under catalytic conditions by stepwise electrophilic cleavage of two C–C bonds of the norcaradiene tautomers **19** (Scheme 15).[23b] The activation energy for the electrophilic cleavage correlates well with the high temperatures required experimentally.

The *in situ* generated aryl gold(I) carbenes **17** can react as catalytic intermediates in intra- and intermolecular cyclopropanation of alkenes **20**,[23a] formal (4+1) cycloaddition with methylenecyclopropenes **22** or cyclobutenes **23** to form cyclopentanes **24**[23c] and formal (3+2) cycloaddition with allenes **25** to form highly substituted indenes **26** (Scheme 15).[23d] Interestingly, only one low yielding example of an intramolecular C(sp^3)–H insertion was found during these investigations (Scheme 15).[23a] In addition, *ortho*-substituted cycloheptatrienes led to the formation of fluorenes **28** and indenes **29** by annulation processes (Scheme 16).[23b] In general, the

23 (a) Solorio-Alvarado, C.; Wang, Y.; Echavarren, A. M. *J. Am. Chem. Soc.* **2011**, *133*, 11952–11955. (b) Wang, Y.; McGonigal, P. R.; Herlé, B.; Besora, M.; Echavarren, A. M. *J. Am. Chem. Soc.* **2014**, *136*, 801–809. (c) Wang, Y.; Muratore, M. E.; Rong, Z.; Echavarren, A. M. *Angew. Chem. Int. Ed.* **2014**, *53*, 14022–14026. (d) Yin, X.; Mato, M.; Echavarren, A. M. *Angew. Chem. Int. Ed.* **2017**, *56*, 14591–14595.

generated intermediate complexes behave more like free or Fischer-type metal carbenes than like benzylic carbocations.

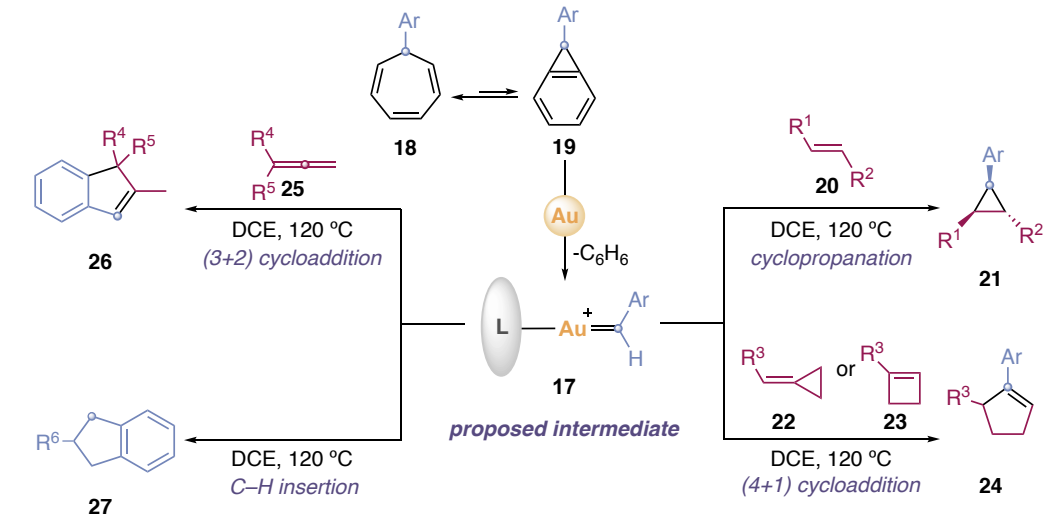

Scheme 15. Gold(I)-catalyzed transformations with cycloheptatrienes.

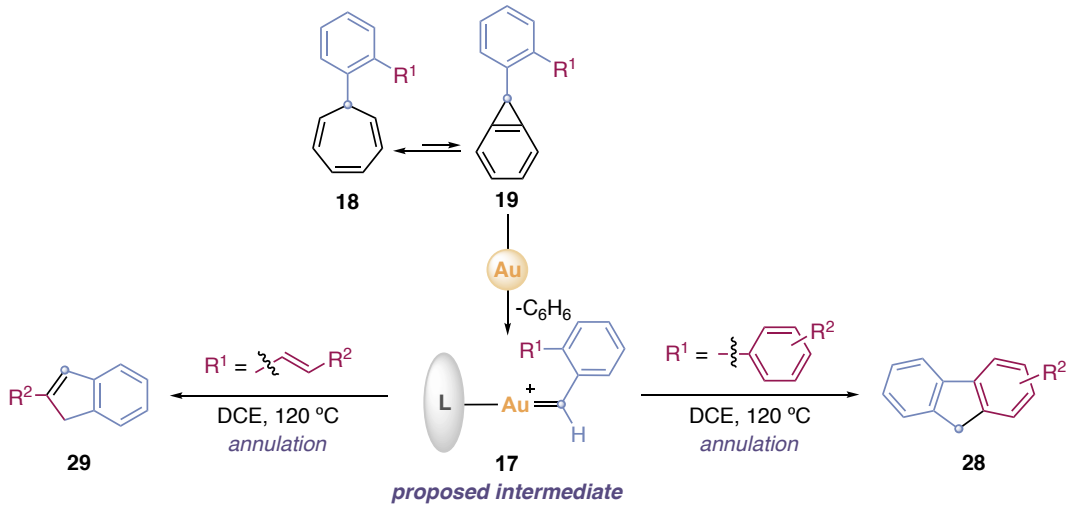

Scheme 16. Gold(I)-catalyzed transformations with *ortho*-substituted cycloheptatrienes.

The organic fragment of the aforementioned invoked intermediates **17** is structurally similar to that of isolated complexes **8**, **12** and **13** and thus, the carbenic carbon could also be stabilized through the π-system of the aryl group (Figure 6). However, besides being attached to an aryl group, the carbenic carbon is also bound to a hydrogen atom which cannot impart any stability to the carbenic carbon.

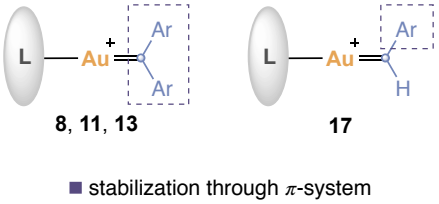

Figure 6. Stabilization effects in diaryl *vs.* aryl gold(I) carbenes

Characterization of aryl gold(I) carbenes in the gas phase

While aryl gold(I) carbenes **17** have not been detected in solution, their existence have been proved in the gas phase by Chen and coworkers.[24,25] On their seminal work, the fragmentation *via* collision-induced dissociation of phosphonium ylide **30** furnishes a species that corresponds to the PPh_3 loss and generation of gold(I) carbene $[(IMes)AuCHPh]^+$ **17a** (Scheme 17).[24a] In the presence of alkenes, species **17a** displays a typical metallocarbene behavior promoting cyclopropanation, alkene loss and, even more interestingly, "cyclopropane metathesis" (Scheme 18). Subsequent experimental data, kinetic studies, and DFT calculations supported that gold(I) carbenes were involved in the aforementioned reactions.[24b-d] In the following years, both the groups of Chen and Gronert demonstrated that the same reactivity patterns were displayed by gold(I) benzylidenes bearing different substitution patterns in the carbene fragment and several ancillary ligands.[24,25,26]

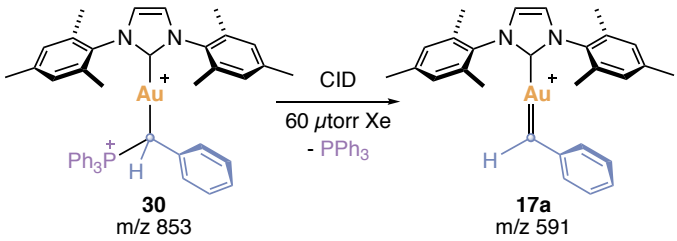

Scheme 17. Generation of aryl gold(I) carbene **17a** in the gas phase.

24 (a) Federov, A.; Moret, M.-E.; Chen, P. *J. Am. Chem. Soc.* **2008**, *130*, 8880–8881. (b) Federov, A.; Chen, P. *Organometallics* **2009**, *28*, 1278–1281. (c) Fedorov, A.; Chen, P. *Organometallics* **2009**, *29*, 2994–3000. (d) Fedorov, A.; Batiste, L.; Bach, A.; Birney, D. M.; Chen, P. *J. Am. Chem. Soc.* **2011**, *133*, 12162–12171.

25 Ringger, D. H.; Kobylianskii, I. J.; Serra, D.; Chen, P. *Chem. –Eur. J.* **2014**, *20*, 14270–14281.

26 Swift, C. A.; Gronert, S. *Organometallics* **2014**, *33*, 7135–7140.

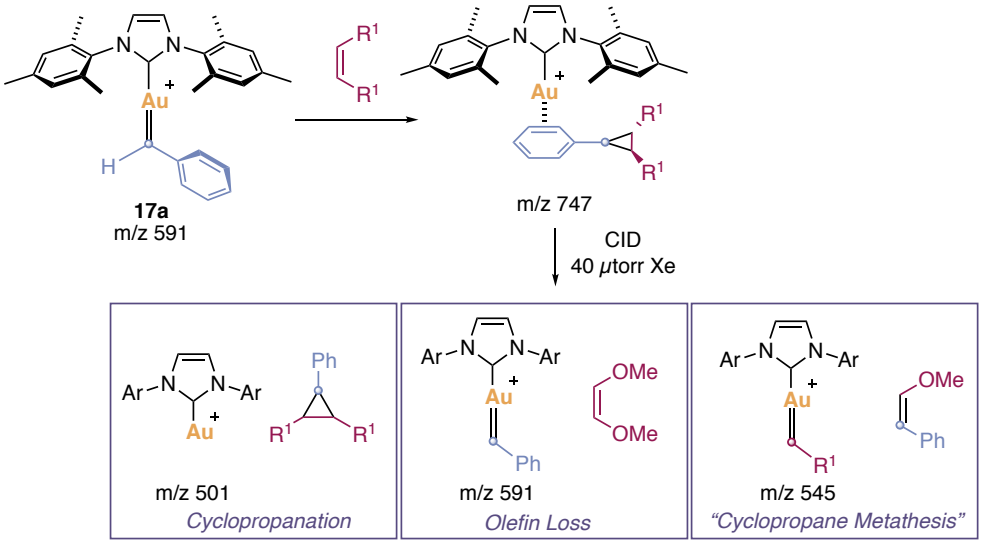

Scheme 18. Reactivity of aryl gold(I) carbene **17a** in gas phase.

The use of phosphonium ylides **30** to characterize gold(I) carbenes upon PPh_3 dissociation in gas phase can be considered as a method in which gold(I) carbenoids generate their corresponding gold(I) carbenes after removal of a good leaving group. In this case, the activation barrier of PPh_3 dissociation from phosphonium ylide **30** was found to be higher than 50.0 $kcalmol^{-1}$ both experimentally and computationally, which limits the possibility of applying this method under thermal conditions in condensed phase.[24a]

To transfer this approach to solution, the group of Chen modified the precursors by installing a SO_2-imidazolylidene moiety as better leaving group, which is capable of thermally dissociate to release SO_2 gas and imidazolylidene.[25] Using precursors **31**, when the thermal dissociation was done in the presence of *p*-methoxystyrene at 120 ºC, the expected cyclopropanes (as *cis* and *trans* mixtures in different ratios) were obtained, supporting the formation of carbene intermediates at high temperatures in solution (Scheme 19). Unfortunately, the corresponding aryl gold(I) carbenes could not be detected in solution and were only characterized in the gas phase using precursor **31**.

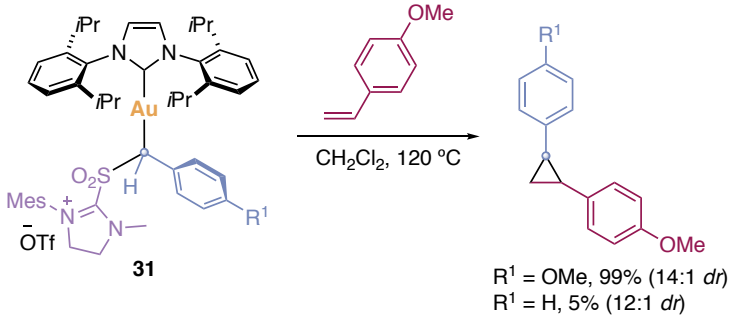

Scheme 19. Stoichiometric cyclopropanation of *p*-methoxystyrene with gold(I) carbene precursors **31**.

Objectives

All the stabilization strategies followed to characterize gold(I) carbenes have led to complexes that are very different to the species involved in catalysis.[4-19] Therefore, despite the significant progress achieved in their isolation,[4-19,21] realistic gold(I) carbene intermediates bearing commonly used ligands have not been characterized yet. Thus, the development of a general and straightforward synthesis of highly reactive gold(I) carbenes resembling real intermediates would be of great interest to fully understand the mechanisms of gold(I)-catalyzed transformations.

During the course of our investigation outlined in Chapter II, preliminary results suggested that [JohnPhosAuCHPhCl] carbenoid, after chloride abstraction, gives rise to stilbene, which undergoes cyclopropanation by an undetected phenyl gold(I) carbene intermediate (Chapter II, Scheme 19).[27] The observed cyclopropanation closely resembles the reactivity displayed by aryl gold(I) carbenes generated by gold(I)-catalyzed retro-Buchner reaction of cycloheptatrienes **18** (Scheme 15 and 16).[23] Although these arylidene complexes have never been observed in solution, such species have been detected in the gas phase.[24-26]

In this context, we envisioned that the dehalogenation of chloro(aryl)methylgold(I) carbenoids could be a general and straightforward manner of generating and, even more relevant, characterizing aryl gold(I) carbenes in solution (Scheme 20). To this end, we decided to tune the aryl substituents and the ancillary ligand of chloro(aryl)methylgold(I) carbenoid precursors in a way that would allow the preparation of stable aryl gold(I) carbenes that could be detected (Scheme 20).

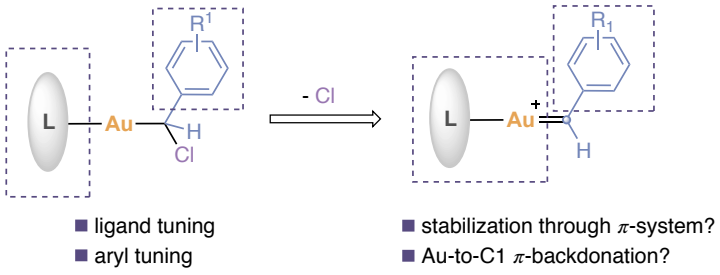

Scheme 20. Proposed synthesis of gold(I) carbenes from gold(I) carbenoids.

27 Sarria Toro, J. M.; García-Morales, C.; Raducan, M.; Smirnova, E. S.; Echavarren, A. M. *Angew. Chem. Int. Ed.* **2017**, *56*, 1859–1863.

Results and Discussion

Design of a Suitable Gold(I) Carbenoid Precursor

As explained in the results and discussion of Chapter II, we found that chloro(organyl)gold(I) carbenoids, after chloride abstraction, display reactivity typical from gold(I) carbenes.[27] Here, we envisaged that tuning the steric and electronic properties of gold(I) carbenoid complexes could be a good strategy to convert them into suitable precursors to access and characterize stable gold(I) carbenes. Bearing in mind the importance of the organic fragment in the stabilization of gold(I) carbenes,[22] we first modified the substituents at the Csp^3 atom of the carbenoid precursors using an electron donating phosphine as ligand (JohnPhos). Specifically, we prepared new gold(I) carbenoids which bear aryls substituents from the reaction of gold(I) chloride **32** with several aryl diazomethane compounds (Scheme 21).

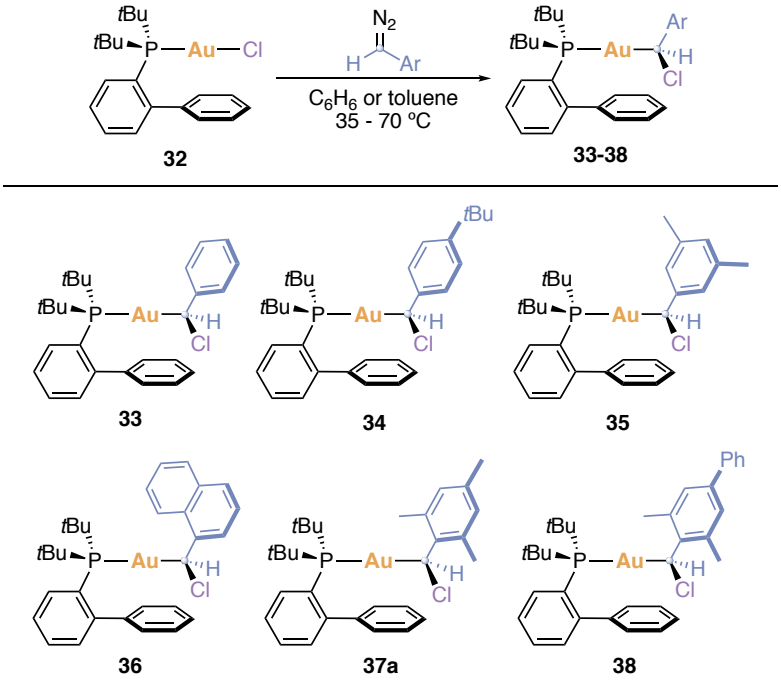

Scheme 21. Synthesis of chloro(aryl)methylgold(I) carbenoids **33-38**.

Subsequently, the aptitude of complexes **33-38**[28] as carbene precursors was evaluated. To this end, $GaCl_3$ was chosen as initial halide scavenger because, after chloride abstraction, generates a non-coordinating counterion, $GaCl_4^-$, without any side product. Therefore, complexes **33-36** were treated with $GaCl_3$ in CD_2Cl_2 at -90 ºC, even if the formation of gold(I) carbenes was supported by the generation of alkenes and further cyclopropanation, these species were not stable enough to be detected by NMR (Scheme 22). Remarkably, upon addition of $GaCl_3$ to carbenoid **37a** in CD_2Cl_2 at -90 ºC, a deep red solution was formed suggesting the formation of mesityl gold(I)

28 The synthesis of complex **33** was already described in Chapter II. Sarria Toro, J. M.; García-Morales, C.; Mihai, R.; Smirnova, E.; Echavarren, A. M. *Angew. Chem. Int. Ed.* **2017**, *56*, 1859–1863.

carbene **39a**, which could be characterized by NMR spectroscopy (Scheme 23). However, complex **39a** was thermally unstable and partially decomposed at temperatures as low as -90 ºC. We hypothesized that gold(I) carbenoids **38** would lead to more stable gold(I) carbene by charge delocalization. However, when complex **38** was treated with $GaCl_3$ under the previous described conditions, the formation of the corresponding gold(I) carbene was not detected (Scheme 22). At this point, we intended to prepare carbenes bearing more electron rich organic fragments. However, we found substantial synthetic limitations with the use of highly electron rich mono- and diaryl diazo compounds[29] in the synthesis of the carbenoid counterparts.

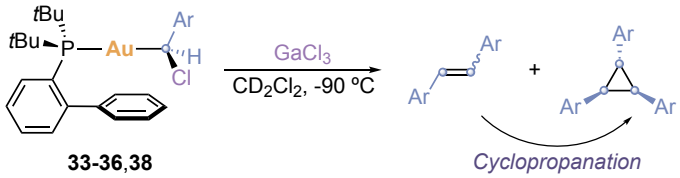

Scheme 22. Activation of gold(I) carbenoids **33-36**,**38** with $GaCl_3$.

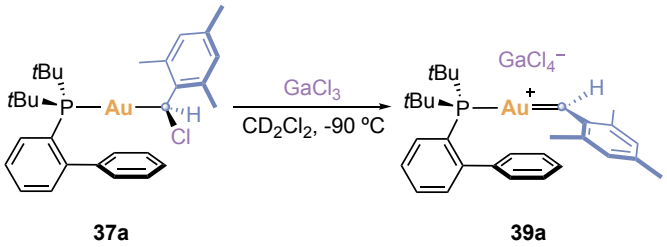

Scheme 23. Synthesis of gold(I) carbene **39a**.

It is worth mentioning that activation of carbenoid **37a** with other chloride scavengers ($B(C_6F_5)_3$, $AlCl_3$, $AlBr_3$, TMSOTf, $TMSNTf_2$ and AgOTf) failed to a gold(I) carbene. Interestingly, when the reaction was carried out in toluene-*d*$_8$ with $GaCl_3$, a red oil was formed all over the walls of the NMR tube and no signal was observed. This red oil was presumably gold(I) carbene **39a** which is not soluble in toluene.

To increase the stability of these aryl gold(I) carbenes, we next sought to modify the ancillary ligand in the carbenoid precursor. Unfortunately, the synthesis of carbenoids did not proceed satisfactorily with NHC carbenes, Ph_3P, Cy_3P, XPhos and BrettPhos. Then, we decided to modify the biaryl moiety of the original JohnPhos ligand. Therefore, a family of chloro(mesityl)methylgold(I) carbenoids **37a-e** bearing JohnPhos-type ligands was prepared (Scheme 24).

29 Bug, T.; Hartnagel, M.; Schlierf, C.; Mayr, H. *Chem. –Eur. J.* **2003**, *9*, 4068–4076.

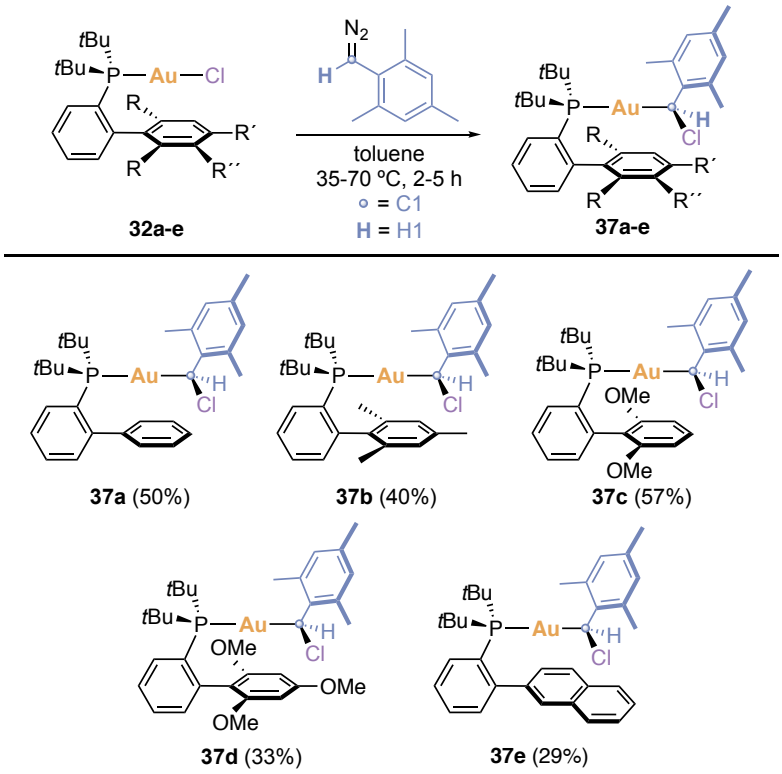

Scheme 24. Synthesis of gold(I) carbenoids **37a-e**.

Complexes **37a-e** were indefinitely stable when stored under argon and their structures were confirmed by X-ray crystallography (Figure 7). The analysis of the NMR data of carbenoids **37a-e** shows that H1 and C1 from the chloromesityl moiety resonate within δ 3.26-4.28 ppm and δ 69.7-71.4 ppm respectively. In the solid state, Au–C1 distances are between 2.038-2.095 Å in agreement with the previously reported chloromethylgold(I) carbenoids.[27] The Au–C1–Cl angle is between 107.1-113.5 º, closer to the ideal tetrahedral angle for a carbon with sp^3 hybridization (Figure 7).

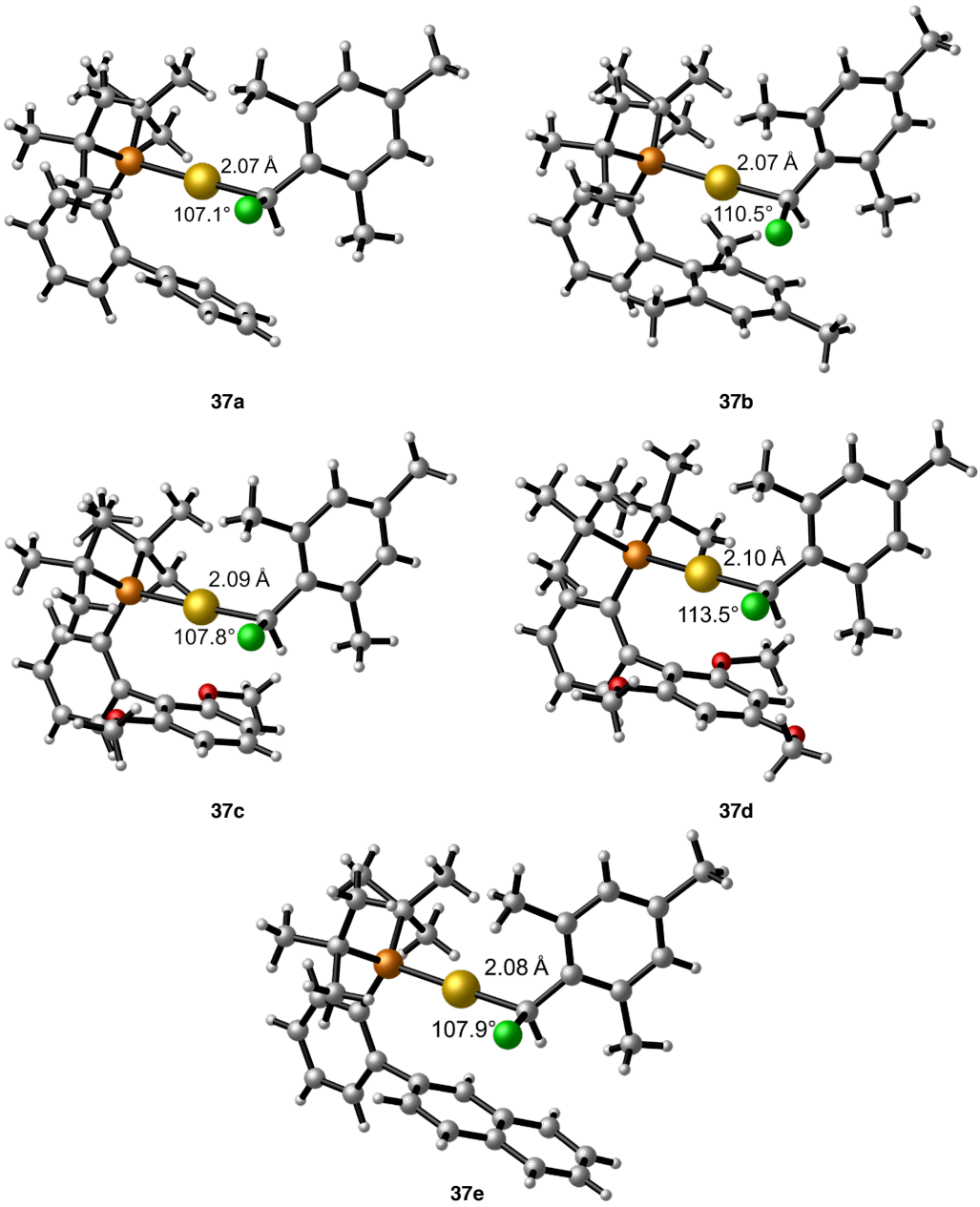

Figure 7. X-ray crystal structure of gold(I) carbenoids **37a-e**.

Mesityl Gold(I) Carbenes Spectroscopy Characterization

When the new chloro(mesityl)methylgold(I) carbenoids **37b-e** were treated with $GaCl_3$ under the optimized conditions for the generation of **39a**, mesityl gold(I) carbenes **39b-e** were also detected by NMR (Scheme 25). Carbenes **39b-e**, were found to be stable until -70 ºC. Furthermore, mesityl gold(I) carbenes **39a-e** were detected in gas phase by ESI-MS from carbenoid complexes **37a-e**.

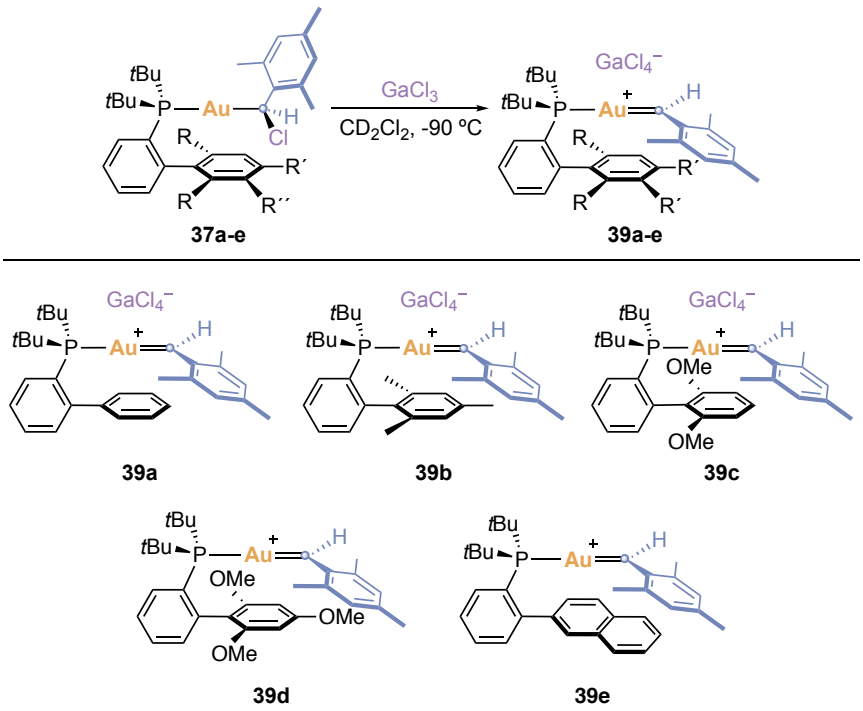

Scheme 25. Synthesis of mesityl gold(I) carbenes **39a-e**.

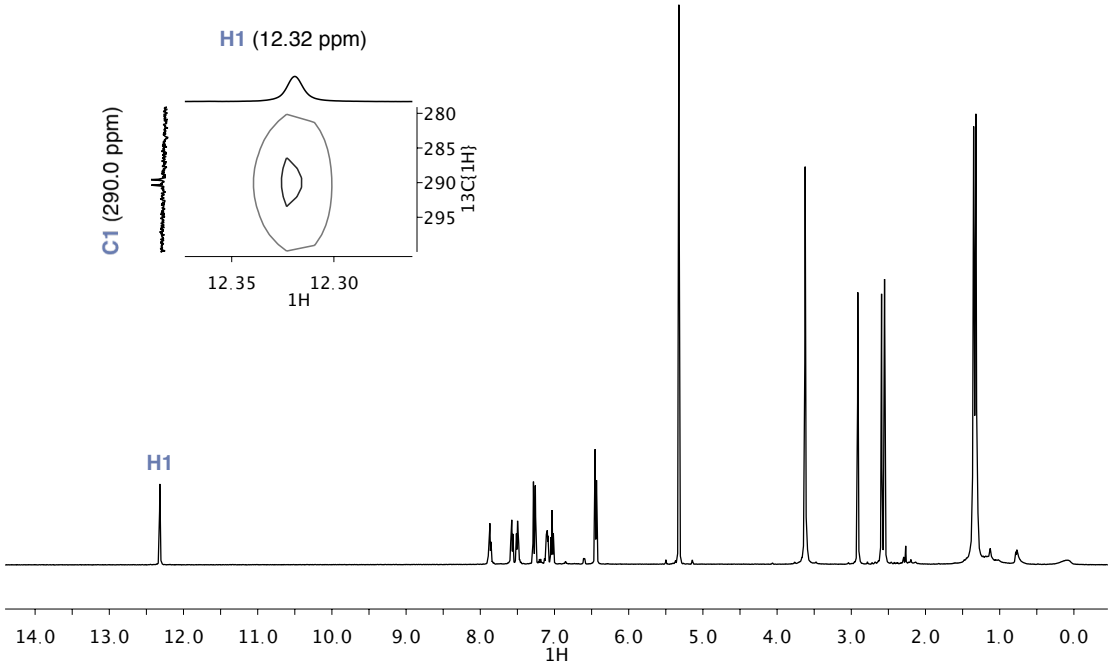

Figure 8. ^{1}H NMR and selected region of ^{1}H-^{13}C HSQC spectra of gold(I) carbene **39c** in CD_2Cl_2 at -90 ºC.

Importantly, these are the first monosubstituted gold(I) carbenes that have been spectroscopically characterized. The ^{1}H NMR and a selected region of ^{1}H-^{13}C HSQC spectra for gold(I) carbene **39c** is shown in Figure 8. Complexes **39a-e** present a characteristic signal in ^{1}H NMR at δ 11.74-

12.67 ppm corresponding to H1 (Table 1).[30] The carbenic carbons (C1) resonate at δ 284.6-290.0 ppm as a doublet (^{2}J (^{13}C-^{31}P) = 96.8-99.8 Hz), within the range of previously characterized gold(I) carbenes (225-321 ppm) (Table 1). In addition, clear correlations between the carbenic carbon (C1) and proton (H1) were observed in the ^{1}H-^{13}C HSQC spectra (Figure 8, correlation for **39c**). Somehow surprisingly was the significant decrease in the ^{1}J (^{13}C1-^{1}H1) of carbenes **39b-c** relative to carbenoids **37b-c**, contrary to what is expected base on the s-character of the carbon orbital involved in the C1–H1 bonds (Table 1). However, these unexpected results can be understood considering that C1 is bounded to an electronegative substituent in complexes **37b-c**. DFT calculations for **37a-e** and **39a-e** complexes at the B3LYP-D3/6-31G(d,p) + SDD(Au) level of theory led to computed ^{1}H NMR, ^{13}C NMR chemical shifts for H1, C1 and ^{1}J (^{1}H1-^{13}C1) constants consistent with the experimental results (Table 1).

Table 1. Selected computed and experimental NMR data for structures **39a-e**.

Entry[a]	Complex	Method	H1 (ppm)	C1 (ppm)	^{1}J (^{1}H1-^{13}C1) [Hz]
1	**39a**	Exp[b]	12.35 (4.92)	290.0 (69.7)[d]	-
		DFT[c]	12.12 (4.22)	280.8 (72.2)	125.2 (144.2)
2	**39b**	Exp[b]	12.67 (4.28)	287.9 (71.8)	129.8 (143.9)
		DFT[c]	12.17 (4.24)	280.2 (71.2)	124.4 (143.4)
3	**39c**	Exp[b]	12.32 (4.17)	290.0 (73.7)	127.8 (144.3)
		DFT[c]	12.09 (4.30	278.9 (75.4)	126.1 (144.6)
4	**39d**	Exp[b]	12.57 (4.24)	289.0 (71.4)[d]	-
		DFT[c]	12.03 (4.69)	274.6 (74.0)	125.6 (144.4)
5	**39e**	Exp[b]	11.74 (3.26)	284.6 (70.7)[d]	-
		DFT[c]	11.06 (-)	272.4 (-)	125.4 (-)

[a] Data for the corresponding carbenoid precursor given within parentheses. [b] -90 ºC in CD_2Cl_2. [c] Computed at 25 ºC in CH_2Cl_2. [d] 25 ºC in toluene-d_8.

Trapping of Gold(I) Carbenes with PPh_3

The thermal instability of mesityl gold(I) carbenes **39a-e** precluded their isolation. Therefore, to obtain structural confirmation, gold(I) carbenes **39b-c** were trapped by PPh_3 at -90 ºC affording phosphonium ylide complexes **40a-b** (Scheme 26), which were easily recognized by NMR due to characteristic signals with doublet of doublet multiplicity both for H1 (**40a** δ 3.67 ppm, **40b** δ 3.40 ppm) and C1 (**40a** δ 35.3 ppm, **40b** δ 35.5 ppm). Furthermore, gold(I) complexes **40a-b** were unambiguously characterized by X-ray diffraction (Figure 9). The trapping is irreversible as shown by heating samples of **40a-b** to 125 ºC in 1,1,2,2-tetrachloroethane-d_2. Complexes **40a-b** resemble the stable phosphonium ylide gold adducts previously used to detect aryl gold(I)

30 See experimental section for full NMR characterization for complexes **39a-e**.

carbenes in gas phase by the group of Chen.[24] The formation and full characterization of complex **40a-b** is a strong structural evidence of the metallocarbene nature of gold(I) complexes **39b-c**.

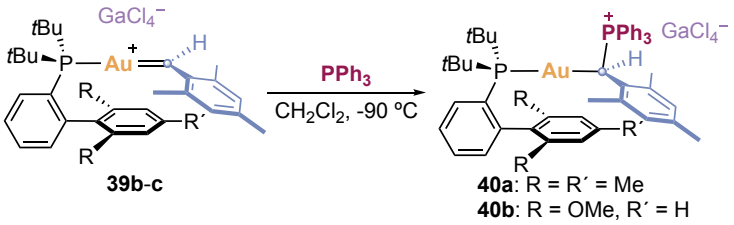

Scheme 26. Synthesis of phosphonium ylide **40a-b**.

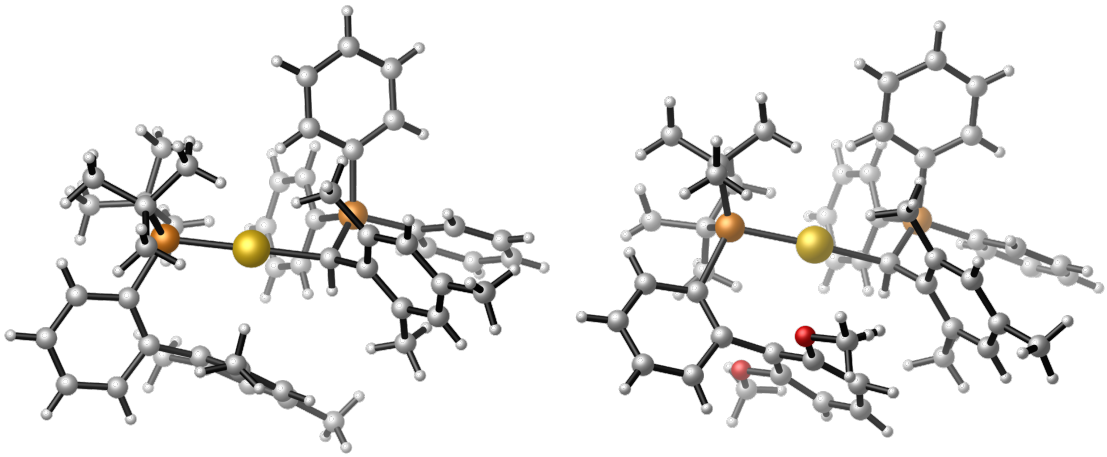

Figure 9. X-ray crystal structure of phosphonium ylide **40a** (left) and **40b** (right). $GaCl_4^-$ omitted for clarity.

Origins of Stability of Mesityl Gold(I) Carbenes

Structural analysis by DFT

To clarify the stabilizing contributions, calculations were performed at the B3LYP-D3/6-31G(d,p) + SDD(Au) level of theory representing CH_2Cl_2 with the PCM. The optimized geometries for gold(I) carbenes **39a-e** are shown in Figure 10 and the most relevant structural information is collected in Table 2. The computed Au–C1 (2.026-2.035 Å) bond distances are slightly shorter than those for carbenoid precursors **37a-e**, Au–C1 (2.095-2.098 Å) (Table 2, entry 2). In all the optimized structures, the mesitylidene fragment lays in horizontal to the lower ring of the biaryl ligand plane. Noteworthy, the mesityl ring is nearly co-planar with the carbene center (Table 2, entry 6) and the C1–C2 (1.399-1.401 Å) (Table 2, entry 4) bonds are considerable contracted compared to those for carbenoid precursor **37a-e** (C1–C2: 1.448-1.500 Å). All in all, these results indicate that the π-system of the aromatic ring participates in the stabilization of the carbene species. Overall, the computed structures are very similar for all the mesityl gold(I) carbenes that have been spectroscopically characterized (**39a-e**) (Figure 10, Table 2).

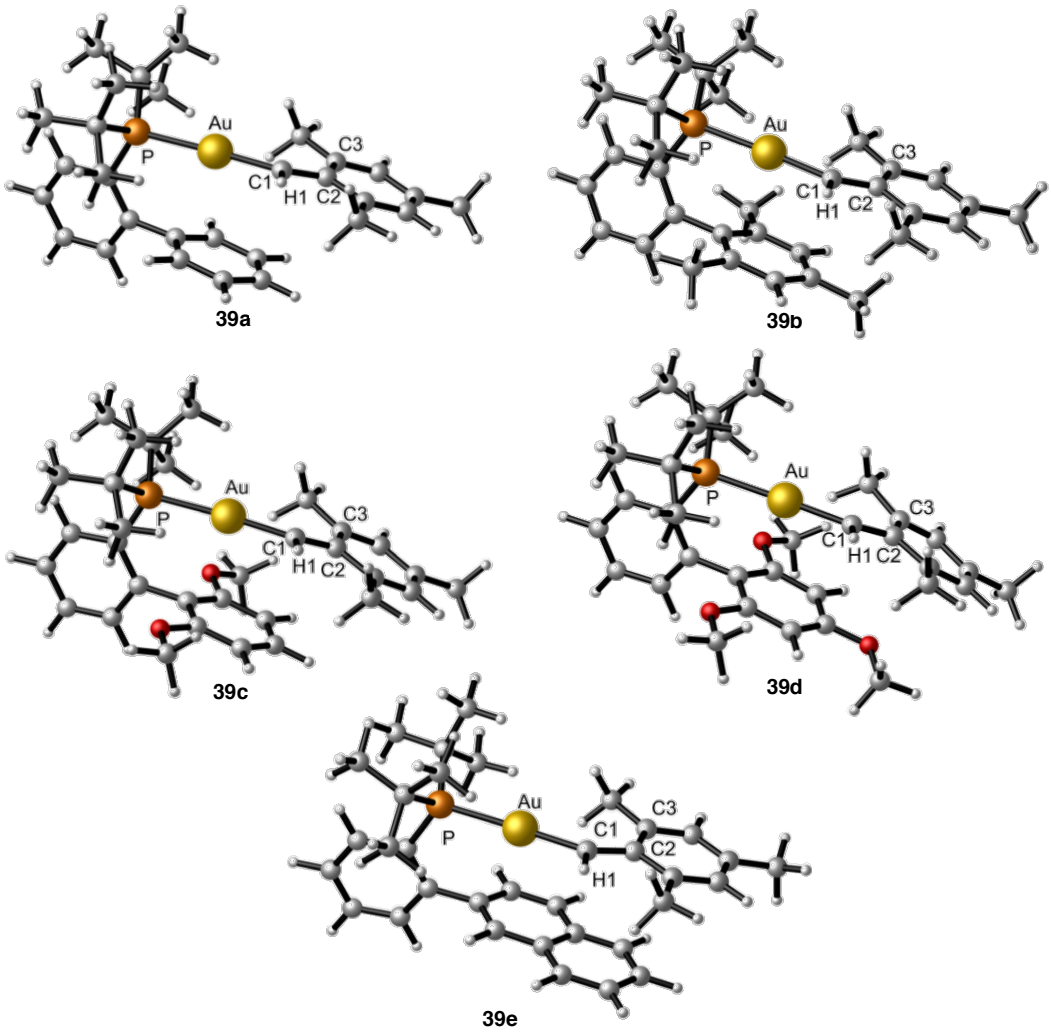

Figure 10. Optimized structures of gold(I) carbenes **39a-e**.

Table 2. Selected computed structural data for structure **39a-e**. Data for the corresponding carbenoid precursor given within parentheses.

Entry	Computed Data	**39a**	**39b**	**39c**	**39d**	**39e**
1	P–Au (Å)	2.384 (2.371)	2.380 (2.366)	2.381 (2.369)	2.382 (2.371)	2.389 (2.378)
2	Au–C1 (Å)	2.030 (2.095)	2.031 (2.095)	2.026 (2.095)	2.027 (2.097)	2.035 (2.098)
3	C1–H1 (Å)	1.091 (1.086)	1.091 (1.085)	1.091 (1.085)	1.091 (1.085)	1.091(1.086)
4	C1–C2 (Å)	1.400 (1.500)	1.400 (1.498)	1.401 (1.498)	1.400 (1.498)	1.399 (1.499)
5	P–Au–C1 (º)	176.6 (176.1)	175.9 (175.1)	176.5 (178.1)	176.2 (178.0)	174.5 (176.0)
6	Au–C1–C2-C3 (º)	11.8 (68.4)	7.7 (71.3)	16.9 (69.6)	14.7 (67.9)	6.0 (68.4)

[a]Computed at the B3LYP-D3/6-31G(d,p) + SDD(Au) level of theory. CH_2Cl_2 represented with PCM.

Non-covalent interactions analysis: ligand stabilization

In solution, complexes **39b-e**, which bear substituted JohnPhos-type ligands, are slightly more stable than **39a**, which carries only JohnPhos (Scheme 25). Therefore, we wondered if non-covalent interaction could be involved in the partial stabilization introduced by ligand

modification. To study non-covalent interactions, we performed a NCIplot analysis which allows simultaneous mapping and visualization of non-covalent interactions as real-space surfaces requiring only molecular geometry information.[31] For simplicity, only the NCIplots for structure **39a** and **39b** will be shown and compared here (Figure 11).[32] Besides the common positive interactions seen in both structures, the NCIplot of **39b** shows stabilizing interactions between the methyl substituents of the ligand and the mesitylidene moiety (green arrows) and also between substituted biaryl rings and *t*Bu substituents on P (red arrows) (Figure 11, right). Similar extra positive interactions were also observed for the substituents in the biaryl ring for complexes **39c,d,e**. This may suggest that steric attractions govern the partial stability introduced by ligand modification.

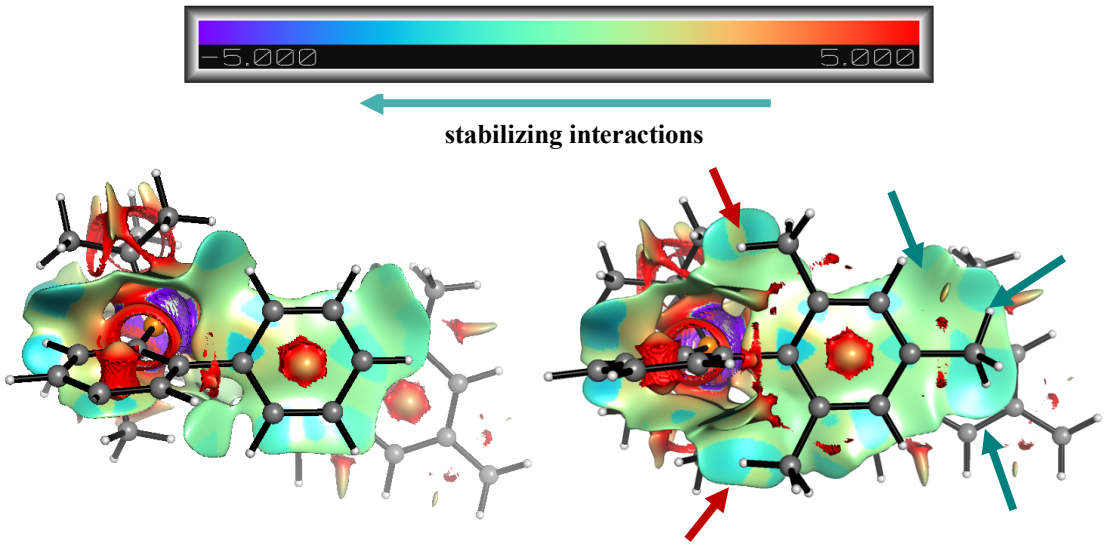

Figure 11. NCIPlots for structures **39a** (left) and **39b** (right). Biaryl moiety of the JohnPhos-type ligand showed in front.

Comparative studies: mesityl stabilization

To further understand the stabilizing ability of the mesityl moiety, we carried out comparative studies tuning the substituents in the aryl group. To do so, gold(I) carbene models with different carbene fragments and the same JohnPhos-type ancillary ligand as **39c** were studied computationally (Figure 12). In particular, we optimized structures bearing highly electron deficient (CF_3, **39c-CF_3**) or electron donating (MeO, **39c-MeO**) substituents in the aryl group (Figure 13).

31 (a) Johnson, E. R.; Keinan, S.; Mori-Sánchez, P.; Contreras-García, J.; Cohen, A. J.; Yang, W. *J. Am. Chem. Soc.* **2010**, *132*, 6498–6506. (b) Contreras-García, J.; Johnson, E. R.; Keinan, S.; Chaudret, R.; Piquemal, J.-P.; Beratan, D. N.; Yang, W. *J. Chem. Theory Comput.* **2011**, *7*, 625–632.

32 See experimental section for further NCIPlots for structures **39a-e**.

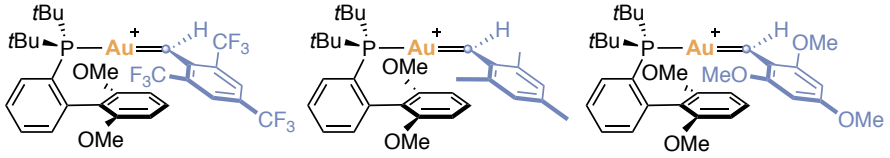

Figure 12. *In silico* optimized gold(I) carbenes tuning the substituents in the aryl moiety.

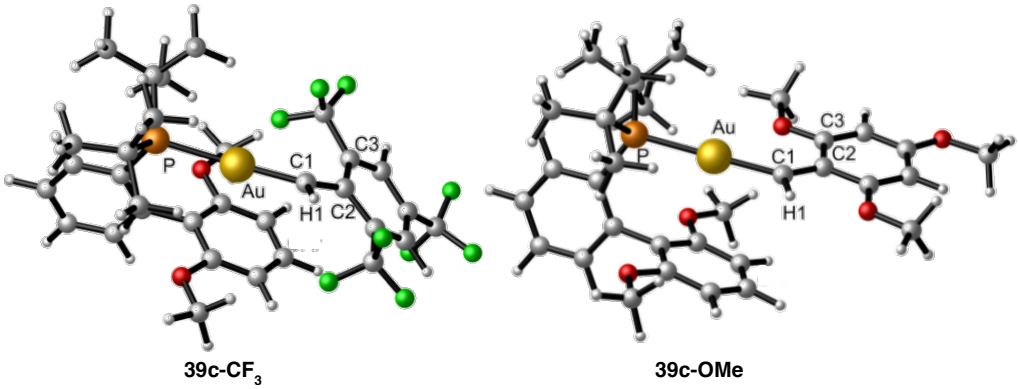

Figure 13. Optimized structures of gold(I) carbenes **39c-CF$_3$** and **39c-MeO**.

Table 3. Selected computed structural data for structure **39c**, **39c-CF$_3$** and **39c-OMe**.

Entry	Computed Data[a]	**39c-CF$_3$**	**39c**	**39c-OMe**
1	P–Au (Å)	2.384	2.381	2.378
2	Au–C1 (Å)	1.996	2.026	2.033
3	C1–H1 (Å)	1.089	1.091	1.091
4	C1–C2 (Å)	1.435	1.401	1.384
5	P–Au–C1 (º)	172.4	176.5	178.5
6	Au–C1–C2–C3 (º)	35.5	16.9	1.8

[a]Computed at the B3LYP-D3/6-31G(d,p) + SDD(Au) level of theory. CH_2Cl_2 represented with PCM.

The optimized geometries of gold(I) carbene models **39c-CF$_3$** and **39c-OMe** are shown in Figure 13. The most relevant structural information of the computed models is collected in Table 3. Clear trends can be observed depending on the electronics properties of the carbene substituents. For aryl gold(I) carbenes, as the aryl becomes more electron-rich, the Au–C1 bonds become longer (**39c-CF$_3$**: 1.996 Å, **39c**: 2.026 Å and **39c-OMe**: 2.033 Å, Table 3, entry 2), the C1–C2 bond length is reduced (**39c-CF$_3$**: 1.435 Å, **39c**: 1.401 Å and **39c-OMe**: 1.384 Å, Table 3, entry 4) and the more coplanar the aryl ring is with respect to the carbene center (Table 3, entry 6). Therefore, the analysis of the aforementioned structures indicates that more electron rich aryls lead to more stable carbenes.

Bonding situation

After studying the optimized structures of the aryl gold(I) carbenes in detail, we decided to analyze in depth the bonding situation to the gold(I) carbenes.

Frontier orbitals

Initially, we studied the frontier orbitals. For complex **39c**, HOMO orbital corresponds to bonding interactions between the filled d_{yz}(Au) and $2p^{\pi}$-system of the lower ring of the biaryl fragment of the ligand (Figure 14, left). It is well-known that the reactivity of electrophilic gold(I) carbenes is dominated by LUMO orbital,[21] which in the case of **39c** corresponds to the antibonding interaction of the occupied d_{xz}(Au) orbital at gold and the $2p^{\pi}$-system of the carbene ligand (Figure 14, right). The aforementioned antibonding overlap between the occupied d_{xz}(Au) orbital at gold and the $2p_y$(C1) is a sign of the existence of some extent of gold-to-carbon π-backdonation.

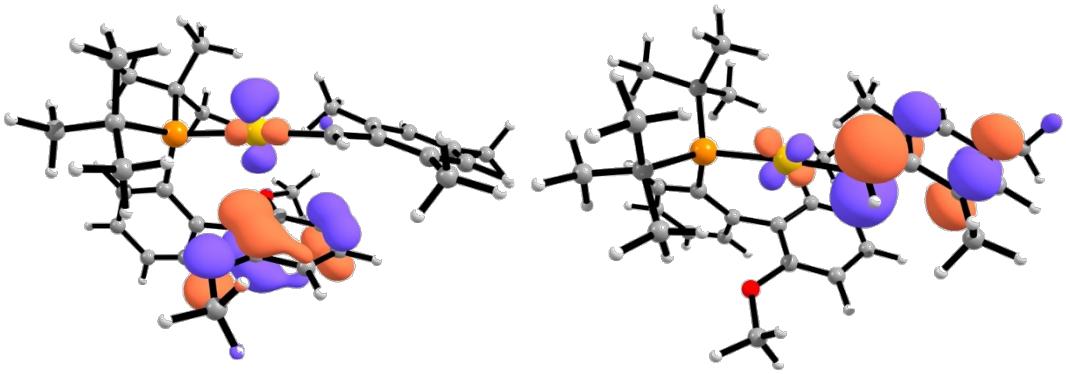

Figure 14. HOMO (left) and LUMO (right) of structure **39c**.

For structures **39c-CF$_3$** and **39c-MeO**, the HOMO and LUMO orbitals are similarly distributed within the molecules as for **39c**.[33] Interestingly, a clear tendency can be seen in the energy of these orbitals (Table 4). As said, the reactivity of gold(I) carbenes is dominated by LUMO orbitals and the obtained data confirmed that the less electron rich the aryl is the lower the LUMO stands and thus, the better electrophile they will be against a common nucleophile (HOMO: **39c-CF$_3$**: -4.41 eV, **39c** = -3.50 eV and **39c-OMe** = -2.98 eV). Furthermore, a larger HOMO-LUMO energy gap is related to higher kinetic stability and lower chemical reactivity. Accordingly, here, the more electron rich the aryl is, the more stable the aryl gold(I) carbene would be (HOMO-LUMO gap: **39c-CF$_3$**: 1.79 eV, **39c** = 2.56 eV and **39c-OMe** = -3.0 eV). Thus, these results underline the stabilization provided by electron rich aryl fragments to the aryl gold(I) carbenes.

33 Plots for the HOMO and LUMO orbitals of aryl gold(I) carbenes **39c-CF$_3$** and **39c-OMe** can be found in the experimental section.

Table 4. Energy of the HOMO and LUMO orbitals.

Structure	HOMO (eV)	LUMO (eV)	Gap (eV)
39c-CF_3	-6.20	-4.41	1.79
39c	-6.06	-3.50	2.56
39c-MeO	-5.98	-2.98	3.00

Natural bond orbital analysis

Recently, Natural Bond Orbital (NBO) analysis has been successfully applied by Bourissou and co-workers to shed light into the bonding situation of gold(I) carbenes.[19,21] The use of this method would also provide useful information in our studies on aryl gold(I) carbenes. Before explaining in detail our results, we will provide a concise description of the theoretical grounds of NBO analysis.

NBO analysis is based on Natural Orbitals (NO), which are used in computational chemistry to calculate the distribution of electron density in atoms and in bonds between atoms. NBO analysis is composed by the calculation of a sequence of different natural localized orbitals that include Natural Atomic Orbitals (NAO), Natural Hybrid Orbitals (NHO), Natural Bond Orbitals (NBO) and Natural Localized Molecular Orbitals (NLMO) (Figure 15).

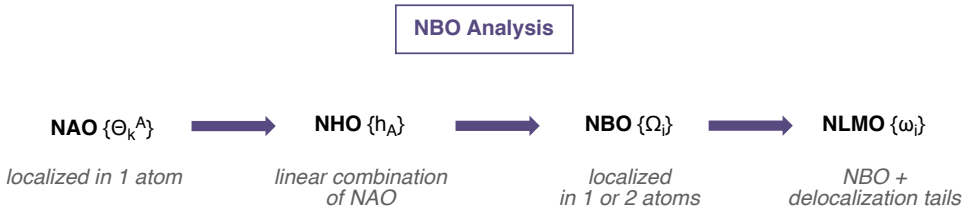

Figure 15. Schematic vision of NBO analysis.

Specifically:

Natural Atomic Orbitals (NAOs) $\{\Theta_k^A\}$ are orbitals localized in one atom and can be described as the effective "natural orbitals of an atom" in the molecular environment.

Natural Hybrid Orbitals (NHOs) $\{h_A\}$ are optimized linear combinations of NAOs for an atom (Equation 1).

$$h_A = \sum_K a_K \Theta_K^A$$

Equation 1. Mathematical definition of NHO (h_A) being A the named atom. Where a: are polarization coefficients and Θ_k^A: NAOs.

Natural Bond Orbitals (NBOs) $\{\Omega_i\}$ are orbitals localized in 1 or 2 atoms, occasionally more, that give the most accurate possible Lewis-like description of the total electron density. The NBOs are composed of NHOs (Equation 2).

$$\Omega_{AB} = a_A h_A + a_B h_B$$

$$\Omega^*_{AB} = a_A h_A - a_B h_B$$

Equation 2. Mathematical definitions of bond (Ω_{AB}, top) and antibond (Ω^*_{AB}, bottom) NBOs. Being A and B the two atoms involved in the NBOs. Where a: are polarization coefficients and h: NHOs.

Natural Localized Molecular Orbitals (NLMOs) $\{\omega_i\}$ are *semi*-localized orbitals that closely resemble a parent NBO $\{\Omega_i\}$, which is strictly localized, but captures the associated delocalization tails needed to describe the density of a full electron pair. Thereby, NLMOs adopt the characteristic bonding pattern of a localized Lewis structure enhancing a bridge between chemical intuition and molecular wave-functions. They can be expressed as combinations of NBOs (Equation 3).

$$\omega_i = \eta\left[\Omega_i + \sum_j \lambda_{i\rightarrow j}\Omega^*_j\right]$$

Equation 3. Mathematical definition of NLMO (ω_i). Where η: is a normalizing constant and $\lambda_{i\rightarrow j}$: are mixing coefficients that reflect the strength of $\Omega_i \rightarrow \Omega^*_j$ donor-acceptor interactions.

Bearing this in mind, we carried out NBO analysis to better understand the gold(I)-to-carbon π-backdonation and the stabilization provided by the π-system of the aryl in gold(I) carbenes **39c-CF_3**, **39c** and **39c-OMe**.

The NBO analysis for **39c** revealed two main electronic contributions involved in the π-orbital stabilization of the carbenic carbon (C1). First, a small π-backdonation with d_{xz}(Au) to $2p^{\pi}$(C1) donor-acceptor interaction (24.4 $kcalmol^{-1}$) and 3.7% contribution of $2p^{\pi}$(C1) in the corresponding NLMO (Figure 16, left), along with a lone pair at C2 ($2p^{\pi}$(C2)) highly polarized towards C1 (23.5% on $2p^{\pi}$(C1)) (Figure 16, right).

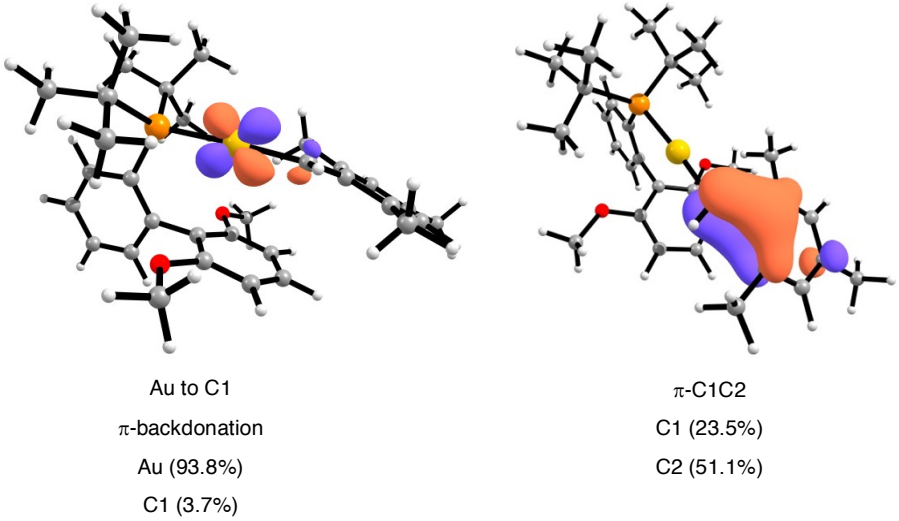

Figure 16. Plot for NLMO associated to π-backdonation from Au to C1 (left) and lone pair at C2 (right) for **39c**. Cutoff: 0.05.

NLMOs associated to π-backdonation were also identified for both models **39c-CF$_3$** (d_{xz}(Au) to $2p^{\pi}$(C1), 10.0% on $2p^{\pi}$(C1), 31.6 kcalmol^{-1}) (Figure 17) and **39c-MeO** (d_{xz}(Au) to $2p^{\pi}$(C1), 2.8% on $2p^{\pi}$(C1), 10.1 kcalmol^{-1}) (Figure 18, left). However, the polarized lone pair at C2 was absent for **39c-CF$_3$**, whereas a NLMO associated to a C1–C2 π-bond was located for **39c-MeO** (Figure 18, right).

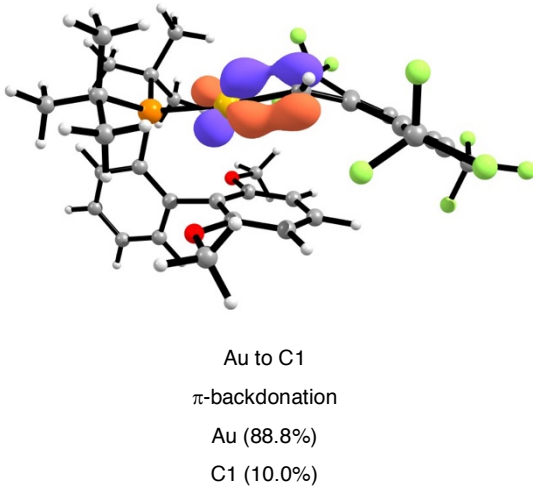

Figure 17. Plot for NLMO associated to π-backdonation from Au to C1 for **39c-CF$_3$**. Cutoff: 0.05.

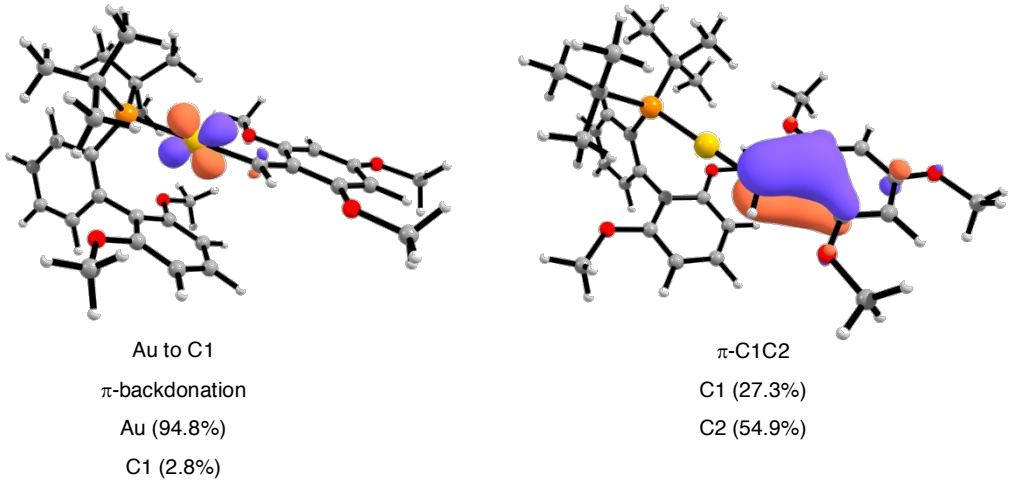

Figure 18. Plot for NLMO associated to π-backdonation from Au to C1 (left) and C1–C2 π-bond (right) for **39c-OMe**. Cutoff: 0.05.

The plots for NLMO associated to the main electronic contributions involved in the π-orbital stabilization of the carbenic carbon are represented in Figures 16, 17 and 18. In these plots, the orbital shapes are an intuitive way to depict the delocalization of the NLMOs. For NLMOs associated to π-backdonation, the delocalization over C1 is appreciably larger for **39c-CF$_3$** (10.0%) than **39c** (3.7%) and **39c-OMe** (2.8%). The corresponding plots visually represent this trend accurately.

Finally, the natural population analysis, which assesses the electron density distribution in a molecular system based on NAO, indicates an increase of the positive charge distribution over the arylidene ligand with the electron donor ability of the aryl substituents, which implies an increase in the arylidene to gold charge transfer (**39c-CF$_3$** (-0.33 e), **39c** (-0.09 e) and **39c-MeO** (-0.02 e)) (Table 5).

Table 5. Charge transfer from carbene to gold based on natural population analysis.

Entry	Natural Charge	**39c-CF$_3$**	**39c**	**39c-MeO**
1	Au	0.46	0.37	0.36
2	Arylidene	0.13	0.28	0.33
3	CT (Carbene to Au)	-0.33	-0.09	-0.02

Barrier to bond rotation

To corroborate the results obtained by NBO analysis, the π-bond character of Au–C1 and C1–C2 bonds was evaluated by calculating the rotational barrier around these bonds for **39c**, **39c-CF$_3$** and **39c-OMe** (Table 6). The activation energy for Au–C1 bond rotation (1.3-3.5 kcalmol^{-1}) did not differ significantly based on the electronics of the aryl and support the low Au–C1 π-backdonation found by NBO studies. On the other hand, the rotational barriers of C1–C2 bond

changed dramatically depending on the substituents. For structure **39c-CF$_3$**, the activation energy required for C1–C2 bond rotation (2.5 kcalmol^{-1}) correlates with the single bond character revealed by NBO analysis. For **39c**, the rotational barrier support a significant C1–C2 π-bond as observed by NBO analysis. Structure **39c-OMe** is an extreme case in which the double bond character of C1–C2 is even stronger due to the stabilization provided by the methoxy substituents.

Table 6. Calculated rotational barriers for Au–C1 and C1–C2 bonds.

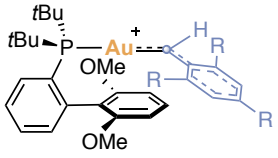

39-CF$_3$: R = CF$_3$
39: R = CH$_3$
39-OMe: R = OMe

Entry	Structure	$\Delta G^{\ddagger}_{Au-C1}$ (kcalmol^{-1})[a]	$\Delta G^{\ddagger}_{C1-C2}$ (kcalmol^{-1})[a]
1	**39c-CF$_3$**	3.5	2.5
2	**39c**	1.3	18.6
3	**39c-MeO**	2.5	32.1

[a] Free energies in solution referred to the lowest energy isomer of gold(I) carbenes.

Full picture for the origin of the stabilization

As outlined above, we applied a set of computational studies to understand the origin of the stabilization of these aryl gold(I) carbenes. The main conclusions of this study are:

- The C1–C2 bond distances are slightly shortened compared to the gold(I) carbenoid precursors.
- The mesityl group is coplanar to the plane formed by gold, C1 and C2.
- For **39c**, NBO analysis reveals two main electronic contributions involved in the π-orbital stabilization of C1. First, a small π-backdonation from gold-to-carbon along with a lone pair at C2 highly polarized towards C1. Furthermore, the positive charge of the molecule is equally distributed over gold and the carbene fragment (CT = -0.07 e$^-$).
- For **39c**, the calculated energy barriers to Au–C1 ($\Delta G^{\ddagger}$ = 1.3 kcalmol^{-1}) and C1–C2 ($\Delta G^{\ddagger}$ = 18.6 kcalmol^{-1}) bond rotation support a low Au–C1 bond π-character and a significant C1–C2 π-bond.
- More electron rich aryls stabilize gold(I) carbenes.
- There is a partial stabilization introduced by the ligand due to non-covalent interactions.

Therefore, these results are consistent with a predominant stabilization resulting from the donation of the π-system of the mesityl group to the electron deficient carbenic carbon. On the other hand, the existence of a low gold-to-carbon π-backdonation was also identified. All in all,

we conclude that the tertiary benzyl carbocation resonance form dominates the structure of gold(I) carbenes **39a-e** (Figure 19). The bonding analysis of these gold(I) carbenes reinforces the previously observation that stabilization by the π-system of the organic fragment is determinant for their characterization.

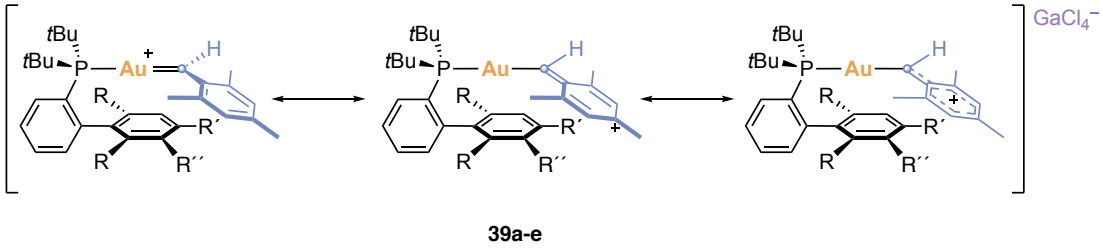

39a-e

Figure 19. Main resonance forms of gold(I) carbenes **39a-e**.

Thermal Instability: Bimolecular Coupling

The stabilization from the mesityl group allowed the spectroscopic characterization of gold(I) carbenes **39a-e** at -90 ºC under inert conditions. Detection of these complexes was also possible due to the absence of any nucleophile during their generation from gold(I) carbenoids **37a-e**. However, complexes **39a-e** were found to be highly thermally unstable.

Table 7. Alkene and cyclopropane formation.[a]

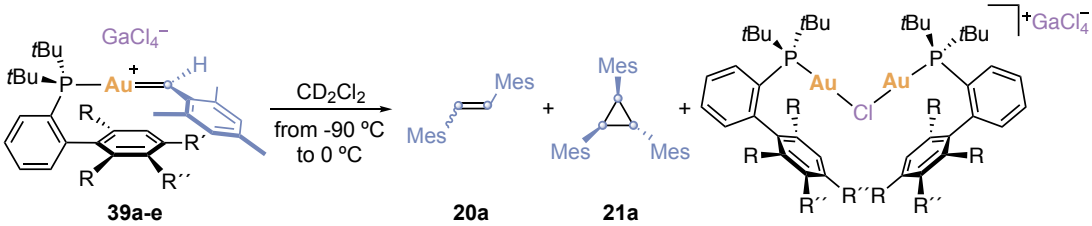

39a-e **20a** **21a** **41a-e**

Entry	Complex	T (ºC)[b]	**20a** (%)[b]	*E*/*Z* ratio	**21a** (%)[c]
1	**39a**	-10	25	12:1	36
2	**39b**	-20	68	> 60:1	< 1
3	**39c**	-10	27	9:1	39
4	**39d**	-30	62	> 60:1	< 1
5	**39e**	0	7	> 60:1	83

[a] Mes = 2,4,6-trimethylphenyl. [b] Temperature at which gold(I) carbene fully decomposed. [c] ^{1}H NMR yield calculated using 1,3,5-tris(trifluoromethyl)benzene as internal standard.

To have a better understanding of the thermal instability of mesityl gold(I) carbenes, solutions of **39a-e** in CD_2Cl_2 were warmed up from -90 ºC to their corresponding decomposition temperatures (-30 to 0 ºC) (Table 7). The analysis of the recorded spectra revealed the formation of *E*-1,2-dimesitylethene (*E*-**20a**), *Z*-1,2-dimesitylethene (*Z*-**20a**) and 1,2,3-trimesitylcyclopropane (**21a**)

in different ratios depending on the specific carbenes. As inorganic species, chloride-bridged digold(I) complexes (**41a-e**) were detected in all the experiments (Table 7).

A closer analysis of the consumption with temperature of gold(I) carbene **39c** shows that *E*-**20b** was initially formed between -70 and -40 ºC. Then, around -40 ºC, small amounts of *Z*-**20b** were also detected together with cyclopropane **21b**, which was formed through cyclopropanation of the previously generated alkenes (Figure 20). However, the distribution of organic products was highly dependent on temperature and on gold(I) carbene complex.

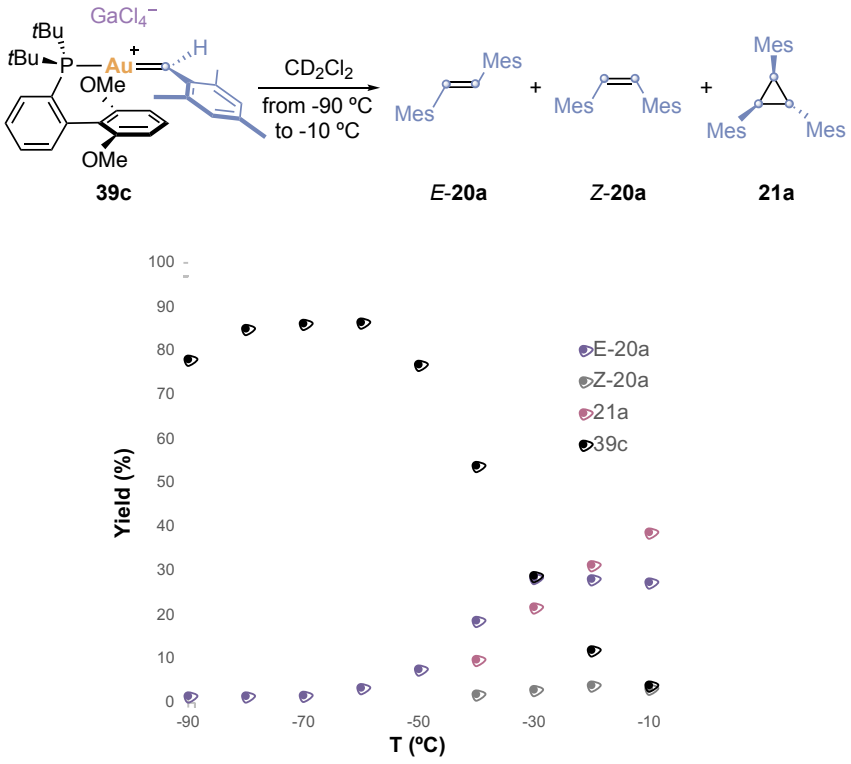

Figure 20. Temperature decay of gold(I) carbene **39c**.

Remarkably, when gold(I) carbenoids **37a-d** were activated with $GaCl_3$ at 0 ºC, alkene *E*-**20a** was immediately observed by NMR preventing the full characterization of mesityl gold(I) carbenes **39a-d** at this temperature (Scheme 27). All the results outlined here suggest that, under inert conditions and absence of nucleophiles, the formation of *E*-**20a** is the main cause to the thermal instability of aryl gold(I) carbenes **39a-e**. This decomposition pathway mirrors the formation of ethylene from chloro(methyl)gold(I) carbenoids explained in Chapter II, which was found to be first order in carbenoid contrary to what would have been expected for a dimerization of two carbene units. The unusual reaction order was explained by the rate-determining formation of a neutral gold(I) carbene that further reacts with another molecule of gold(I) carbenoid. However, in this case, the formation of alkene *E*-**20a** takes place directly from well-characterized gold(I) carbenes complexes at low temperatures and therefore, the mechanism could now involve the

direct dimerization of two gold(I) carbene complexes. Therefore, to clarify the mechanism of formation of *E*-**20a** we performed both kinetics and DFTs studies.

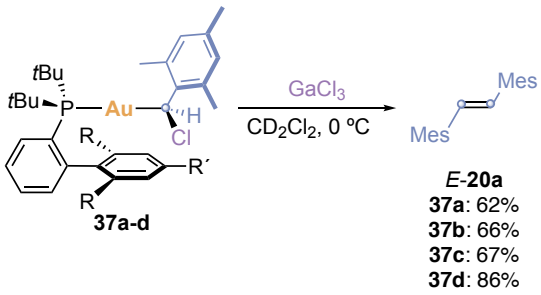

Scheme 27. Reaction of gold(I) carbenoids **37a-d** with $GaCl_3$ at 0 ºC.

Kinetics studies

In this case, finding a proper system to perform kinetic studies was not trivial because gold(I) carbenes were involved in several transformations at the same time. Furthermore, the initial consumption of gold(I) carbenes was very fast, which forced us to discard the initial-rate method used in Chapter I to calculate the kinetic order of gold(I) carbenes. After an extensive screening of reaction conditions, we finally found out that gold(I) carbene **39b** was consumed at -40ºC in approximately 6 hours leading to *E*-**20a**, traces of *Z*-**20a** and cyclopropane **21a** (Figure 21).

To accurately analyze these data, we needed to be sure that there was no competition between the cyclopropanation of *E*- and *Z*-**20a** under these conditions. To this end, we examined theoretically the reaction pathways for the cyclopropanation of *Z*-**20a** and *E*-**20a** by gold carbene **39b**. These reactions proceed by an asynchronous concerted mechanism with an activation barrier for *E*-**20a** ($\Delta G^{\ddagger}$ = 12.7 kcalmol^{-1}) lower than for *Z*-**20a** ($\Delta G^{\ddagger}$ = 21.2 kcalmol^{-1}).[34] Considering $\Delta\Delta G^{\ddagger}_{E\text{-}Z}$ = 8.5 calmol^{-1}, we assumed that cyclopropane **21a** is only being formed *via* cyclopropanation of *E*-**20a** at -40 ºC. Based on this assumption, the amount of **39b** related to the formation of *E*-**20a** (mmol $\mathbf{39b}_{E\text{-}\mathbf{20a}}$) at any time were calculated using Equation 4.

$$mmol\ \mathbf{39b}_{E-\mathbf{20a}} = mmol\ \mathbf{39b}_{remaining} + (2 * mmol\ Z\mathbf{20a}) + mmol\ \mathbf{21a}$$

Equation 4. Where mmol $\mathbf{39b}_{E\text{-}\mathbf{20a}}$ = mmol $\mathbf{39b}_{\mathbf{initial}}$ - mmol **39b** consumed to form *E*-**20a** at time t, mmol $\mathbf{39b}_{\mathbf{remaining}}$ = mmol **39b** remaining at time t, mmol *Z*-**20a** = mmol of *Z*-**20a** formed at time t and mmol **21a** = mmol of cyclopropane **21a** at time t.

34 Full energy profile for cyclopropanation reactions can be found in the experimental section.

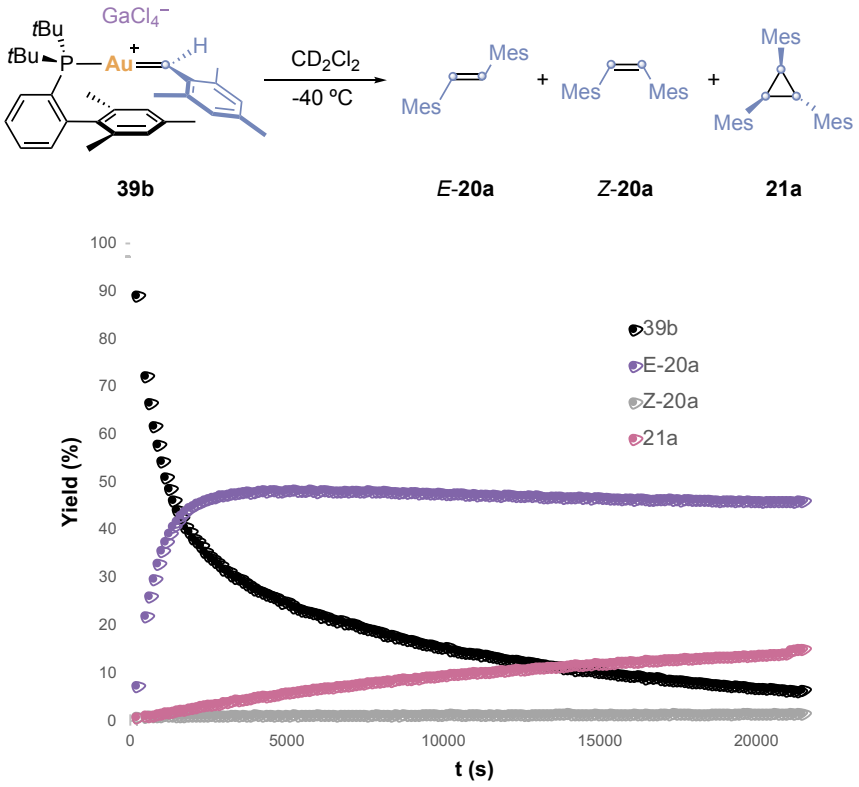

Figure 21. ^{1}H NMR monitoring of gold(I) carbene **39b** consumption at -40 ºC to generate *E*-**20a**, *Z*-**20a** and **21a**.

With these data in hand, we applied the integral method to determine the kinetic order with respect to the gold(I) carbene **39b** for the formation of *E*-**20a**. The integral method is based on fitting the experimental data to the integration of the rate law for different orders. For the formation of symmetrical alkene *E*-**20a**, the integrated equations for first (Equation 5) and second orders (Equation 6) are shown below:

$$\mathbf{ln[39b}_{\boldsymbol{E-20a}}\mathbf{]}_t = -\boldsymbol{k}\mathbf{t} + \mathbf{ln[39b]}_0$$

Equation 5. Integrated order law for first order reaction.

$$\frac{\mathbf{1}}{\mathbf{[39b}_{\boldsymbol{E-20a}}\mathbf{]}_t} = \frac{\mathbf{1}}{\mathbf{[39b]}_0} + \boldsymbol{k}\mathbf{t}$$

Equation 6. Integrated order law for second order reaction.

We next plotted the reaction rate data in terms of concentration of **39b**$_{E\text{-}20a}$ *vs.*time following the integrated equations for first (Equation 5, Figure 22) and second order reactions (Equation 6, Figure 23). The experimental data fall on a straight line for Equation 6 (Figure 22). Therefore, under the employed conditions, the formation of *E*-**20a** follows a second order regime in complex **39b**, consistent with a rate-limiting bimolecular coupling of two carbene complexes as the slowest step for the generation of *E*-**20a**. The rate equation of the formation of *E*-**20a** is shown in Equation 7.

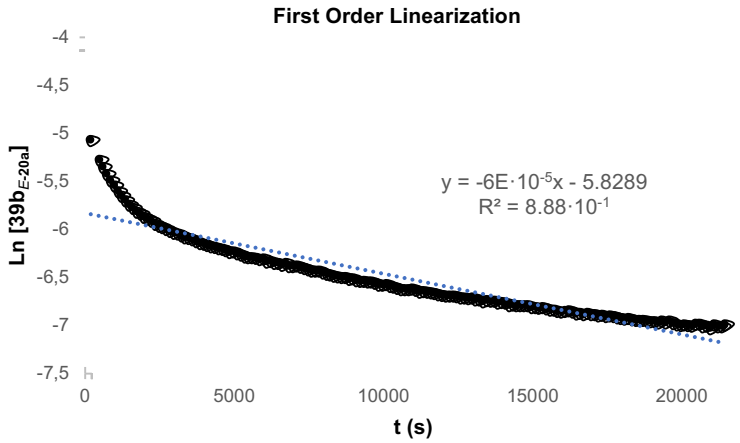

Figure 22. First order linearization plot for the consumption of gold(I) carbene **39b** in the formation of *E*-**2b** at -40 ºC.

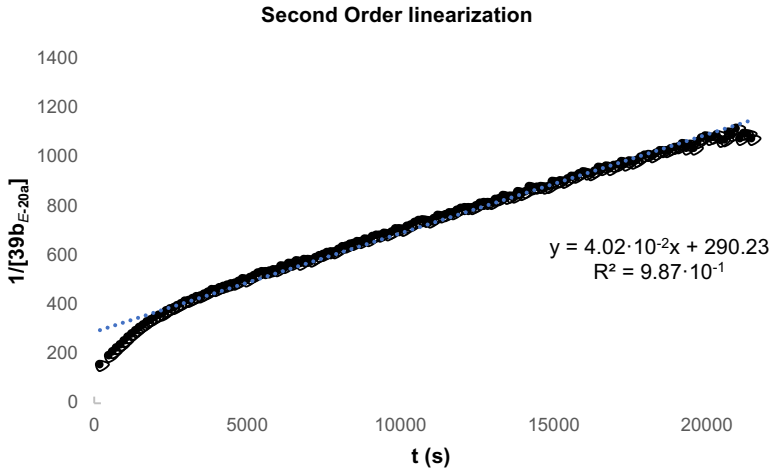

Figure 23. Second order linearization plot for the consumption of gold(I) carbene **39b** in the formation of *E*-**2b** at -40 ºC.

$$rate = k_{obs}[\mathbf{39b}_{E-\mathbf{20a}}]^2$$

Equation 7. Calculated rate law for the formation of *E*-**20a** at -40 ºC.

It is important to note that related bimolecular couplings to form symmetrical alkenes have been observed as common decomposition pathways for rhenium methylidenes [(η^5-C_5H_5)Re(NO)(PPh_3)(CH_2)]PF_6,[35] [Cp_2ReCH_2]BAr_4^F,[36] ruthenium alkylidene

35 (a) J. H. Merrifield, G. Y. Lin, W. A. Kiel, J. A. Gladysz, *J. Am. Chem. Soc.* **1983**, *105*, 5811–5819. (b) Roger, C.; Bodner, G. S.; Hatton, W. G.; Gladysz, J. A. *Organometallics* **1991**, 10, 3266–3274.

36 D. M. Heinekey, C. E. Radzewich, *Organometallics* **1998**, *17*, 51–58.

[(H$_2$IMes)RuCl$_2$(py)$_2$(CHPh)][37] and other ruthenium carbenes,[38] as well as typical Fischer[39] and Schrock carbenes such as [Cp$_2$Ta(CH$_2$)(CH$_3$)].[40]

DFT studies

To get a deeper insight into the mechanism of this rate-limiting bimolecular coupling, we performed DFT calculations with complex **39b** (Scheme 28).

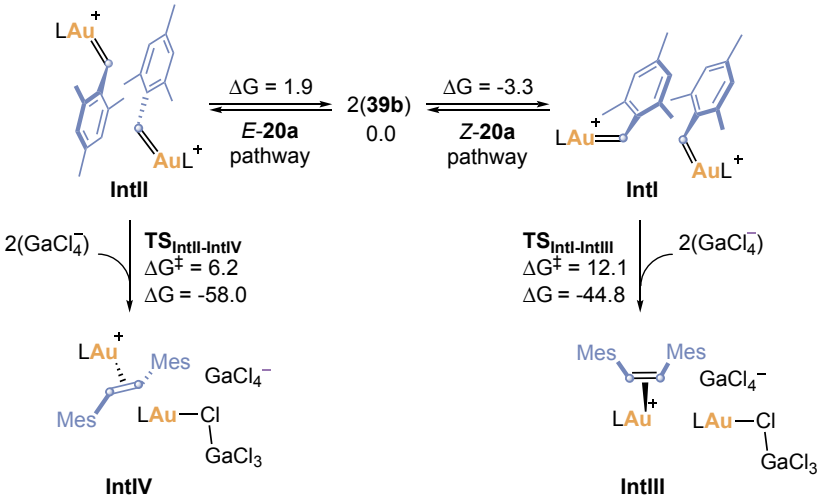

Scheme 28. Calculated reaction profile for the bimolecular coupling of gold(I) carbene **39b**. L = 2-Di-*tert*-butylphosphino-2′,4′,6′-trimethylbiphenyl. Free energies in kcalmol^{-1}.

Kinetics results point towards the coupling of two carbene complexes as the pathway for alkene formation. The prediction and characterization of bimetallic structures for similar transformations suggest the importance of dimers in these processes.[35-40] Indeed, our calculations suggest that association complex **IntI**, which is stabilized by face-to-face π-π interactions between the two mesitylidene fragments, as revealed by NCIPlot analysis (Figure 23), is preferentially formed (ΔG = -3.3 kcalmol^{-1}) (Scheme 28). **IntI** shows a relatively short C1–C1 distance (3.13 Å) and can evolve through **TS$_{\text{IntI-IntIII}}$** (ΔG‡ = 12.1 kcalmol^{-1}) to form (η^2-*Z*-**20a**)gold(I) complex (**IntIII**) in a highly exothermic process (ΔG = -44.8 kcalmol^{-1}). Alternatively, less stable association complex **IntII** (ΔG = 1.9 kcalmol^{-1}) (Scheme 28), with the optimal orientation of the mesitylidenes for *trans*-C1-C1 bond formation, can evolve *via* **TS$_{\text{IntII-IV}}$** (ΔG‡ = 6.2 kcalmol^{-1}) to

37 G. A. Bailey, M. Foscato, C. S. Higman, C. S. Day, V. R. Jensen, D. E. Fogg, *J. Am. Chem. Soc.* **2018**, *140*, 6931–6944.

38 E. Graban, F. R. Lemke, *Organometallics* **2002**, *21*, 3823–3826.

39 (a) C. P. Casey, R. L. Anderson, *J. Chem. Soc., Chem. Commun.* **1975**, 895–896. (b) C. Masters, C. Van der Woude, J. A. Van Doorn, *J. Am. Chem. Soc.* **1979**, *101*, 1633–1634.

40 (a) R. R. Schrock, P. R. Sharp, *J. Am. Chem. Soc.* **1978**, *100*, 2389–2399. (b) D. H. Berry, T. S. Koloski, P. J. Carroll, *Organometallics* **1990**, *9*, 2952–2962. (c) R. R. Schrock, C. Copeŕet, *Organometallics* **2017**, 36, 1884−1892.

form (η^2-*E*-**20a**)gold(I) complex (**IntIII**) in a similarly highly exothermic process (ΔG = -58.0 kcalmol^{-1}).

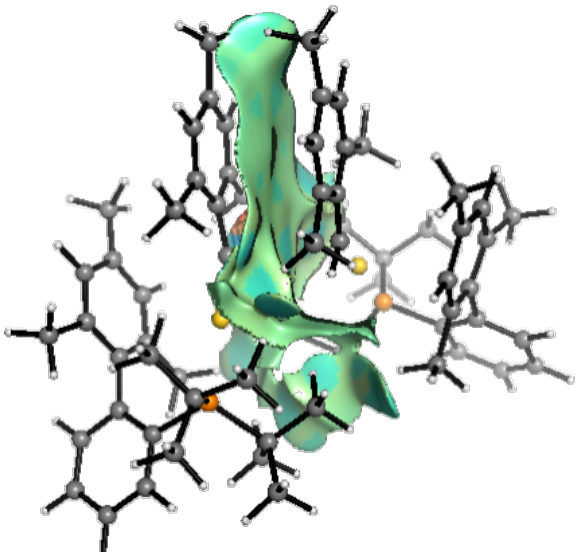

Figure 23. NCIPlot for **IntI**.

Transition states $\mathbf{TS_{IntII\text{-}IV}}$ and $\mathbf{TS_{IntI\text{-}IntIII}}$ can be considered early transition states that, according to the Hammond postulate, are characteristic of rapid exothermic reactions as the one described here (Figure 24).

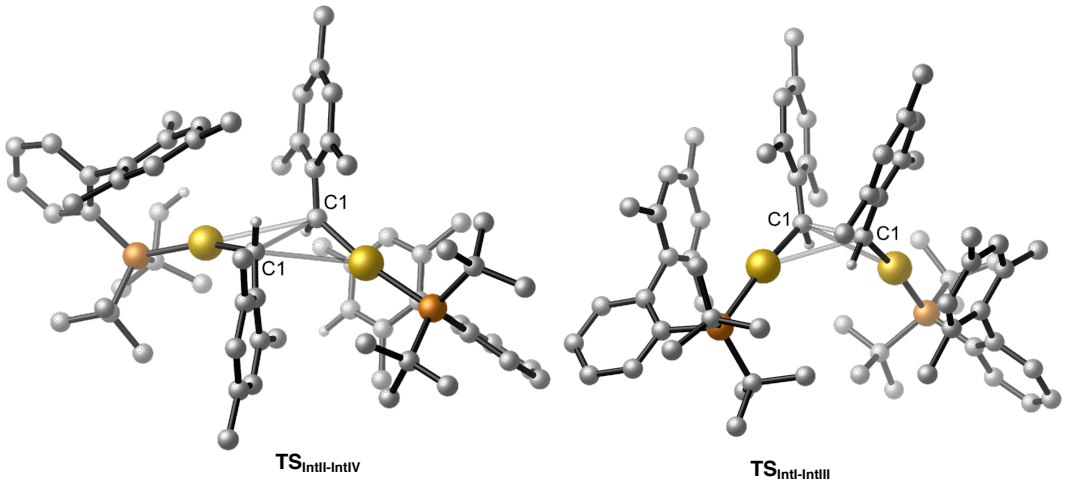

Figure 24. Plot for the $\mathbf{TS_{IntII\text{-}IntIV}}$ (left) and $\mathbf{TS_{IntI\text{-}IntIII}}$ (right), all the hydrogens but carbene hydrogens (H1) omitted for clarity.

At -35 ºC, assuming that the system is under Curtin-Hammett control, the calculated *E*/*Z*-**20a** ratio ($\Delta\Delta G^{\ddagger}$= 0.6 kcalmol^{-1}, 3.8:1 *E*/*Z*) is in agreement with the experimental results (3.7:1 *E*/*Z*) (Scheme 29). Related mechanisms have been proposed for the formation of alkenes from rhenium[36] and ruthenium[37] carbenes.

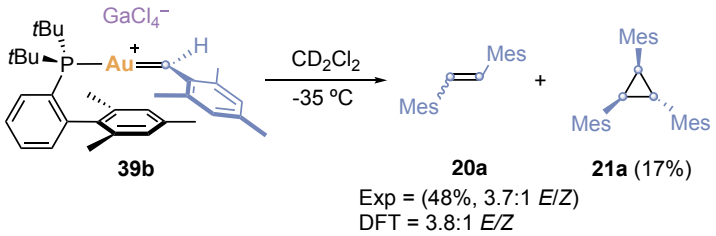

Scheme 29. Decay of gold(I) carbene **39b** at -35 ºC. Mes = 2,4,6-trimethylphenyl.

Gold(I)-Promoted Oxidation

In the previous dimerization studies, small amounts of 2,4,6-trimesitylbenzaldehyde (**42**) were detected resulting presumably from the oxidation of gold(I) carbenes by traces of oxygen.[41] To probe our hypothesis, we bubbled oxygen through solutions of gold(I) carbenes **39a-d** at -90 ºC and we observed instantaneous consumption of the carbenes to form aldehyde **42** and small amounts of *E*-**20a** (Scheme 30, right). Very fast oxygen atom transfer also took place by treating gold(I) carbenes **39a-d** with pyridine *N*-oxide at -90 ºC (Scheme 30, left). The reaction proceeds through nucleophilic attack to the carbenic carbon C1 forming 2,4,6-trimesitylbenzaldehyde **42**, small amounts of *E*-**20a** and LAuCl as inorganic species. Similar reactivity was observed before for characterized gold(I) carbene **9** (Scheme 9).[17]

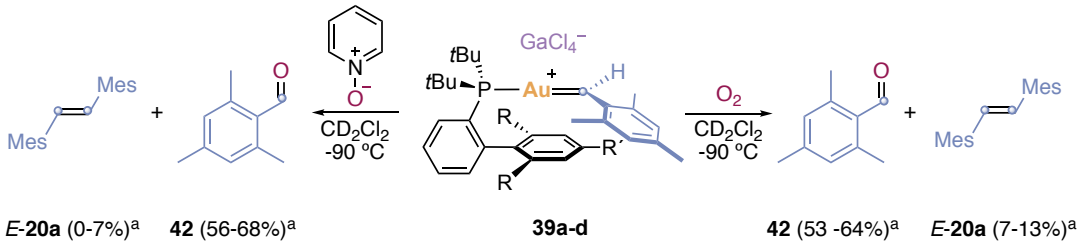

Scheme 30. Gold(I)-promoted oxygen transfer. [a] ^{1}H NMR yield using diphenylmethane as internal standard. Mes = 2,4,6-trimethylphenyl.

Gold(I)-Promoted Cyclopropanation of Alkenes

The competitive cyclopropanation observed in the formal dimerization of the carbene fragments hinted at the possibility of using gold(I) carbenes **39a-e** to cyclopropanate external alkenes. Therefore, mono-, di- and tri- substituted alkenes **20b-d** readily react at -90 ºC with gold(I) carbenes **39a-e** to form the corresponding cyclopropanes **21b-d** in very high to quantitative yields (Scheme 31, left).

41 Oxidation of gold(I) carbenes under air: H. Zhan, L. Zhao, J. Liao, N. Li, Q. Chen, S. Qiu, H. Cao, *Adv. Synth. Catal.* **2015**, *357*, 46–50.

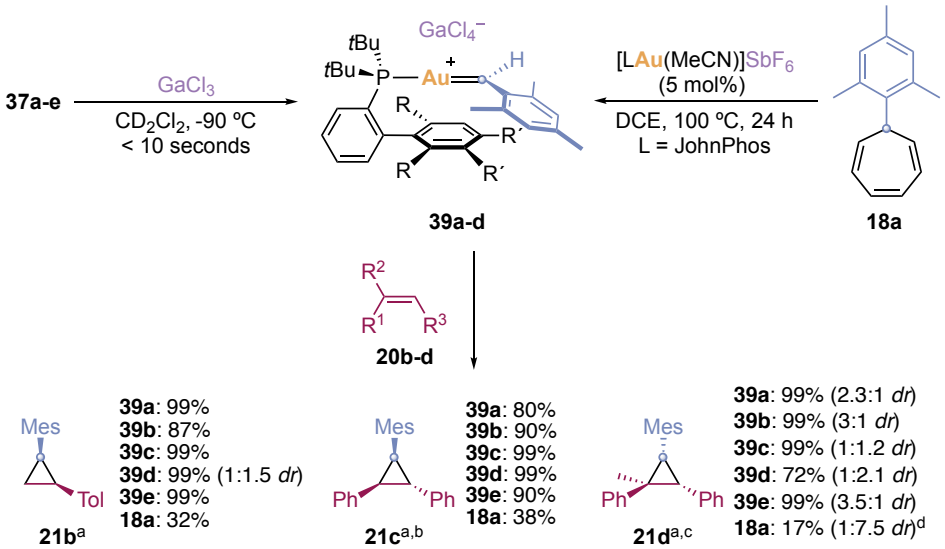

Scheme 31. Gold(I)-promoted/catalyzed cyclopropanation of alkenes **20b-d**. [a] ^{1}H NMR yield using diphenylmethane as internal standard. [b] *trans*-stilbene as alkene. [c] *trans*-α-methylstylbene as alkene. [d] Catalyst loading (10 mol%).

As explained in the introduction, aryl gold(I) carbenes can be catalytically generated *via* decarbenation reaction (retro-Buchner) of aryl cycloheptatrienes **18** in gold(I)-catalyzed cyclopropanation of alkenes (Schemes 15).[23a] Importantly, the gold(I)-catalyzed retro-Buchner reaction of mesityl cycloheptatriene **18a** in the presence of alkenes **20b-d** also leads to cyclopropanes **21b-d**, which strongly suggests that mesityl gold(I) carbene **39a** is the genuine intermediate of these transformations (Scheme 31, right) . The lower yields of **21b-d** obtained under catalytic conditions can be explained by the steric hindrance introduced by the mesityl group in the rate-determining cleavage of the cyclopropane bond of the norcaradiene in tautomeric equilibrium with the cycloheptatriene (Scheme 15). For cyclopropane **21b**, the diastereomeric ratio vary along the experiments because small amounts of $GaCl_3$ can catalyze the isomerization of *cis*-**20a** to *trans*-**20a** (Table 8). This catalytic isomerization can also explain the variation in the diastereomeric ratio for cyclopropane **21d**.

Table 8. ^{1}H NMR monitoring of the *cis* to *trans* isomerization of **21b**.

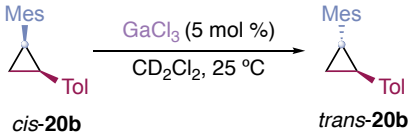

cis-**20b** *trans*-**20b**

Entry	t (s)	*cis*-**21b** (mmol)[a]	*trans*-**21b** (mmol)[a]
1	0	0.020	0
2	352	0.016	0.004
3	906	0.014	0.006
4	1829	0.013	0.007
5	10529	0.004	0.016

[a] mmol calculated by ^{1}H NMR using diphenylmethane as internal standard.

Gold(I)-Promoted C–H Insertion

Intermolecular C–H insertion

As explained in the introduction, our group reported a single example in very low yield of an intermolecular C(sp^3)-H insertion *via* gold(I) catalyzed retro-Buchner reaction of *ortho*-cycloheptatrienes (Scheme 15). Recently, Xiang Yin and Giuseppe Zuccarello expanded this reaction in our group using using *ortho*-substituted arylcycloheptatrienes, which have C–H bonds closer to the generated carbene (Scheme 31).[42]

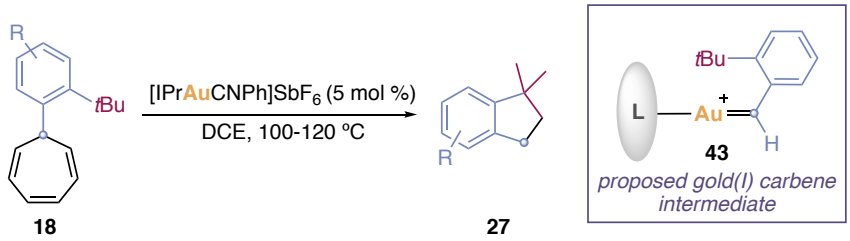

18 **27**

Scheme 32. Gold(I)-catalyzed intermolecular C(sp^3)-H insertion and proposed gold(I) carbene key intermediate.

The proposed mechanism for this transformation proceeds through the formation of an *ortho*-substituted aryl gold(I) carbene **43**, which undergoes intramolecular carbene transfer to a C(sp^3)-H bond to finally deliver indanes **27** (Scheme 32).

Hence, we wondered if we could detect the proposed *ortho*-substituted aryl gold(I) carbene intermediate by activation of the corresponding gold(I) carbenoid. To do so, gold(I) carbenoid **44** was synthesized and subjected to the optimized conditions for the generation of mesityl gold(I) carbenes (Scheme 33). However, the C–H insertion took place immediately upon activation of gold(I) carbenoid **44** with $GaCl_3$ at -90 ºC and the corresponding gold(I) carbene **43a** could not

42 Ying, X.; Zuccarello, G.; García-Morales, C.; Zhang, G.; Echavarren, A. M. unpublished results.

be detected (Scheme 33). On the other hand, gold(I) carbene **43a** was detected upon ESI-MS of gold(I) carbenoid **44**. Considering that we have demonstrated that gold(I) carbenes are generated upon activation of gold(I) carbenoids, the quantitative formation of indane **27a** after dehalogenation of **44** supports the involvement of *ortho*-substituted aryl gold(I) carbene **43a** in the aforementioned intermolecular C(sp^3)–H insertion.

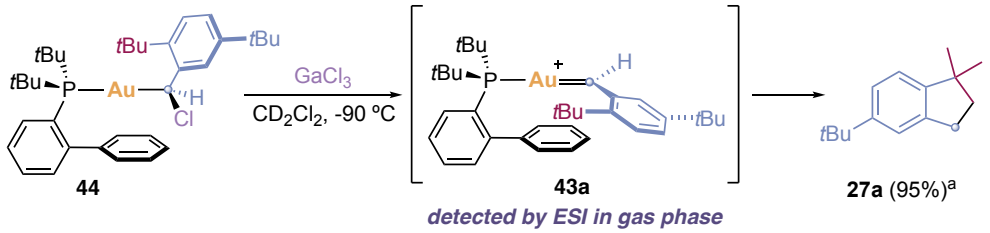

Scheme 33. Activation of gold(I) carbenoid **44** with $GaCl_3$ at -90 ºC.

Intramolecular C–H insertion

Knowing that aryl gold(I) carbenes could promote intermolecular C–H insertion, we wondered if highly electrophilic complexes **39a-e** would be able to transfer the carbene moiety to cyclohexane. Unlike cyclopropanation and oxidation, the more challenging intermolecular C–H insertion into a secondary carbon did not take place at -90 ºC. It was not until the solutions of carbenes **39a-e** were warmed up to -40 ºC that compound **43** was observed together with *E*-**20a** and **21a** as major products. To avoid competitive dimerization and cyclopropanation, gold(I) carbenes **39a-e** were generated at -30 ºC in the presence of an excess of cyclohexane. At this temperature, **43** was the major product, formed together with small amounts of *E*-**20a** (Scheme 34).

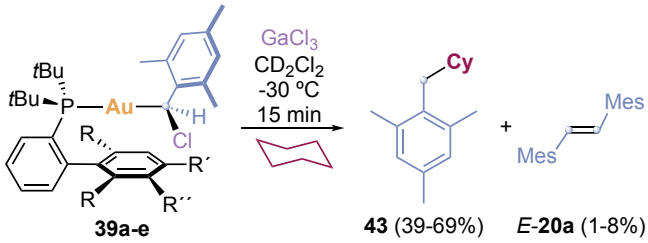

Scheme 34. Gold(I)-promoted C–H insertion. [a] Yields determined by ^{1}H NMR using diphenylmethane as internal standard.

The gold(I)-catalyzed retro-Buchner of cycloheptatrienes and further carbene transfer to alkanes has not been achieved so far. Indeed, the reaction of cycloheptratriene **18a** and 10 mol% of [JohnPhosAu(CH_3CN)]SbF_6 in cyclohexane led only to traces of C–H insertion product **43** (Scheme 35).

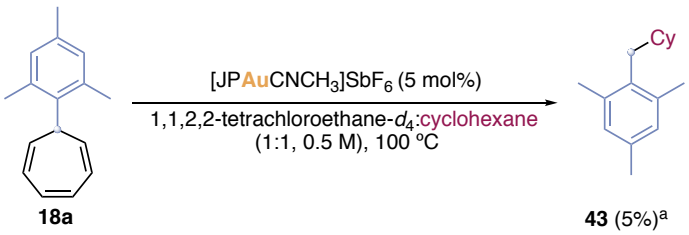

Scheme 35. C–H insertion of cyclohexane by gold(I)-catalyzed retro-Buchner reaction. [a] Yield determined by ^{1}H NMR using diphenylmethane as internal standard.

The energy profile for the insertion of mesitylidene ligand from **39a** into a C–H bond of cyclohexane is shown in Scheme 36. The initial approximation between carbene and alkane yields intermediate **IntV** (ΔG = 3.8 kcalmol^{-1}), which is slightly higher in energy as the two individual fragments. **IntV** evolves to $\mathbf{TS_{IntV\text{-}IntVI}}$ ($\Delta G^{\ddagger}$ = 19.0 kcalmol^{-1}), in which the formation of the C1–H2 and C1–C2 bonds is coupled with the breaking of the Au–C1 and C2–H2 bonds. The C–H insertion into cyclohexane has a higher energy barrier (*ca* 8 kcalmol^{-1}) than dimerization and cyclopropanation reactions, which reflects the dominance of these transformations over C–H insertion under competitive conditions in accordance with the experimental results.

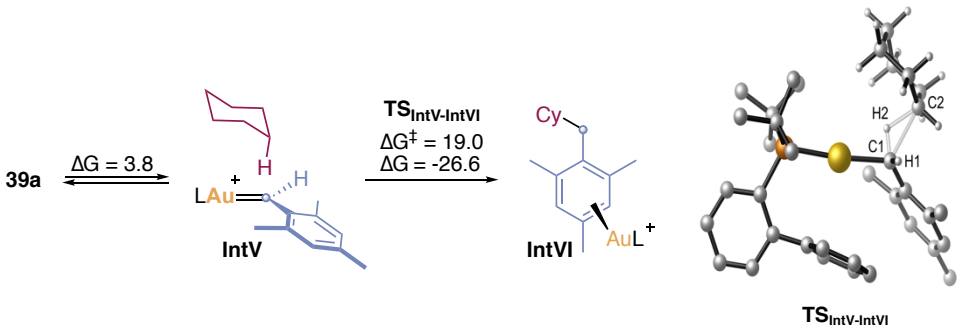

Scheme 36. Calculated reaction profile for the gold(I)-promoted C–H insertion in cyclohexane. L = JohnPhos. Free energies in kcalmol^{-1}.

Conclusions

We have generated and spectroscopically characterized monosubstituted gold(I) carbenes for the first time in solution. The mesityl group directly attached to the electron deficient carbenic carbon is essential for their detection and, in fact, NBO analysis revealed that these gold(I) carbenes are predominantly stabilized by the π-system of the mesityl group (Scheme 37).

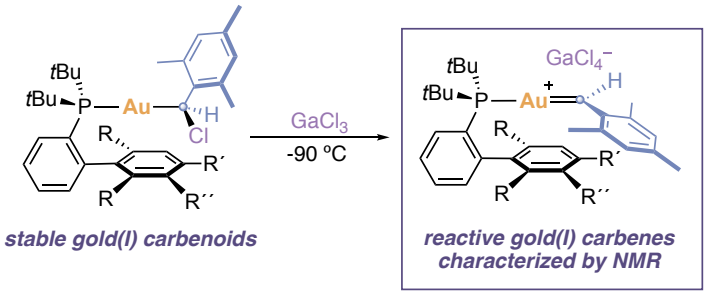

Scheme 37. Synthesis of mesityl gold(I) carbenes

The aforementioned mesityl gold(I) carbenes undergo representative transformations of intermediate gold(I) carbenes formed under catalytic conditions such as oxidation, cyclopropanation and C–H insertion reactions (Scheme 38). In addition, the reactivity studies support that they correspond to the intermediates generated in the gold(I)-catalyzed retro-Buchner reaction of cycloheptatrienes. In the absence of other reagents, we observed dimerization to form preferentially the *E*-configured alkene by a process similar to that followed by other well-known metal carbenes, which places these highly electrophilic species among the metal carbene family, despite the weak gold-to-carbon π-backdonation revealed in our computational studies (Scheme 8).

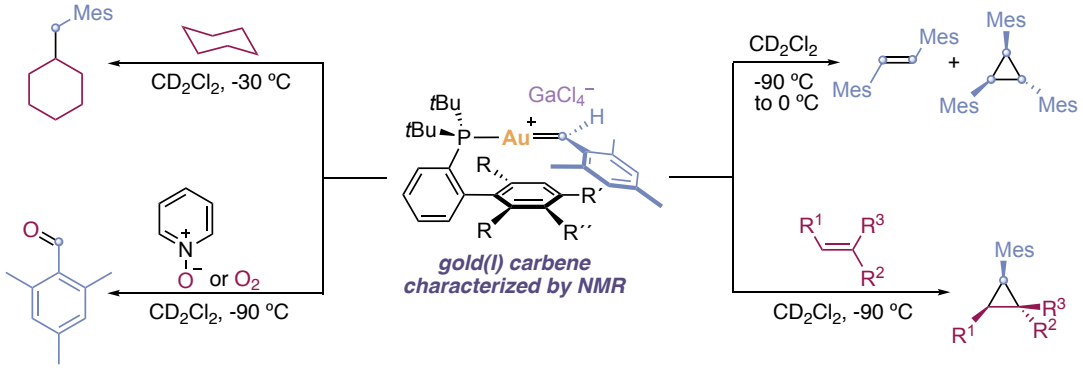

Scheme 38. Reactivity of mesityl gold(I) carbenes.

Experimental Section

General Methods

Unless otherwise stated, the reactions were carried out under argon using standard Schlenk techniques and solvents dried by passing through an activated alumina column on a PureSolvTM solvent purification system. Deuterated solvents were dried over activated MS 3Å for at least three days and deoxygenated by bubbling argon for 30 minutes before storing them in the glovebox. All the glassware used was dried in the oven at 100 ºC for at least 12 hours before use. Thin layer chromatography was carried out using TLC aluminium sheets coated with 0.2 mm of silica gel (Merck GF_{234}) using UV light as the visualizing agent and a solution of vanillin as stain. Reactions were followed using NMR techniques, GCMS apparatus or TLC. Chromatographic purifications were carried out using flash grade silica gel (SDS Chromatogel 60 ACC, 40-60 μm) or automated flash chromatographer CombiFlash Companion. Preparative TLC was performed on 20 cm × 20 cm silica gel plates (2.0 mm or 1.0 mm thick, Analtech).

NMR data were recorded in deuterated solvents on a Bruker Advance 400 Ultra Shield (400 MHz for ^{1}H, 100 MHz for ^{13}C, 162 MHz for ^{31}P and 376 MHz for ^{19}F), Bruker 500 Ultrashield (500 MHz for ^{1}H, 125 MHz for ^{13}C and 202 MHz for ^{31}P) apparatus and Bruker 300 Ultrashield (300 MHz for ^{1}H and 75 MHz for ^{13}C). Chemical shifts (δ) are reported in parts per million (ppm) and referenced to residual solvent or tetramethylsilane. Coupling constants (J) are reported in Hertz (Hz). Mass Spectra were recorded on a Waters LCT Premier Spectrometer (ESI) and Bruker Daltonics Autoflex (MALDI) spectrometers. Elemental analyses were performed on a LECO CHNS 932 micro-analyzer at the Universidad Complutense de Madrid. Melting points were determined using a Büchi melting point apparatus. Single crystal X-ray diffraction data were recorded on a Bruker Kappa APEX II DUO diffractometer equipped with an APPEX 2 4K CCD area detector, a Microsource with Mo_{ka} radiation and an Oxford Cryostream 700 low temperature device (T = -173 ºC).

2-Di-*t*-butylphosphino-2',4',6'-trimethylbiphenyl,[43] 2′-bromo-2′,6′-dimethoxybiphenyl,[44] 2′-bromo-2′,4′,6′-trimethoxybiphenyl,[44] and benzenesulfonic acid, 4-methyl-, 2-[(2′,4′,6′-trimethylphenyl)methylene]hydrazide[45] were prepared following previously reported procedures. [JohnPhosAuCl] was purchased from commercial sources and used without further purification.

43 Burgos, C. H.; Barder, T. E.; Huang, X.; Buchwald, S. L. *Angew. Chem. Int. Ed.* **2006**, *45*, 4321–4326.

44 Becht, J.-M.; Ngouela, S.; Wagner, A.; MiosKowski, C. *Tetrahedron* **2004**, *60*, 6853–6857.

45 Aggarwal, V. K.; Alonso, E.; Bae, I.; Hynd, G.; Lydon, M. K.; Palmer, M. J.; Patel, M.; Marina, P.; Richardson, J.; Stenson, R. A.; Studley, J. R.; Vasse, J.-L.; Winn, C. *J. Am. Chem. Soc.* **2003**, *125*, 10926–10940.

Synthetic Procedures and Analytical Data

General procedure for the synthesis of ligands

An oven-dried three-neck round-bottom flask equipped with a condenser was charged with magnesium turnings, the corresponding 2´-bromo-1,1´-biphenyl and dry THF under argon. Magnesium was activated by the addition of 1,2-dibromoethane (50 μL) via syringe. The mixture was stirred at 70 °C for 2 h and then allowed to cool down to room temperature. It was filtered through a canula filter to a new oven-dried three-neck round-bottom flask charged with argon. Anhydrous CuCl was added in a single portion, followed by the slow addition of di-*tert*-butylchlorophosphine via syringe over a period of 30 minutes. The reaction mixture was stirred at 70 °C for 24 h. The mixture was allowed to cool down to room temperature and then washed with 30% aqueous NH_4OH and extracted with ethyl acetate. Brine was added as needed to help in the phase separation. This process was repeated at least six times until the aqueous phase was not blue colored. The organic phase was dried over Na_2SO_4, filtered and concentrated *in vacuo*. The crude was purified by flash column chromatography on silica gel under nitrogen.

2-Di-*tert*-butylphosphino-2´,6´-dimethoxybiphenyl

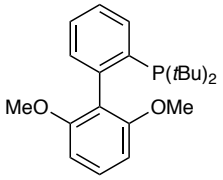

The title ligand was synthesized according to the general procedure from 2´-bromo-2´,6´-dimethoxy-1,1´-biphenyl (550 mg, 1.88 mmol), magnesium turnings (137 mg, 5.63 mmol), anhydrous CuCl (186 mg, 1.88 mmol) and di-*tert*-butylchlorophosphane (0.463 ml, 2.44 mmol). The crude was purified by silica gel flash column chromatography using a 95:5 to 9:1 mixture of cyclohexane:ethyl acetate as eluent to give the tittle ligand as a crystalline solid (300 mg, 0.84 mmol, 45% yield). The compound was stored in the glovebox.

mp 132.6 °C **^{1}H NMR** (400 MHz, $CDCl_3$) δ 7.84 (dt, J = 7.6 Hz, J = 1.5 Hz, 1H), 7.41 – 7.36 (m, 1H), 7.34 – 7.28 (m, 2H), 7.17 (ddd, J = 7.6 Hz, J = 3.7 Hz, J = 1.5 Hz, 1H), 6.58 (d, J = 8.4 Hz, 2H), 3.66 (s, 6H), 1.14 (d, J (^{1}H-^{31}P) = 11.5 Hz, 18H). **^{13}C NMR** (126 MHz, $CDCl_3$) δ 157.45 (d, J (^{13}C-^{31}P) = 1.1 Hz), 143.6 (d, J (^{13}C-^{31}P) = 35.1 Hz), 137.7 (d, J (^{13}C-^{31}P) = 25.8 Hz), 135.4 (d, J (^{13}C-^{31}P) = 3.4 Hz), 131.6 (d, J (^{13}C-^{31}P) = 6.8 Hz), 128.7, 128.4 (d, J (^{13}C-^{31}P) = 1.2 Hz), 125.7, 120.7 (d, J (^{13}C-^{31}P) = 7.2 Hz), 103.3, 55.2, 32.2 (d, J (^{13}C-^{31}P) = 24.5 Hz). **^{31}P NMR** (162 MHz, $CDCl_3$) δ 27.31. **HRMS** (APCI+) calculated for $C_{22}H_{32}O_2P$ $(M+H)^+$: 359.2134; found: 359.2120. **Elemental Analysis** calculated for $C_{22}H_{31}O_2P$: C, 73.72; H, 8.72; found: C, 73.64; H, 8.48.

2-Di-*tert*-butylphosphino-2´,4´,6´-trimethoxybiphenyl

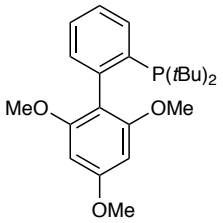

The title ligand was synthesized according to the general procedure from 2´-bromo-2´,4´,6´-dimethoxy-1,1´-biphenyl (6.37 g, 19.7 mmol), magnesium turnings (1.44 g, 59.1 mmol), anhydrous CuCl (1.95 mg, 19.71 mmol) and di-*tert*-butylchlorophosphane (4.87 ml, 25.6 mmol). The crude was purified by silica gel column chromatography using a 95:5 to 9:1 mixture of cyclohexane: ethyl acetate as eluent to give the tittle ligand as a crystalline solid (5.03 mg, 12.95 mmol, 65.7 % yield). The compound was stored in the glovebox.

mp 115.4 °C **^{1}H NMR** (500 MHz, $CDCl_3$) δ 7.82 (dt, J = 7.6, 1.5 Hz, 1H), 7.40 – 7.34 (m, 1H), 7.29 (td, J = 7.6, 1.5 Hz, 1H), 7.15 (ddd, J = 7.6, 3.8, 1.5 Hz, 1H), 6.16 (s, 2H), 3.87 (s, 3H), 3.64 (s, 6H), 1.14 (d, J (^{1}H-^{31}P) = 11.5 Hz, 18H). **^{13}C NMR** (101 MHz, $CDCl_3$) δ 160.7, 158.0 (d, J (^{13}C-^{31}P) = 0.8 Hz), 143.6 (d, J (^{13}C-^{31}P) = 34.7 Hz), 138.2 (d, J (^{13}C-^{31}P) = 25.0 Hz), 135.4 (d, J (^{13}C-^{31}P) = 3.4 Hz), 132.2 (d, J (^{13}C-^{31}P) = 6.7 Hz), 128.4 (d, J (^{13}C-^{31}P) = 1.4 Hz), 125.6, 113.7 (d, J (^{13}C-^{31}P) = 7.5 Hz), 90.0, 55.3, 55.2, 32.2 (d, J (^{13}C-^{31}P) = 24.3 Hz), 30.8 (d, J (^{13}C-^{31}P) = 15.6 Hz). **^{31}P NMR** (202 MHz, $CDCl_3$) δ 27.35. **HRMS** (ESI+) calculated for $C_{23}H_{34}OP$ $(M+H)^+$: 389.2240; found: 389.2245.

2-Di-*tert*-butylphosphino-2-naphthyl

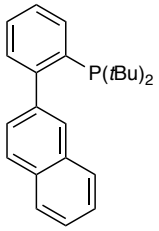

The title ligand was synthesized according to the general procedure from 2-(2-bromophenyl)naphthalene (6.37 g, 19.7 mmol), magnesium turnings (0.463 g, 6.36 mmol), anhydrous CuCl (0.629 mg, 6.36 mmol) and di-*tert*-butylchlorophosphane (1.57 ml, 19.07 mmol). The crude was purified by silica gel column chromatography using a 95:5 to 9:1 mixture of cyclohexane: ethyl acetate as eluent to give the tittle ligand as a crystalline solid (1.13 g, 3.24 mmol, 51 % yield). The compound was stored in the glovebox.

mp 90.4 °C **^{1}H NMR** (400 MHz, $CDCl_3$) δ 7.97 – 7.92 (m, 1H), 7.89 – 7.84 (m, 1H), 7.83 – 7.78 (m, 2H), 7.68 – 7.64 (m, 1H), 7.50 – 7.44 (m, 3H), 7.44 – 7.36 (m, 1H), 7.36 – 7.30 (m, 1H), 1.15 (d, J (^{1}H-^{31}P) = 11.6 Hz, 18H). **^{13}C NMR** (101 MHz, $CDCl_3$) δ 151.2 (d, J (^{13}C-^{31}P) = 32.3 Hz), 141.7 (d, J (^{13}C-^{31}P) = 7.2 Hz), 135.8 (d, J (^{13}C-^{31}P) = 27.9 Hz), 135.4 (d, J (^{13}C-^{31}P) = 3.2 Hz), 133.0 (d, J (^{13}C-^{31}P) = 1.7 Hz), 132.2, 130.9 (d, J (^{13}C-^{31}P) = 6.4 Hz), 129.7 (d, J (^{13}C-^{31}P) = 4.9

Hz), 128.83 (d, J (^{13}C-^{31}P) = 2.2 Hz), 128.5, 128.0, 127.8, 126.2, 126.0, 125.8 (d, J (^{13}C-^{31}P) = 1.6 Hz), 125.5 (d, J (^{13}C-^{31}P) = 1.7 Hz), 32.9 (d, J (^{13}C-^{31}P) = 25.4 Hz), 30.8 (dd, J (^{13}C-^{31}P) = 15.3, 1.8 Hz). **^{31}P NMR** (162 MHz, $CDCl_3$) δ 21.32. **HRMS** (ESI+) calculated for $C_{24}H_{30}P$ $(M+H)^+$: 349.2080; found: 349.2085.

General procedure for the synthesis of gold(I) chloride complexes:

In a Schlenk, [(Me_2S)AuCl] was added to a solution of the corresponding phosphine in dry CH_2Cl_2 under argon at 25 ºC. The solution was stirred for 1 h, filtered through a pad of cotton/Celite/cotton and concentrated under vacuum. The crude was purified by flash column chromatography on silica gel.

2-Di-*tert*-butylphosphino-2´,4´,6´-trimethylbiphenyl gold(I) chloride (32b)

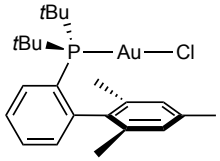

Gold(I) chloride complex **32b** was synthesized according to the general procedure from 2-di-*t*-butylphosphino-2´,4´,6´-trimethylbiphenyl (90 mg, 0.264 mmol) and (Me_2S)AuCl (78 mg, 0.264 mmol). A white crystalline solid was obtained in 65% yield (98 mg, 0.172 mmol) after purification by flash column chromatography using a mixture of cyclohexane:ethyl acetate (8:2) as eluent.

^{1}H NMR (500 MHz, $CDCl_3$) δ 7.89 (td, J = 8.0, 1.5 Hz, 1H), 7.58 (tt, J = 7.5, 1.5 Hz, 1H), 7.49 (ddt, J = 8.0, 7.5, 1.5 Hz, 1H), 7.25 (ddd, J = 7.5, 4.5, 1.5 Hz, 1H), 7.02 (s, 2H), 2.47 (s, 3H), 1.95 (s, 6H), 1.44 (d, J (^{1}H-^{31}P) = 15.5 Hz, 18H). **^{13}C NMR** (126 MHz, $CDCl_3$) δ 149.4 (d, J (^{13}C-^{31}P) = 13.6 Hz), 138.9, 137.5 (d, J (^{13}C-^{31}P) = 5.9 Hz), 135.4, 134.5 (d, J (^{13}C-^{31}P) = 3.0 Hz), 133.9 (d, J (^{13}C-^{31}P) = 7.8 Hz), 131.5 (d, J (^{13}C-^{31}P) = 2.4 Hz), 129.4, 127.8 (d, J (^{13}C-^{31}P) = 43.6 Hz), 126.5 (d, J (^{13}C-^{31}P) = 6.9 Hz), 38.3 (d, J (^{13}C-^{31}P) = 26.4 Hz), 31.5 (d, J (^{13}C-^{31}P) = 6.5 Hz), 21.7, 21.5. **^{31}P NMR** (202 MHz, $CDCl_3$) δ. 62.38. **HRMS** (ESI+) calculated for $C_{23}H_{33}AuClP$ $(M + Na)^+$: 595.1566; found: 595.1576. **Elemental Analysis** calculated for $C_{23}H_{33}AuClP$: C, 48.22; H, 5.81; found: C, 48.13; H, 5.56.

2-Di-*tert*-butylphosphino-2´,6´-dimethoxybiphenyl gold(I) chloride (32c)

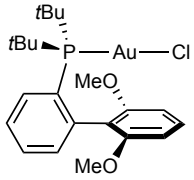

Gold(I) chloride complex **32c** was synthesized according to the general procedure from 2-di-*t*-butylphosphino-2´,6´-dimethoxybiphenyl (100 mg, 0.279 mmol) and (Me_2S)AuCl (82 mg, 0.279 mmol). A white crystalline solid was obtained in 43% yield (70 mg, 0.120 mmol) after purification by flash column chromatography using a mixture of cyclohexane:ethyl acetate (8:2)

as eluent.

^{1}H NMR (500 MHz, $CDCl_3$) δ 7.88 – 7.83 (m, 1H), 7.57 – 7.50 (m, 2H), 7.46 – 7.41 (m, 1H), 7.21 (ddd, J = 7.7, 4.3, 1.4 Hz, 1H), 6.64 (d, J = 8.4 Hz, 2H), 3.65 (s, 6H), 1.40 (d, J (^{1}H-^{31}P) = 15.5 Hz, 18H).**^{13}C NMR** (126 MHz, $CDCl_3$) δ 157.3, 143.7 (d, J (^{13}C-^{31}P) = 13.3 Hz), 134.0 (d, J (^{13}C-^{31}P) = 7.8 Hz), 133.8 (d, J (^{13}C-^{31}P) = 3.0 Hz), 131.2 (d, J (^{13}C-^{31}P) = 2.4 Hz), 130.3, 128.4 (d, J (^{13}C-^{31}P) = 47.5 Hz), 126.4 (d, J (^{13}C-^{31}P) = 7.0 Hz), 119.2 (d, J (^{13}C-^{31}P) = 6.7 Hz), 104.4, 55.3, 37.8 (d, J (^{13}C-^{31}P) = 26.0 Hz), 31.0 (d, J (^{13}C-^{31}P) = 6.9 Hz). **^{31}P NMR** (202 MHz, $CDCl_3$) δ 64.26. **HRMS** (ESI+) calculated for $C_{22}H_{31}AuClO_2P$ (M + Na)$^{+}$: 613.1308; found: 613.1323. **Elemental Analysis** calculated for $C_{22}H_{31}AuClO_2P$: C, 44.72; H, 5.29; found: C, 45.47; H, 5.18.

2-Di-*tert*-butylphosphino-2´,4´,6´-trimethoxybiphenyl gold(I) chloride (32d)

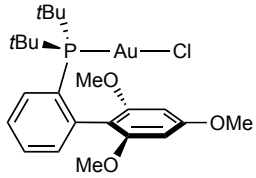

Gold chloride complex **32d** was synthesized according to the general procedure from 2-di-*t*-butylphosphino-2´,4´,6´-trimethoxybiphenyl (250 mg, 0.644 mmol) and (Me_2S)AuCl (190 mg, 0.644 mmol). A white crystalline solid was obtained in 92% yield (367 mg, 0.592 mmol) after purification by flash column chromatography using a mixture of cyclohexane:ethyl acetate (8:2) as eluent.

mp 251.4 °C **^{1}H NMR** (500 MHz, $CDCl_3$) δ 7.86 (td, J = 8.0, 1.5 Hz, 1H), 7.55 (tt, J = 7.6, 1.5 Hz, 1H), 7.44 (ddt, J = 8.0, 7.6, 1.5 Hz, 1H), 7.24 (ddd, J = 7.6, 4.3, 1.5 Hz, 1H), 6.26 (s, 2H), 3.97 (s, 3H), 3.66 (s, 7H), 1.41 (d, J (^{1}H-^{31}P) = 15.4 Hz, 18H). **^{13}C NMR** (126 MHz, $CDCl_3$) δ 162.9, 157.7, 143.7 (d, J (^{13}C-^{31}P) = 13.3 Hz), 134.6 (d, J (^{13}C-^{31}P) = 7.6 Hz), 133.7 (d, J (^{13}C-^{31}P) = 3.2 Hz), 131.1 (d, J (^{13}C-^{31}P) = 2.3 Hz), 128.7 (d, J (^{13}C-^{31}P) = 48.3 Hz), 126.3 (d, J (^{13}C-^{31}P) = 7.2 Hz), 111.8 (d, J (^{13}C-^{31}P) = 6.9 Hz), 91.7, 56.0, 55.2, 37.7 (d, J (^{13}C-^{31}P) = 26.0 Hz), 31.0 (d, J (^{13}C-^{31}P) = 6.9 Hz). **^{31}P NMR** (202 MHz, $CDCl_3$) δ 64.16. **HRMS** (ESI+) calculated for $C_{23}H_{33}AuClO_3NaP$ (M + Na): 643.1414; found: 643.1436. **Elemental Analysis** calculated for $C_{23}H_{33}AuClO_3P$: C, 44.49; H, 5.36; found: C, 44.82; H, 5.25.

2-Di-*tert*-butylphosphino-2-naphthyl gold(I) chloride (32e)

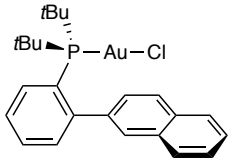

Gold chloride complex **32e** was synthesized according to the general procedure from 2-di-*t*-butylphosphino-2-naphthyl (559.2 mg, 1.605 mmol) and (Me_2S)AuCl (500 mg, 1.605 mmol). A white crystalline solid was obtained in 36.4% yield (338.9 mg, 0.58 mmol) after purification by flash column chromatography using a mixture of cyclohexane: ethyl acetate (4:1) as eluent.

mp 241.2 °C **^{1}H NMR** (400 MHz, $CDCl_3$) δ 8.03 – 7.87 (m, 3H), 7.84 – 7.77 (m, 1H), 7.64 – 7.60 (m, 1H), 7.60 – 7.48 (m, 4H), 7.41 – 7.34 (m, 1H), 7.26 – 7.21 (m, 1H), 1.44 (d, J = 4.1 Hz, 11H), 1.40 (d, J (^{1}H-^{31}P) = 4.1 Hz, 11H). **^{13}C NMR** (101 MHz, $CDCl_3$) δ 150.3 (d, J (^{13}C-^{31}P) = 13.7 Hz), 139.7 (d, J (^{13}C-^{31}P) = 6.5 Hz), 133.6 (d, J (^{13}C-^{31}P) = 2.8 Hz), 133.6, 133.5, 133.3, 130.7 (d, J (^{13}C-^{31}P) = 2.2 Hz), 129.0, 128.4, 128.3, 128.0, 127.1, 127.0 (d, J (^{13}C-^{31}P) = 2.3 Hz), 126.4, 126.0, 38.0 (d, J (^{13}C-^{31}P) = 22.2 Hz), 37.8 (d, J (^{13}C-^{31}P) = 22.1 Hz), 31.0 (d, J (^{13}C-^{31}P) = 7.1 Hz), 31.0 (d, J (^{13}C-^{31}P) = 7.0 Hz). **^{31}P NMR** (162 MHz, $CDCl_3$) δ 63.02. **HRMS** (ESI+) calculated for $C_{24}H_{29}AuClNaP$ $(M + Na)^+$: 603.1254; found: 603.1254.

Synthesis of Gold(I) Carbenoids

Preparation of mesityldiazomethane in toluene solution

The used of protective shielding screens is highly recommended during the preparation of mesityldiazomethane solution due to the risk of explosion of aryl diazomethane compounds.

A 250 ml two-neck round-bottom flask with a findenser condenser was charged with an aqueous solution of NaOH (50 ml, 7 g, 24.5 mmol), benzyltriethylammonium chloride (0.968 g, 4.25 mmol and toluene (50 ml). Benzenesulfonic acid, 4-methyl-, 2-[(2,4,6-trimethylphenyl)methylene]hydrazide (0.538 g, 1.70 mmol) was sequentially added, *the addition must be done following the noted order*. The flask was covered with aluminum foil and protected by a three-walls shielding screen. The resulting mixture was stirred for 2 h at 70 ºC. After being allowed to cool down to room temperature, the mixture was transferred to a separatory funnel. The orange organic phase was separated from the aqueous phase and transferred to a round-bottom flask charged with NaOH pellets and covered with aluminum foil under argon. The mesityldiazomethane solution was deoxygenated by bubbling argon through it for 30 minutes. The dry and deoxygenated solution was transferred to an oven-dried Schlenk under argon using a syringe connected to a Teflon filter. It was concentrated to 2 ml under vacuum in the Schlenk line and layered with 2 ml of dry pentane. After being cooled down to -70 ºC for 30 minutes, white solid precipitated and the orange solution was filtered at -70 ºC to a new oven-dried Schlenk using a cannula filter. The solution was concentrated to dryness in the Schlenk line (***be especially careful at that point!!!)***. Followed by the addition of dry and deoxygenated toluene (5 ml). It was stored under argon and covered with aluminum foil in the freezer at -20 ºC until it was used the very next day.

Synthesis of Chloromesityl(methyl)gold(I) Carbenoids

The used of protective shielding screens is highly recommended during the synthesis of gold(I) carbenoids due to the risk of explosion of aryl diazomethane compounds.

2-Di-*tert*-butylphosphinobiphenyl chloromesityl(methyl)gold(I) carbenoid (37a)

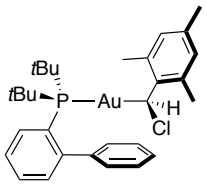

2-Di-*tert*-butylphosphinobiphenyl gold(I) chloride (150 mg, 0.283 mmol) was added to a Schlenk charged with a freshly prepared solution of mesityldiazomethane (1.695 mmol of starting hydrazide, 5 ml) under argon and protected by a three-walls shielding screen. The Schlenk was located in an aluminum heating block with sand and heated up to 35 ºC for 2 h. The solution was concentrated to 2 ml and stirred at 45 ºC until full conversion was observed by ^{31}P NMR. Once the starting material was consumed, the solution was allowed to cool down to room temperature. At this point, toluene was evaporated to dryness leading to a red oil, ***be especially careful!!*** The orange oil was dissolved in 2 ml of pentane that were subsequently evaporated leading to an orange solid, the process was repeated twice. The orange solid was dissolved in dry toluene (0.5 ml) and dry pentane (2 ml). The resulting solution was cooled down to -30 ºC and stirred until white solid precipitated. The solvent was filtered off using a cannula filter leading to a pinkish-white solid that was washed with dry pentane (1 ml x 3) at -30 ºC. The resulting solid was dried for 24 h. 2-Di-*tert*-butylphosphinobiphenylchloromesityl(methyl) gold(I) carbenoid (**37a**) was obtained as a white solid in 48% yield, (90 mg, 0.136 mmol). The complex was stored in the glovebox at room temperature. X-ray quality crystals were obtained layering a toluene solution of the complex with pentane at -20 ºC under argon.

^{1}H NMR (400 MHz, toluene-d_8) δ 7.54 – 7.48 (m, 1H), 7.43 – 7.38 (m, 1H), 7.17 – 7.08 (m, 2H), 7.03 – 6.92 (m, 5H), 6.82 (bs, 2H), 4.92 (d, J (^{1}H-^{31}P) = 6.6 Hz, 1H), 2.70 (bs, 6H), 2.23 (s, 3H), 1.21 (d, J (^{1}H-^{31}P) = 14.5 Hz, 9H), 1.04 (d, J (^{1}H-^{31}P) = 14.5 Hz, 9H). **^{13}C NMR** (101 MHz, toluene-d_8) δ 150.9 (d, J (^{13}C-^{31}P) = 16.5 Hz), 144.4 (d, J (^{13}C-^{31}P) = 0.9 Hz), 143.1 (d, J (^{13}C-^{31}P) = 5.7 Hz), 134.8, 133.5, 133.1 (d, J (^{13}C-^{31}P) = 7.7 Hz), 130.1 (d, J (^{13}C-^{31}P) = 2.2 Hz), 129.6, 129.2, 129.2, 128.9, 128.5, 127.8, 126.3 (d, J (^{13}C-^{31}P) = 5.0 Hz), 69.7 (d, J (^{13}C-^{31}P) = 107.7 Hz), 37.1 (d, J (^{13}C-^{31}P) = 19.2 Hz), 36.9 (d, J (^{13}C-^{31}P) = 19.0 Hz), 30.8 (d, J (^{13}C-^{31}P) = 6.9 Hz), 30.6 (d, J (^{13}C-^{31}P) = 7.0 Hz), 22.3, 21.0. **^{31}P NMR** (162 MHz, toluene-d_8) δ 66.42. **HRMS** (ESI+) calculated for $C_{30}H_{39}AuP$ $(M\text{-}Cl)^+$: 627.2450; found: 627.2436.

2-Di-*tert*-butylphosphino-2´,4´,6´-trimethylbiphenyl chloromesityl(methyl)gold(I) carbenoid (37b)

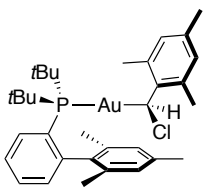

2-Di-*tert*-butylphosphino-2´,4´,6´-trimethylbiphenyl gold(I) chloride (200 mg, 0.349 mmol) was added to a Schlenk charged with a freshly prepared solution of mesityldiazomethane (3.490 mmol of starting hydrazide, 5 ml) under argon and protected by a three-walls shielding screen. The Schlenk was located in an aluminum heating block with sand and heated up to 55 ºC for 2 h. The solution was concentrated to 2 ml and stirred at 55 ºC until full conversion was observed by ^{31}P NMR. Once the starting material was consumed, the solution was allowed to cool down to room temperature. At this point, toluene was evaporated to dryness leading to an orange oil, ***be especially careful!!*** The orange oil was dissolved in 2 ml of pentane that was subsequently evaporated giving an oily orange solid, the process was repeated twice. The oily solid was dissolved in dry pentane (2 ml) and stirred until a white solid precipitated. The solvent was filtered off using a cannula filter leading to a pinkish-white solid that was washed with dry pentane (1 ml x 3). The resulting solid was dried for 24 h. 2-Di-*tert*-butylphosphino-2´,4´,6´-trimethylbiphenyl chloromesityl(methyl)gold(I) carbenoid (**37b**) was obtained as a white solid in 41% yield, (100 mg, 0.143 mmol). The complex was stored in the glovebox at room temperature. X-ray quality crystals were obtained layering a toluene solution of the complex with pentane at -20 ºC under argon.

^{1}H NMR (400 MHz, toluene-d_8) δ 7.55 – 7.48 (m, 1H), 7.18 (s, 1H), 7.12 – 7.08 (m, 1H), 7.07 – 7.01 (m, 2H), 6.86 – 6.78 (m, 3H), 4.90 (d, J (^{1}H-^{31}P) = 6.9 Hz, 1H), 2.75 (bs, 6H), 2.49 (s, 3H), 2.20 (s, 3H), 2.06 (s, 3H), 1.88 (s, 3H), 1.22 (d, J (^{1}H-^{31}P) = 14.4 Hz, 9H), 0.98 (d, J (^{1}H-^{31}P) = 14.4 Hz, 9H). **^{13}C{^{1}H} NMR** (101 MHz, toluene-d_8) δ 150.1 (d, J (^{13}C-^{31}P) = 16.9 Hz), 144.3, 139.2 (d, J (^{13}C-^{31}P) = 4.5 Hz), 137.4, 136.0, 135.7, 135.4, 133.8 (d, J (^{13}C-^{31}P) = 8.2 Hz), 133.3, 131.0, 130.8 (d, J (^{13}C-^{31}P) = 2.3 Hz), 130.7, 129.9, 125.9 (d, J (^{13}C-^{31}P) = 5.1 Hz), 70.1 (d, J (^{13}C-^{31}P) = 108.4 Hz), 37.5 (d, J (^{13}C-^{31}P) = 7.5 Hz), 37.3 (d, J (^{13}C-^{31}P) = 7.9 Hz), 31.4 (d, J (^{13}C-^{31}P) = 6.8 Hz), 31.0 (d, J (^{13}C-^{31}P) = 6.7 Hz), 22.2, 21.9, 21.5, 21.0. **^{13}C {^{1}H} NMR** (126 MHz, CD_2Cl_2, -90 ºC) C1 71.8 (d, J (^{13}C-^{31}P) = 107.2 Hz). **^{13}C NMR** (126 MHz, CD_2Cl_2, -90 ºC) C1 71.8 (d, J (^{13}C-^{1}H) = 143.9 Hz, J (^{13}C-^{31}P) = 107.2 Hz). **^{31}P NMR** (162 MHz, toluene-d_8) δ 67.16. **HRMS** (ESI+) calculated for $C_{33}H_{45}AuP$ $(M\text{-}Cl)^+$: 669.2919; found: 669.2916. **Elemental Analysis** calculated for $C_{33}H_{45}AuClP$: C, 56.21; H, 6.43; found: C, 54.41; H, 6.51.

2-Di-*tert*-butylphosphino-2´,6´-dimethoxybiphenyl chloromesityl(methyl)gold(I) carbenoid (37c)

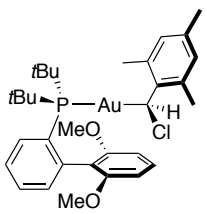

2-Di-*tert*-butylphosphino-2´,6´-dimethoxybiphenyl gold(I) chloride (200 mg, 0.338 mmol) was added to a Schlenk charged with a freshly prepared solution of mesityldiazomethane (4.06 mmol

of starting hydrazide, 20 ml) under argon and protected by a three-walls shielding screen. The Schlenk was located in an aluminum heating block with sand and heated up to 65 ºC for 1 h. The solution was concentrated to 5 ml and stirred for 2 h. The solution was further concentrated to 2 ml and stirred until full conversion was observed by ^{31}P NMR. Once the starting material was consumed, the solution was allowed to cool down to room temperature. At this point, toluene was evaporated to dryness leading to an orange solid, ***be especially careful!!*** The orange solid was washed with 2 ml of pentane that were subsequently evaporated. The orange solid was dissolved in dry toluene (0.5 ml) and dry pentane (2 ml). Instantaneously, solid precipitated and the solvent was filtered off using a cannula filter leading to a pale rose solid that was washed with dry pentane (1 ml x 3). The resulting solid was dried for 24 h. 2-Di-*tert*-butylphosphino-2´,6´-dimethoxybiphenyl chloromesityl(methyl)gold(I) carbenoid (**37c**) was obtained as a pinkish-white solid in 57% yield, (140 mg, 0.192 mmol). The complex was stored in the glovebox at room temperature. X-ray quality crystals were obtained layering a toluene solution of the complex with pentane at -20 ºC under argon.

^{1}H NMR (400 MHz, toluene-d_8) δ 7.59 (t, J = 7.0 Hz, 1H), 7.23 (t, J = 8.4 Hz, 1H), 7.09 – 7.02 (m, 1H), 6.84 (s, 2H), 6.65 (d, J = 8.4 Hz, 1H), 6.26 (d, J = 8.3 Hz, 1H), 4.84 (d, J (^{1}H-^{31}P) = 6.7 Hz, 1H), 3.50 (s, 3H), 3.16 (s, 3H), 2.76 (bs, 6H), 2.22 (s, 3H), 1.33 (d, J (^{1}H-^{31}P) = 14.3 Hz, 10H), 1.10 (d, J (^{1}H-^{31}P) = 14.3 Hz, 9H). **^{13}C{^{1}H} NMR** (126 MHz, CD_2Cl_2, -90 ºC) δ 156.8 (d, J (^{13}C-^{31}P) = 3.4 Hz), 142.9, 142.6 (d, J (^{13}C-^{31}P) = 16.0 Hz), 137.5, 135.2, 134.0, 133.8 (d, J (^{13}C-^{31}P) = 3.6 Hz), 132.7 (d, J (^{13}C-^{31}P) = 8.2 Hz), 130.7, 130.4, 128.9 (d, J (^{13}C-^{31}P) = 50.1 Hz), 128.7, 127.9, 127.7, 126.4 (d, J (^{13}C-^{31}P) = 4.8 Hz), 124.9, 119.5 (d, J (^{13}C-^{31}P) = 5.6 Hz), 102.9 (d, J (^{13}C-^{31}P) = 165.8 Hz), 73.7 (C1, d, J (^{13}C-^{31}P) = 107.4 Hz), 55.3, 54.9, 36.3 (d, J (^{13}C-^{31}P) = 10.5 Hz), 36.1 (d, J (^{13}C-^{31}P)= 10.5 Hz), 30.7, 29.6, 21.8, 21.6, 20.4. **^{13}C NMR** (126 MHz, CD_2Cl_2, -90 ºC) C1 73.7 (d, J (^{13}C-^{1}H) = 144.3 Hz, J (^{13}C-^{31}P) = 107.4 Hz). **^{31}P NMR** (162 MHz, toluene-d_8) δ 67.76. **HRMS** (ESI+) calculated for $C_{32}H_{43}AuO_2P$ (M-Cl)$^{+}$: 687.2661; found: 687.2652.

2-Di-*tert*-butylphosphino-2´,4´,6´-trimethoxybiphenyl chloromesityl(methyl)gold(I) carbenoid (37d)

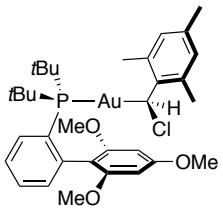

2-Di-*tert*-butylphosphino-2´,4´,6´-trimethoxybiphenyl gold(I) chloride (150 mg, 0.242 mmol) was added to a Schlenk charged with a freshly prepared solution of mesityldiazomethane (2.416 mmol of starting hydrazide, 5 ml) under argon and protected by a three-walls shielding screen. The Schlenk was located in an aluminum heating block with sand and heated up to 65 ºC until full conversion was observed by ^{31}P NMR. Once the starting material was consumed, the solution

was allowed to cool down to room temperature. At this point, toluene was evaporated to dryness leading to an orange oil, ***be especially careful!!*** The orange oil was dissolved in 2 ml of pentane that was subsequently evaporated giving an oily solid, the process was repeated twice. The oily solid was dissolved in dry diethyl ether (2 ml) and stirred at -20 ºC until white solid precipitated. The solvent was filtered off using a cannula filter leading to a pinkish-white solid that was washed with dry pentane (1 ml x 3). The resulting solid was dried for 24 h. 2-Di-*tert*-butylphosphino-2′,4′,6′-trimethoxybiphenyl chloromesityl(methyl)gold(I) carbenoid (**37d**) was obtained as a white solid in 33% yield, (60 mg, 0.080 mmol). The complex was stored in the glovebox at room temperature.

^{1}H NMR (500 MHz, toluene-d_8) δ 7.59 (ddd, J = 7.8, 6.4, 1.6 Hz, 1H), 7.17 (ddd, J = 7.8, 4.1, 1.6 Hz, 1H), 7.14 – 7.10 (m, 1H), 7.04 – 6.99 (m, 1H), 6.82 (s, 2H), 6.45 (d, J = 2.2 Hz, 1H), 6.29 (d, J = 2.1 Hz, 1H), 4.88 (d, J (^{1}H-^{31}P) = 6.7 Hz, 1H), 3.81 (s, 3H), 3.59 (s, 3H), 3.17 (s, 3H), 2.81 (bs, 6H), 2.19 (s, 3H), 1.34 (d, J (^{1}H-^{31}P) = 14.3 Hz, 9H), 1.03 (d, J (1H-31P) = 14.3 Hz, 9H). **^{13}C NMR** (126 MHz, toluene-d_8) δ 161.8, 158.0 (d, J (^{13}C-^{31}P) = 33.8 Hz), 144.0 (d, J (^{13}C-^{31}P) = 16.4 Hz), 143.9 (d, J (^{13}C-^{31}P) = 1.3 Hz), 134.7, 134.5, 133.0, 131.1 (d, J (^{13}C-^{31}P) = 35.9 Hz), 130.1 (d, J (^{13}C-^{31}P) = 2.2 Hz), 125.4 (d, J (^{13}C-^{31}P) = 5.5 Hz), 125.0, 113.2 (d, J (^{13}C-^{31}P) = 5.7 Hz), 91.8, 89.8, e (d, J (^{13}C-^{31}P) = 109.6 Hz), 54.7, 54.5, 54.2, 36.6 (d, J (^{13}C-^{31}P) = 14.4 Hz), 36.5 (d, J (^{13}C-^{31}P) = 14.4 Hz), 31.0 (d, J (^{13}C-^{31}P) = 7.1 Hz), 30.1 (d, J (^{13}C-^{31}P) = 7.0 Hz), 21.8, 20.6. **^{31}P NMR** (202 MHz, toluene-d_8) δ 67.53. **HRMS** (ESI+) calculated for $C_{33}H_{45}AuO_3P$ (M-Cl)$^{+}$: 717.2767; found: 717.2771.

2-Di-*tert*-butylphosphino-2-naphthyl chloromesityl(methyl)gold(I) carbenoid (37e)

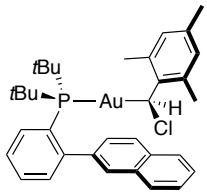

2-Di-*tert*-butylphosphinobiphenyl gold(I) chloride (338.9 mg, 0.583 mmol) was added to a Schlenk charged with a freshly prepared solution of mesityldiazomethane (3.56 mmol of starting hydrazide, 10 ml) under argon and protected by a three-walls shielding screen. The Schlenk was located in an aluminum heating block with sand and heated up to 35 ºC for 1 h. The solution was concentrated to 2 ml and stirred at 45 ºC until full conversion was observed by ^{31}P NMR. Once the starting material was consumed, the solution was allowed to cool down to room temperature. At this point, toluene was evaporated to dryness leading to an orange oil, ***be especially careful!!*** The orange oil was dissolved in 2 ml of pentane that were subsequently evaporated leading to an orange solid, the process was repeated twice. The orange solid was dissolved in dry toluene (0.5 ml) and dry pentane (2 ml). The resulting solution was cooled down to -30 ºC and stirred until white solid precipitated. The solvent was filtered off using a cannula filter leading to a pinkish-white solid that was washed with dry pentane (1 ml x 3) at -30 ºC. The resulting solid was dried

for 24 h. 2-Di-*tert*-butylphosphino-2-naphthyl chloromesityl(methyl)gold(I) carbenoid (**37e**) was obtained as a white solid in 29% yield, (120 mg, 0.168 mmol). The complex was stored in the glovebox at room temperature. X-ray quality crystals were obtained layering a toluene solution of the complex with pentane at -20 ºC under argon. The complex was a 3:1 (A:B) mixture of two regioisomers in solution.

^{1}H NMR (500 MHz, CD_2Cl_2, -90 ºC) δ 8.08 – 8.03 (A, m, 1H), 8.01 (A, d, J = 8.3 Hz, 1H), 7.91 (B, q, J = 4.7 Hz, 0.66H), 7.89 – 7.85 (B, m, 1H), 7.81 – 7.77 (B, m, 0.66H), 7.72 (B, d, J = 1.7 Hz, 0.33H), 7.61 – 7.45 (A, m, 7H), 7.37 (A, dd, J = 8.3, 1.7 Hz, 1H), 7.25 – 7.19 (B, m, 0.66H), 7.16 (B, dd, J = 8.3, 1.7 Hz, 0.33H), 6.62 (B, d, J = 9.3 Hz, 0.66H), 6.56 (A, d, J = 2.0 Hz, 1H), 6.44 (A, d, J = 2.0 Hz, 1H), 3.25 (A, d, J (^{1}H-^{31}P) = 6.0 Hz, 1H), 3.22 (B, d, J (^{1}H-^{31}P) = 6.0 Hz, 0.33H), 2.50 (A, s, 3H), 2.48 (B, s, 1H), 2.10 (B, s, 1H), 2.03 (A, s, 3H), 1.93 (B, s, 1H), 1.46 (A, d, J (^{1}H-^{31}P) = 14.7 Hz, 9H), 1.39 (B, d, J (^{1}H-^{31}P) = 14.8 Hz, 3H), 1.27 – 1.18 (B, m, 3H), 1.17 – 1.08 (A, m, 9H), 1.07 (A, s, 3H). **^{13}C NMR** (126 MHz, CD_2Cl_2, -90 ºC) δ 149.1 (d, J (^{13}C-^{31}P) = 16.1 Hz), 142.3, 140.8 (d, J (^{13}C-^{31}P) = 5.4 Hz), 137.1, 134.6, 133.6 (d, J (^{13}C-^{31}P) = 2.8 Hz), 132.6 (d, J (^{13}C-^{31}P) = 7.5 Hz), 132.5, 131.9, 129.8, 128.9, 127.8, 127.5, 127.5, 127.3 (d, J (^{13}C-^{31}P) = 5.0 Hz), 127.2 (d, J (^{13}C-^{31}P) = 3.3 Hz), 126.6, 126.4, 126.0, 99.5, 70.7 (d, J (^{13}C-^{31}P) = 107.0 Hz), 36.5 (d, J (^{13}C-^{31}P) = 20.4 Hz), 36.4 – 36.1 (m), 30.6, 29.9 (d, J (^{13}C-^{31}P) = 59.0 Hz), 21.5 (A), 20.3, 19.5. **^{31}P NMR** (162 MHz, CD_2Cl_2, -90 ºC) δ 66.47, 66.37. **HRMS** (ESI+) calculated for $C_{34}H_{41}AuP$ $(M\text{-}Cl)^+$: 677.2590; found: 677.2606.

Preparation of 1,4-di-*tert*-butyl-2-benzyldiazomethane in toluene solution

The used of protective shielding screens is highly recommended during the preparation of mesityldiazomethane solution due to the risk of explosion of aryl diazomethane compounds.

A 250 ml two-neck round-bottom flask with a findenser condenser was charged with an aqueous solution of NaOH (50 ml, 7 g, 24.5 mmol), benzyltriethylammonium chloride (0.968 g, 4.25 mmol and toluene (50 ml). (*Z*)-N'-(2,5-Di-*tert*-butylbenzylidene)-4-methylbenzenesulfonohydrazide (0.657 g, 1.70 mmol) was sequentially added, *the addition must be done following the noted order*. The flask was covered with aluminum foil and protected by a three-walls shielding screen. The resulting mixture was stirred for 2 h at 70 ºC. After being allowed to cool down to room temperature, the mixture was transferred to a separatory funnel. The red organic phase was separated from the aqueous phase and transferred to a round-bottom flask charged with NaOH pellets and covered with aluminum foil under argon. The 1,4-di-*tert*-butyl-2-benzyldiazomethane solution was deoxygenated by bubbling argon through it for 30 minutes. The dry and deoxygenated solution was transferred to an oven-dried Schlenk under argon using a syringe connected to a Teflon filter. It was concentrated to 2 ml under vacuum in the Schlenk line and layered with 2 ml of dry pentane. After being cooled down to -90 ºC for 50 minutes, white solid precipitated and the red solution was filtered at -90 ºC to a new oven-dried

Schlenk using a cannula filter. The solution was concentrated to dryness in the Schlenk line (***be especially careful at that point!!!)***. Followed by the addition of dry and deoxygenated toluene (5 ml). It was stored under argon and covered with aluminum foil in the freezer at -20 ºC until it was used the very next day.

2-Di-*tert*-butylphosphinobiphenyl chloro(1,4-di-*tert*-butyl-2-benzylmethyl)gold(I) carbenoid (37a)

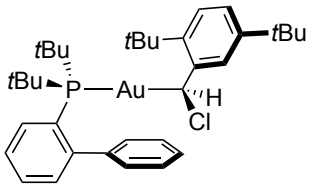

2-Di-*tert*-butylphosphinobiphenyl gold(I) chloride (100 mg, 0.188 mmol) was added to a Schlenk charged with a freshly prepared solution of mesityldiazomethane (1.7 mmol of starting hydrazide, 5 ml) under argon and protected by a three-walls shielding screen. The Schlenk was located in an aluminum heating block with sand and heated up to 55 ºC for 1 h. The solution was concentrated to 2 ml and stirred at 55 ºC until full conversion was observed by ^{31}P NMR. Once the starting material was consumed, the solution was allowed to cool down to room temperature. At this point, toluene was evaporated to dryness leading to a red oil, ***be especially careful!!*** The red oil was dissolved in 2 ml of pentane that were subsequently evaporated leading to an red solid, the process was repeated twice. A white solid precipitated and the solvent was filtered off using a cannula filter leading to a pale rose solid that was washed with dry pentane (1 ml x 3). The resulting solid was dried for 24 h. 2-Di-*tert*-butylphosphinobiphenyl chloro(1,4-di-*tert*-butyl-2-benzylmethyl) (methyl)gold(I) carbenoid (**37a**) was obtained as a white solid in 48% yield, (90 mg, 0.136 mmol). The complex was stored in the glovebox at room temperature. X-ray quality crystals were obtained layering a toluene solution of the complex with pentane at -20 ºC under argon.

^{1}H NMR (500 MHz, toluene-d_8) δ 8.03 (d, J = 2.4 Hz, 1H), 7.66 (t, J = 7.9 Hz, 1H), 7.55 – 7.49 (m, 1H), 7.49 – 7.44 (m, 1H), 7.31 (t, J = 7.9 Hz, 1H), 7.28 – 7.24 (m, 1H), 7.21 (d, J = 8.4 Hz, 1H), 7.12 – 7.08 (m, 1H), 7.05 –6.94 (m, 4H), 4.91 (d, J (^{1}H-^{31}P) = 5.2 Hz, 1H), 1.53 (s, 9H), 1.39 (s, 9H), 1.25 (d, J (^{1}H-^{31}P) = 14.4 Hz, 9H), 0.96 (d, J (^{1}H-^{31}P) = 14.5 Hz, 9H). **^{13}C NMR** (126 MHz, toluene-d_8) δ 151.0 (d, J (^{13}C-^{31}P) = 16.8 Hz), 149.8 (d, J (^{13}C-^{31}P) = 2.6 Hz), 146.8, 143.2 (d, J (^{13}C-^{31}P) = 5.5 Hz), 141.5 (d, J (^{13}C-^{31}P) = 3.3 Hz), 134.7, 133.1 (d, J (^{13}C-^{31}P) = 7.5 Hz), 132.9, 130.1 (d, J (^{13}C-^{31}P) = 2.2 Hz), 129.9, 129.6, 129.2, 128.2, 126.3 (d, J (^{13}C-^{31}P) = 5.0 Hz), 125.4, 121.1, 73.9 (d, J (^{13}C-^{31}P) = 105.3 Hz), 37.2 (d, J (^{13}C-^{31}P) = 19.1 Hz), 36.8 (d, J (^{13}C-^{31}P) = 19.0 Hz), 35.5, 34.3, 32.2, 31.7, 31.0 (d, J (^{13}C-^{31}P) = 7.1 Hz), 30.4 (d, J (^{13}C-^{31}P) = 7.0 Hz).

^{31}P NMR (202 MHz, toluene-d_8) δ 65.98. **HRMS** (ESI+) calculated for $C_{35}H_{49}AuP$ $(M\text{-}Cl)^+$: 697.3232; found: 697.3258.

General procedure for the generation of gold(I) carbenes in solution

In a glovebox, the corresponding chloromesityl(methyl)gold(I) carbenoid was weighed in an oven-dried standard NMR tube and capped with a rubber septum. Separately, $GaCl_3$ (1.2 equiv) was dissolved in CD_2Cl_2 (0.5 ml) in a HPLC vial and taken in a syringe with a long needle protected from air. Besides that, CD_2Cl_2 (0.5 ml) was taken in a syringe protected from air. Outside the glovebox, the capped NMR tube was cooled down to -90 ºC in an acetone/liquid nitrogen bath and cold CD_2Cl_2 (0.5 ml) was injected into the NMR tube. The NMR tube was shacked until the solution was homogeneous. Afterwards, the cold $GaCl_3$ solution was added over the mixture in the NMR tube at -90 ºC. The solution turned deep red instantaneously. The sample was transferred to the NMR instrument set at -90 ºC as fast as possible. The mesityl gold(I) carbenes generated were characterized by ^{1}H NMR, ^{13}C NMR, ^{31}P NMR, ^{1}H-^{13}C HSQC and ^{1}H-^{31}P HMBC.

2-Di-*tert*-butylphosphinobiphenyl mesityl gold(I) carbene (39a)

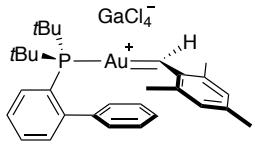

Gold(I) carbene **39a** was generated according to the general procedure from gold(I) carbenoid **37a** (5 mg, 7.5 µmol) and $GaCl_3$ (1.52 mg, 8.8 µmol). Deep red solution.

^{1}H NMR (400 MHz, CD_2Cl_2, -90 ºC) δ 12.35 (bs, 1H, *carbenic proton*), 7.90 – 7.83 (m, 1H), 7.58 – 7.49 (m, 3H), 7.27 – 7.16 (m, 5H), 7.02 – 6.94 (m, 1H), 2.87 (s, 3H), 2.54 (bs, 3H), 2.53 (bs, 3H), 1.35 (d, J (^{1}H-^{31}P) = 15.3 Hz, 18H). **^{13}C NMR** (101 MHz, CD_2Cl_2, -80 ºC) δ 290.0 (d, J (^{13}C-^{31}P) = 98.3 Hz, *carbenic carbon*), 172.4, 159.8, 156.6 (d, J (^{13}C-^{31}P) = 5.4 Hz), 151.4, 148.7 (d, J (^{13}C-^{31}P) = 14.4 Hz), 143.7 (d, J (^{13}C-^{31}P) = 5.8 Hz), 134.9, 134.1, 130.1, 128.9, 38.1 (d, J (^{13}C-^{31}P) = 26.3 Hz), 30.6, 25.2, 25.2, 22.7. *The complete assignment of carbon signals was not possible due to decomposition of the compound over time.* **^{31}P NMR** (162 MHz, CD_2Cl_2, -90 ºC) δ 64.96. Important correlations: **^{1}H-^{13}C HSQC** (CD_2Cl_2, -90 ºC), correlation between carbenic proton (12.35 ppm) and carbenic carbon (290.0 ppm). **^{1}H-^{31}P HMBC** (CD_2Cl_2, -90 ºC), correlation between carbenic proton (12.35 ppm) and ^{31}P signal (64.96 ppm).

[(2-Di-*tert*-butylphosphinobiphenylAu)$_2$Cl]$GaCl_4$ (**41a**), *E*-1,2-dimesitylethene (*E*-**20a**), *Z*-1,2-dimesitylethene (*Z*-**20a**) and 2,4,6-trimethylbenzaldehyde (**42**) were detected by NMR as minor products at -90 ºC.

2-Di-*tert*-butylphosphino-2´,4´,6´-trimethylbiphenyl mesityl gold(I) carbene (39b)

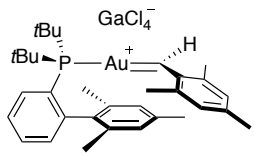

Gold(I) carbene **39b** was generated according to the general procedure from gold(I) carbenoid **37b** (5 mg, 7.09 μmol) and $GaCl_3$ (1.5 mg, 8.5 μmol). Deep red solution.

^{1}H NMR (500 MHz, CD_2Cl_2, -90 ºC) δ 12.67 (s, 1H), 7.87 (t, J = 7.6 Hz, 1H), 7.58 – 7.47 (m, 2H), 7.28 (s, 2H), 7.08 – 7.03 (m, 1H), 6.68 (s, 2H), 2.83 (s, 3H), 2.58 (s, 3H), 2.57 (s, 3H), 1.91 (s, 6H), 1.45 (s, 3H), 1.37 (d, J (^{1}H-^{31}P) = 15.3 Hz, 18H). **^{13}C{^{1}H} NMR** (126 MHz, CD_2Cl_2, -90 ºC) 288.4 (d, J (^{13}C-^{31}P) = 99.4 Hz), 171.6, 159.4, 156.1 (d, J (^{13}C-^{31}P) = 5.3 Hz), 150.4, 147.3 (d, J (^{13}C-^{31}P) = 14.9 Hz), 138.3 (d, J (^{13}C-^{31}P) = 5.3 Hz), 136.9, 136.5, 135.3, 133.7, 132.8 (d, J (^{13}C-^{31}P) = 7.7 Hz), 131.4, 128.1, 127.0 (d, J (^{13}C-^{31}P) = 6.1 Hz), 38.1 (d, J (^{13}C-^{31}P) = 27.0 Hz), 37.82 (d, J (^{13}C-^{31}P) = 27.2 Hz), 30.6, 30.6, 25.0, 24.7, 22.1, 21.3, 19.8. **^{13}C NMR** (126 MHz, CD_2Cl_2, -90 ºC) selected signals 288.4 (dd, ^1J (^{13}C-^{1}H) = 129.1 Hz, ^2J (^{13}C-^{31}P) = 99.4 Hz) **^{31}P NMR** (202 MHz, CD_2Cl_2, -90 ºC) δ 65.69. Important correlations: **^{1}H-^{13}C HSQC** (CD_2Cl_2, -90 ºC), correlation between carbenic proton (12.67 ppm) and carbenic carbon (288.4 ppm). **^{1}H-^{31}P HMBC** (CD_2Cl_2, -90 ºC), correlation between carbenic proton (12.67 ppm) and ^{31}P signal (65.69 ppm).

[(2-Di-*tert*-butylphosphino-2′,4′,6′-trimethylbiphenylAu)$_2$Cl]$GaCl_4$ (**41b**), *E*-1,2-dimesitylethene (*E*-**20a**) and 2,4,6-trimethylbenzaldehyde (**42**) were detected by NMR as minor products at -90 ºC.

2-Di-*tert*-butylphosphino-2′,6′-dimethoxybiphenyl mesityl gold(I) carbene (39c)

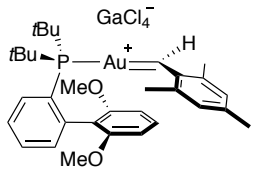

Gold(I) carbene **39c** was generated according to the general procedure from gold(I) carbenoid **37c** (5 mg, 6.9 μmol) and $GaCl_3$ (1.5 mg, 8.3 μmol). Deep red solution.

^{1}H NMR (500 MHz, CD_2Cl_2, -90 ºC) δ 12.32 (s, 1H), 7.87 (t, J = 7.7 Hz, 1H), 7.57 (t, J = 7.7 Hz, 1H), 7.50 (t, J = 7.7 Hz, 1H), 7.27 (d, J = 12.9 Hz, 2H), 7.12 – 7.08 (m, 1H), 7.03 (t, J = 8.3 Hz, 1H), 6.44 (d, J = 8.4 Hz, 2H), 3.62 (s, 6H), 2.91 (s, 3H), 2.59 (s, 3H), 2.55 (s, 3H), 1.33 (d, J (^{1}H-^{31}P) = 15.1 Hz, 18H). **^{13}C NMR** (126 MHz, CD_2Cl_2, -90 ºC) 290.0 (d, J (^{13}C-^{31}P) = 99.8 Hz), 172.4, 159.6, 158.0, 156.6 (d, J (^{13}C-^{31}P) = 5.2 Hz), 151.4 (d, J (^{13}C-^{31}P) = 3.3 Hz), 142.4 (d, J (^{13}C-^{31}P) = 14.8 Hz), 135.6, 134.1, 133.2 (d, J (^{13}C-^{31}P) = 7.8 Hz), 129.9, 129.4, 129.2, 128.4, 103.4, 55.8, 38.0 (d, J (^{13}C-^{31}P) = 26.9 Hz), 37.7 (d, J (^{13}C-^{31}P) = 27.1 Hz), 30.6 (d, J (^{13}C-^{31}P) = 5.1 Hz), 25.3, 25.1, 22.8. **^{31}P NMR** (202 MHz, CD_2Cl_2, -90 ºC) δ 66.31. Important correlations: **^{1}H-^{13}C HSQC** (CD_2Cl_2, -90 ºC), correlation between carbenic proton (12.32 ppm) and carbenic carbon (290.0 ppm). **^{1}H-^{31}P HMBC** (CD_2Cl_2, -90 ºC), correlation between carbenic proton (12.32 ppm) and ^{31}P signal (66.32 ppm).

[(2-Di-*tert*-butylphosphino-2´,6´-dimethoxybiphenylAu)$_2$Cl]$GaCl_4$ (**41c**), *E*-1,2-dimesitylethene (*E*-**20a**), *Z*-1,2-dimesitylethene (*Z*-**20a**) and 2,4,6-trimethylbenzaldehyde (**42**) were detected by NMR as minor products at -90 ºC.

2-Di-*tert*-butylphosphino-2´,4´,6´-trimethoxybiphenyl mesityl gold(I) carbene (39d)

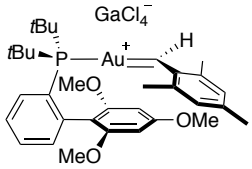

Gold(I) carbene **39d** was generated according to the general procedure from gold(I) carbenoid **37d** (5 mg, 6.6 µmol) and $GaCl_3$ (1.4 mg, 8.0 µmol). Deep red solution.

^{1}H NMR (500 MHz, CD_2Cl_2, -90 ºC) δ 12.57 (s, 1H), 7.88 – 7.82 (m, 1H), 7.56 – 7.51 (m, 1H), 7.51 – 7.44 (m, 1H), 7.29 (d, J = 13.1 Hz, 2H), 7.07 – 7.01 (m, 1H), 5.92 (s, 2H), 3.64 (bs, 6H), 3.13 (bs, 3H), 2.93 (bs, 3H), 2.61 (bs, 3H), 2.57 (bs, 3H), 1.33 (d, J (^{1}H-^{31}P) = 15.5 Hz, 18H). **^{13}C NMR** (126 MHz, CD_2Cl_2, -90 ºC) 289.0 (d, J (^{13}C-^{31}P) = 96.8 Hz), 172.2, 161.0, 158.7, 157.4 (d, J (^{13}C-^{31}P) = 5.1 Hz), 150.9 (d, J (^{13}C-^{31}P) = 3.5 Hz), 142.4 (d, J (^{13}C-^{31}P) = 17.12 Hz), 135.4, 134.1, 133.8 (d, J (^{13}C-^{31}P) = 7.6 Hz), 132.36, 129.7, 127.5 (d, J (^{13}C-^{31}P) = 6.6 Hz), 111.5, 89.6, 55.9, 55.1, 37.8 (m), 30.6 (d, J (^{13}C-^{31}P) = 3.7 Hz), 25.2, 22.4. **^{31}P NMR** (202 MHz, CD_2Cl_2, -90 ºC) δ 66.47. Important correlations: **^{1}H-^{13}C HSQC** (CD_2Cl_2, -90 ºC), correlation between carbenic proton (12.57 ppm) and carbenic carbon (289.0 ppm). **^{1}H-^{31}P HMBC** (CD_2Cl_2, -90 ºC), correlation between carbenic proton (12.57 ppm) and ^{31}P signal (66.47 ppm).

[(2-Di-*tert*-butylphosphino-2´,4´,6´-trimethoxybiphenylAu)$_2$Cl]$GaCl_4$ (**41d**), *E*-1,2-dimesitylethene (*E*-**20a**) and 2,4,6-trimethylbenzaldehyde (**42**) were detected by NMR as minor products at -90 ºC.

2-Di-*tert*-butylphosphinonapthylphenyl mesityl gold(I) carbene (39e)

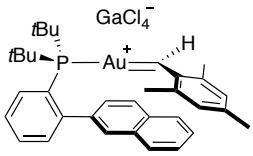

Gold(I) carbene **39e** was generated according to the general procedure from gold(I) carbenoid **37e** (4.99 mg, 7 µmol) and $GaCl_3$ (1.2 mg, 7.0 µmol). Deep red solution.

^{1}H NMR (500 MHz, CD_2Cl_2, -90 ºC) δ 11.74 (s, 1H), 7.91 (td, J = 6.9, 3.2 Hz, 1H), 7.78 (d, J = 8.4 Hz, 1H), 7.66 (s, 1H), 7.65 – 7.61 (m, 1H), 7.59 – 7.54 (m, 2H), 7.46 (d, J = 7.9 Hz, 1H), 7.34 – 7.26 (m, 2H), 7.11 – 7.04 (m, 3H), 6.99 (ddd, J = 8.1, 6.9, 1.3 Hz, 1H), 2.67 (s, 3H), 2.52 (s, 3H), 2.17 (s, 3H), 1.37 (t, J (^{1}H-^{31}P) = 16.4 Hz, 18H). **^{13}C NMR** (126 MHz, CD_2Cl_2, -90 ºC) 284.6 (d, J (^{13}C-^{31}P) = 97.8 Hz), 171.2, 158.9, 155.8 (d, J (^{13}C-^{31}P) = 5.1 Hz), 149.9 (d, J (^{13}C-^{31}P) = 3.5 Hz), 148.1 (d, J (^{13}C-^{31}P) = 14.7 Hz), 140.2 (d, J (^{13}C-^{31}P) = 6.1 Hz), 134.3, 133.2, 132.2, 132.1 (d, J (^{13}C-^{31}P) = 7.4 Hz), 131.8, 130.9, 130.4, 127.9, 127.8 (d, J (^{13}C-^{31}P) = 3.1 Hz), 127.4 (d, J (^{13}C-^{31}P) = 6.5 Hz), 126.9, 126.5 (d, J (^{13}C-^{31}P) = 12.2 Hz), 126.2, 125.6, 36.7 (d, J (^{13}C-^{31}P) =

22.1 Hz), 36.5 (d, J (^{13}C-^{31}P)= 22.3 Hz), 30.2, 29.9, 24.6, 24.5, 21.7. **^{31}P NMR** (202 MHz, CD_2Cl_2, -90 ºC) δ 65.38. Important correlations: **^{1}H-^{31}P HMBC** (CD_2Cl_2, -90 ºC), correlation between carbenic proton (11.74 ppm) and ^{31}P signal (65.38 ppm).

[(2-Di-*tert*-butylphosphinonapthylphenylAu)$_2$Cl]$GaCl_4$ (**41e**) and 2,4,6-trimethylbenzaldehyde (**42**) were detected by NMR as minor products at -90 ºC.

General procedure for the synthesis of phosphonium ylide complexes 40

In a glovebox, the corresponding gold(I) carbenoid was weighed in a Schlenk. Separately, $GaCl_3$ (1 equiv) was dissolved in dry CH_2Cl_2 (1 ml) in a HPLC vial and taken out in a syringe protected from air. A solution of PPh_3 (1 equiv) in dry CH_2Cl_2 (1 ml) was prepared and taken in a syringe protected from air. Besides that, dry CH_2Cl_2 (2 ml) was also taken in a syringe protected from air. The Schlenk was cooled down to -90 ºC and CH_2Cl_2 (2 ml) was added. Followed by the addition of $GaCl_3$ solution at the same temperature leading to a dark red solution. Afterwards, the PPh_3 solution was added over the mixture at -90 ºC. The color faded away immediately after the addition of PPh_3 generating a colorless solution. The sample was allowed to warm up to room temperature. A white solid was obtained after evaporation of the solvent under vacuum in the line. The white solid was washed with dry pentane (1 ml x 3) and dried in the line. A mixture of two inseparable gold(I) complexes **40** and **S1/S2** was obtained. The complexes were stored in the glovebox at room temperature.

Synthesis of phosphonium ylide complex 40a

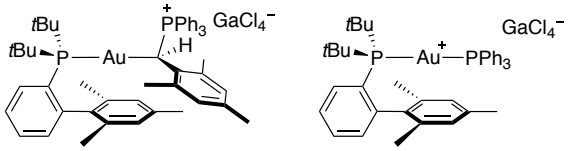

40a **S1**

Phosphonium ylide complex **40a** was synthetized following the general procedure from gold(I) carbenoid **37b** (30.0 mg, 0.043 mmol), $GaCl_3$ (7.5 mg, 0.043 mmol) and PPh_3 (11.16 mg, 0.043 mmol). Complex **40a** was obtained as a mixture with complex **S1** (29.2 mg, **40a**:**S1** = 7:1). The complexes were stored in the glovebox at room temperature. X-ray quality crystals were obtained layering a CD_2Cl_2 solution of the complex with dry toluene under argon at -20 ºC.

^{1}H NMR (500 MHz, CD_2Cl_2) δ 7.93 (td, J = 7.4, 1.8 Hz, 1H), 7.74 – 7.68 (m, 2H), 7.53 – 7.43 (m, 8H), 7.34 – 7.28 (m, 7H), 6.86 (ddd, J = 7.4, 4.4, 1.8 Hz, 1H), 6.78 (d, J = 3.9 Hz, 2H), 6.77 (s, 1H), 6.27 (s, 1H), 3.67 (dd, J (^{1}H-^{31}P) = 18.9, 9.1 Hz, 1H), 2.31 (d, J (^{1}H-^{31}P) = 3.1 Hz, 3H), 2.03 (d, J (^{1}H-^{31}P) = 1.9 Hz, 3H), 1.96 (s, 3H), 1.92 (s, 3H), 1.72 (s, 3H), 1.66 (d, J (^{1}H-^{31}P) 1.5 Hz, 3H), 1.47 (d, J (^{1}H-^{31}P) = 15.0 Hz, 9H), 1.07 (d, J (^{1}H-^{31}P) = 15.0 Hz, 9H). **^{13}C NMR** (126 MHz, CD_2Cl_2) δ 149.2 (d, J (^{13}C-^{31}P) = 14.6 Hz), 139.9 (dd, J (^{13}C-^{31}P) = 7.6, 3.5 Hz), 139.3 (d, J (^{13}C-^{31}P) = 4.41 Hz),138.0, 137.6 (dd, J (^{13}C-^{31}P) = 6.0, 2.9 Hz), 136.7, 136.4, 136.1, 134.5 (d, J (^{13}C-^{31}P) = 9.1 Hz), 134.4 (d, J (^{13}C-^{31}P) = 2.7 Hz), 132.1 (d, J (^{13}C-^{31}P) = 2.5 Hz), 131.1 (d, J

(^{13}C-^{31}P) = 4.4 Hz), 130.9 (d, *J* (^{13}C-^{31}P) = 3.9 Hz), 129.9, 129.0 (d, *J* (^{13}C-^{31}P) = 8.2 Hz), 127.1 (d, *J* (^{13}C-^{31}P) = 6.1 Hz), 123.8, 123.1, 38.4 (d, *J* (^{13}C-^{31}P) = 21.3 Hz), 35.2 (dd, *J* (^{13}C-^{31}P) = 80.2, 28.5 Hz), 31.8 (d, *J* (^{13}C-^{31}P) = 5.9 Hz), 31.25 (d, *J* (^{13}C-^{31}P) = 6.4 Hz), 23.9, 22.5, 22.3, 21.5, 21.0. **^{31}P NMR** (202 MHz, CD_2Cl_2) δ 69.50 (d, *J* (^{31}P-^{31}P) = 4.3 Hz), 27.21 (d, *J* (^{31}P-^{31}P) = 4.9 Hz). **^{1}H-^{13}C HSQC** (CD_2Cl_2, 25 ºC), correlation between H1 (3.67 ppm) and C1 (35.2 ppm) signals. **^{1}H-^{31}P HMBC** (CD_2Cl_2, 25 ºC), correlation between H1 (3.67 ppm) and ^{31}P signals (69.50 and 27.21 ppm). **HRMS** (ESI+) calculated for $C_{51}H_{60}AuP_2$ (M-$GaCl_4$)$^+$: 931.3830; found: 931.3811.

Synthesis of phosphonium ylide complex 40b

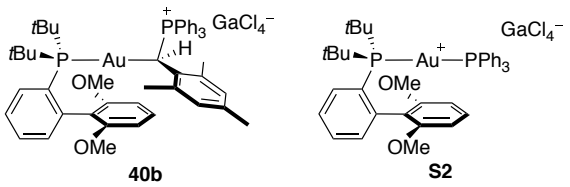

Phosphonium ylide complex **40b** was synthetized following the general procedure from gold(I) carbenoid **37c** (30.0 mg, 0.041 mmol), $GaCl_3$ (7.3 mg, 0.041 mmol) and PPh_3 (10.9 mg, 0.041 mmol). Complex **40b** was obtained as a mixture with complex **S2** (41.5 mg, **40b**:**S2** = 6:1). The complexes were stored in the glovebox at room temperature. X-ray quality crystals were obtained layering a CD_2Cl_2 solution of the complex with dry pentane under argon at -20 ºC.

Data listed as a mixture of gold(I) complexes **40b**:**S2** (6:1).

^{1}H NMR (400 MHz, CD_2Cl_2) δ 7.88 (**S2**, td, *J* = 7.6, 1.5 Hz, 1H), 7.76 – 7.69 (**40b**, m, 3H), 7.66 (**S2**, td, *J* = 7.3, 1.8 Hz, 0.5H), 7.62 – 7.52 (**S2**, m, 1.5H), 7.51 – 7.44 (**40b**, m, 8H), 7.42 (**S2**, t, *J* = 1.5 Hz, 0.5H), 7.41 (**S2**, t, *J* = 1.5 Hz, 0.35H), 7.40 – 7-31 (**40b**, m, 7H), 7.11 – 7.05 (**S2**, m, 0.17H), 6.94 (**40b**, ddd, *J* = 7.5, 4.2, 1.7 Hz, 1H), 6.82 (**40b**, d, *J* = 7.5 Hz, 1H), 6.75 (**40b**, t, *J* = 8.3 Hz, 1H), 6.60 (**40b**, dd, *J* = 8.4, 0.9 Hz, 1H), 6.45 (**S2**, t, *J* = 8.4 Hz, 0.17H), 6.11 (**S2**, d, *J* = 8.4 Hz, 0.35H), 5.58 (**40b**, d, *J* = 8.5 Hz, 1H), 3.71 (**40b**, s, 3H), 3.61 (**S2**, s, 1H), 3.40 (**40b**, dd, *J* (^{1}H-^{31}P) = 18.8, 9.1 Hz, 1H), 3.22 (**40b**, s, 3H), 2.33 (**40b**, d, *J* (^{1}H-^{31}P) = 3.1 Hz, 3H), 2.12 (**S2**, s, 0.5H), 2.09 (**40b**, d, *J* (^{1}H-^{31}P) = 1.9 Hz, 3H), 1.67 (**40b**, s, 3H), 1.48 (**S2**, d, *J* (^{1}H-^{31}P) = 15.7 Hz, 3H), 1.47 (**40b**, d, *J* (^{1}H-^{31}P) = 15.0 Hz, 9H), 1.04 (**40b**, d, *J* (^{1}H-^{31}P)= 15.1 Hz, 9H). **^{13}C NMR** (101 MHz, CD_2Cl_2) δ 157.8 (**40b**, d, *J* (^{13}C-^{31}P) = 39.4 Hz), 143.5 (**40b**, d, *J* (^{13}C-^{31}P) = 14.9 Hz), 140.9 (**40b**, dd, *J* (^{13}C-^{31}P) = 7.4, 3.4 Hz), 137.7 (**40b**, d, *J* (^{13}C-^{31}P) = 4.4), 136.7 (**40b**, d, *J* (^{13}C-^{31}P) = 4.4 Hz), 135.2 (**40b**, d, *J* (^{13}C-^{31}P) = 1.7 Hz), 134.7 (**S2**, d, *J* (^{13}C-^{31}P) = 13.0 Hz), 134.5 (**40b**, d, *J* (^{13}C-^{31}P) = 8.7 Hz), 134.1 (**40b**, d, *J* (^{13}C-^{31}P) = 8.2 Hz), 133.1 (**S2**, d, *J* (^{13}C-^{31}P) = 2.6 Hz), 131.5 (**40b**, d, *J* (^{13}C-^{31}P) = 2.2 Hz), 131.4 (**40b**), 131.2 (**S2**, d, *J* (^{13}C-^{31}P) = 2.2 Hz), 131.1 (**S2**, d, *J* (^{13}C-^{31}P) = 2.3 Hz), 131.0 (**40b**, d, *J* (^{13}C-^{31}P) = 4.2 Hz), 130.7 (**S2**), 130.4 (**40b**, d, *J* (^{13}C-^{31}P) = 4.0 Hz), 130.1 (**S2**, d, *J* (^{13}C-^{31}P) = 11.3 Hz), 129.9 (**40b**, d, *J* (^{13}C-^{31}P) = 11.5 Hz), 127.0 (**40b**, d, *J* (^{13}C-^{31}P) = 6.4 Hz), 123.9 (**40b**), 123.1 (**40b**), 119.8 (**S2**, d, *J* (^{13}C-^{31}P) = 5.9 Hz), 104.9 (**S2**), 103.7 (**40b**), 102.9 (**40b**), 55.9 (Y), 55.9 (**40b**), 55.0 (**40b**), 38.9 (Y, d, *J* (^{13}C-^{31}P) =22

Hz), 38.1 (**40b**, d, *J* (^{13}C-^{31}P) = 19.4 Hz), 37.9 (**40b**, d, *J* (^{13}C-^{31}P) = 18.9 Hz), 35.5 (**40b**, dd, *J* (^{13}C-^{31}P) = 81.4, 28.8 Hz), 34.7 (**S2**), 31.56 (**S2**, d, *J* (^{13}C-^{31}P) = 5.6 Hz), 31.5 (**40b**, d, *J* (^{13}C-^{31}P) = 6.5 Hz), 30.7 (**40b**, d, *J* (^{13}C-^{31}P) = 6.5 Hz), 24.1 (**40b**, d, *J* (^{13}C-^{31}P) = 1.9 Hz), 22.9 (**S2**), 22.8 (**40b**, d, *J* (^{13}C-^{31}P) = 1.3 Hz), 21.1 (**40b**, d, *J* (^{13}C-^{31}P) = 1.7 Hz), 14.38 (**S2**). **^{31}P NMR** (162 MHz, CD_2Cl_2) δ 73.22 (**S2**, d, *J* (^{31}P-^{31}P) = 300.4 Hz), 69.68 (**40b**, d, *J* (^{31}P-^{31}P) = 5.0 Hz), 47.27 (**S2**, d, *J* (^{31}P-^{31}P) = 300.3 Hz), 26.82 (**40b**, d, *J* (^{31}P-^{31}P) = 4.9 Hz). **^{1}H-^{31}P HMBC** (CD_2Cl_2, 25 ºC), correlation between carbenic proton (3.40 ppm) and ^{31}P signals (69.68 and 26.82 ppm). Some signals coming from **S2** are missing due to the low amount of complex present in the analysed mixture. **HRMS** (ESI+) calculated for $C_{50}H_{58}AuO_2P_2$ (M-$GaCl_4$)$^+$: 949.3572; found: 949.3527.

Synthesis of [oMeOJPAuPPh$_3$]GaCl$_4$ (S2)

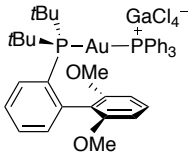

Inside the glovebox, 2-Di-*t*-butylphosphino-2´,6´-dimethoxybiphenyl gold(I) chloride (10.0 mg, 0.017 mmol) was dissolved in dry CD_2Cl_2 (0.4 ml) in an oven-dried standard NMR tube and capped with a rubber septum. Separately, $GaCl_3$ (3.0 mg, 0.017 mmol) was dissolved in CD_2Cl_2 (0.3 ml) in a HPLC vial and taken in a syringe protected from air. Besides that, a solution of PPh_3 (4.4 mg, 0.017 mmol) in dry CD_2Cl_2 (0.3 ml) was also taken in a syringe protected from air. Outside the glovebox, the PPh_3 solution was injected into the NMR tube. Followed by the addition of the $GaCl_3$ solution. The solution was analyzed by NMR. X-ray quality crystals were obtained layering a CD_2Cl_2 solution of the complex with dry pentane under argon at -20 ºC.

^{1}H NMR (500 MHz, CD_2Cl_2) δ 7.94 (td, *J* = 7.7, 1.4 Hz, 1H), 7.74 – 7.66 (m, 2H), 7.64 – 7.58 (m, 8H), 7.42 – 7.36 (m, 7H), 7.12 (ddd, *J* = 7.7, 4.5, 1.6 Hz, 1H), 6.49 (t, *J* = 8.3 Hz, 1H), 6.15 (d, *J* = 8.4 Hz, 2H), 3.65 (s, 6H), 1.52 (d, *J* (^{1}H-^{31}P) = 15.8 Hz, 18H). **^{13}C NMR** (126 MHz, CD_2Cl_2) δ 157.9, 135.2 (dd, *J* (^{13}C-^{31}P) = 4.6, 2.3 Hz), 134.7 (d, *J* (^{13}C-^{31}P) = 13.4 Hz), 134.4, 134.2 (d, *J* (^{13}C-^{31}P) = 8.4 Hz), 133.0 (d, *J* (^{13}C-^{31}P) = 2.7 Hz), 132.4 (d, *J* (^{13}C-^{31}P) = 2.4 Hz), 130.7, 130.1 (d, *J* (^{13}C-^{31}P) = 11.4 Hz), 129.8 (d, *J* (^{13}C-^{31}P) = 24.3 Hz), 128.6 (d, *J* (^{13}C-^{31}P) = 1.7 Hz), 128.1 (d, *J* (^{13}C-^{31}P) = 1.8 Hz), 127.8 (d, *J* (^{13}C-^{31}P) = 6.6 Hz), 104.9, 55.9, 38.9 (d, *J* (^{13}C-^{31}P) = 21.9 Hz), 31.6 (d, *J* (^{13}C-^{31}P) = 6.3 Hz). **^{31}P NMR** (203 MHz, CD_2Cl_2) δ 73.18 (d, *J* (^{31}P-^{31}P) = 300.4 Hz), 47.25 (d, *J* (^{31}P-^{31}P) = 300.3 Hz).

General procedure for the thermal stability test of complexes 40a-b

In a glovebox, phosphonium ylide gold(I) complexes **40a-b** (5 mg) were weighed in an oven-dried NMR tube and dissolved in dry 1,1,2,2-tethrachloroethane-*d*$_4$ (0.5 ml). ^{1}H NMR and ^{31}P NMR spectra were taken every 10 ºC from 25 to 125 ºC. No decomposition was observed through any experiment.

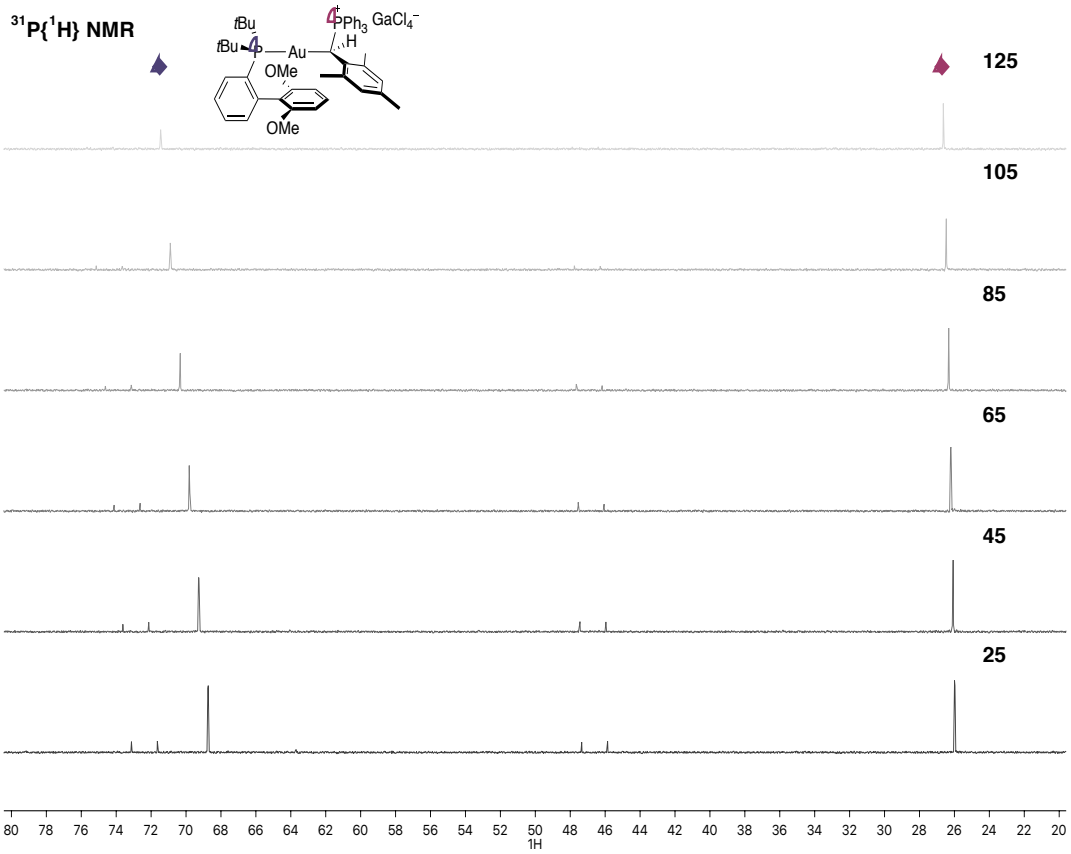

Figure 25. Thermal stability of phosphonium ylide complex **40a**

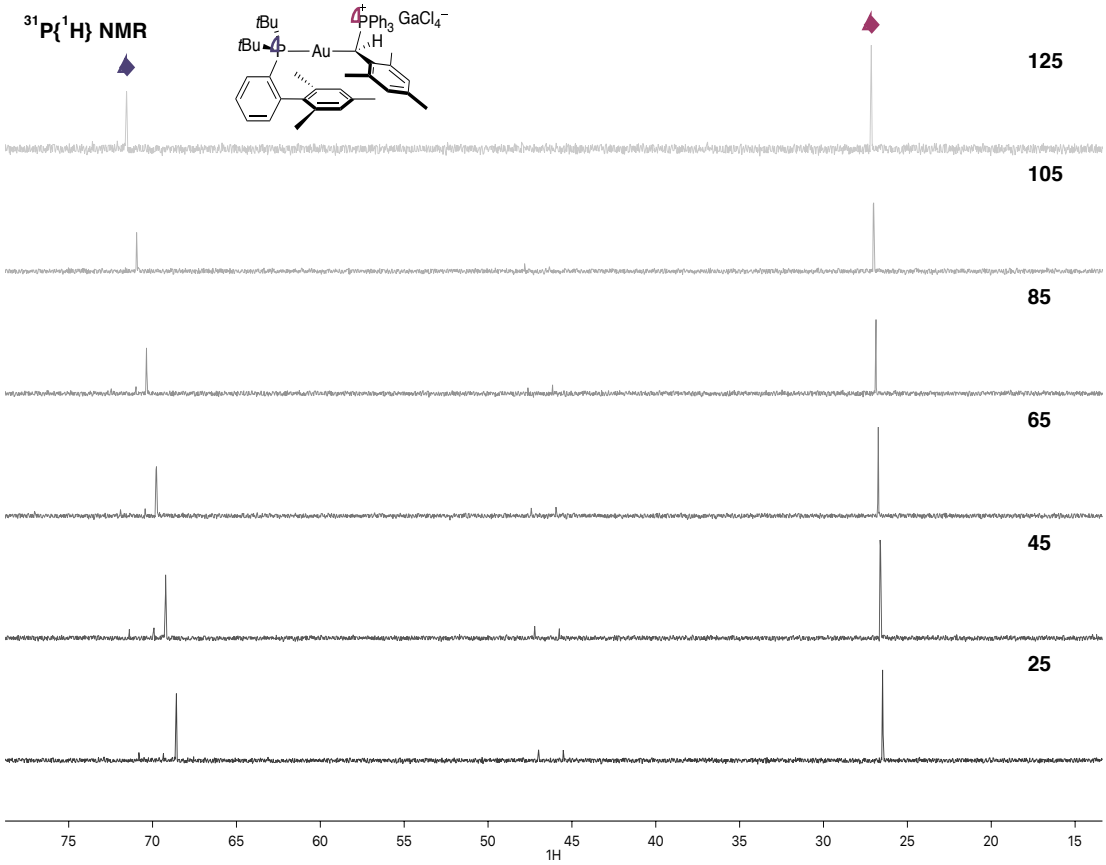

Figure 26. Thermal stability of phosphonium ylide complex **40b**

Thermal stability of mesityl gold(I) carbenes

General procedures for the quantification of the decay of gold(I) carbenes in solution

Procedure A: In a glovebox, the corresponding chloromesityl(methyl)gold(I) carbenoid (0.007 mmol) was weighed in an oven-dried standard NMR tube and capped with a rubber septum. Separately, $GaCl_3$ (1.0 equiv) was dissolved in CD_2Cl_2 (0.4 ml) in a HPLC vial and taken in a syringe with a long needle protected from air. Besides that, CD_2Cl_2 (0.5 ml) and a solution of 1,3,5-trifluoromethylbenzene used as internal standard (0.1 ml, 0.007 mmol, 0.07 M) was taken in a syringe protected from air. Outside the glovebox, the capped NMR tube was cooled down to -90 ºC in an acetone/liquid nitrogen cooling bath and CD_2Cl_2 (0.5 ml) was injected into the NMR tube. The NMR tube was shacked until the solution was homogeneous. Afterwards, a solution of the internal standard (0.1 ml) was added to the previous solution at -90 ºC. A ^1H NMR was taken at -90 ºC to calculate the exact amount of chloromesityl(methyl) gold(I) carbenoid in every case. The NMR tube was ejected and cooled down to -90 ºC in the acetone/liquid nitrogen cooling bath again. Ultimately, the $GaCl_3$ solution was added over the mixture in the NMR tube at -90 ºC. The solution turned deep red instantaneously. The sample was transferred to the NMR instrument set at -90 ºC as fast as possible. ^1H and ^{31}P NMR experiments were taken every ten degrees, from -90 ºC to the mesityl gold(I) carbene decomposition temperature.

Procedure B: In a glovebox, the corresponding chloromesityl(methyl)gold(I) carbenoid (0.007 mmol) was weighed in an oven-dried standard NMR tube and capped with a rubber septum. Separately, $GaCl_3$ (1.0 equiv) was dissolved in CD_2Cl_2 (0.4 ml) in a HPLC vial and taken in a syringe with a long needle protected from air. Besides that, CD_2Cl_2 (0.5 ml) and a solution of 1,3,5-trifluoromethylbenzene used as internal standard (0.1 ml, 0.007 mmol, 0.07 M) was taken in a syringe protected from air. Outside the glovebox, the capped NMR tube was cooled down to 0 ºC in and CD_2Cl_2 (0.5 ml) was injected into the NMR tube. The NMR tube was shacked until the solution was homogeneous. Afterwards, a solution of the internal standard (0.1 ml) was added to the previous solution at 0 ºC. Ultimately, the $GaCl_3$ solution was added over the mixture in the NMR tube at 0 ºC. The turned deep red and the color faded away instantaneously. After 10 minutes at 0 ºC, the solution was warmed up to room temperature and the yield was calculated by ^1H NMR.

Kinetics Measurements

In a glovebox, gold(I) carbenoid **39b** (0.007 mmol) was weighed in an oven-dried standard NMR tube and capped with a rubber septum. Separately, $GaCl_3$ solution in CD_2Cl_2 (0.4 ml, 0.007 mmol, 0.11 M) was taken out with a Hamilton syringe connected to a long protected from air. Besides that, CD_2Cl_2 (0.5 ml) and a solution of 1,3,5-trifluoromethylbenzene used as internal standard (0.1 ml, 0.007 mmol, 0.07 M) were taken in Hamilton syringes protected from air. Outside the glovebox, the capped NMR tube was cooled down to -90 ºC in an acetone/liquid nitrogen cooling

bath and CD_2Cl_2 (0.5 ml) was injected into the NMR tube. The NMR tube was shacked until the solution was homogeneous. Afterwards, the internal standard (0.1 ml) was added to the previous solution at -90 ºC. Ultimately, the $GaCl_3$ solution was added over the mixture in the NMR tube at -90 ºC. The solution turned deep red instantaneously. The sample was transferred to the NMR instrument set at -40 ºC or -35 ºC as fast as possible. ^{1}H experiments were taken every two minutes until full consumption of gold(I) carbene **39b**.

General procedure for the synthesis of chloride bridge digold(I) complexes

In a Schlenk in the glovebox, the corresponding gold(I) chloride complex was dissolved in dry CH_2Cl_2. Followed by the one pot addition of a dichloromethane solution of $GaCl_3$ at 25 ºC. The Schlenk was taken out from the glovebox and stirred under argon. After 15 minutes, the solution was concentrated to dryness in the Schlenk line giving a solid that was washed with pentane (x3). The complexes were stored in the glovebox.

[(2-Di-*tert*-butylphosphinobiphenylAu)$_2$Cl]GaCl$_4$ (41a)

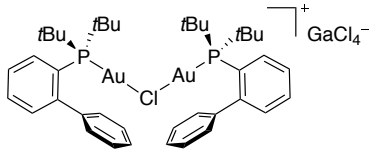

Complex **41a** was synthetized according to the general procedure from 2-di-*t*-butylphosphinobiphenyl gold(I) chloride (**32a**) (50 mg, 0.094 mmol) and $GaCl_3$ (8.3 mg, 0.047 mmol). A white solid was obtained in 52% yield (60 mg, 0.048 mmol). X-ray quality crystals were obtained layering a CD_2Cl_2 solution of the complex with dry pentane under argon at -20 ºC. **^{1}H NMR** (400 MHz, CD_2Cl_2) δ 7.93 – 7.84 (m, 2H), 7.64 – 7.56 (m, 4H), 7.55 – 7.48 (m, 2H), 7.43 – 7.35 (m, 4H), 7.34 – 7.28 (m, 2H), 7.17 – 7.11 (m, 4H), 1.40 (d, J (^{1}H-^{31}P) = 16.1 Hz, 36H). **^{13}C NMR** (101 MHz, CD_2Cl_2) δ 149.8 (d, J (^{13}C-^{31}P) = 12.4 Hz), 143.1 (d, J (^{13}C-^{31}P) = 6.7 Hz), 133.9 (d, J (^{13}C-^{31}P) = 3.3 Hz), 133.8, 131.9, 130.0, 129.3, 128.8, 128.1 (d, J (^{13}C-^{31}P) = 7.3 Hz), 125.0 (d, J (^{13}C-^{31}P) = 49.5 Hz), 38.7 (d, J (^{13}C-^{31}P) = 26.0 Hz), 31.3 (d, J (^{13}C-^{31}P) = 6.4 Hz). **^{31}P NMR** (162 MHz, CD_2Cl_2) δ 64.68. **HRMS** (ESI+) calculated for $C_{40}H_{54}Au_2ClP_2$ (M-$GaCl_4$)$^+$: 1025.2715; found: 1025.2667.

[(2-Di-*tert*-butyl-2´,4´,6´-trimethylphosphinobiphenylAu)$_2$Cl]GaCl$_4$ (41b)

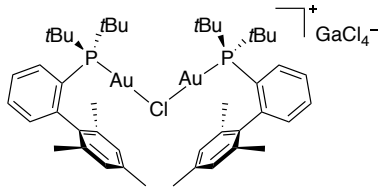

Complex X was synthetized according to the general procedure from 2-di-*t*-butyl-2´,4´,6´-trimethylphosphinobiphenyl gold(I) chloride (**32b**) (30 mg, 0.052 mmol) and $GaCl_3$ (4.62 mg, 0.026 mmol). A white solid was obtained in 43% yield (30 mg, 0.023 mmol).

^{1}H NMR (400 MHz, CD_2Cl_2) δ 7.93 – 7.85 (m, 2H), 7.68 – 7.60 (m, 2H), 7.60 – 7.52 (m, 2H), 7.21 (ddd, J = 7.8, 4.7, 1.6 Hz, 2H), 6.92 (s, 4H), 2.40 (s, 6H), 1.90 (s, 12H), 1.42 (d, J (^{1}H-^{31}P) = 16.1 Hz, 36H). **^{13}C NMR** (101 MHz, CD_2Cl_2) δ 148.9 (d, J (^{13}C-^{31}P) = 12.8 Hz), 138.9, 138.3 (d, J (^{13}C-^{31}P) = 6.2 Hz), 136.6, 134.8 (d, J (^{13}C-^{31}P) = 3.9 Hz), 134.4 (d, J (^{13}C-^{31}P) = 8.0 Hz), 132.8, 129.7, 127.8 (d, J (^{13}C-^{31}P) = 7.4 Hz), 126.4 (d, J (^{13}C-^{31}P) = 47.9 Hz), 39.1 (d, J (^{13}C-^{31}P) = 26.8 Hz), 31.8 (d, J (^{13}C-^{31}P) = 6.2 Hz), 22.0, 21.7. **^{31}P NMR** (162 MHz, CD_2Cl_2) δ 63.78. **HRMS** (ESI+) calculated for $C_{46}H_{66}Au_2ClP_2$ (M-$GaCl_4$)$^{+}$: 1109.3654; found: 1109.3687.

[(2-Di-*tert*-butyl-2´,6´-dimethoxyphosphinobiphenylAu)$_2$Cl]GaCl$_4$ (41c)

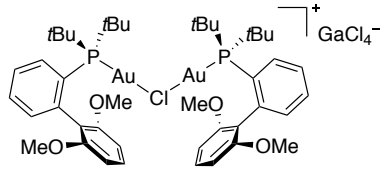

Complex **41c** was synthetized according to the general procedure from 2-di-*tert*-butyl-2´,6´-dimethoxyphosphinobiphenyl gold(I) chloride (**32c**) (20 mg, 0.034 mmol) and $GaCl_3$ (2.98 mg, 0.017 mmol). A white solid was obtained in 28.3% yield (13 mg, 0.010 mmol). X-ray quality crystals were from the decomposition of gold(I) carbene **41c** at -90 ºC in toluene.

^{1}H NMR (400 MHz, CD_2Cl_2) δ 7.91 – 7.82 (m, 1H), 7.63 – 7.56 (m, 1H), 7.55 – 7.45 (m, 2H), 7.18 (ddd, J = 7.7, 4.4, 1.6 Hz, 1H), 6.61 (d, J = 8.4 Hz, 2H), 3.64 (s, 6H), 1.38 (d, J (^{1}H-^{31}P) = 16.0 Hz, 18H). **^{13}C NMR** (126 MHz, CD_2Cl_2) δ 158.1, 143.6 (d, J (^{13}C-^{31}P) = 12.0 Hz), 134.5 (d, J (^{13}C-^{31}P) = 7.8 Hz), 134.1 (bs), 132.0 (bs), 130.8, 127.4 (d, J (^{13}C-^{31}P) = 6.0 Hz), 119.9 (d, J (^{13}C-^{31}P) = 7.0 Hz), 104.7, 55.8, 38.4 (d, J (^{13}C-^{31}P) = 26.6 Hz), 31.3 (d, J (^{13}C-^{31}P) = 6.7 Hz). **^{31}P NMR** (203 MHz, CD_2Cl_2) δ 65.79 (bs). **HRMS** (ESI+) calculated for $C_{44}H_{62}Au_2ClP_2$ (M-$GaCl_4$)$^{+}$: 1145.3138; found: 1145.3157.

Characterization of detected organic products

E-1,2-dimesitylethene (*E*-**20a**), *Z*-1,2-dimesitylethene (*Z*-**20a**), 2,4,6-trimethylbenzaldehyde (**42**) and 1,2,3-trimesitylcyclopropane (**21a**) were detected by ^{1}H NMR and GCMS as organic products from the decomposition of mesityl gold(I) carbenes **39a-e** from the reaction crudes.

The ^{1}H NMR data of *E*-1,2-dimesitylethene (*E*-**20a**)[46] and *Z*-1,2-dimesitylethene (*Z*-**20a**)[46] were identical to the previously reported. The ^{1}H NMR data of 2,4,6-trimethylbenzaldehyde (**42**) was compared to an original sample purchased from commercial sources. However, 1,2,3-trimesitylcyclopropane (**21a**) was isolated from the reaction crude and characterized.

46 Zhao, Y.-P.; Yang, Y.-L.; Liu, R. S. H. *Green Chem.* **2009**, *11*, 837–842.

1,2,3-trimesitylcyclopropane (21a)

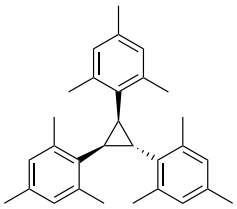

Gold(I) carbene **39c** was generated according to the general procedure for the generation of gold(I) carbenes in solution from gold(I) carbenoid **39c** (20 mg, 0.028 mmol) and $GaCl_3$ (5.84 mg, 0.033 mmol) at -90 ºC. The tube NMR was allowed to warm up to room temperature and the solution was filtered through a small pad of celite. Cyclopropane **21a** was obtained from the reaction crude as a yellowish oil after purification by preparative TLC with pentane as eluent.

^{1}H NMR (500 MHz, CD_2Cl_2) δ 6.83 (s, 2H), 6.70 (s, 4H), 3.79 (t, J = 7.1 Hz, 1H), 2.63 (d, J = 7.1 Hz, 2H), 2.36 (s, 6H), 2.24 (s, 3H), 2.22 (s, 12H), 2.18 (s, 6H). **^{13}C NMR** (126 MHz, CD_2Cl_2) δ 137.8, 137.5, 136.1, 135.41, 135.0, 132.2, 129.8, 129.3, 31.9, 26.3, 21.4, 20.7, 20.4, 20.3. The configuration was assigned by COSY, ^{1}H-^{13}C HSQC and NOESY. **HRMS** (APCI+) calculated for $C_{30}H_{37}$ $(M+H)^+$: 397.2886; found: 397.2890.

Gold(I) promoted oxidation

Procedure A: Generation of mesityl gold(I) carbenes in the presence of pyridine N-oxide.

In a glovebox, the corresponding chloromesityl(methyl)gold(I) carbenoid (0.007 mmol) was weighed in an oven-dried microwave vial and capped. Separately, $GaCl_3$ (1 equiv) was dissolved in dry CD_2Cl_2 (0.3 ml) in a HPLC vial and taken in a syringe protected from air. A solution of pyridine N-oxide (10 equiv) in dry CD_2Cl_2 (0.2 ml) was prepared and taken in a syringe protected from air. Besides that, dry CD_2Cl_2 (0.5 ml) was also taken in a syringe protected from air. The microwave vial was cooled down to -90 ºC and CD_2Cl_2 (0.5 ml) was added. Afterwards, the $GaCl_3$ solution was added over the solution in the microwave vial at -90 ºC. Followed by the addition of the pyridine N-oxide solution. The sample was kept at -90 ºC for two minutes and allowed to warm up to room temperature. Followed by the addition of a CD_2Cl_2 solution of diphenylmethane (0.05 mmol, 0.1 ml, 0.5 M). The reaction was opened to air and transferred to a NMR tube. The yield was calculated by integration of the ^{1}H NMR of the product and the internal standard.

2,4,6-trimethylbenzaldehyde **42** was detected by ^{1}H NMR and GCMS from the crude reactions of the oxidation. The ^{1}H NMR data of 2,4,6-trimethylbenzaldehyde **42** was identical to the data of an original sample.

Procedure B: Generation of mesityl gold(I) carbenes in the presence of oxygen.

In a glovebox, the corresponding chloromesityl(methyl)gold(I) carbenoid (0.007 mmol) was weighed in an oven-dried microwave vial and capped. Separately, $GaCl_3$ (1 equiv) was dissolved in dry CD_2Cl_2 (0.5 ml) in a HPLC vial and taken in a syringe protected from air. Besides that, dry CD_2Cl_2 (0.5 ml) was also taken in a syringe protected from air. The microwave vial was cooled

down to -90 ºC and CD_2Cl_2 (0.5 ml) was added. Afterwards, the $GaCl_3$ solution was added over the mixture in the microwave vial at -90 ºC. Oxygen was bubble through the mixture until the dark red color of the solution faded away, approximately 1 minute. The sample was allowed to warm up to room temperature. Followed by the addition of a CD_2Cl_2 solution of diphenylmethane (0.05 mmol, 0.1 ml, 0.5 M). The reaction was opened to air and transferred to a NMR tube. The yield was calculated by integration of the ^{1}H NMR of the product and the internal standard.
2,4,6-trimethylbenzaldehyde **42** was detected by ^{1}H NMR and GCMS from the crude reactions of the oxidation.

Gold(I)-promoted/catalyzed cyclopropanation of alkenes

7-mesitylcyclohepta-1,3,5-triene (18a)

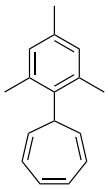

This compound was prepared following a reported procedure for the synthesis of cyclohepta-1,3,5-trienes.[23a] An oven-dried two-neck round-bottom flask equipped with a condenser was charged with magnesium turnings (243 mg, 10.0 mmol), dry THF (30 ml) and two drops of 1,2-dibromoethane. A solution of 2-bromo-1,3,5-trimethylbenzene (995 mg, 5 mmol) in dry THF (10 ml) was added slowly over a period of 30 minutes at room temperature. The mixture was heated up to 70 °C for 1 h and then allowed to cool down to room temperature. Then tropylium tetrafluoroborate (1.335 g, 7.5 mmol) was added in one portion and the reaction was stirred at room temperature for 14 h. Then, the mixture was washed with sat. NH_4Cl solution and extracted with ethyl acetate. The combined organic extracts were dried over $MgSO_4$, filtered and concentrated *in vacuo*. 7-Mesitylcyclohepta-1,3,5-triene (**18a**) was obtained as a white solid in 40% yield (420 mg, 2 mmol) after purification by flash column chromatography using cyclohexane as eluent.
^{1}H NMR (300 MHz, $CDCl_3$) δ 6.90 (s, 2H), 6.61 (t, J = 3.3 Hz, 2H), 6.21 – 6.12 (m, 2H), 5.38 – 5.27 (m, 2H), 3.50 – 3.41 (m, 1H), 2.28 (s, 9H). **^{13}C NMR** (126 MHz, $CDCl_3$) δ 137.3, 136.5, 135.9, 130.9, 130.0, 129.3, 124.7, 40.4, 27.1, 21.6, 20.9. **HRMS** (APCI+) calculated for $C_{16}H_{19}$ (M+H): 211.1481; found: 211.1480.

General procedure for the gold(I)-promoted alkene cyclopropanation

Procedure A: Generation of mesityl gold(I) carbenes in the presence of alkenes
In a glovebox, the corresponding chloromesityl(methyl)gold(I) carbenoid (0.007 mmol) was weighed in an oven-dried microwave vial and capped. Separately, $GaCl_3$ (1 equiv) was dissolved in dry CD_2Cl_2 (0.3 ml) in a HPLC vial and taken in a syringe protected from air. A solution of the corresponding alkene (10 equiv) in dry CD_2Cl_2 (0.2 ml) was prepared and taken in a syringe

protected from air. Besides that, dry CD_2Cl_2 (0.5 ml) was also taken in a syringe protected from air. Outside the glovebox, the microwave vial was cooled down to -90 ºC and cold CD_2Cl_2 was added. The vial was shaken until the solution was homogenous. Afterwards, the cold $GaCl_3$ solution was injected into the microwave vial at -90 ºC. Followed by the addition of the alkene solution at -90 ºC. The deep red color corresponding to the carbene complexes faded away as soon as the alkene solution was added due to the fast cyclopropanation reaction in all cases. The sample was kept at -90 ºC for 2 minutes and allowed to warm up to room temperature. Followed by the addition of a CD_2Cl_2 solution of diphenylmethane (0.05 mmol, 0.1 ml, 0.5 M). The reaction was opened to air and transferred to a NMR tube. The yield was calculated by integration of the ^{1}H NMR of the cyclopropanes and the internal standard.

Procedure B: Gold(I)-catalyzed cyclopropanation by retro-Buchner reaction

A microwave vial was charged with 7-mesitylcyclohepta-1,3,5-triene (**18a**) (0.2 mmol), the corresponding alkene (0.4 mmol) and [JohnPhosAu(NCCH$_3$)]SbF$_6$ (5 mol %). 1,2-Dichloroethane (0.5 M) was added via syringe and the vial was capped with a microwave cap with septum. The reaction was heated to 100 ºC until 7-mesitylcyclohepta-1,3,5-triene (**18a**) was consumed (6-24 h). The reaction was allowed to cool down to room temperature, filtered through a pad of celite and concentrated *in vacuo*. ^{1}H NMR yield was calculated by integration of the ^{1}H NMR of the cyclopropanes and the internal standard.

These reactions are carried out in a microwave vial at a temperature higher of the boiling point of 1,2-dichloroethane.

Cyclopropane *trans*-**20b**

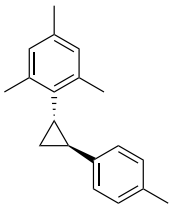

Cyclopropane *trans*-**20b** was synthesized according to procedure A from 1-methyl-4-vinylbenzene (10 equiv), the corresponding chloromesithyl(methyl)gold(I) carbenoid (5 mg) and $GaCl_3$ (1.2 equiv). ^{1}H NMR yield was calculated from the reaction crude. A colorless oil was obtained after purification by preparative TLC using pentane as eluent.

^{1}H NMR (500 MHz, CD_2Cl_2) δ 7.13 – 7.04 (m, 4H), 6.80 (s, 2H), 2.33 (s, 6H), 2.32 (s, 3H), 2.22 (s, 3H), 1.99 – 1.93 (m, 1H), 1.90 (dt, J = 8.8, 5.5 Hz, 1H), 1.39 (ddd, J = 8.8, 5.5, 4.8 Hz, 1H), 1.18 (ddd, J = 8.8, 6.6, 4.8 Hz, 1H). **^{13}C NMR** (126 MHz, CD_2Cl_2) δ 140.3, 138.4, 135.6, 135.4, 135.0, 128.9, 128.6, 125.2, 25.5, 24.7, 20.6, 20.5, 20.5, 19.3. The configuration was assigned by COSY, NOESY, ^{1}H-^{13}C HSQC, ^{1}H-^{13}C HMBC. **HRMS** (APCI+) calculated for $C_{19}H_{23}$ $(M+H)^+$: 251.1794; found: 251.1793.

Cyclopropane *cis*-20b

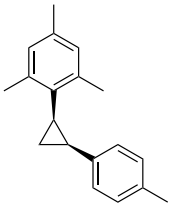

Cyclopropane *cis*-**20b** was synthesized according to procedure B from 1-methyl-4-vinylbenzene (47.3 mg, 0.4 mmol), 7-mesitylcyclohepta-1,3,5-triene (**18a**) (42.1 mg, 0.2 mmol) and [JohnPhosAu(NCCH$_3$)]SbF$_6$ (7.7 mg, 0.01 mmol). 32% ^{1}H NMR yield was calculated from the crude. A colorless oil was obtained in 20% yield (10 mg, 0.04 mmol) after purification by preparative TLC using pentane as eluent.

^{1}H NMR (500 MHz, $CDCl_3$) δ 6.84 – 6.80 (m, 2H), 6.71 (s, 2H), 6.55 – 6.50 (m, 2H), 2.37 – 2.10 (m, 14H), 1.73 – 1.66 (m, 1H), 1.10 – 1.05 (m, 1H). **^{13}C NMR** (126 MHz, $CDCl_3$) δ 139.1, 138.1, 135.6, 134.4, 131.2, 128.8, 128.2, 126.3, 23.3, 22.9, 21.1, 21.0, 20.9, 17.8. The configuration was assigned by COSY, NOESY, ^{1}H-^{13}C HSQC, ^{1}H-^{13}C HMBC. **HRMS** (APCI+) calculated for $C_{19}H_{23}$ $(M+H)^+$: 251.1794; found: 251.1795.

Cyclopropane 21c

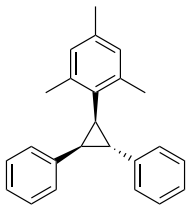

Cyclopropane **21c** was synthesized according to procedure B from *trans*-stilbene (72 mg, 0.4 mmol), 7-mesitylcyclohepta-1,3,5-triene (**18a**) (42.1 mg, 0.2 mmol) and [JohnPhosAu(NCCH$_3$)]SbF$_6$ (7.7 mg, 0.01 mmol). 38% ^{1}H NMR yield was calculated from the crude. A yellowish oil was obtained in 25% yield (15.5 mg, 0.05 mmol) after purification by preparative TLC using pentane as eluent. Cyclopropane **18a** was also obtained by procedure A.

^{1}H NMR (400 MHz, $CDCl_3$) δ 7.39 – 7.33 (m, 2H), 7.32 – 7.28 (m, 2H), 7.26 – 7.21 (m, 1H), 7.09 – 7.03 (m, 3H), 6.76 (bs, 2H), 6.73 – 6.68 (m, 2H), 2.78 – 2.71 (m, 1H), 2.64 (dd, J = 9.0, 5.4 Hz, 1H), 2.54 (dd, J = 7.0, 5.4 Hz, 1H), 2.24 (s, 3H), 2.21 – 2.09 (m, 6H).**^{13}C NMR** (101 MHz, $CDCl_3$) δ 142.2, 140.1, 138.3, 135.9, 130.3, 128.9, 128.7, 128.5, 127.5, 126.5, 126.0, 125.4, 35.6, 35.5, 32.6, 21.0, 20.9, 20.6. The configuration was assigned by COSY, NOESY, ^{1}H-^{13}C HSQC, ^{1}H-^{13}C HMBC. **HRMS** (APCI+) calculated for $C_{24}H_{25}$ $(M+H)^+$: 313.1951; found: 313.1948.

Cyclopropanes 21d

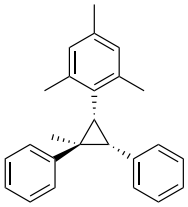

Cyclopropanes **21d** was synthesized according to procedure A from (*E*)-prop-1-ene-1,2-diyldibenzene (10 equiv), the corresponding chloromesithyl(methyl)gold(I) carbenoid (5 mg) and $GaCl_3$ (1.2 equiv). ^{1}H NMR yield was calculated from the reaction crude. Both enantiomers could be separately after two TLC plates in a row with pentane as eluent. Yellowish oil.

^{1}H NMR (500 MHz, CD_2Cl_2) δ 7.52 – 7.47 (m, 2H), 7.39 – 7.34 (m, 2H), 7.26 – 7.21 (m, 1H), 7.13 – 7.09 (m, 3H), 6.85 (s, 2H), 6.81 – 6.75 (m, 2H), 3.00 (d, J = 9.7 Hz, 1H), 2.56 (d, J = 9.7 Hz, 1H), 2.29 (s, 3H), 2.21 (s, 6H), 1.25 (s, 3H). **^{13}C NMR** (126 MHz, CD_2Cl_2) δ 149.6, 139.5, 135.7, 129.9, 128.9, 128.8, 128.5, 127.4, 126.8, 125.8, 125.1, 36.2, 31.7, 31.3, 29.7, 20.6 (d, J = 1.7 Hz), 17.9. A quaternary carbon is missing. The configuration was assigned by COSY, NOESY, GOESY, ^{1}H-^{13}C HSQC, ^{1}H-^{13}C HMBC. **HRMS** (APCI+) calculated for $C_{25}H_{27}$ $(M+H)^+$: 327.2107; found: 327.2108.

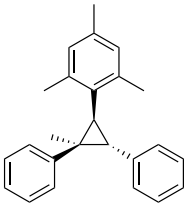

^{1}H NMR (500 MHz, CD_2Cl_2) δ 7.40 – 7.32 (m, 4H), 7.30 – 7.22 (m, 1H), 7.10 – 7.02 (m, 3H), 6.95 – 6.89 (m, 2H), 6.81 – 6.57 (m, 2H), 3.13 (d, J = 8.0 Hz, 1H), 2.66 (d, J = 8.0 Hz, 1H), 2.39 (s, 3H), 2.23 (s, 3H), 2.20 (s, 3H), 1.36 (s, 3H).**^{13}C NMR** (126 MHz, CD_2Cl_2) δ 143.5, 138.8, 138.1, 135.5, 135.5, 135.3, 131.3, 129.2, 128.2, 127.2, 126.3, 125.4, 40.2, 35.4, 31.4, 20.6, 20.5, 20.4, 19.7. The configuration was assigned by COSY, NOESY, ^{1}H-^{13}C HSQC, ^{1}H-^{13}C HMBC. **HRMS** (APCI+) calculated for $C_{25}H_{27}$ $(M+H)^+$: 327.2107; found: 327.2103.

Gold(I)-promoted C–H insertion

Procedure A: Generation of mesityl gold(I) carbenes in the presence of cyclohexane

In a glovebox, the corresponding chloromesityl(methyl)gold(I) carbenoid (0.007 mmol) and cyclohexane (50 equiv) were weighed in an oven-dried microwave vial and capped. Separately, $GaCl_3$ (1.0 equiv) was dissolved in dry CD_2Cl_2 (0.5 ml) in a HPLC vial and taken in a syringe protected from air. Besides that, dry CD_2Cl_2 (0.5 ml) were also taken in a syringe protected from air. Outside the glovebox, both syringes containing $GaCl_3$ solution and CD_2Cl_2 were cooled down with dry ice. The microwave vial was cooled down to -30 ºC and dissolved in cold CD_2Cl_2 (0.5 ml). Afterwards, the cold $GaCl_3$ solution was added over the mixture in the microwave vial at -

30 ºC. The sample was kept at -30 ºC for 15 minutes and allowed to warm up to room temperature. Followed by the addition of a CD_2Cl_2 solution of diphenylmethane (0.05 mmol, 0.1 ml, 0.5 M). The reaction was opened to air and transferred to a NMR tube. The yield was calculated by integration of the ^{1}H NMR of the product and the internal standard.

Generation of mesityl gold(I) carbene followed by addition of cyclohexane at -90 ºC also generated 2-(cyclohexylmethyl)-1,3,5-trimethylbenzene **43** together with *E*-1,2-dimesitylethene (*E*-**20a**), *Z*-1,2-dimesitylethene (*Z*-**20a**), 2,4,6-trimethylbenzaldehyde (**42**) and 1,2,3-trimesitylcyclopropane (**21a**). To avoid competitive transformations, gold(I) carbenes **39a-b** were generated in the presence of an excess of cyclohexane at -30 ºC.

2-(cyclohexylmethyl)-1,3,5-trimethylbenzene **42** was detected by ^{1}H NMR and GCMS from the crude reactions of the CH insertion of cyclohexane. The ^{1}H NMR data of 2-(cyclohexylmethyl)-1,3,5-trimethylbenzene **42** was identical to the previously reported.[47]

Procedure B: Gold(I)-promoted C–H insertion by retro-Buchner reaction

A microwave vial was charged with 7-mesitylcyclohepta-1,3,5-triene (**18a**) (0.3 mmol) and [JohnPhosAu(NCCH$_3$)]SbF$_6$ (5 mol %). 1,1,2,2-Tetrachloroethane-*d*$_4$ (0.3 ml, 0.5 M) and cyclohexane (0.3 ml, 0.5M) was added via syringe. The vial was capped with a microwave cap with septum and the reaction was heated to 100 ºC until 7-mesitylcyclohepta-1,3,5-triene (**18a**) was consumed (12 h). The mixture was allowed to cool down to room temperature, internal standard was added and it was transferred to a NMR tube. ^{1}H NMR yield was calculated by integration of the ^{1}H NMR of the product and the internal standard.

These reactions are carried out in a microwave vial at a temperature higher of the boiling point of cyclohexane.

47 Admasu, A.; Platz, M. S.; Marcinek, A.; Michalak, J.; Gudmundsdóttir, A. D.; Gebicki, J. *Journal of physical organic chemistry* **1997**, *10*, 207–220.

Crystallographic Data

Gold(I) carbenoid 37a

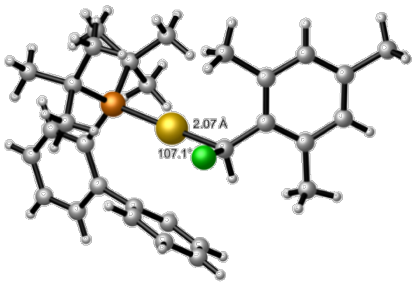

Table 9. Crystal data and structure refinement for **37a**.

Identification code	mo_CGJS020109_0m	
Empirical formula	C30 H39 Au Cl P	
Formula weight	663.00	
Temperature	100(2) K	
Wavelength	0.71073 Å	
Crystal system	Triclinic	
Space group	P-1	
Unit cell dimensions	a = 8.7383(6)Å	a= 93.9248(17)°.
	b = 10.6161(6)Å	b = 105.5298(17)°.
	c = 16.2054(11)Å	g = 107.0370(17)°.
Volume	1367.15(15) $Å^3$	
Z	2	
Density (calculated)	1.611 Mg/m^3	
Absorption coefficient	5.553 mm^{-1}	
F(000)	660	
Crystal size	0.05 x 0.05 x 0.05 mm^3	
Theta range for data collection	2.032 to 24.711°.	
Index ranges	-8<=h<=10,-12<=k<=9,-18<=l<=19	
Reflections collected	9039	
Independent reflections	4539[R(int) = 0.0157]	
Completeness to theta =24.711°	97.399994%	
Absorption correction	Multi-scan	
Max. and min. transmission	0.769 and 0.688	
Refinement method	Full-matrix least-squares on F^2	
Data / restraints / parameters	4539/ 0/ 307	
Goodness-of-fit on F^2	1.056	
Final R indices [I>2sigma(I)]	R1 = 0.0228, wR2 = 0.0527	
R indices (all data)	R1 = 0.0255, wR2 = 0.0537	
Largest diff. peak and hole	3.227 and -0.793 e.$Å^-$	

Gold(I) carbenoid 37b

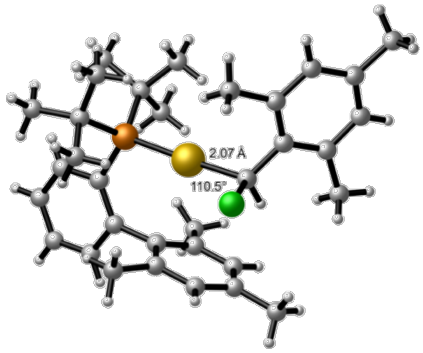

Table 10. Crystal data and structure refinement for **37b**

Identification code	CGS-02-316	
Empirical formula	C33 H45 Au Cl P	
Formula weight	705.07	
Temperature	100(2) K	
Wavelength	0.71073 Å	
Crystal system	Monoclinic	
Space group	P2(1)/n	
Unit cell dimensions	a = 12.16734(6)Å	α= 90°.
	b = 16.07131(6)Å	β = 101.6845(5)°.
	c = 15.75663(8)Å	γ = 90°.
Volume	3017.28(2) $Å^3$	
Z	4	
Density (calculated)	1.552 Mg/m^3	
Absorption coefficient	5.037 mm^{-1}	
F(000)	1416	
Crystal size	0.1 x 0.1 x 0.05 mm^3	
Theta range for data collection	1.830 to 27.485°.	
Index ranges	-15<=h<=15,-20<=k<=20,-20<=l<=20	
Reflections collected	178839	
Independent reflections	6911[R(int) = 0.0349]	
Completeness to theta =27.485°	99.9%	
Absorption correction	Multi-scan	
Max. and min. transmission	0.787 and 0.605	
Refinement method	Full-matrix least-squares on F^2	
Data / restraints / parameters	6911/ 0/ 337	
Goodness-of-fit on F^2	1.559	
Final R indices [I>2sigma(I)]	R1 = 0.0168, wR2 = 0.0582	
R indices (all data)	R1 = 0.0182, wR2 = 0.0587	
Largest diff. peak and hole	2.417 and -1.043 $e.Å^{-3}$	

Gold(I) carbenoid 37c

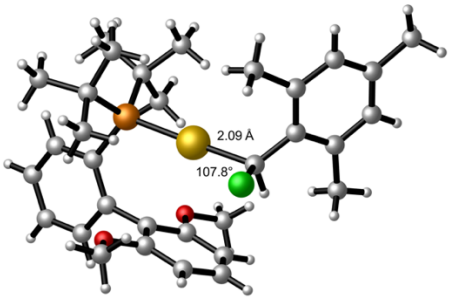

Table 11. Crystal data and structure refinement for **37c**.

Identification code	mo_CGJS02264_0m	
Empirical formula	C32 H43 Au Cl O2 P	
Formula weight	723.05	
Temperature	100(2) K	
Wavelength	null Å	
Crystal system	Monoclinic	
Space group	P2(1)/n	
Unit cell dimensions	a = 15.3944(10)Å	a= 90°.
	b = 9.3499(6)Å	b = 100.6183(16)°.
	c = 21.2741(14)Å	g = 90°.
Volume	3009.7(3) $Å^3$	
Z	4	
Density (calculated)	1.596 Mg/m^3	
Absorption coefficient	5.057 mm^{-1}	
F(000)	1448	
Crystal size	0.10 x 0.10 x 0.02 mm^3	
Theta range for data collection	2.386 to 24.712°.	
Index ranges	-18<=h<=18,-10<=k<=8,-25<=l<=24	
Reflections collected	21583	
Independent reflections	5109[R(int) = 0.0326]	
Completeness to theta =24.712°	99.9%	
Absorption correction	Multi-scan	
Max. and min. transmission	_exptl_absorpt_correction_T_max 0.7467 and	
_exptl_absorpt_correction_T_min 0.6322		
Refinement method	Full-matrix least-squares on F^2	
Data / restraints / parameters	5109/ 0/ 345	
Goodness-of-fit on F^2	1.009	
Final R indices [I>2sigma(I)]	R1 = 0.0215, wR2 = 0.0517	
R indices (all data)	R1 = 0.0242, wR2 = 0.0528	
Largest diff. peak and hole	2.848 and -0.668 e.Å$^-$	

Gold(I) carbenoid 37d

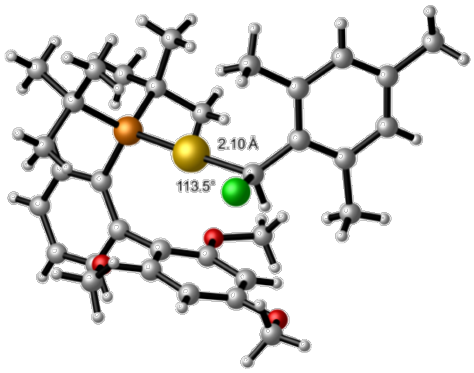

Table 12. Crystal data and structure refinement for **37d.**

Identification code	CGJS02-332	
Empirical formula	C33 H45 Au Cl O3 P	
Formula weight	753.07	
Temperature	100(2) K	
Wavelength	0.71073 Å	
Crystal system	Monoclinic	
Space group	I2/a	
Unit cell dimensions	a = 22.3984(10)Å	a= 90°.
	b = 9.8047(3)Å	b = 104.245(4)°.
	c = 30.7411(10)Å	g = 90°.
Volume	6543.5(4) $Å^3$	
Z	8	
Density (calculated)	1.529 Mg/m^3	
Absorption coefficient	4.657 mm^{-1}	
F(000)	3024	
Crystal size	? x ? x ? mm^3	
Theta range for data collection	2.187 to 31.912°.	
Index ranges	-31<=h<=31,-13<=k<=14,-44<=l<=22	
Reflections collected	27147	
Independent reflections	10192[R(int) = 0.0417]	
Completeness to theta =31.912°	90.3%	
Absorption correction	Multi-scan	
Max. and min. transmission	0.955 and 0.735	
Refinement method	Full-matrix least-squares on F^2	
Data / restraints / parameters	10192/ 0/ 364	
Goodness-of-fit on F^2	0.940	
Final R indices [I>2sigma(I)]	R1 = 0.0307, wR2 = 0.0701	
R indices (all data)	R1 = 0.0514, wR2 = 0.0774	
Largest diff. peak and hole	2.604 and -0.691 e.$Å^{-3}$	

Gold(I) carbenoid 37e

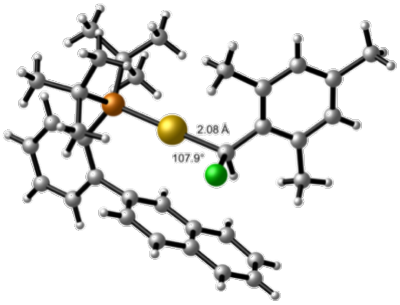

Table 13. Crystal data and structure refinement for **37e**.

Identification code	mo_CGJS02560_0m	
Empirical formula	C34 H41 Au Cl P	
Formula weight	713.05	
Temperature	100(2) K	
Wavelength	0.71073 Å	
Crystal system	Monoclinic	
Space group	P2(1)	
Unit cell dimensions	a = 11.1431(5)Å	a= 90°.
	b = 16.2846(7)Å	b = 100.0600(10)°.
	c = 16.7392(7)Å	g = 90°.
Volume	2990.8(2) $Å^3$	
Z	4	
Density (calculated)	1.584 Mg/m^3	
Absorption coefficient	5.083 mm^{-1}	
F(000)	1424	
Crystal size	0.15 x 0.15 x 0.06 mm^3	
Theta range for data collection	1.235 to 32.714°.	
Index ranges	-16<=h<=16,-24<=k<=24,-25<=l<=25	
Reflections collected	80205	
Independent reflections	20682[R(int) = 0.0265]	
Completeness to theta =32.714°	96.100006%	
Absorption correction	Multi-scan	
Max. and min. transmission	0.750 and 0.515	
Refinement method	Full-matrix least-squares on F^2	
Data / restraints / parameters	20682/ 585/ 789	
Goodness-of-fit on F^2	1.215	
Final R indices [I>2sigma(I)]	R1 = 0.0222, wR2 = 0.0483	
R indices (all data)	R1 = 0.0252, wR2 = 0.0491	
Flack parameter	x =0.361(6)	
Largest diff. peak and hole	1.432 and -0.747 $e.Å^{-3}$	

Phosphonium ylide complex 41a

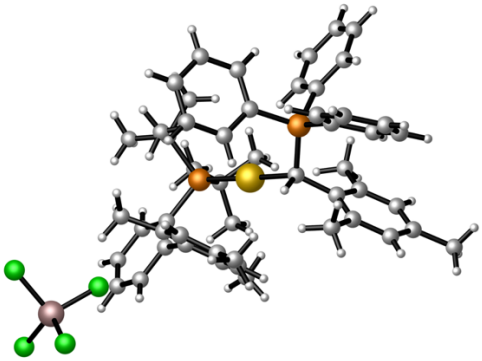

Table 14. Crystal data and structure refinement for **41a**.

Identification code	mo_CGJS02512_0m	
Empirical formula	C51 H60 Au Cl4 Ga P2	
Formula weight	1143.41	
Temperature	100(2) K	
Wavelength	0.71073 Å	
Crystal system	Monoclinic	
Space group	P2(1)/n	
Unit cell dimensions	a = 15.1297(5)Å	a= 90°.
	b = 15.1006(5)Å	b = 101.4222(18)°.
	c = 22.1469(8)Å	g = 90°.
Volume	4959.6(3) $Å^3$	
Z	4	
Density (calculated)	1.531 Mg/m^3	
Absorption coefficient	3.811 mm^{-1}	
F(000)	2296	
Crystal size	0.20 x 0.20 x 0.20 mm^3	
Theta range for data collection	1.643 to 33.344°.	
Index ranges	-22<=h<=12,-18<=k<=22,-32<=l<=31	
Reflections collected	42998	
Independent reflections	16383[R(int) = 0.0393]	
Completeness to theta =33.344°	85.299995%	
Absorption correction	Multi-scan	
Max. and min. transmission	0.516 and 0.397	
Refinement method	Full-matrix least-squares on F^2	
Data / restraints / parameters	16383/ 48/ 580	
Goodness-of-fit on F^2	1.019	
Final R indices [I>2sigma(I)]	R1 = 0.0318, wR2 = 0.0563	
R indices (all data)	R1 = 0.0503, wR2 = 0.0611	
Largest diff. peak and hole	0.926 and -1.018 $e.Å^{-3}$	

Phosphonium ylide complex 40b

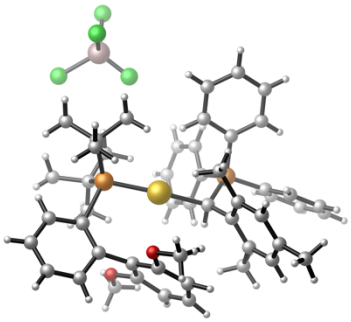

Table 15. Crystal data and structure refinement for **40b**.

Identification code	mo_CGJS460_0m	
Empirical formula	C57 H66 Au Cl4 Ga O2 P2	
Formula weight	1253.52	
Temperature	100(2) K	
Wavelength	0.71073 Å	
Crystal system	Triclinic	
Space group	P-1	
Unit cell dimensions	a = 11.5933(5)Å	a= 80.4789(11)°.
	b = 15.5453(7)Å	b = 76.1721(10)°.
	c = 16.4650(7)Å	g = 75.7588(11)°.
Volume	2774.8(2) $Å^3$	
Z	2	
Density (calculated)	1.500 Mg/m^3	
Absorption coefficient	3.416 mm^{-1}	
F(000)	1264	
Crystal size	0.20 x 0.20 x 0.10 mm^3	
Theta range for data collection	1.760 to 33.881°.	
Index ranges	-15<=h<=18,-23<=k<=24,-25<=l<=24	
Reflections collected	45728	
Independent reflections	21068[R(int) = 0.0366]	
Completeness to theta =33.881°	93.8%	
Absorption correction	Multi-scan	
Max. and min. transmission	0.726 and 0.601	
Refinement method	Full-matrix least-squares on F^2	
Data / restraints / parameters	21068/ 804/ 1013	
Goodness-of-fit on F^2	1.038	
Final R indices [I>2sigma(I)]	R1 = 0.0376, wR2 = 0.0749	
R indices (all data)	R1 = 0.0531, wR2 = 0.0796	
Largest diff. peak and hole	1.204 and -1.114 $e.Å^{-3}$	

Complex S1

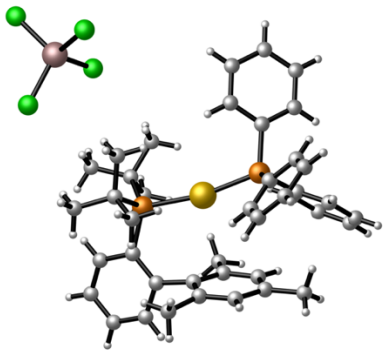

Table 16. Crystal data and structure refinement for **S1**.

Identification code	mo_CGJS02512_b_0m	
Empirical formula	C41 H48 Au Cl4 Ga P2	
Formula weight	1011.22	
Temperature	100(2) K	
Wavelength	0.71073 Å	
Crystal system	Triclinic	
Space group	P-1	
Unit cell dimensions	a = 9.8240(3)Å	α= 90.8386(11)°.
	b = 13.8807(5)Å	β = 102.3072(10)°.
	c = 15.8756(6)Å	γ = 99.3037(10)°.
Volume	2084.58(13) $Å^3$	
Z	2	
Density (calculated)	1.611 Mg/m^3	
Absorption coefficient	4.522 mm^{-1}	
F(000)	1004	
Crystal size	0.20 x 0.10 x 0.10 mm^3	
Theta range for data collection	1.935 to 30.561°.	
Index ranges	-9<=h<=13,-14<=k<=19,-22<=l<=21	
Reflections collected	22182	
Independent reflections	11705[R(int) = 0.0296]	
Completeness to theta =30.561°	91.7%	
Absorption correction	Multi-scan	
Max. and min. transmission	0.661 and 0.462	
Refinement method	Full-matrix least-squares on F^2	
Data / restraints / parameters	11705/ 56/ 452	
Goodness-of-fit on F^2	1.028	
Final R indices [I>2sigma(I)]	R1 = 0.0304, wR2 = 0.0555	
R indices (all data)	R1 = 0.0386, wR2 = 0.0581	
Largest diff. peak and hole	0.890 and -1.068 $e.Å^{-3}$	

Complex S2

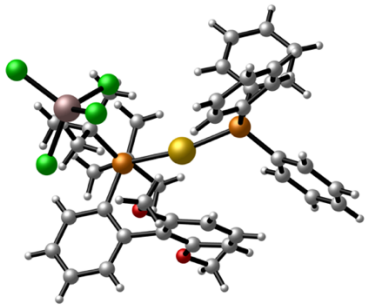

Table 17. Crystal data and structure refinement for **S2**.

Identification code	mo_CGJS02489B_0m	
Empirical formula	C60 H69 Au1.50 Cl6 Ga1.50 O3 P3	
Formula weight	1543.79	
Temperature	100(2) K	
Wavelength	0.71073 Å	
Crystal system	Monoclinic	
Space group	P2(1)/n	
Unit cell dimensions	a = 14.858(5)Å	a= 90°.
	b = 25.357(8)Å	b = 92.193(12)°.
	c = 33.572(7)Å	g = 90°.
Volume	12640(6) $Å^3$	
Z	8	
Density (calculated)	1.623 Mg/m^3	
Absorption coefficient	4.480 mm^{-1}	
F(000)	6120	
Crystal size	? x ? x ? mm^3	
Theta range for data collection	1.521 to 25.505°.	
Index ranges	-17<=h<=14,-30<=k<=30,-40<=l<=38	
Reflections collected	70460	
Independent reflections	22417[R(int) = 0.0987]	
Completeness to theta =25.505°	95.3%	
Absorption correction	Multi-scan	
Max. and min. transmission	0.916 and 0.752	
Refinement method	Full-matrix least-squares on F^2	
Data / restraints / parameters	22417/ 3/ 1375	
Goodness-of-fit on F^2	0.929	
Final R indices [I>2sigma(I)]	R1 = 0.0511, wR2 = 0.0892	
R indices (all data)	R1 = 0.1221, wR2 = 0.1124	
Largest diff. peak and hole	1.021 and -0.772 $e.Å^{-3}$	

Complex 41a

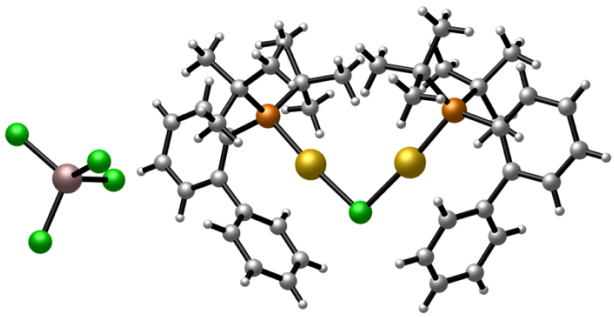

Table 18. Crystal data and structure refinement for **41a**.

Identification code	cgs-02-340	
Empirical formula	C40 H54 Au2 Cl5 Ga P2	
Formula weight	1237.67	
Temperature	100(2) K	
Wavelength	0.71073 Å	
Crystal system	Triclinic	
Space group	P-1	
Unit cell dimensions	a = 11.34310(10)Å	a= 66.0970(10)°.
	b = 15.01070(10)Å	b = 69.0110(10)°.
	c = 15.71570(10)Å	g = 71.1750(10)°.
Volume	2234.10(4) $Å^3$	
Z	2	
Density (calculated)	1.840 Mg/m^3	
Absorption coefficient	7.547 mm^{-1}	
F(000)	1196	
Crystal size	? x ? x ? mm^3	
Theta range for data collection	2.026 to 26.372°.	
Index ranges	-14<=h<=14,-18<=k<=18,-19<=l<=19	
Reflections collected	125845	
Independent reflections	9134[R(int) = 0.0381]	
Completeness to theta =26.372°	99.9%	
Absorption correction	Multi-scan	
Max. and min. transmission	0.805 and 0.619	
Refinement method	Full-matrix least-squares on F^2	
Data / restraints / parameters	9134/ 0/ 463	
Goodness-of-fit on F^2	1.070	
Final R indices [I>2sigma(I)]	R1 = 0.0224, wR2 = 0.0615	
R indices (all data)	R1 = 0.0238, wR2 = 0.0624	
Largest diff. peak and hole	2.278 and -1.947 $e.Å^{-3}$	

Complex 41b

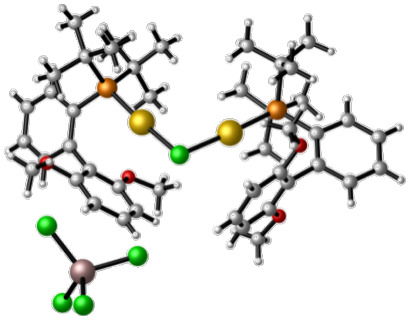

Table 19. Crystal data and structure refinement for **41c**.

Identification code	CGJS-02-0409	
Empirical formula	C51 H70 Au2 Cl5 Ga O4 P2	
Formula weight	1449.91	
Temperature	100(2) K	
Wavelength	0.71073 Å	
Crystal system	Triclinic	
Space group	P-1	
Unit cell dimensions	a = 13.3973(3)Å	α= 78.113(2)°.
	b = 14.6629(4)Å	β = 68.581(2)°.
	c = 16.4950(3)Å	γ = 69.576(2)°.
Volume	2815.43(12) $Å^3$	
Z	2	
Density (calculated)	1.710 Mg/m^3	
Absorption coefficient	6.008 mm^{-1}	
F(000)	1424	
Crystal size	0.05 x 0.01 x 0.01 mm^3	
Theta range for data collection	1.802 to 26.371°.	
Index ranges	-15<=h<=16,-15<=k<=18,-20<=l<=20	
Reflections collected	39526	
Independent reflections	11520[R(int) = 0.0432]	
Completeness to theta =26.371°	100.0%	
Absorption correction	Multi-scan	
Max. and min. transmission	0.942 and 0.725	
Refinement method	Full-matrix least-squares on F^2	
Data / restraints / parameters	11520/ 99/ 655	
Goodness-of-fit on F^2	1.073	
Final R indices [I>2sigma(I)]	R1 = 0.0318, wR2 = 0.0787	
R indices (all data)	R1 = 0.0436, wR2 = 0.0828	
Largest diff. peak and hole	2.480 and -1.860 $e.Å^{-3}$	

DFT Calculations

All density functional calculations were performed using the Gaussian09 suit.[48] The functional B3LYP[49] was used in conjunction with Grimme's D3 dispersion correction. The basis set for Au and Ga used was SDD,[50] and 6-31G(d,p)[51] for all other atoms. All structures were fully optimized and frequency calculations were undertaken. No imaginary frequencies for minima and a single imaginary frequency corresponding to the reaction coordinate in the case of the transition states were found. Additionally, single point of the optimized structures using the Polarizable Continuum Model (PCM)[52] to simulate dichloromethane ($\varepsilon = 8.93$) as solvent were performed throughout all calculations. All the energies presented are potential (E) and free energies (G) in solution at 298.15 K and 1 atm in $kcalmol^{-1}$. Optimized geometries were visualized using CYLview.[53]

NMR data was calculated at B3LYP/6-311+G(2d,p) level of theory in dichloromethane (PCM) using previously calculated scaling factor.[54]

Non-covalent interaction analysis was performed with NCIplot.[31]

The bonding situation was analyzed using Natural Bond Orbital analysis (NBO 6.0).[55] Charge transfer between the carbene moiety and gold atom has been calculated using Natural Population

48 Gaussian 09, Revision D.01,
Frisch, M. J.; Trucks, G. W.; Schlegel, H. B.; Scuseria, G. E.; Robb, M. A.; Cheeseman, J. R.; Scalmani, G.; Barone, V.; Mennucci, B.; Petersson, G. A.; Nakatsuji, H.; Caricato, M.; Li, X.; Hratchian, H. P.; Izmaylov, A. F.; Bloino, J.; Zheng, G.; Sonnenberg, J. L.; Hada, M.; Ehara, M.; Toyota, K.; Fukuda, R.; Hasegawa, J.; Ishida, M.; Nakajima, T.; Honda, Y.; Kitao, O.; Nakai, H.; Vreven, T.; Montgomery, Jr., J. A.; Peralta, J. E.; Ogliaro, F.; Bearpark, M.; Heyd, J. J.; Brothers, E.; Kudin, K. N.; Staroverov, V. N.; Keith, T.; Kobayashi, R.; Normand, J.; Raghavachari, K.; Rendell, A.; Burant, J. C.; Iyengar, S. S.; Tomasi, J.; Cossi, M.; Rega, N.; Millam, J. M.; Klene, M.; Knox, J. E.; Cross, J. B.; Bakken, V.; Adamo, C.; Jaramillo, J.; Gomperts, R.; Stratmann, R. E.; Yazyev, O.; Austin, A. J.; Cammi, R.; Pomelli, C.; Ochterski, J. W.; Martin, R. L.; Morokuma, K.; Zakrzewski, V. G.; Voth, G. A.; Salvador, P.; Dannenberg, J. J.; Dapprich, S.; Daniels, A. D.; Farkas, O.; Foresman, J. B.; Ortiz, J. V.; Cioslowski, J.; Fox, D. J. Gaussian, Inc., Wallingford CT, **2013**.

49 (a) Becke, A. D. *J. Chem. Phys.* **1993**, *98*, 5648-5652. (b) Lee, C.; Yang, W.; Parr, R. G. *Phys. Rev. B.* **1988**, *37*, 785–789. (c) Stephens, P. J.; Devlin, F. J.; Chabalowsky, C. F.; Frisch, M. J. *J. Phys. Chem.* **1994**, *98*, 11623–11627.

50 Andrae, D.; Haussermann, U.; Dolg, M.; Stoll, H.; Preuss, H. *Theor. Chim. Acta* **1990**, *77*, 123–141.

51 Hehre, W. J.; Ditchfield, R.; Pople, J. A. *J. Chem. Phys.* **1972**, *56*, 2257–2261.

52 Marenich, A. V.; Cramer, C. J.; Truhlar, D. G. *J. Phys. Chem. B.* **2009**, *113*, 6378–6396.

53 Legault, C. Y. CYLview; Universite de Sherbrooke: Sherbrooke, Canada, **2009**; http://www.cylview.org.

54 Pierens, G. K. *J. Comput. Chem.* **2014**, *35*, 1388–1394.

55 Glendening, E. D.; Badenhoop, J. K.; Reed, A. E.; Carpenter, J. E.; Bohmann, J. A.; Morales, C. M.; Landis, C. R.; Weinhold, F. Theoretical Chemistry Institute, University of Wisconsin, Madison, **2013**.

Analysis (NPA).[56] The Natural Localized Molecular Orbitals (NLMO) associated to the Au–C1 and C1–C2 interactions have been determined.[57] The NLMOs isosurface were visualized using ChemCraft, with the surface contour set at 0.05.[58]

56 Reed, A. E.; Weinstock, R. B.; Weinhold, F. *J. Chem. Phys.* **1985**, *83*, 735–746.

57 Reed, A. E.; Weinhold, F. *J. Chem. Phys.* **1985**, *83*, 1736–1740.

58 Chemcraft - graphical software for visualization of quantum chemistry computations. https://www.chemcraftprog.com.

NMR predictions

Previously calculated scaling factor[54] were employed to achieve high-accuracy chemical shifts from the computed isotropic shielding constants of the optimized gold(I) complexes using Equation 8.

$$\delta = \frac{intercept - \sigma}{-slope}$$

Equation 8. Where δ = chemical shift in ppm, σ = isotropic value, intercept = 31.9351 for ^{1}H and 181.2747 for ^{13}C, slope = 1.0463 for ^{1}H and 1.0272 for ^{13}C.

Non-covalent interaction analysis

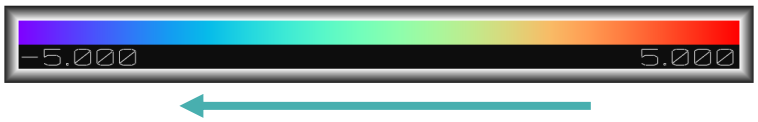

Stabilizing interaction

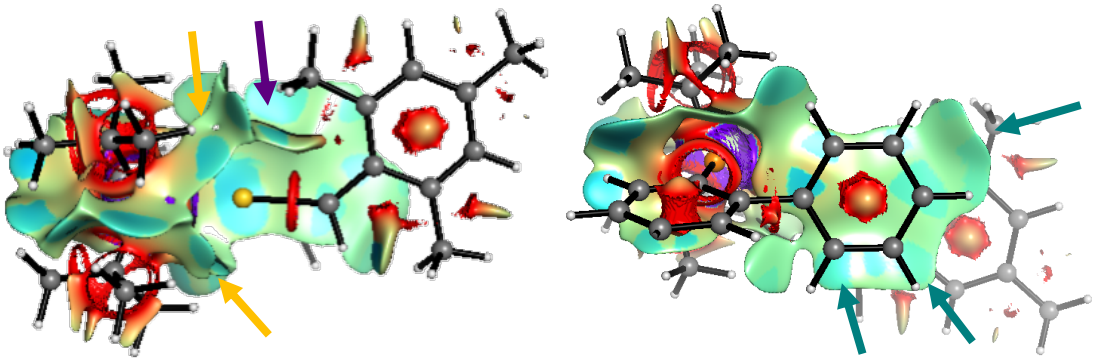

Figure 27. Non-covalent interaction plot for structure **39a**. Left: the mesitylidene moiety is showed in front. Right: the biaryl moiety is showed in front.

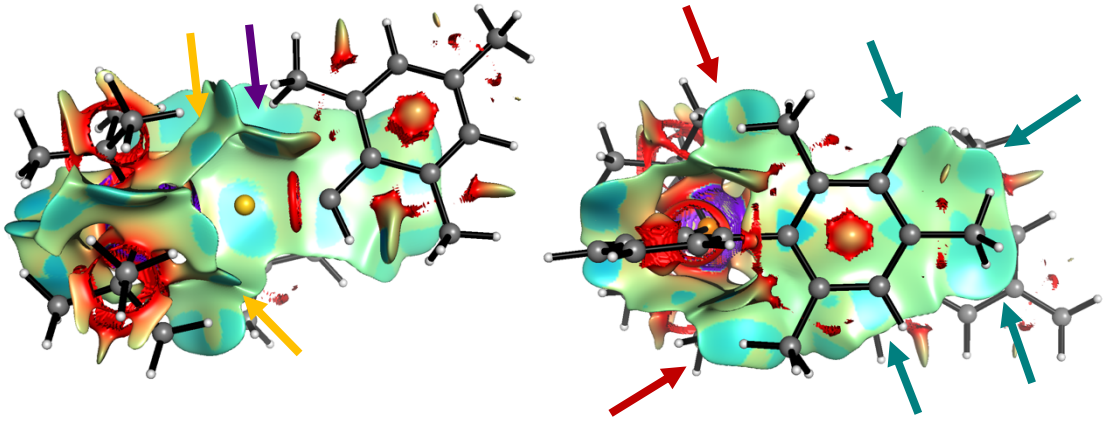

Figure 28. Non-covalent interaction plot for structure **39b**. Left: the biaryl moiety is showed in front. Right: the mesitylidene moiety is showed in front.

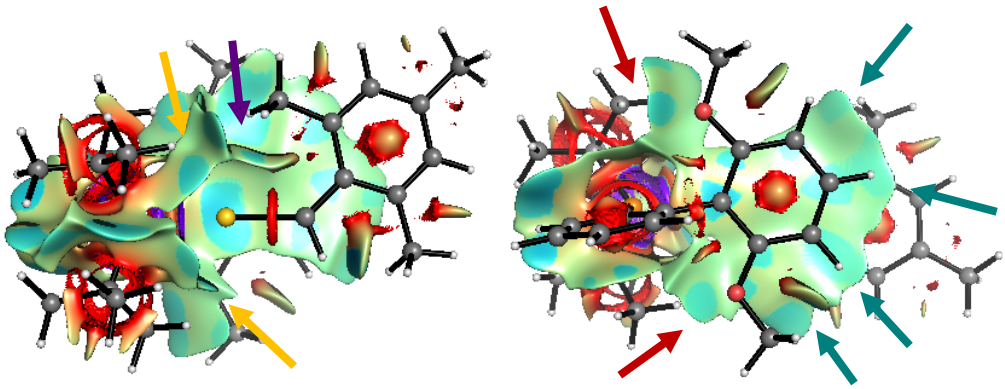

Figure 29. Non-covalent interaction plot for structure **39c**. Left: the biaryl moiety is showed in front. Right: the mesitylidene moiety is showed in front.

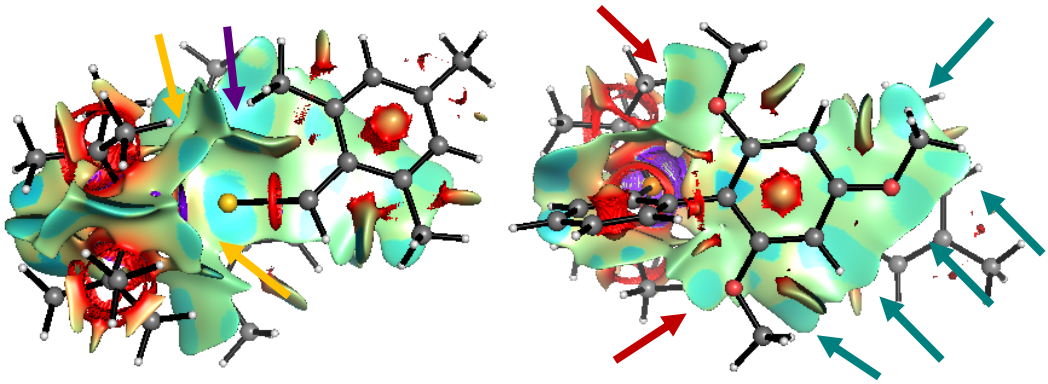

Figure 30. Non-covalent interaction plot for structure **39d**. Left: the biaryl moiety is showed in front. Right: the mesitylidene moiety is showed in front.

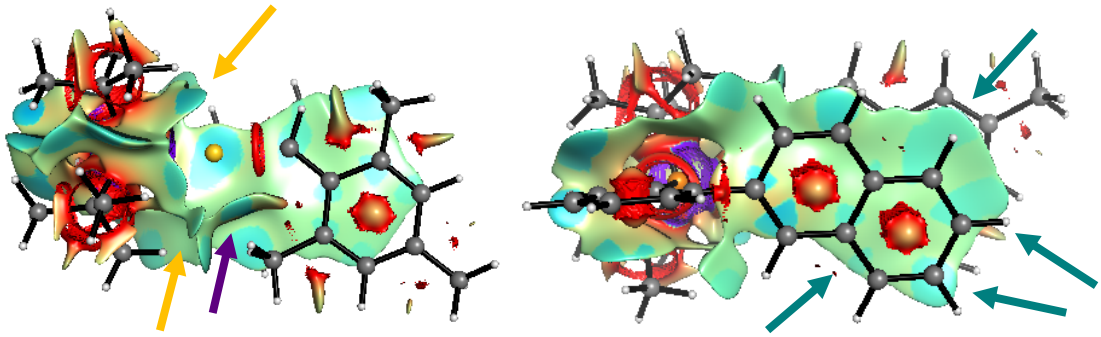

Figure 31. Non-covalent interaction plot for structure **39e**. Left: the biaryl moiety is showed in front. Right: the mesitylidene moiety is showed in front.

Frontier orbitals

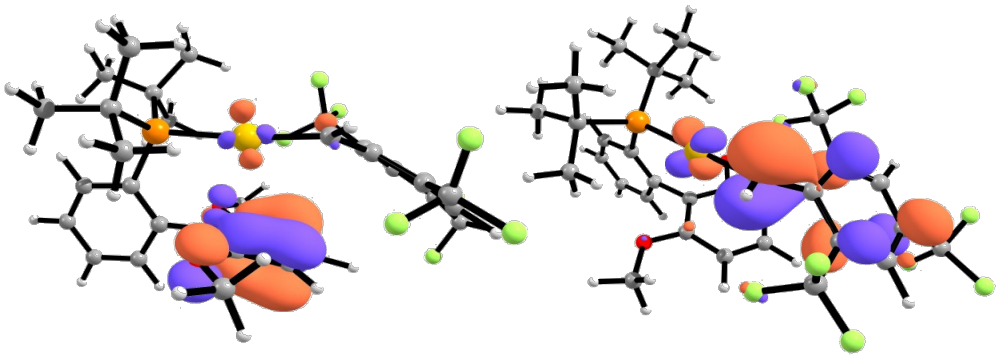

Figure 32. HOMO (left) and LUMO (right) for structure **39c-CF_3**.

Figure 33. HOMO (left) and LUMO (right) of structure **39c-MeO**.

Bond orbital analysis

Table 20. Natural localized molecular orbitals associated to C1 stabilization for **39c-CF_3**, **39c** and **39c-MeO**. Contribution of main atoms in percent and NBOs donor-acceptor related to the analyzed NLMO.

Interaction	Analysis	**39c-CF_3**	**39c**	**39c-MeO**
π-backdonation	NLMO	d_{xz}(Au)	d_{xy}(Au)	d_{xz}(Au)
	Au	88.8%	93.8%	94.8
	C1	10.0%	3.7%	2.8
	$C_{Aryl\text{-}system}$	0.5%	1.5%	1.2%
	NBO donor	n_{Au}	n_{Au}	n_{Au}
	NBO acceptor	n_{C1}* (31.6 Kcal/mol)	n_{C1}* (24.4 Kcal/mol)	Ω^*_{C1-C2} (10.1 Kcal/mol)
	Interaction	d_{xz}(Au) to $2p_z$(C1)	d_{xy}(Au) to $2p_y$(C1)	d_{xz}(Au) to $2p_z$(C1)
π_{C1-C2} bond	NLMO	No NLMO	$2p_y$(C2)	π_{C1-C2}
	C1		23.5	27.3
	C2		51.1	54.9
	C3		8.5	5.36
	C4		8.6	6.0
	C5		0.8	0.8
	C6		0.8	0.8
	C7		6.2	3.0
	NBO donor		n_{C2}	Ω_{C1-C2}
	NBO acceptor		Ω^*_{C3-C5} (82.3 Kcal/mol) Ω^*_{C4-C6} (81.8 Kcal/mol)	Ω^*_{C1-C2} (6.0 Kcal/mol) Ω^*_{C3-C5} (27.4 Kcal/mol) Ω^*_{C4-C6} (29.9 Kcal/mol)
	Interaction		$2p^{\pi}$(C2) to $2p^{\pi}$(C1)	Ω_{C1-C2} to $\Omega^*_{C=C^{aryl}}$

NBO types: n_A = nonbonded lone pair (1 center, valence), n_A* = unfilled nonbonded (1 center, valence), Ω_{A-B} = bond (2 centers, valence), Ω^*_{A-B} = antibond (2 centers, valence).

Cyclopropanation of E-20a by gold(I) carbene 39b

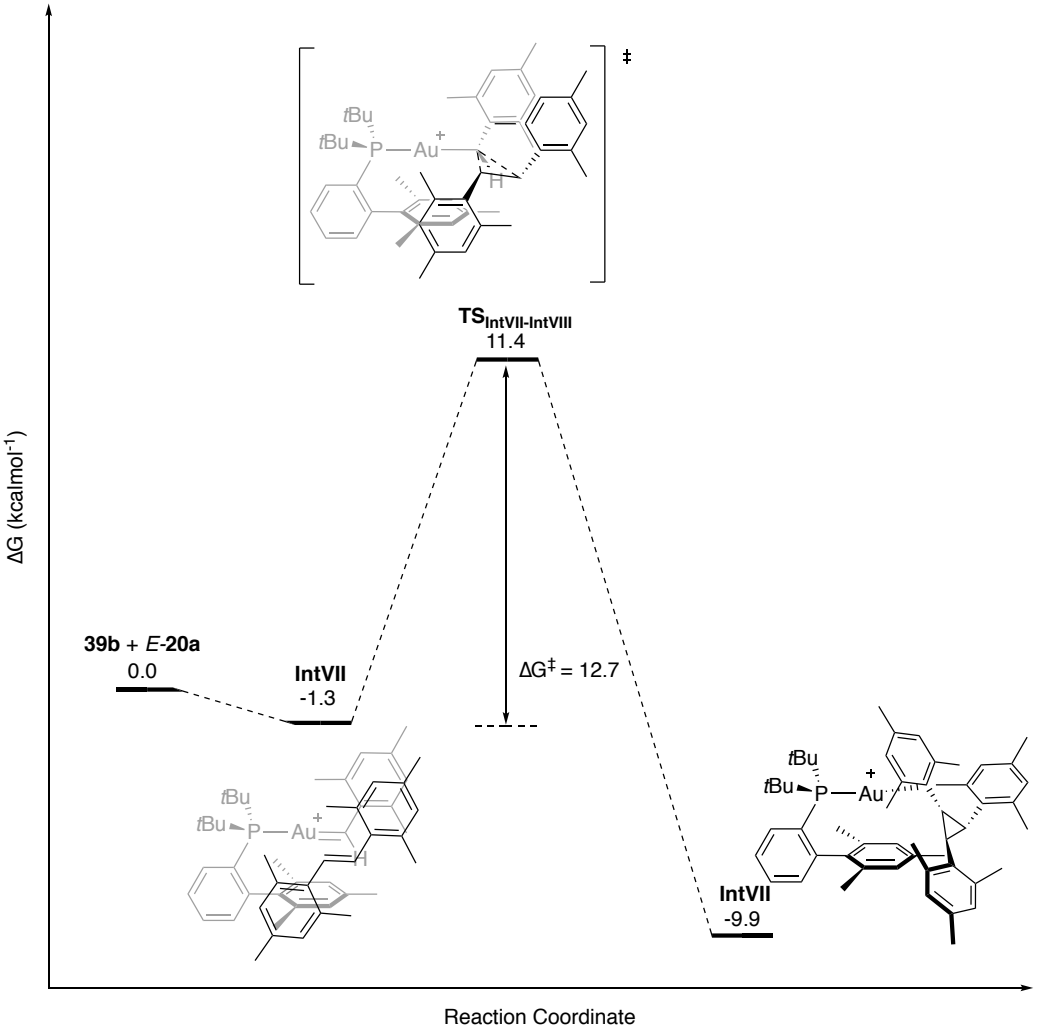

Figure 34. Calculated free energy profile for the cyclopropanation of *E*-**20a** with gold(I) carbene **39b**. PCM(CH_2Cl_2)-B3LYP-D3, SDD(Au), 6-31G(d,p) (C, H, O, P, Cl, F).

Cyclopropanation of Z-20a by gold(I) carbene 39b

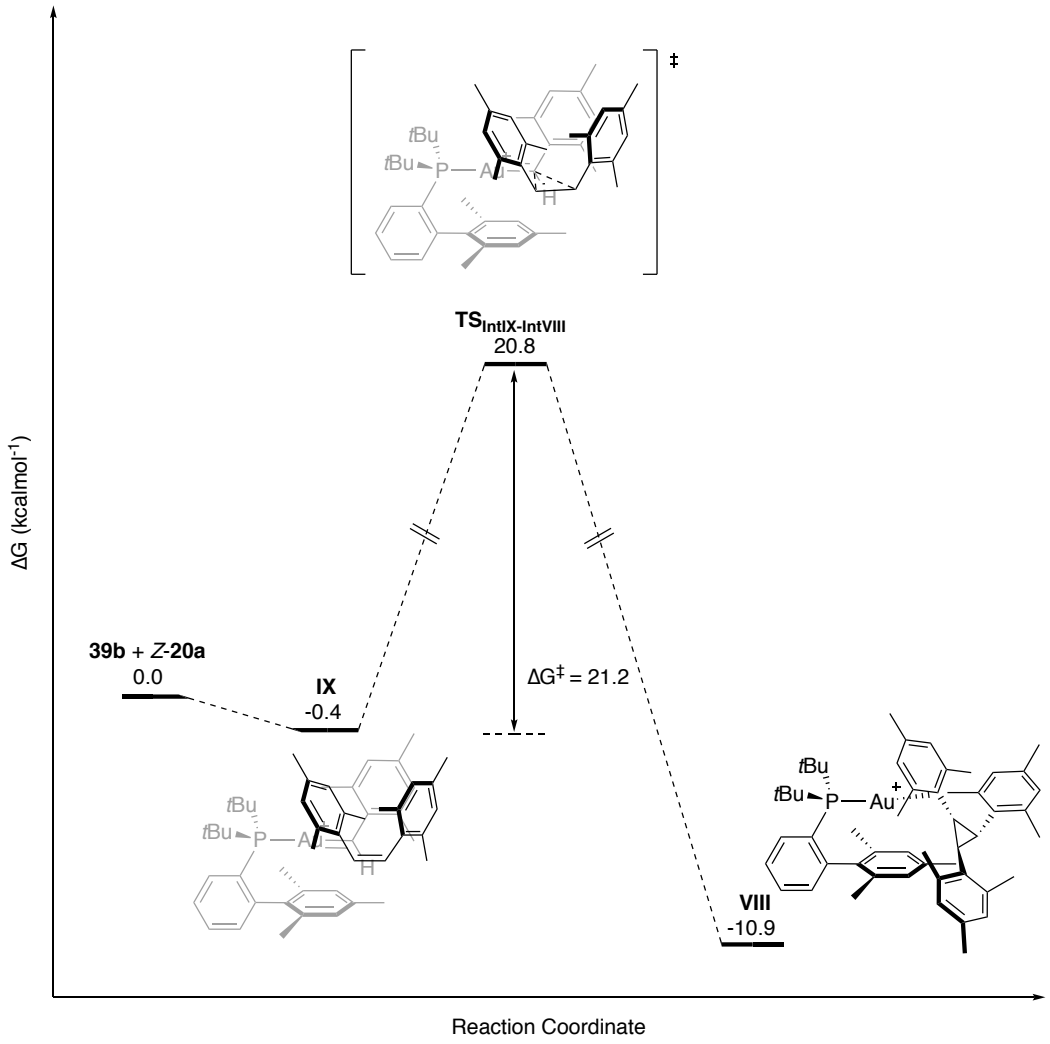

Figure 35. Calculated free energy profile for cyclopropanation of *Z*-**20a** with gold(I) carbene **39b**. PCM(CH_2Cl_2)-B3LYP-D3, SDD(Au), 6-31G(d,p) (C, H, O, P, Cl, F).

Optimized structures and absolute energies (a. u.) for all stationary points

In some structures hydrogens have been omitted for clarity.

Gold(I) carbenoid 37a

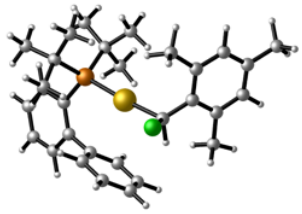

E = -2104.21100429

G = -2103.668056

Gold(I) carbenoid 37b

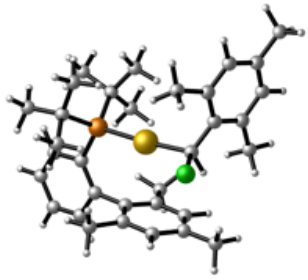

E = -2222.18169603

G = -2221.558599

Gold(I) carbenoid 37c

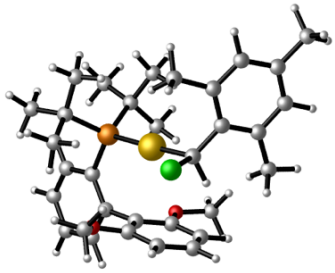

E = -2333.27610932

G = -2332.673481

Gold(I) carbenoid 37d

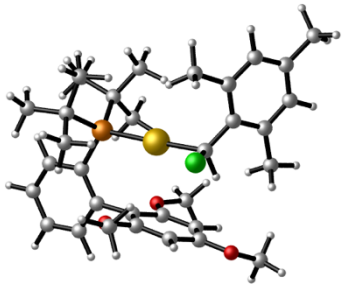

E = -2447.78290171

G = -2447.171876

Gold(I) carbenoid 37e

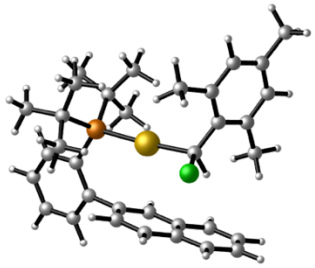

E = -2257.86566694

G = -2257.278242

Gold(I) carbene 39a

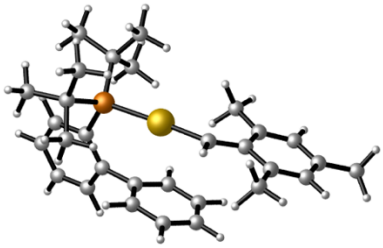

E = -1643.78502029

G = -1643.242214

Gold(I) carbene 39b

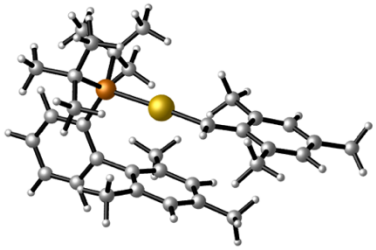

E = -1761.75758572

G = -1761.133641

Gold(I) carbene 39c

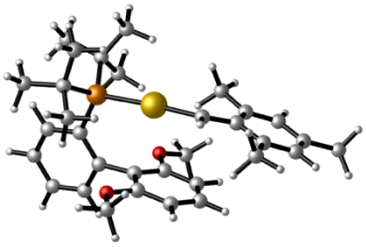

E = -1872.85105731

G = -1872.246067

Gold(I) carbene 39d

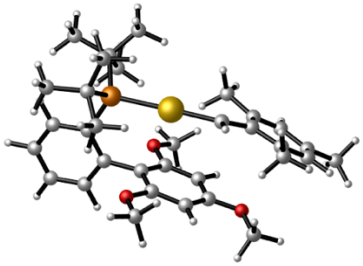

E = -1987.38360385

G = -1986.749420

Gold(I) carbene 39e

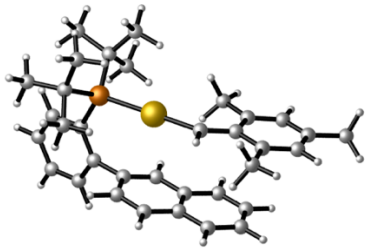

E = -1797.41542281

G = -1796.854818

Gold(I) carbene 39c-CF_3

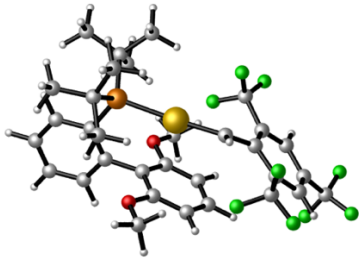

E = -2765.96617146

G = -2765.439993

Gold(I) carbene 39c-OMe

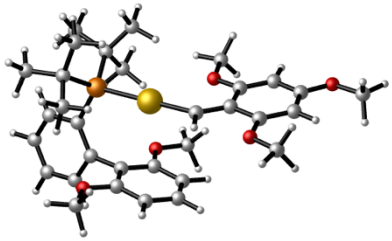

E = -2098.49115080

G = -2097.874195

39c-CF_3-TSAuC1

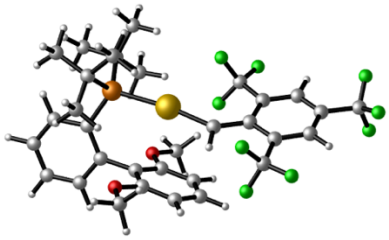

E = -2765.96245330

G = -2765.433746

39c-CF_3-TSC1C2

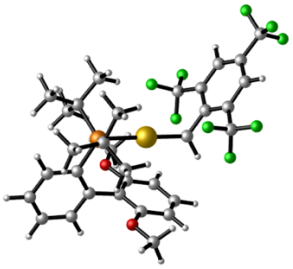

E = -2765.95775925

G = -2765.433400

39c-TSAuC1

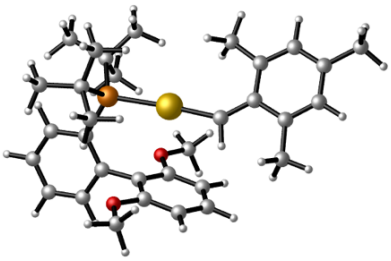

E = -1872.84898542

G = -1872.243720

39c-TSC1C2

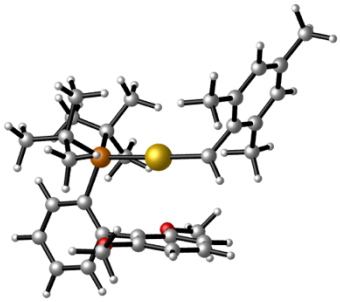

E = -1872.81272074

G = -1872.211560

39c-OMe-TSAuC1

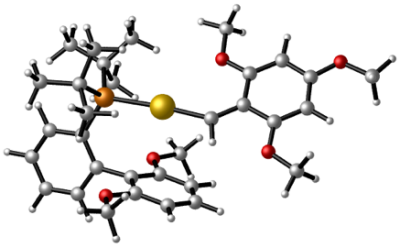

E = -2098.48867744

G = -2097.871147

39c-OMe-TSC1C2

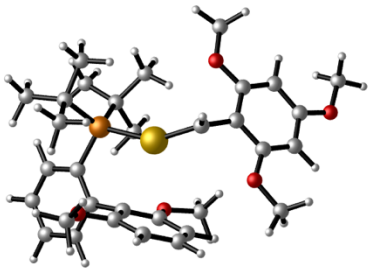

E =-2098.43666198

G = -2097.821877

IntI

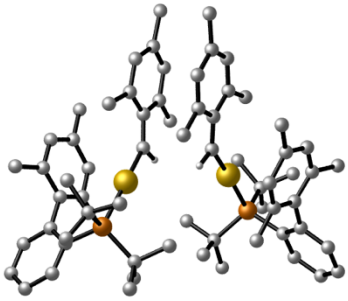

E = -3523.4979415

G = -3522.223411

IntII

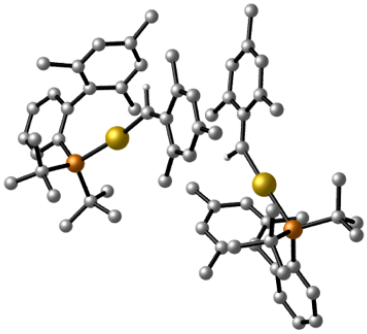

E = -3523.48887184

G = -3522.214727

IntIII

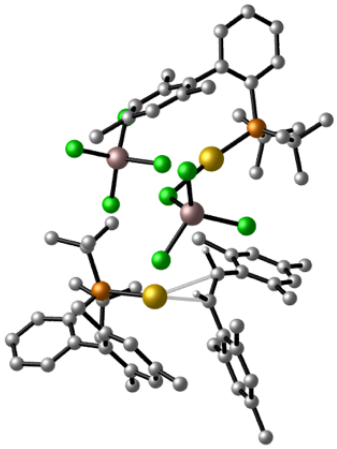

E = -7210.23024734

G = -7208.962554

IntIV

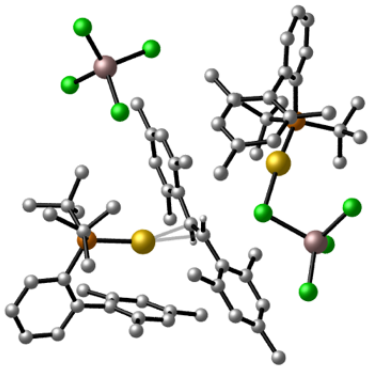

E = -7210.11884637

G = -7210.11884637

TSIntI-IntIII

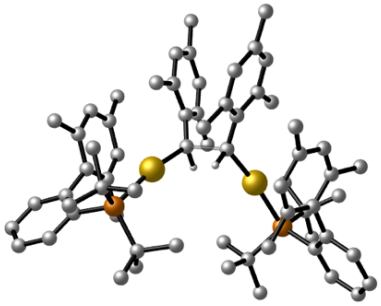

E = -3523.48092795

G = -3522.204607

$TS_{IntII-IntIV}$

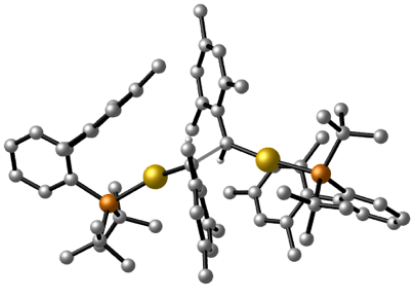

E = -3523.48130721

G = -3522.201591

$GaCl_4^-$

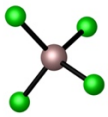

E = -1843.17908099

G = -1843.208109

Cyclohexane

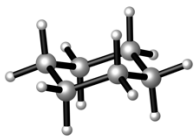

E = -235.905839640

G = -235.763520

IntV

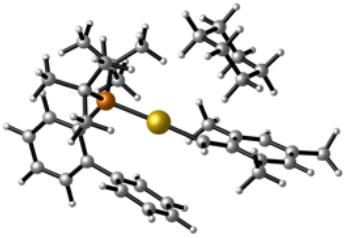

E = -1879.70877338

G = -1879.002881

IntVI

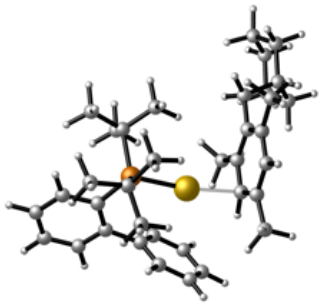

G = -1879.049886

E = -1879.76193325

$TS_{IntV-IntVI}$

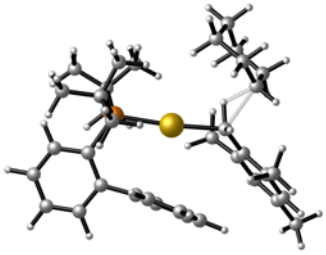

G = -1878.976404

E = -1879.68369158

***E*-20a**

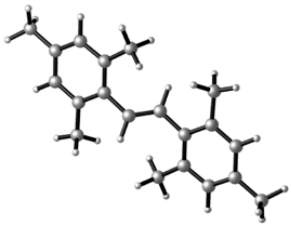

E = -776.661926601

G = -776.330594

_Z_-20a

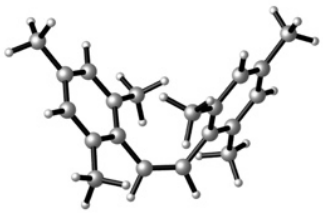

E = -776.664356897

G = -776.331611

IntVII

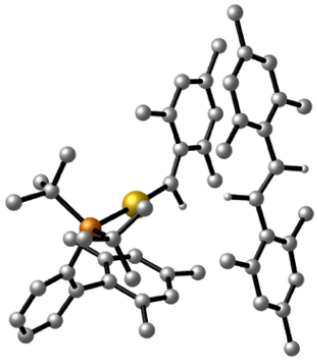

E = -2538.46370751

G = -2537.478038

IntVIII

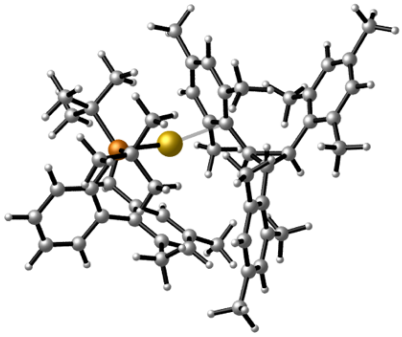

E = -2538.47450977

G = -2537.487003

$TS_{IntVII-IntVIII}$

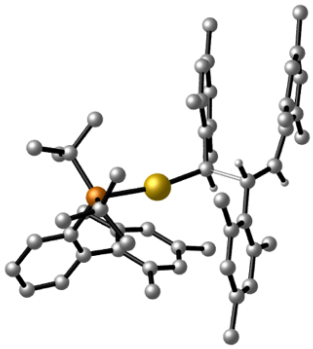

E = -2538.44698933

G = -2537.457826

IntIX

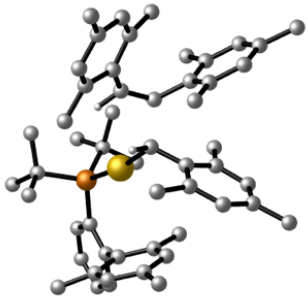

E = -2538.42862309

G = -2537.441486

$TS_{IntIX-IntVIII}$

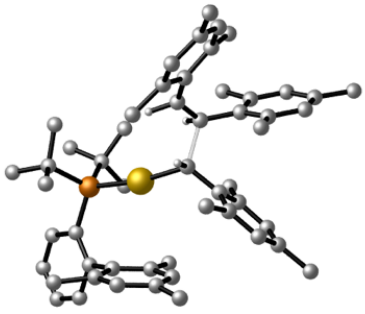

E = -2538.42866477

G = -2537.441012

Selected NMR spectra

Gold(I) carbene 39a

1H NMR -90 °C

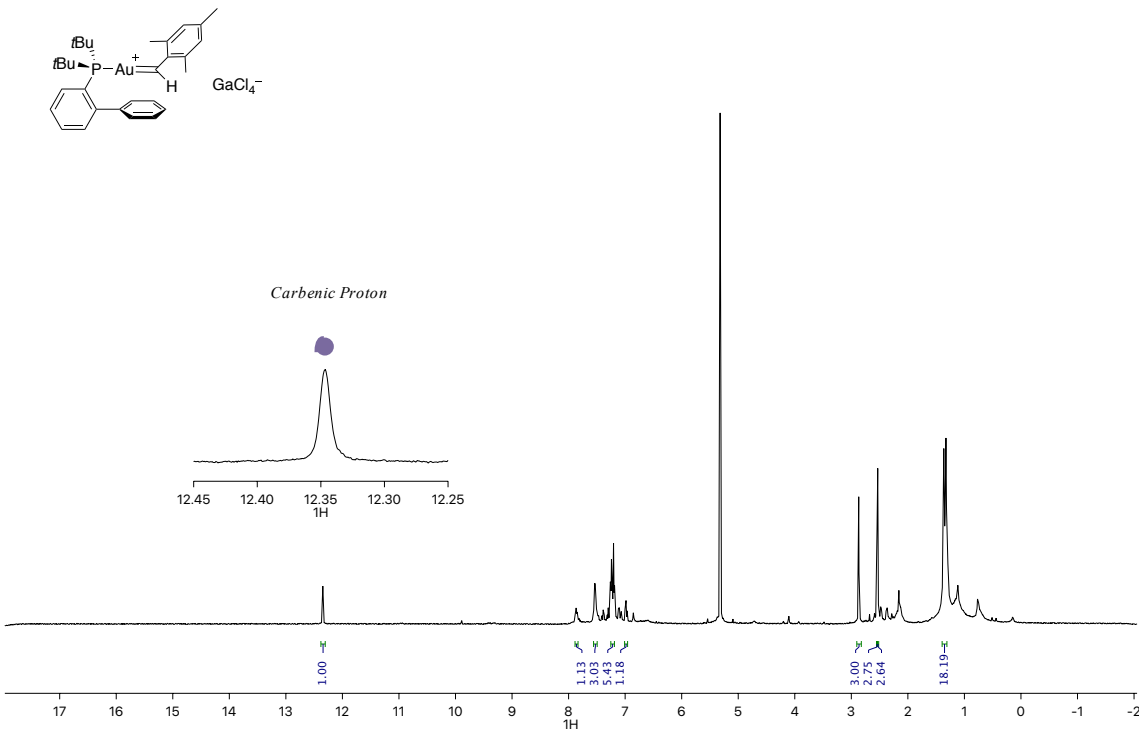

13C{1H} NMR -80 °C

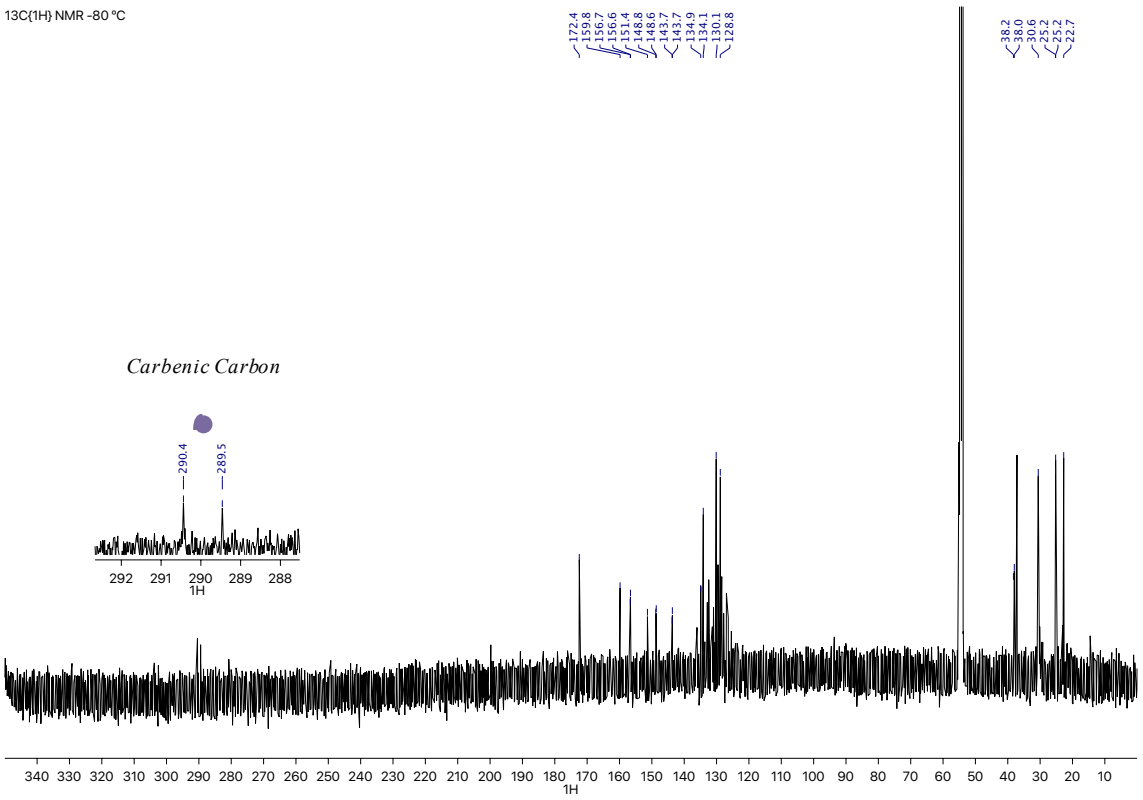

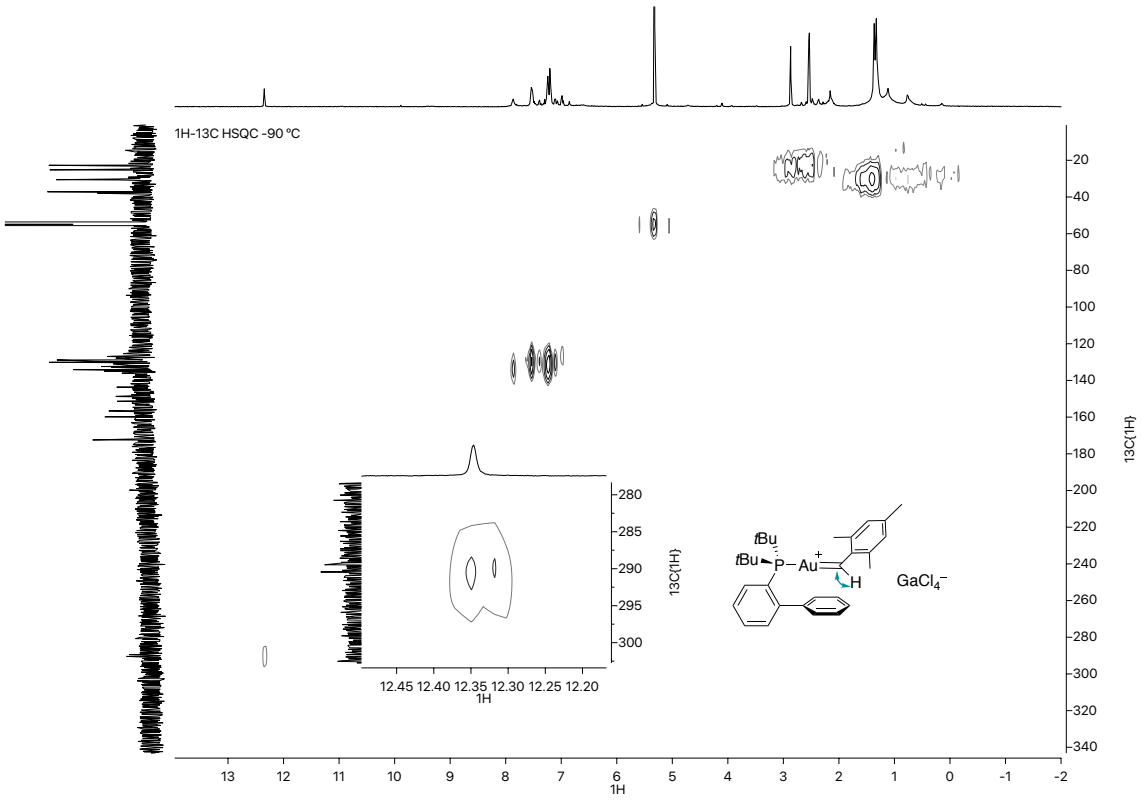
1H-13C HSQC -90 °C
13C{1H}
1H
tBu
tBu
P
Au
H
GaCl4−

Gold(I) carbene 39b

1H NMR -90 °C

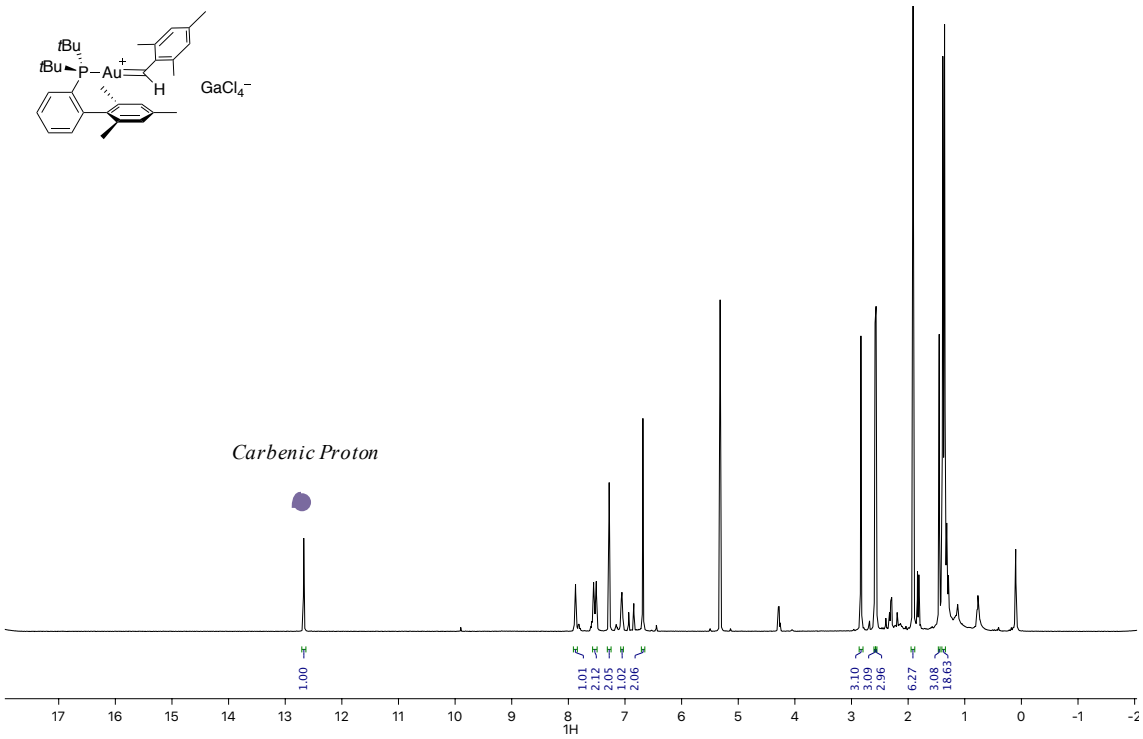

13C{1H} NMR -90 °C

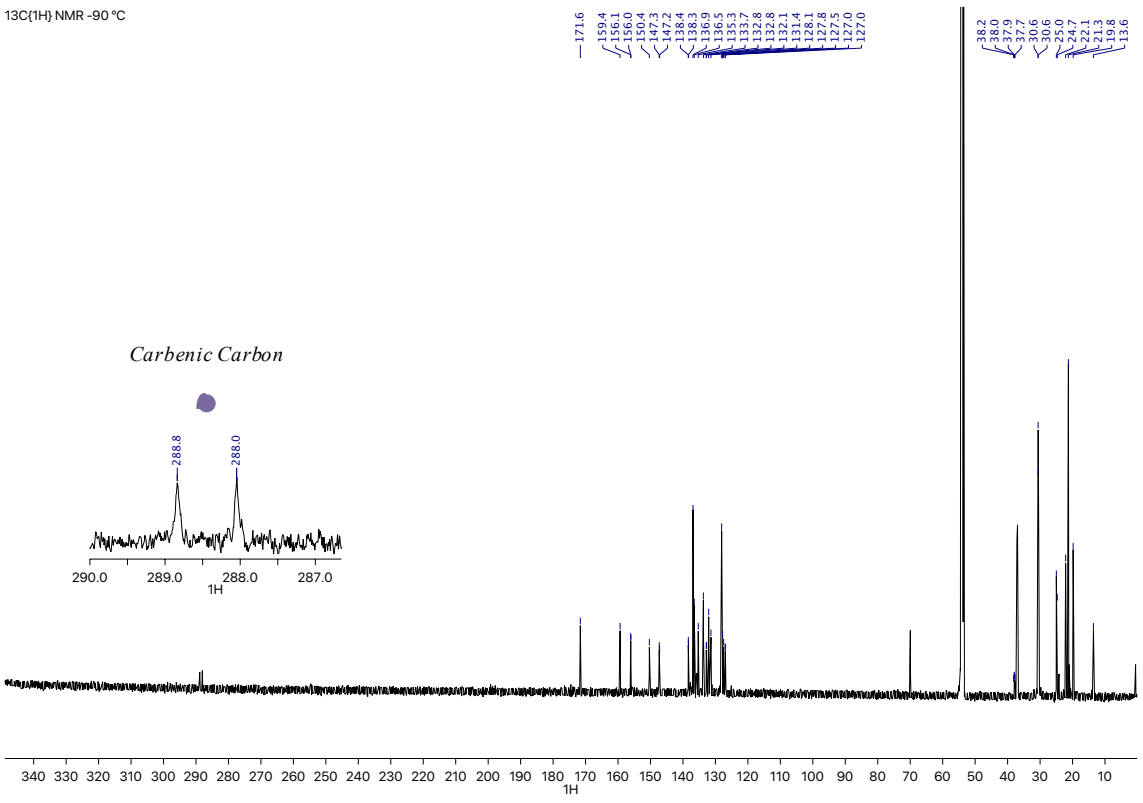

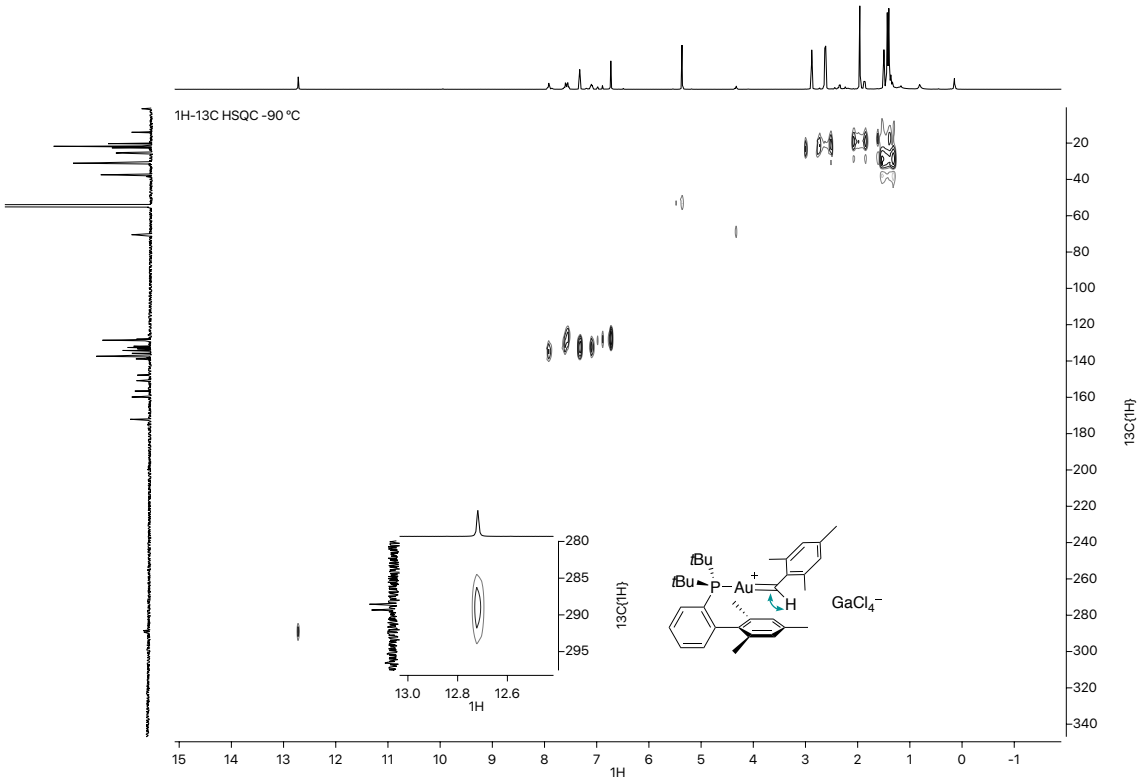
1H-13C HSQC -90 °C
13C{1H}
1H
tBu
tBu
P
Au
H
GaCl4−

Gold(I) carbene 39c

1H NMR -90 °C

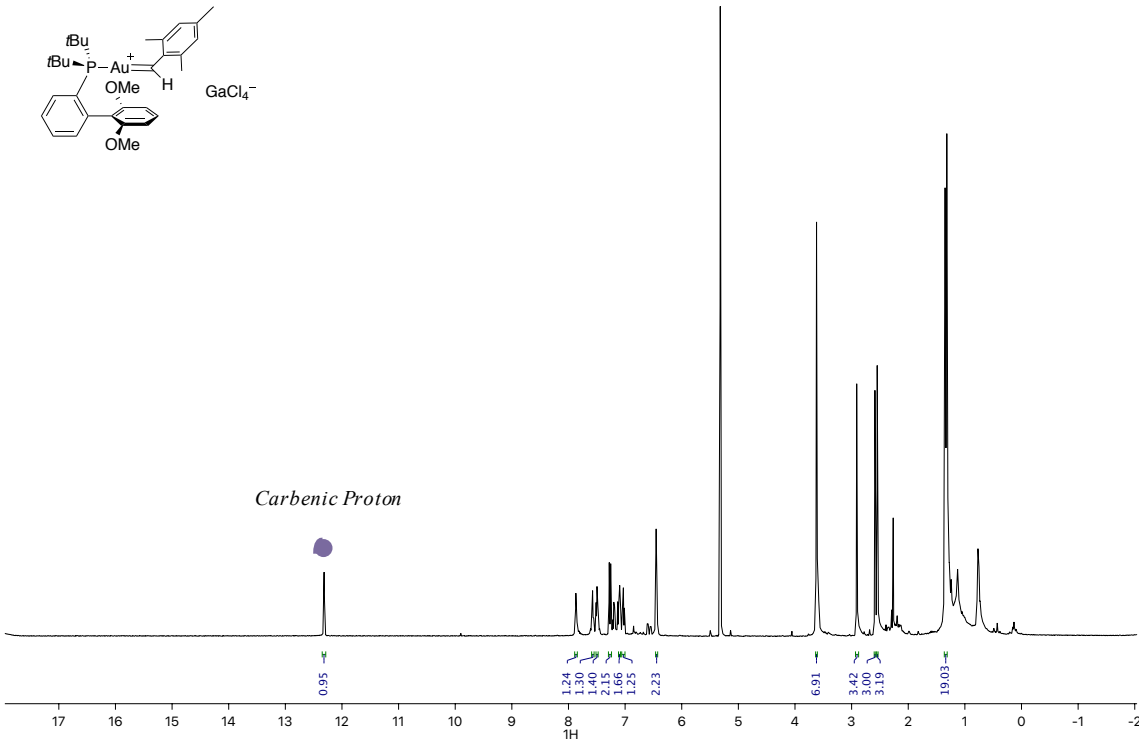

13C{1H} NMR -90 °C

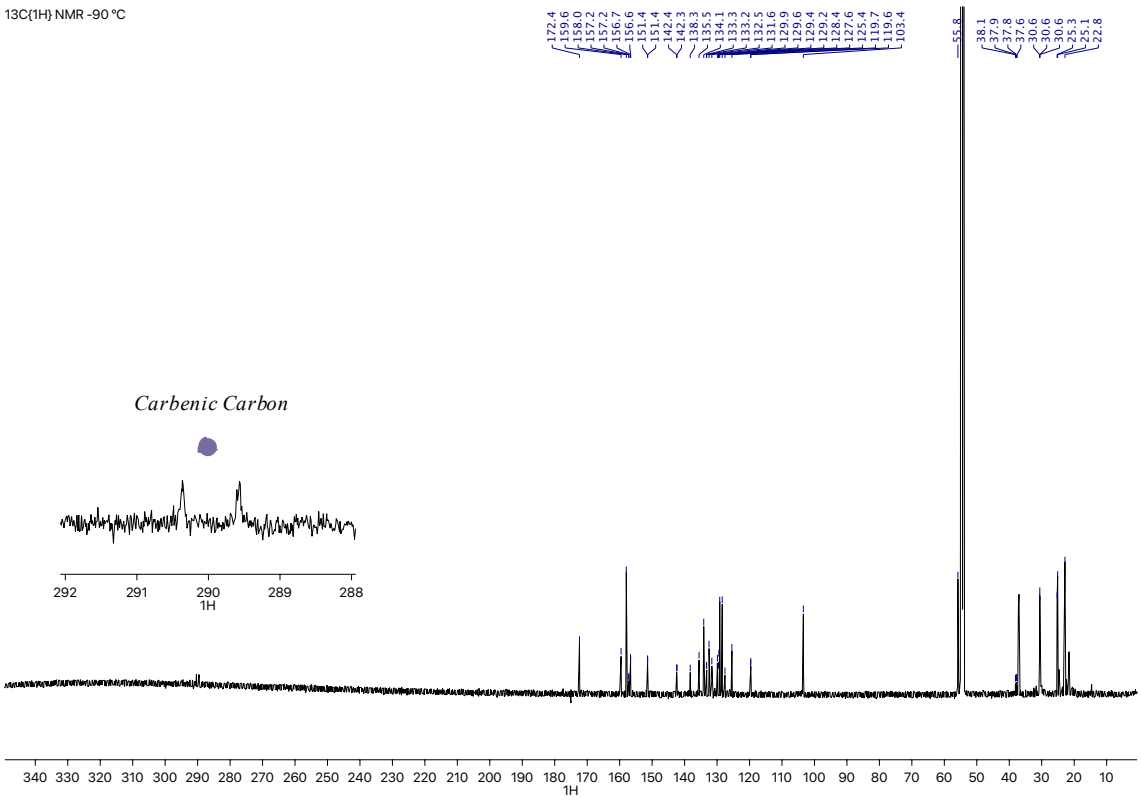

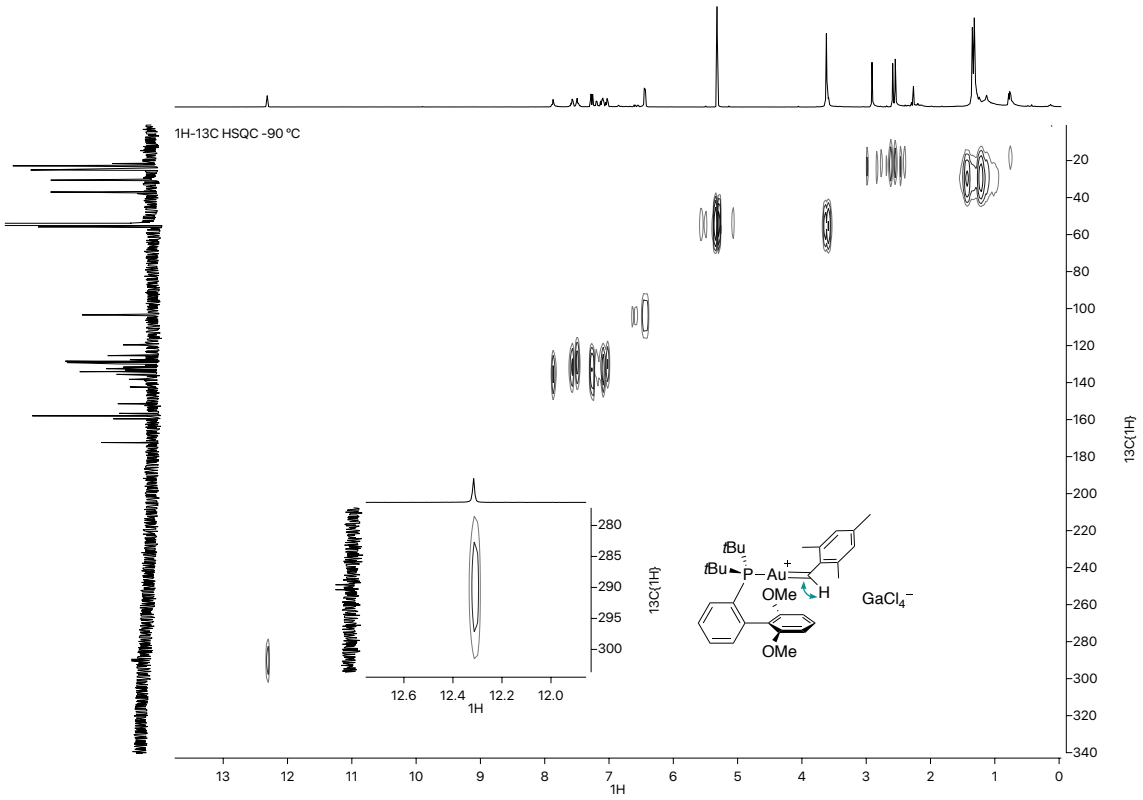
1H-13C HSQC -90 °C
13C{1H}
1H
tBu
tBu
P
Au
OMe
H
OMe
GaCl4−

Gold(I) carbene 39d

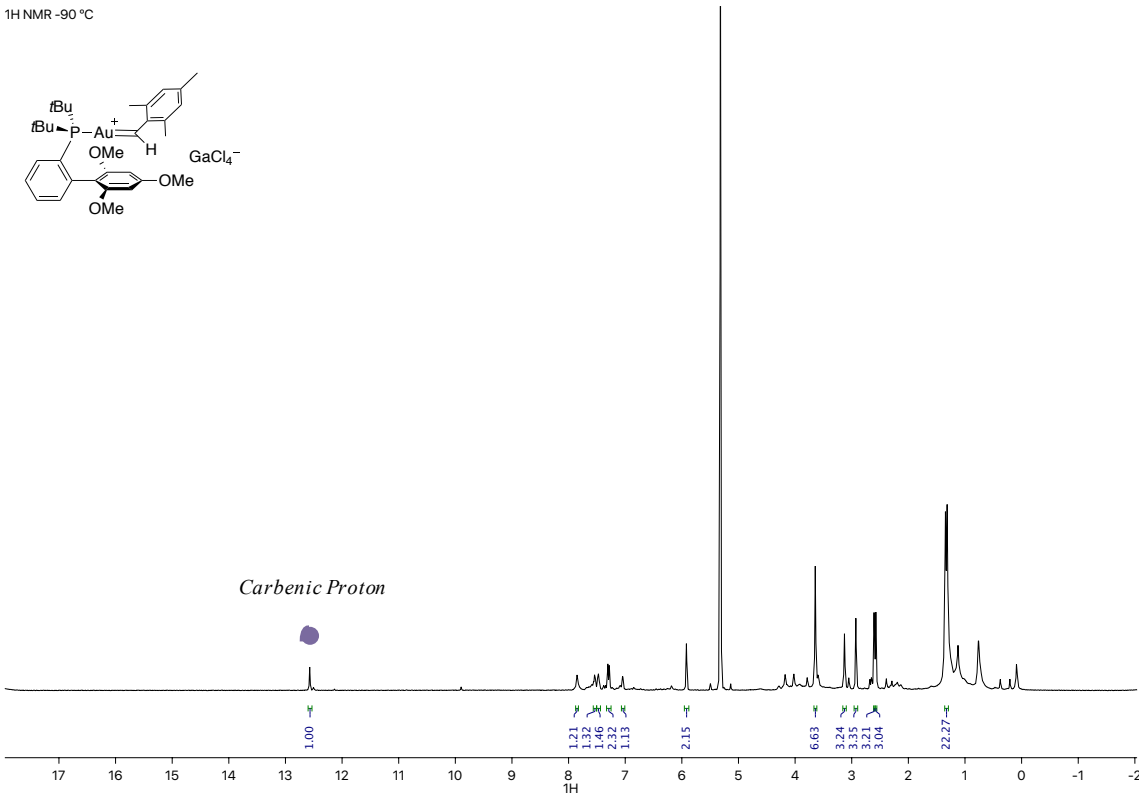

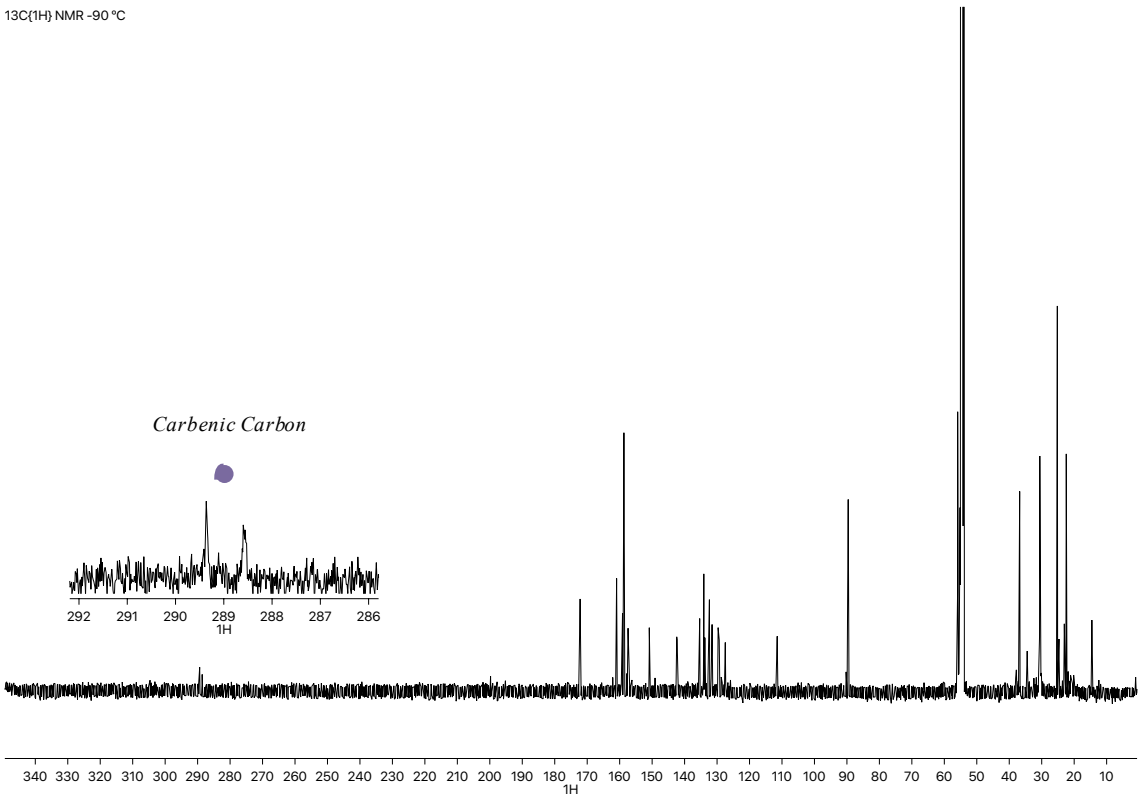

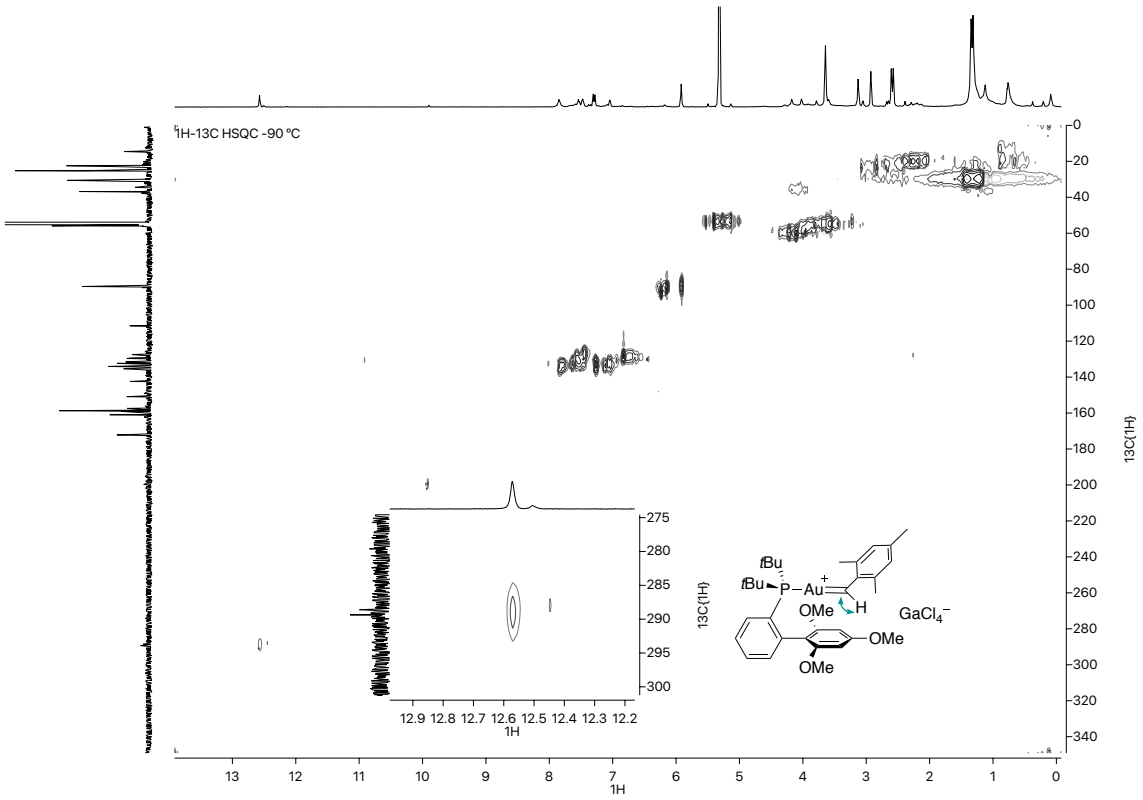
1H-13C HSQC -90 °C
13C{1H}
1H
tBu
tBu
P
Au
OMe
H
GaCl4−
OMe
OMe

Gold(I) carbene 39e

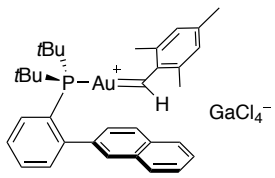

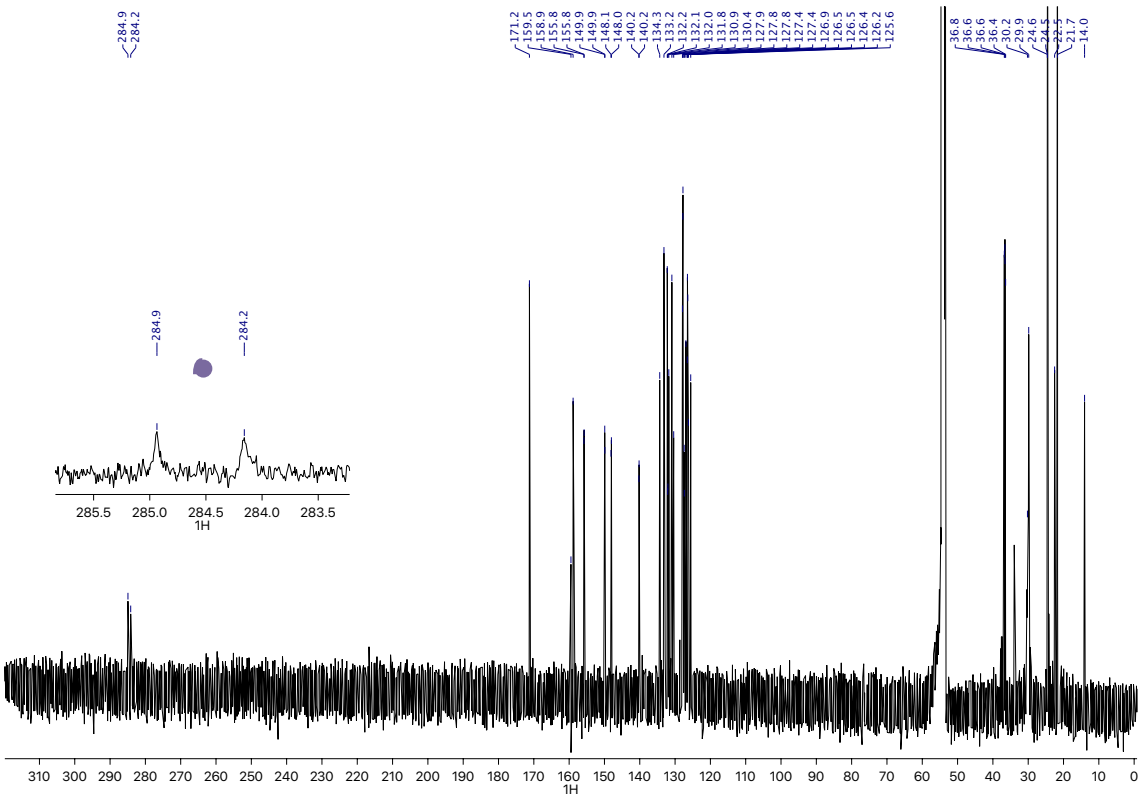

General Conclusions

The research developed in this Doctoral Thesis has led to the following results:

The first general strategy for the enantioselective synthesis of cyclobutenes by intermolecular gold(I)-catalyzed [2+2] cycloaddition has been developed (see Chapter I), (Scheme 1). This was enabled by the use of a chiral non-C_2 symmetrical Josiphos digold(I) precatalysts, through the generation of monocationic complexes *in situ*. The reaction proceeds satisfactorily with aryl alkynes and di- or trisubstituted alkenes. Following efforts in mechanistic investigations suggest that both ligand exchange and electrophilic addition can be turnover-limiting steps of the catalytic cycle depending on the electronic nature of the alkene.

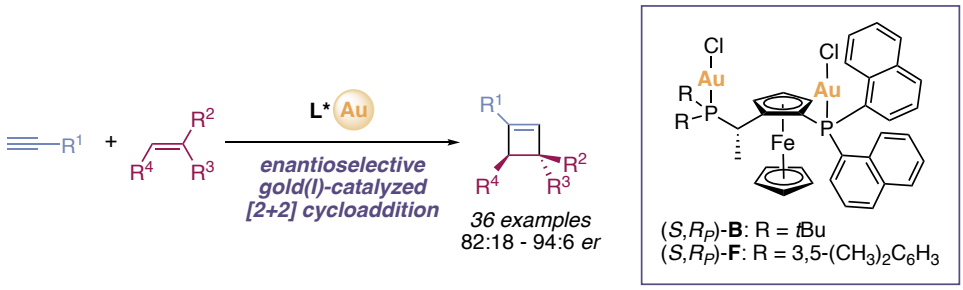

Scheme 1. Enantioselective gold(I)-catalyzed [2+2] cycloaddition.

A novel simple and reliable method for the preparation of chloro(methyl)gold carbenoid complexes was developed (see Chapter II). Activation of these new carbenoid complexes with a variety of chloride scavengers promotes reactivity typical of metallocarbenes in solution, namely homocoupling to ethylene, olefin cyclopropanation and Buchner ring expansion of benzene (Scheme 2). Kinetic studies together with DFT calculations suggest that the generation of ethylene proceeds *via* the rate-determining formation of a tri-coordinated neutral methylidene gold(I) carbene. On the other hand, the cyclopropanation occurs through a Simmons-Smith like transition state.

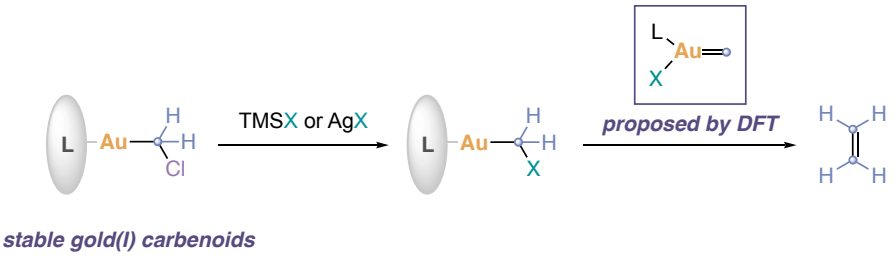

Scheme 2. Activation of chloro(methyl)gold(I) carbenoids and ethylene formation.

We have also demonstrated that aryl gold(I) carbenes can be certainly generated and characterized from the corresponding gold(I) carbenoids upon chloride abstraction, which stresses the different nature of gold(I) carbene and carbenoid complexes (see Chapter III). These aryl gold(I) carbene complexes undergo representative transformations of gold(I) carbene intermediates formed under catalytic conditions such as cyclopropanation, oxidation, and C–H insertion reactions.

Furthermore, they correspond to the reactive intermediates generated in the gold(I)-catalyzed decarbenation of cycloheptatrienes (retro-Buchner reaction). In the absence of other reagents, we observed dimerization to form preferentially the *E*-configured alkene by a process similar to that followed by other well-known metal carbenes, which places these highly electrophilic species among the metal carbene family, despite the weak π-backdonation from gold(I)-to-carbon calculated by NBO analysis.

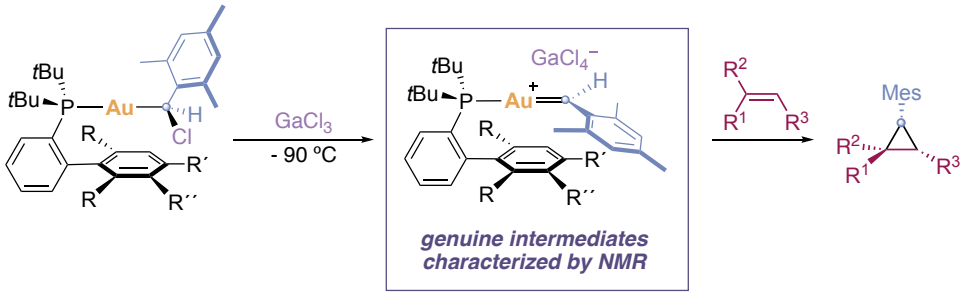

Scheme 3. Synthesis of aryl gold(I) carbenes from gold(I) carbenoids.

UNIVERSITAT ROVIRA I VIRGILI
REACTIVITY AND CHARACTERIZATION OF GOLD(I) CARBENES: KEY INTERMEDIATES IN GOLD(I) CATALYSIS
Cristina García Morales

UNIVERSITAT
ROVIRA i VIRGILI